# AGGREGATE CHARACTERISTICS AFFECTING RESPONSE AND PERFORMANCE OF UNSURFACED PAVEMENTS ON WEAK SUBGRADES

BY

DEBAKANTA MISHRA

DISSERTATION

Submitted in partial fulfillment of the requirements
for the degree of Doctor of Philosophy in Civil Engineering
in the Graduate College of the
University of Illinois at Urbana-Champaign, 2012

Urbana, Illinois

Doctoral Committee:

Professor Erol Tutumluer, Chair
Professor Imad L. Al-Qadi
Professor Emeritus Marshall R. Thompson
Professor William G. Buttlar
Dr. Abbas A. Butt

# ABSTRACT

Design of low volume roads and unsurfaced pavements traditionally involves covering the prepared subgrade with an unbound aggregate layer of sufficient thickness such that traffic-induced wheel loads are adequately distributed and stresses on the subgrade can be tolerated. Aggregate gradation and field-density requirements are commonly the only considerations for constructing "acceptable" aggregate cover layers. Aggregate quality aspects and properties are not considered in detail while selecting aggregate sources often with the lowest material hauling and transportation costs. This approach based solely on economic considerations may result in the selection of locally available poor quality material for routine use as the primary pavement load bearing layer. The primary objective of this PhD research was to evaluate individual effects of selected aggregate physical properties (test factors), such as particle shape, texture and angularity, type and amount of fines, and compaction (moisture-density) conditions on the response and performance of unsurfaced pavements.

Three different aggregate types, namely crushed limestone, crushed dolomite and uncrushed gravel were selected to first quantify the effects of individual test factors on aggregate shear strength, permanent deformation and directional modulus characteristics through a controlled laboratory test matrix. Laboratory test results showed that the effects of individual test factors on aggregate behavior changed significantly depending on the levels assigned to other test factors. Crushed aggregates showed consistently higher shear strength and modulus, and lower permanent deformations due to improved particle interlock when compared to the uncrushed gravel. The effect of type of fines on aggregate behavior was erratic at low fines contents, and was more pronounced when the fines fraction occupied a significant proportion of the voids in the aggregate matrix. Plastic fines when combined with excessive moisture, were found to destroy the inter-particle load transfer in the aggregate matrix, thus inducing excessive deformations under loading leading to specimen failure. The concept of anisotropic modulus ratio, an indicator of

compaction induced anisotropy in aggregates, was successfully applied as a material quality indicator for predicting unbound aggregate behavior.

Important findings from laboratory testing of aggregates served as the basis for material selection and thickness design of full-scale unsurfaced pavement sections for accelerated testing. Five different test "cells" were constructed at different combinations of aggregate material quality and engineered subgrade strength, and were tested to failure using an Accelerated Transportation Loading Assembly (ATLAS) under near-optimum and flooded aggregate moisture conditions. Test section performances under simulated traffic loading were monitored through surface profile measurements and transverse scanning with Ground Penetrating Radar (GPR) for assessment of subsurface deformations. Transverse trenches were subsequently excavated for visual identification of different mechanisms contributing to pavement failure. The use of non-destructive field modulus measurement techniques was pursued to establish their applicability as means of identifying anomalies in construction quality. Earth pressure cells were installed on top of the subgrade at the aggregate-subgrade interface to evaluate the effects of aggregate material type and quality on the dissipation of traffic-induced stresses within the aggregate layer. Depending on the type and quality of aggregates used, internal shear movement of the aggregate layer or subgrade deformation was found to be the primary mechanism contributing to pavement failure. Recommendations regarding the material selection and construction practices for unsurfaced pavements were finally presented to ensure improved performance of such pavement systems.

*To My Parents for their Unconditional Love & Support*

# ACKNOWLEDGMENTS

This PhD thesis is a product of the combined efforts and team work of several individuals. It is impossible to express my gratitude towards them in a limited number of words. This "Acknowledgments" section symbolizes my humble attempt at thanking those who have taught me anything and everything I have learned during my graduate studies.

It is common practice for a PhD thesis to start by acknowledging one's research supervisor for his/her contribution. However, I believe that "thanking" my PhD advisor Prof. Erol Tutumluer will be pretentious on my part, and would indicate an attempt to quantify his contribution towards my education. Prof. Tutumluer has long since transcended the role of merely serving as my PhD research supervisor, and epitomized a teacher and a mentor who laid the foundation for, and subsequently shaped my professional career. The thirst for conducting consistent high quality research, making the extra surge to improve the quality of research products, as well as collaborating with others towards the achievement of common research goals, are some of the virtues that Prof. Tutumluer has communicated to me during my PhD. Every graduate student wishes to work with an understanding, but at the same time motivating research supervisor. I have been blessed in this regard, and have enjoyed every moment of my life while working with Prof. Tutumluer. A fellow researcher once asked me how it felt to be working with the most-recognized professor in my area of expertise. My simple answer was, "Merely classifying Prof. Tutumluer as the most-recognized professor in transportation geotechnics will be an insult to the great human being. He is an ideal mentor, and has made my PhD a great learning experience".

Other members of my PhD committee have jointly contributed towards improving the intellectual quality of my PhD research, as well as motivating me to become a life-long "student" of transportation engineering. Prof. Imad Al-Qadi has taught me the art of smiling through

demanding work days, and enjoying every moment along the research path while striving to achieve the ultimate objective. Starting from seeking his feedback on the application of ground penetrating radar (GPR) to study pavement performance, to learning the art of pavement instrumentation, I have constantly relied on Prof. Al-Qadi's knowledge and experience to improve my research quality. I aim to borrow from his ever-positive attitude and leadership qualities while trying to establish myself as an academic researcher in pavement engineering.

Prof. Marshall Thompson encouraged me to conduct state of the art academic research, while at the same time ensuring its applicability in practice to improve the quality of the society's infrastructure. I will miss having frequent long discussions with Prof. Thompson while waiting in the department office for the coffee to brew. I have constantly relied on his immense knowledge and unfathomable memory to learn different aspects of unbound aggregate material characteristics and layer behavior. Running back to my desk after our discussions, and taking notes to implement some of his research ideas, have been routine activities that I have thoroughly enjoyed.

Dr. Abbas Butt and his staff contributed significantly towards completion of the laboratory testing of aggregates under the scope of this research study. The art of paying immaculate attention to details for ensuring repeatability and accuracy of laboratory test results, was the most important quality I learned from Dr. Butt. He has always been available and eager to help during the course of my PhD research. Prof. William Buttlar taught me to "ask the right questions" while working on a research problem. His feedback and suggestions have helped me significantly in developing the right hypotheses related to my research topic, and have driven me to conduct goal-oriented research. Thanks to Prof. Jeff Roesler for his valuable inputs aimed at enhancing the quality of my research.

The research reported in this thesis was primarily sponsored by the Illinois Department of Transportation (IDOT). I am thankful to all present and past members of the University of Illinois (U of I) Transportation Geotechnics research group, as well as other students and researchers at the U of I Advanced Transportation Research and Engineering Laboratory (ATREL) and the Illinois Center for Transportation (ICT). Thanks to Dr. Joseph Anochie-Boateng for getting me familiarized with different laboratory test methods, and above all, the U of I FastCell. My sincere thanks to Jim Meister for his constant help during the

construction and accelerated testing of the full-scale test sections. The field modulus measurement work reported in this thesis would not have been possible without the support of Ed Hall from Humboldt®, as well as Erwin Kohler and Gary Mitchell of Dynatest®. Thanks to Yuanjie Xiao, Maziar Moaveni, Hasan Kazmee, Yu Qian, Huseyin Boler, Zhen Leng, Pengcheng Shangguan, Marcus Dersch, Anthony Mareno, Armen Amirkhanian, Hasan Ozer, and Altan Yilmaz for their help during the laboratory and field testing phases of this research study. Ed Bartholomew of ERI and Steve Summers of Open Road Paving helped during the laboratory testing and field construction phases, respectively. Levi Koppmann, Dan Oberg, Connor Smith, and Nora Al-Qadi worked with me as undergraduate research assistants during different stages of my PhD research. The contributions of Tim Prunkard, Darold Marrow, Marc Killion, and Chester Riggin of the Newmark Civil Engineering Machine Shop are greatly appreciated. Phil Donovan, Atul Dixit, Behzad Behnia, and Eshan Dave made my social life in Urbana-Champaign immensely enjoyable.

My family members provided me with constant guidance and encouragement throughout my PhD. I am grateful to my brother and sister-in-law Dr. Sukant Misra and Mrs. Rina Misra for being my guardians and "substitute parents" in the United States. It was their love and affection that never let me feel away from home, and has given me a family environment to spend some of the most memorable times of my life. Thanks to my sister Debajani Misra for being my best friend and biggest critique. Talking to her and fighting with her has always rejuvenated me, and I intend to utilize that for the rest of my life.

My wife Bipasha has patiently put up with my indifference and unavailability towards all household related activities over the last two years. She has never complained about my work schedule, and has always supported me in my personal and professional endeavors. I am eternally grateful for her understanding nature, and must confess that I have always taken undue advantage of this quality.

Finally, this thesis is dedicated to my parents, Mr. Janamohan Misra and Mrs. Chitrarekha Misra. Their love for me remains unchanged as I ride the waves of success and failure in personal as well as professional matters. Thank you Nana and Bou for always loving me the way I am. I hope someday I can make the two of you proud.

# TABLE OF CONTENTS

# LIST OF TABLES

# LIST OF FIGURES

# CHAPTER 1

# INTRODUCTION

Based on the nature of stress and deflection transfer between its layers, a pavement structure can be categorized as flexible, rigid, or composite [1, 2]. A flexible pavement involves the transmission of uniform stresses and non-uniform deflections between layers, whereas a rigid pavement is idealized by the downward transmission of uniform deflections and non-uniform stresses [2]. Several different material and layer combinations can be used by engineers to build a pavement structure that facilitates safe, reliable, and comfortable movement of traffic without undergoing excessive damage. Among the materials used to build pavement surface layers, Hot Mix Asphalt (HMA) and Portland Cement Concrete (PCC) are the most common. Owing to the general behavior of these two materials under loading, pavements constructed with HMA are usually categorized as "flexible" whereas those built with PCC are called "rigid".

A conventional flexible pavement structure consists of an HMA surface layer with one or more layers of unbound aggregates set on top of the subgrade. Rigid pavements, on the other hand comprise a PCC slab on top of the subgrade with or without the intermediate unbound aggregate layers. Composite pavement structures consist of both HMA and PCC layers in different possible configurations. The thickness and order of layers in each of the different pavement types are governed by their structural and functional demands. Figure 1.1 shows a variety of layer configurations commonly used in pavement structures [3].

## 1.1 Unsurfaced Pavements and Construction Platforms

Besides the above mentioned pavement types with bound surface layers, "unsurfaced pavements" or "unpaved roads" constitute a major portion of the road network in any country. In the United States (US), over 1.6 million miles of unpaved roads (53 % of all roads) were reported in the year 2000 [4]. Moreover, in "under-developed" to "developing" countries, unsurfaced pavements

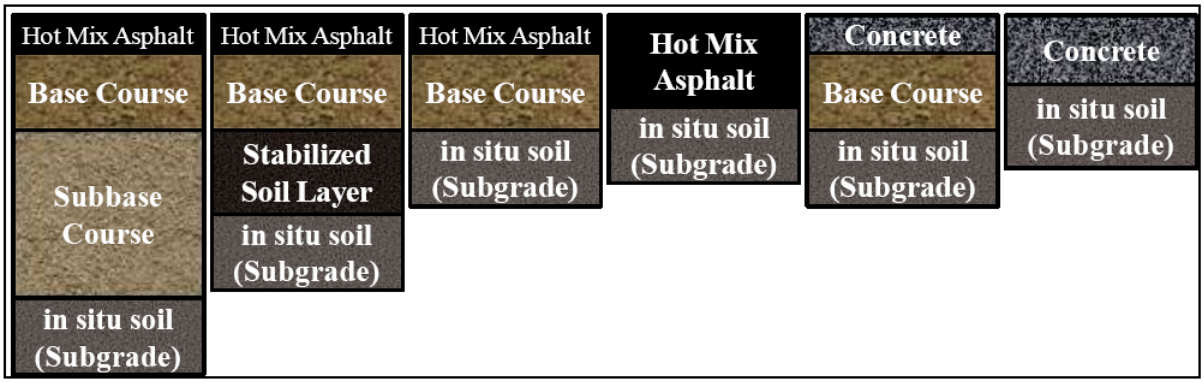


Figure 1.1: Typical Pavement System Configurations [3]

account for an even larger proportion in the total number of road miles. These roads (also referred to as "gravel roads" or "dirt roads") are often constructed by direct placement of an unbound granular layer (UGL) on top of the subgrade, and generally carry local traffic between rural lands and villages besides providing connecting links between paved roads. The surface of such a pavement is given a relatively smooth finish through adequate compaction of the UGL. The absence of stronger bound surface layers in these pavements results in direct load application on the UGL. In certain cases, a thin bituminous seal is applied on top of the UGL to prevent material attrition, as well as to provide insulation against surface water infiltration. In either configuration, the UGL functions as the primary load bearing component [5].

Another common instance of direct traffic loading on the UGL is observed in pavement working platforms constructed to ensure adequate subgrade stability. Subgrade stability refers to the strength and deformation characteristics of subgrade soils that impact pavement construction activities [6]. For both the short-term and long-term stability requirements, the following are the guidelines [7]:

- The subgrade should be "stable" enough to prevent excessive rutting and shoving during construction;
- The subgrade should provide a sound "platform" for the placement and compaction of overlying layers; and
- The subgrade should be "stiff" enough to limit permanent deformation accumulation during the pavement service life.

In areas with soft unstable soils inadequate to support heavy construction equipment, a "construction platform" often needs to be built. These layers are usually constructed by "capping" the soft subgrade with an unbound granular layer. Besides providing sufficient support for equipment mobility and paving operations, these layers also provide a stable foundation for compaction of overlying layers. Similar to unpaved roads, the UGL in a construction platform is subjected to very high stress levels from heavy construction equipment.

## 1.2 Unbound Granular Layer Functionality

The primary functionality of an UGL as the base course or subbase in a conventional pavement system involves spreading the traffic induced stresses through particle to particle load transmission at the contact points [8]. The lateral stress dissipation and resulting reduction with depth protects the subgrade (weakest layer) from overloading, and excessive deformations. For unsurfaced pavements and construction platforms characterized by direct application of heavy loads on the UGL, the layer should be thick enough to achieve sufficient stress reduction at the subgrade level. Moreover, the aggregate layer must have adequate resistance to prevent internal shear failure. One additional requirement for unsurfaced pavement applications is that the aggregate material must be cohesive enough to prevent material loss through attrition [4, 8].

Fluctuating oil prices in recent years have magnified the importance of unbound granular layers functioning as the primary load bearing structural components in pavements. High price of crude oil and high maintenance costs associated with paved roads have forced several transportation agencies to build more unsurfaced pavements along low volume routes [4]. To function adequately and facilitate smooth movement of traffic over these pavements, the UGL must be designed for adequate structural capacity.

## 1.3 Problem Statement

Most methods used for thickness design of unsurfaced pavements and construction platforms are based on subgrade strength as the primary input. Some indicator of subgrade (shear) strength is used in empirically developed equations to determine the UGL thickness. "Subgrade protection" is the primary underlying principle behind most of these "recipe" approaches that do not consider

aggregate material quality while recommending the UGL design thickness.

For construction platform applications in the US, the aggregate cover thickness is mostly determined as a function of the subgrade shear strength or unconfined compressive strength ($Q_u$) [6]. Similarly, pavement foundation specifications traditionally used in other countries like the Netherlands and United Kingdom (until recently) are based on the California Bearing Ratio (CBR) of the subgrade soil as an indicator of shear strength. These approaches do not consider the effects of different aggregate properties affecting its behavior while recommending UGL design thicknesses. The use of a wide range of aggregate materials for constructing these layers often leads to unpredictable behavior under loading. Depending on the quality of the aggregate material, a recipe approach may lead to failure of the subgrade from excessive stress levels, or internal shear failure of the UGL. On the other hand, these methods may sometimes lead to overdesigning when "good quality" aggregate material is available.

The performances of unbound granular layers are greatly influenced by different aggregate properties, namely: particle shape, texture, and angularity, type and amount of fines, moisture content, and moisture-density or compaction conditions. Although several research studies have focussed on evaluating the effect of one or more of these factors on aggregate performance, no study has explored the combined effect of all these factors in a factorial experimental design [9, 10, 11, 12]. Quantification of the relative effects of individual aggregate physical properties influencing performance would greatly aid safe and economical design of unbound granular layers in pavements. This is particularly important for unsurfaced pavements where the UGL is the primary structural component.

As state and federal agency specifications often allow for a wide variety of aggregate materials to be used in pavement applications, it is important to evaluate the effects of different aggregate physical properties on UGL performance. In states like Illinois, a common aggregate specification is often used for different pavement applications. An experimental study aimed at quantifying the effects of different aggregate physical properties on behavior will therefore impact the design and construction all pavement structures significantly.

## 1.4 Research Objective

The primary objective of this PhD research was to evaluate individual effects of selected aggregate physical properties, such as particle shape, texture and angularity, type and amount of fines, and compaction (moisture-density) conditions on the response and performance of unsurfaced pavement systems using particle size distribution (gradation) as the primary control parameter, and thereby develop guidelines for "adequate" material selection and construction practices.

## 1.5 Research Scope

The research work conducted under the scope of this PhD study comprised two distinct phases, namely: (1) Laboratory experimentation, and (2) accelerated testing of full-scale unsurfaced pavement sections. The primary tasks associated with each of the two phases, and the research approach adopted to accomplish these tasks are listed below.

### 1.5.1 Laboratory Experimentation

*Tasks:*

1. Identify and select important aggregate physical properties affecting behavior to be studied in the laboratory.
2. Develop a database of aggregate shear strength, permanent deformation and resilient modulus test results through completion of a laboratory test matrix at different combinations of selected aggregate properties.
3. Statistically analyze the laboratory database to evaluate the significance of individual aggregate properties affecting strength, permanent deformation and resilient modulus behavior and thus impacting material characterization models.
4. Evaluate the effects of aggregate physical properties, and compactive effort on directional dependency (anisotropy) of unbound aggregate resilient response and modulus characteristics, and the ratio of horizontal and vertical resilient moduli linked to aggregate performance.

*Research Approach:*

Based on an extensive review of technical literature, the following aggregate physical properties (test factors) were identified as most significant in governing UGL behavior: (1) particle shape, surface texture, and angularity, (2) type and amount of fines, and (3) compaction (moisture-density) conditions. Another factor, identified as critical in governing UGL performance was gradation or particle size distribution. To single out and evaluate individual effects of the selected test factors on UGL behavior, it was decided to use particle size distribution as the primary control parameter for conducting the laboratory experiments.

Two types of crushed stones (limestone and dolomite) and an uncrushed river gravel often used in pavement applications throughout state of Illinois were selected for laboratory characterization. A laboratory test matrix was designed to characterize the (shear) strength, permanent deformation, and resilient modulus behavior of the above aggregate types under factorial combinations of aggregate shape (including flatness and elongation, texture and angularity), type of fines (plastic and nonplastic), amount of fines (ranging in increments from low to high), and moisture content (in relation to the optimum compaction conditions). Ranges for the above test factors were established considering allowable limits specified by different transportation agencies.

Commonly used material characterization models to predict the resilient modulus and permanent deformation behavior of unbound granular materials were fitted to the laboratory test results. Analyses of Variance (ANOVA) were conducted to identify the significance of aggregate physical properties affecting material characterization model parameters.

Applicability of aggregate anisotropic modulus ratios as quality indicators for unbound granular materials was evaluated through analyses of the directional modulus test results. The anisotropic modulus ratio was defined as the ratio of resilient modulus values determined from independent pulsing in the horizontal and vertical directions (Modulus Ratio = $M_{Rh}/M_{Rv}$). Possible changes in anisotropic modulus ratio values as a function of compaction level were investigated through repeated load triaxial testing of aggregate specimens compacted using the standard [13] as well as modified [14] efforts.

### 1.5.2 Accelerated Testing of Full-Scale Unsurfaced Pavement Sections

*Tasks:*

1. Synthesize important findings from the laboratory testing of aggregates to select different aggregate types for use in construction of full-scale unsurfaced pavement sections and verify the laboratory test results through accelerated pavement testing.
2. Characterize the selected aggregate types in the laboratory for (shear) strength, resilient modulus and permanent deformation behavior.
3. Conduct Finite Element (FE) based pavement analyses of the layered pavement systems for thickness design of unsurfaced pavement sections, and use the vertical deviator stress on top of the subgrade as a critical pavement response parameter to evaluate effects of aggregate quality on subgrade rutting potential.
4. Construct full-scale unsurfaced pavement test sections using different aggregate types over an engineered subgrade of controlled strength for accelerated pavement testing and performance monitoring.
5. Perform accelerated testing of field sections with an Accelerated Transportation Loading Assembly (ATLAS) and use "rut depth" to measure and quantify pavement performance.
6. Use non-destructive field modulus measurement and subsurface visualization techniques for construction quality assurance and pavement performance assessment.

*Research Approach:*

Based on important findings from the laboratory testing of aggregates, four different aggregate types were selected representing different combinations of the test factors, for construction of full-scale unsurfaced test sections. These aggregate types were subsequently characterized in the laboratory for shear strength, permanent deformation, and resilient modulus behaviors.

Nonlinear, stress dependent material characterization model parameters determined from laboratory testing of aggregates at different test factor combinations were used in a Finite Element (FE) pavement analysis program to calculate the critical pavement response values for

typical unsurfaced pavement sections under wheel loading. Unsurfaced pavement sections constructed using aggregates at different combinations of the test factors were analyzed, and subgrade rutting potential was evaluated using the concept of Subgrade Stress Ratio (SSR). Failure of unsurfaced pavements through subgrade deformation was distinguished from that due to internal shear movement of the unbound granular layer, through combined analyses of the SSR values and results from laboratory testing of aggregates. Based on the analysis results, three different unsurfaced pavement configurations were selected for construction and accelerated pavement testing to verify results from the laboratory phase of the research study.

Important findings from the laboratory phase of the research regarding individual effects of the test factors on aggregate behavior were verified through accelerated testing of full-scale unsurfaced pavement sections. Five different test "cells" were constructed at the University of Illinois Advanced Transportation Research and Engineering Laboratory (ATREL) representing different combinations of aggregate quality and subgrade strength. The pavement sections were constructed over a subgrade of controlled CBR to simulate "weak" subgrade conditions often encountered in unsurfaced pavement construction.

The full-scale unsurfaced pavement sections were loaded using an Accelerated Transportation Loading Assembly (ATLAS) to assess the effects of aggregate quality on pavement performance. Each test cell was loaded up to a maximum of 1,000 applications of a 44.5 kN (10,000 lb) single wheel load at a tire pressure of 758 kPa (110 psi) and performance was monitored through surface profile measurements after different number of load applications. The effect of moisture conditions on unsurfaced pavement performance was studied by loading each cell along two wheel paths separated by a distance of 2.4 m (8 ft.). Earth pressure cells were installed on top of the subgrade at the aggregate-subgrade interface to monitor the vertical subgrade stress levels under loading, and evaluate the effects of aggregate material type and quality on the degree of stress dissipation achieved within the aggregate layer. Possible mechanisms contributing towards failure of the test sections were proposed, and the hypotheses were corroborated through excavation of transverse trenches in the test sections. Conclusions were drawn regarding the effect aggregate quality on the failure mechanisms of unsurfaced pavement sections.

The use of several non-destructive modulus measurement and substructure visualization techniques was also pursued in this research study for construction quality assurance and performance assessment of the full scale test sections. In-situ moduli of the constructed layers were measured using a Dynatest® Light Weight Deflectometer (LWD) (model 3031) and a Humboldt® Soil Stiffness Gauge (GeoGauge™). Tests were conducted on the engineered subgrade as well as on the finished aggregate layer with data collected consistently from the same locations using the two devices. Moreover, transverse scanning of the pavement sections was conducted using Ground Penetrating Radar (GPR) to introduce an innovative application of GPR technology in subsurface deformation assessment of unsurfaced pavement sections.

## 1.6 Thesis Organization

Chapter 2 of this PhD thesis presents an overview of unbound granular material properties and behavior. Different theories developed over the years to explain the UGL behavior in pavements are first discussed followed by commonly used material characterization models to explain resilient as well as permanent deformation behavior of aggregates. Commonly used methods for design of unsurfaced pavements and construction platforms are listed, and their primary features are highlighted. Finally, common aggregate physical properties identified by researchers as primarily responsible for governing the (shear) strength, (resilient) modulus and (permanent) deformation behavior of unbound granular layers in pavements are summarized.

The scientific approach adopted during this research study to evaluate the effects of different aggregate physical properties on behavior is outlined in Chapter 3. Development of a laboratory test matrix representing different combinations of the test factors is explained along with details on the different aggregate materials tested. The importance of using a common engineered gradation for laboratory testing of the aggregates is emphasized, and the procedure adopted for developing the engineered gradations is outlined. Finally, shape, texture and angularity characteristics of the three aggregate types tested in the laboratory are quantified through imaging based morphological indices.

Chapters 4 and 5 present findings from the laboratory testing of the selected aggregates at different combinations of the test factors. Aggregate compaction characteristics and shear

strength results are presented in Chapter 4 whereas results from repeated load triaxial testing to characterize aggregate directional modulus and permanent deformation behavior are discussed in Chapter 5. Significant effects of test factors on strength, modulus and deformation behavior are identified and are later used as guidelines in Chapter 6 for aggregate materials selected for construction and testing of full-scale unsurfaced pavement sections.

Chapter 6 covers the design and construction of full-scale unsurfaced pavement sections for accelerated pavement testing and verification of the laboratory test results. Material quality information on the aggregates used in construction is presented along with results from different laboratory tests conducted to characterize the (shear) strength, resilient modulus and permanent deformation behavior of the different aggregate types. Thickness designs of the full-scale test sections are described based on Finite Element (FE) analyses of typical unsurfaced pavement sections, and the effects of different test factors on critical pavement response parameters are analyzed. Finally, layout and cross-sectional details of the full-scale test sections are presented along with procedures for subgrade preparation, instrumentation, and aggregate placement.

Chapter 7 presents details on the use of different non-destructive modulus measurement and subsurface visualization techniques used in the current research for construction quality assurance and performance assessment of the full-scale unsurfaced pavement sections under loading. The effectiveness of these technologies for establishing links between material quality and field section performance is also discussed.

Observed performance trends of full-scale test sections under loading are presented in Chapter 8. Different mechanisms contributing towards the accumulation of rutting are analyzed using surface profile measurements, Ground Penetrating Radar (GPR) scans, as well as visual inspection of pavement layer boundaries obtained from excavation of transverse trenches across the wheel paths. Field-measured subgrade vertical stress levels are presented to justify the trends observed in test section performance under loading. Results from finite element analyses of the full-scale test sections are presented and discrepancies between the predicted and observed behavior are justified. Finally, guidelines are presented highlighting "adequate" material selection and construction practices to aid the design and construction of better performing unsurfaced pavements.

Finally, Chapter 9 summarizes important findings from this PhD research, and presents recommendations for future research activities to better assess the effects of aggregate physical properties on unsurfaced pavement performance and accordingly incorporate those effects into improved designs of unsurfaced pavements.

# CHAPTER 2

# OVERVIEW OF UNBOUND GRANULAR MATERIAL CHARACTERISTICS AND LAYER BEHAVIOR

## 2.1 Introduction

This chapter presents an overview of unbound granular material (UGM) characteristics and layer behavior as the primary structural component in unsurfaced pavement systems. A thorough understanding of different approaches commonly used to model granular layer behavior in pavements, is imperative to facilitate better design of pavement systems, and ultimately ensure adequate performance under loading. This is particularly important in unsurfaced pavement systems where heavy wheel loads are directly applied on top of the granular layers.

Different theories developed over the years to explain UGM behavior under loading are first highlighted. Commonly used models to characterize the resilient as well as permanent deformation behavior of UGMs are discussed next with a review of their primary features. Commonly used methods for the design of unsurfaced pavements and construction platforms are also summarized by listing their advantages and limitations. Different mechanisms contributing to the failure of unsurfaced pavement systems are reviewed to emphasize the importance of aggregate material quality governing unsurfaced pavement performance. Finally, common aggregate physical properties affecting granular layer strength, modulus and permanent deformation behavior are discussed in detail.

## 2.2 UGM Behavior under Repeated Loading

Unbound granular layers (UGL) in pavements are subjected to repeated load applications due to traffic. They undergo both elastic (commonly known as resilient for pavement applications) as well as plastic (permanent) deformations with the every load repetition. Figure 2.1 presents a schematic of UGM behavior under repeated loading with the help of a stress-strain diagram.

Note, that the relative magnitudes of elastic and plastic components of the total strain depend on several different factors, i.e. traffic load levels and speed of operation, thickness and quality of overlying pavement layers (if any), quality of aggregates used in construction of the UGL, and subgrade conditions.

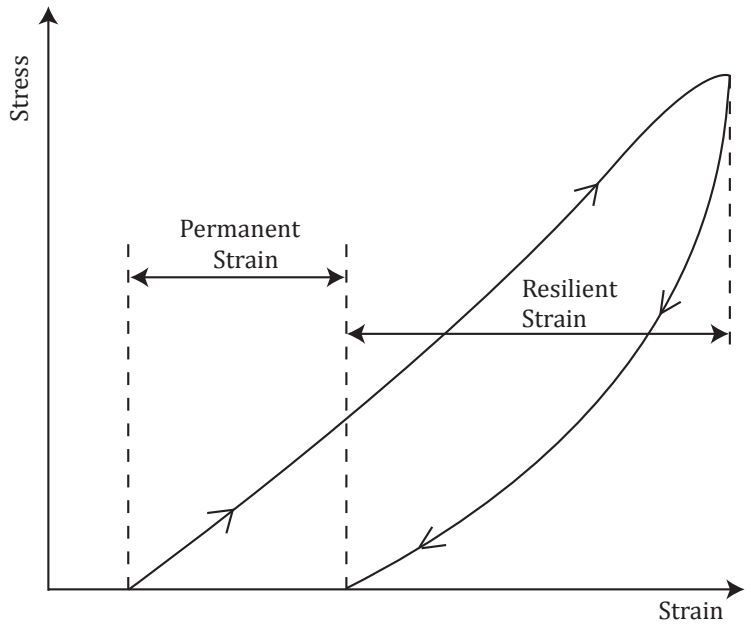


Figure 2.1: Strains in Granular Materials during One Cycle of Load Application

In a typical unbound granular layer the accumulation of permanent deformation for each load repetition gradually decreases with increased number of load applications. Once the layer has been well compacted to achieve a densely packed matrix, all the subsequent load applications should ideally result in deformations that are mostly elastic in nature. The resilient and permanent deformations of an unbound granular layer can be attributed to different mechanisms. Werkmeister [15] summarized the Hertz contact theory, and suggested that resilient deformation in UGMs is primarily because of deformation of individual grains, whereas permanent deformation takes place due to relative movement of the particles with respect to each other.

Figure 2.2 shows a schematic of typical unbound granular material behavior under application of repeated wheel loads [16]. As shown in the figure, the rate of permanent deformation accumulation in the UGM gradually decreases, and becomes negligible beyond a certain number of load applications (represented by the horizontal nature of the curve). The initial rapid

accumulation of permanent deformation typically corresponds to the rearrangement of particles during initial compaction, and subsequent loading of the pavement layers. After adequate "shakedown" of the material is reached under this initial loading phase, the pavement layers show predominantly resilient deformation provided that the load levels remain below permissible limits.

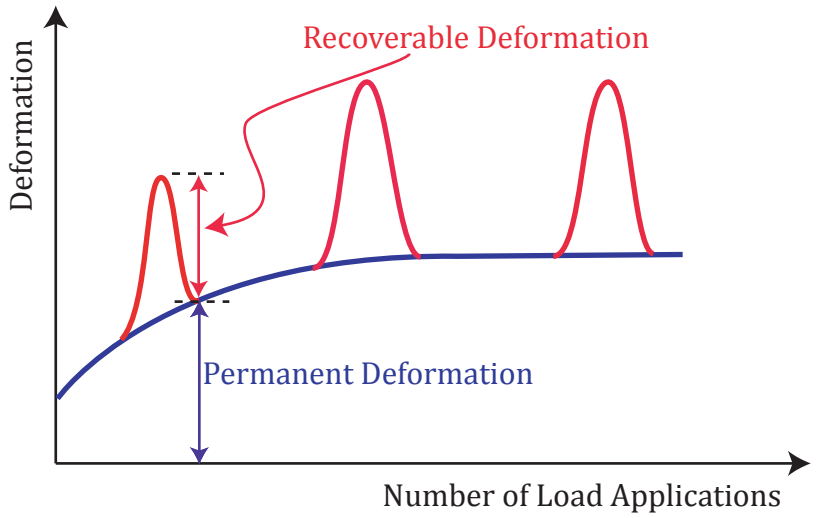


Figure 2.2: Behavior of Unbound Granular Materials under Repeated Loading [16]

## 2.3 Resilient Response of Unbound Granular Materials

Ideally, pavement layer response under traffic loading should be purely elastic, and thus no accumulation of permanent deformation should occur during its service life. Accordingly, mechanistic-based pavement design approaches have traditionally focused on the elastic or resilient response of unbound granular layers to predict the critical pavement responses under traffic loading. The most important property for incorporating repeated load behavior of UGL behavior into pavement analysis has been the "resilient modulus". Defined as a secant modulus representing hysteretic stress-strain behavior of materials, the resilient modulus ($M_R$) is a critical material input property into mechanistic-empirical (M-E) pavement design methods. Figure 2.3 shows a schematic of typical hysteretic response exhibited by unbound granular materials under repeated loading [16].

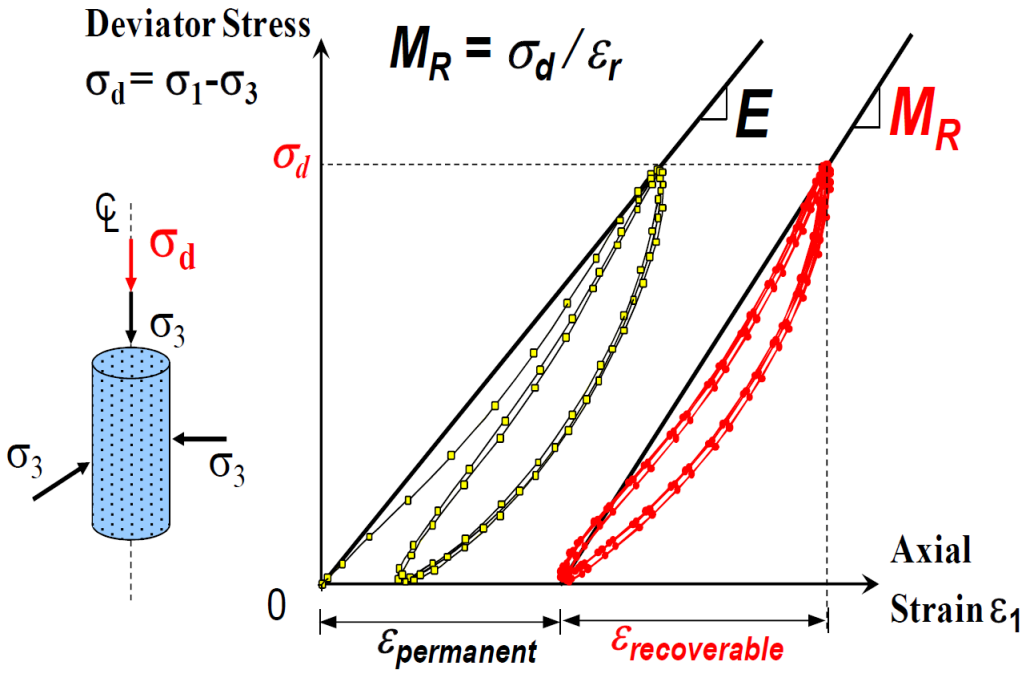


Figure 2.3: Resilient Modulus Defined as the Elastic Modulus of a Deformed Material [16]

As shown in Figure 2.3, the resilient modulus ($M_R$) of a material is defined as the elastic modulus after the material has already accumulated a certain amount of permanent deformation. The difference between elastic or Young's modulus (E) and the resilient modulus ($M_R$) of a material is clearly highlighted in the figure. Equation 2.1 can be used to determine the resilient modulus of a material from repeated load triaxial test results. Note that in the equation, $\sigma_d$ represents the deviator stress or repeated wheel load stress, and $\epsilon_r$ represents the recoverable strain.

$$M_R = \frac{\sigma_d}{\epsilon_r} \tag{2.1}$$

### 2.3.1 Characterization Models for UGM Resilient Behavior

Several material characterization models have been proposed by researchers over the years to model the resilient and permanent deformation behavior of unbound granular materials as functions of the applied stress states and material characteristics. Some of the most commonly used resilient modulus and permanent deformation models are discussed below.

K-Theta Model

Originally proposed by Hicks and Monismith 1971 [17], the K-$\theta$ model is the most commonly used model relating the resilient modulus and applied stress states for unbound granular materials. This model expresses the resilient modulus of unbound granular materials as a function of the stress states using the bulk stress or first stress invariant.

$$M_R = K\theta^n \tag{2.2}$$

where $M_R$ is the resilient modulus; $\theta$ is the bulk stress or first stress invariant ($\theta = \sigma_1 + \sigma_2 + \sigma_3$); K and n are model parameters usually determined through linear regression of laboratory experimental data. Rada and Witczak [18] reported an inverse power relationship ($logK = 4.657 - 1.807n$) between K and n, where an increase in the 'K' parameter was often accompanied by a reduction in the 'n' parameter. In their comprehensive study of granular material $M_R$ test results Rada and Witczak reported higher K values of the K-$\theta$ model for "higher quality" granular materials such as crushed stone. Although the K-$\theta$ model can adequately represent the stress-hardening behavior of coarse grained aggregates, it cannot account for the stress-softening behavior observed in fine-grained soils. Moreover, the K-$\theta$ model does not account for effects of shear stresses imposed, particularly for low stress ratios $\sigma_1/\sigma_3$ applied during initial stages of resilient modulus testing [19, 20].

Uzan Model

Uzan in 1985 [19] proposed an improvement to the K-$\theta$ model by incorporating the shear stress (deviator stress in case of repeated load triaxial testing) level into $M_R$ prediction models. Equation 2.3 shows the formulation of the resilient modulus model proposed by Uzan [19].

$$M_R = k_1\theta^{k_2}\sigma_d^{k_3} \tag{2.3}$$

where $M_R$ is the resilient modulus; $\theta$ is the bulk stress or first stress invariant ($\theta = \sigma_1 + \sigma_2 + \sigma_3$); $\sigma_d$ is the deviator stress ($\sigma_d = \sigma_1 - \sigma_3$); $k_1$, $k_2$, and $k_3$ are model parameters usually determined from multiple linear regression of laboratory experimental data. Due to its ability to handle shear stress-strain effects, the Uzan model adequately models unbound granular material behavior during analyses of layered pavement structures [21]. However, the Uzan model cannot account for

the effects of three-dimensional (3-D) stress states in an unbound granular layer.

Modified Uzan Model

Witczak and Uzan in 1988 [22] modified the Uzan model to replace the deviator stress ($\sigma_d$) term in Equation 2.3 by the octahedral shear stress term. Equation 2.4 shows the modified Uzan model (also known as the octahedral shear stress model) using normalized bulk stress and octahedral shear stress terms.

$$M_R = k_1.p_a.\left(\frac{\theta}{p_a}\right)^{k_2}.\left(\frac{\tau_{oct}}{p_a}\right)^{k_3} \tag{2.4}$$

where: $M_R$is the resilient modulus; $\theta$ is the bulk stress or first stress invariant ($\theta = \sigma_1 + \sigma_2 + \sigma_3$); $\tau_{oct}$ is the octahedral shear stress ($\tau_{oct} = \frac{1}{3}\sqrt{(\sigma_1 - \sigma_2)^2 + (\sigma_2 - \sigma_3)^2 + (\sigma_3 - \sigma_1)^2}$); $p_a$ is the atmospheric pressure (101.3 kPa, or 14.7 psi); $k_1$, $k_2$ and $k_3$ are model parameters determined through multiple linear regression of laboratory experimental data. By considering octahedral shear stress in place of the deviator stress as in the original Uzan model, the modified Uzan model can account for dilative behavior shown by unbound granular materials at extreme stress ratios ($\sigma_1/\sigma_3$) [21]. Moreover, incorporating the octahedral shear stress term ($\tau_{oct}$) into the resilient modulus formulation, this model can adequately account for 3-D stress states in a pavement layer. Kim and Tutumluer used the modified Uzan model to simulate nonlinear three dimensional behavior of unbound aggregate layers using ABAQUS$^{TM}$ [23].

MEPDG Model

The MEPDG model used in the new Mechanistic-Empirical Pavement Design Guide [24], is similar to the modified Uzan model and considers both the bulk stress and octahedral shear stress terms to account for both the stress hardening and stress-softening behavior of pavement geomaterials. Equation 2.5 gives the MEPDG model.

$$M_R = k_1 p_a \left(\frac{\theta}{p_a}\right)^{k_2} \left(\frac{\tau_{oct}}{p_a} + 1\right)^{k_3} \tag{2.5}$$

where $M_R$is the resilient modulus; $\theta$ is the bulk stress or first stress invariant ($\theta = \sigma_1 + \sigma_2 + \sigma_3$); $\tau_{oct}$ is the octahedral shear stress ($\tau_{oct} = \frac{1}{3}\sqrt{(\sigma_1 - \sigma_2)^2 + (\sigma_2 - \sigma_3)^2 + (\sigma_3 - \sigma_1)^2}$); $p_a$ is the atmospheric pressure (101.3 kPa, or 14.7 psi); and $k_1$, $k_2$ and $k_3$ are model parameters determined through multiple linear regression of experimental data. In Equation 2.5, the first

term ($\theta/p_a$) accounts for the stress-hardening behavior of pavement geomaterials (particularly coarse-grained particles), and therefore, the $k_2$ parameter typically takes non-negative values ($k_2 \geq 0$). Similarly, the second term ($\tau_{oct} + 1$) captures the stress-softening behavior of fine-grained soils (subgrade). Accordingly, the $k_3$ values are typically less than zero ($k_3 \leq 0$). Note that the '+1' term in Equation 2.5 was added to ensure that the ($\tau_{oct}/p_a$) term does not take values less than unity ($< 1$) which would ultimately lead to nonlinear convergence problems during finite element (FE) analyses of pavement systems.

Conducting regression analyses of resilient modulus test results from the Long Term Pavement Performance (LTPP) database, Yau and Von Quintus [25] reported typical values for the $k_1$, $k_2$, and $k_3$ model parameters in Equation 2.5. Analyzing results from 1920 different resilient modulus tests, they reported that the values of $k_1$, $k_2$, and $k_3$ ranged between 0 to 3, 0 to 1.5, and 0 to -7, respectively. Table 2.1 lists typical mean and median values of the above model parameters as reported by Yau and Von Quintus [25]. In Table 2.1, the median value for $k_2$ decreases as the amount of fines in the material/soil increases. Similarly, the median value for $k_3$ becomes more negative as the material/soil becomes more fine-grained. They also reported zero values for the $k_3$ parameter for approximately 25 percent of the $M_R$tests for unbound aggregate base/subbase materials and 10 percent of the tests for coarse-grained subgrade soils.

Table 2.1: Summary of the Mean and Median Values for MEPDG Model Parameters [25]

| **Model Parameter** | **Unbound Base-Subbase Materials** | | **Coarse-Grained Soils** | | **Fine-Grained Soils** | |
|---|---|---|---|---|---|---|
| | **Mean** | **Median** | **Mean** | **Median** | **Mean** | **Median** |
| $k_1$ | 0.873 | 0.853 | 0.802 | 0.764 | 0.896 | 0.804 |
| $k_2$ | 0.626 | 0.628 | 0.452 | 0.446 | 0.282 | 0.243 |
| $k_3$ | -0.170 | -0.129 | -1.140 | -1.052 | -1.576 | -1.399 |

Among the above listed resilient modulus models, the K-$\theta$ model and the MEPDG models were selected and used in this research study to conduct statistical analyses of different aggregate physical properties affecting material characterization model parameters (see Chapter 5) and thickness design of typical unsurfaced pavement structures using finite element analyses (see Chapter 6).

## 2.4 Permanent Deformation Response of Unbound Granular Materials

Permanent deformation in pavement geomaterials is represented by the non-recoverable or plastic strain accumulation under repeated loading as shown in Figure 2.1. The plastic strain accumulation in pavement layers is a result of large number of load applications on the pavement structure exposing the layers to stresses of magnitude well below their failure stress levels. For conventional pavement structures, these stress magnitudes are often only a fraction of the geomaterial shear strength. However, for unsurfaced pavements and pavement construction platforms characterized by direct application of heavy loads on the unbound granular layers, these stress levels may approach the material shear strength.

The development of plastic strains in pavement geomaterials is a result of primarily two contributing mechanisms, namely: consolidation (reduction in volume), and plastic flow (particle re-arrangement). These two mechanisms are graphically illustrated in Figure 2.4 [26]. While consolidation is the primary contributing mechanism for permanent deformation of subgrade soils, plastic flow accounts for most permanent strain accumulation in granular aggregates. Note that the rate of plastic flow in an unbound granular layer is primarily dependent on the ratio of the applied stress levels to the shear strength of the material [26, 27]. Note that shear flow in unbound granular layers can be considered to be an extreme case of the plastic flow shown in Figure 2.4(b).

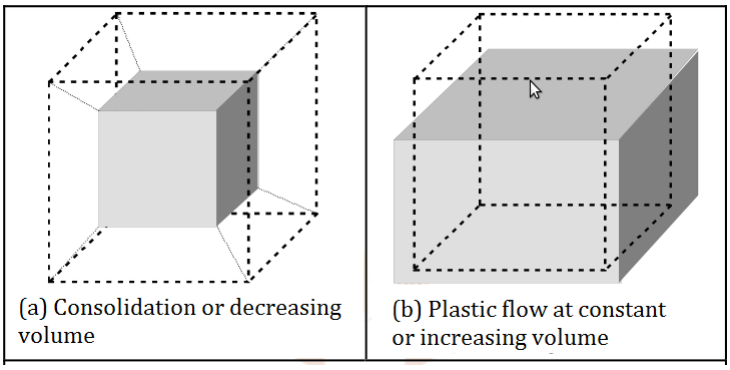


Figure 2.4: Mechanisms for Permanent Deformation Accumulation in Pavement Geomaterials [26]

Another theory used to describe UGM permanent deformation behavior is based on the "shakedown" concept. Originally developed to analyze the behavior of pressure vessels to cyclic

thermal loading, the shakedown theory has been extended by researchers to study permanent deformation accumulation in unbound granular layers [28, 29, 30, 31, 32, 33]. This theory divides the stress-strain response of materials under repeated loading into different regimes based on the magnitude of the applied stress levels with respect to certain material specific threshold values.

Werkmeister et al. [31] studied the applicability of shakedown theory to unbound granular materials through repeated load triaxial testing of crushed aggregates and grouped the behavior of unbound granular materials under repeated loading into the following three ranges: (A) Plastic Shakedown, (B) Plastic Creep, and (C) Incremental Collapse (see Figure 2.5) [15].

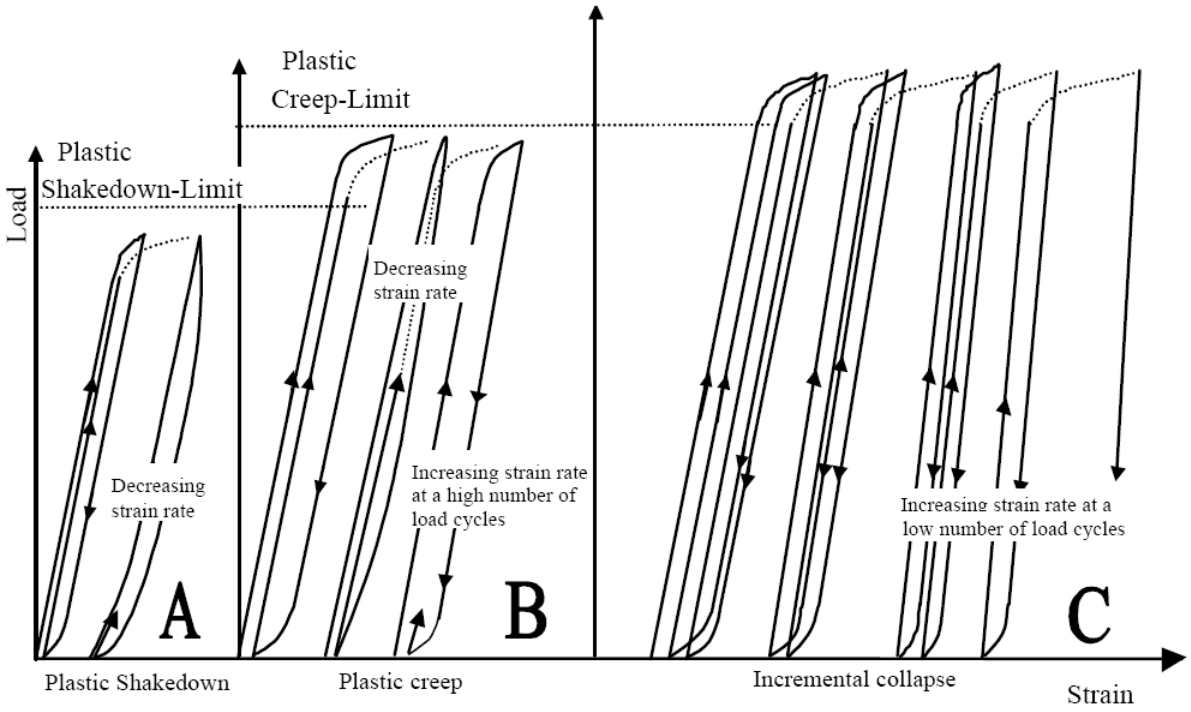


Figure 2.5: Stress-Strain Response of Unbound Granular Materials under Repeated Loading Presented using the Shakedown Concept [31]

Note that range A shown in Figure 2.5 corresponds to load levels that are significantly smaller than the material shear stress, and is represented by decreasing permanent strain rates with increase in load applications. Range C behavior results when the applied stress levels are significantly close to shear strength of the material and represents rapid shear failure of the material under low number of load applications. Range B is intermediate between A and C, and corresponds to load levels larger than the plastic shakedown limit (Range A), but smaller than the

plastic creep limit (Range C). Under these conditions, the material shows decreasing permanent strain rates up to a certain number of load cycles. However, upon further load application, the permanent strain rates start increasing once again. The material subjected to load levels corresponding to Range B fails eventually at very high number of load applications. Note that unbound granular layer behavior in conventional pavement systems typically corresponds to Range B. However, as unsurfaced pavements and construction platforms are typically subjected to low number of load applications, the UGL behavior in such structures corresponds to range A or C depending on the magnitudes of applied loads with respect to aggregate shear strength.

Theyse [32] proposed slight modifications to the shakedown theory, and presented it in the form of a set of individual permanent deformation response lines (permanent deformation vs. number of load repetitions) depending on applied stress states. Figure 2.6 shows the "extended" shakedown theory proposed by Theyse including the limits separating material response in different regimes. Note that the "zero stress loading" and "static failure" lines represent the lower and upper boundaries of shakedown theory, respectively. In-depth understanding of different mechanisms contributing to the accumulation of permanent deformation in unbound granular layers is particularly important for design and analysis of unsurfaced pavements, as the unbound granular layer is the primary structural load bearing components in these pavement systems.

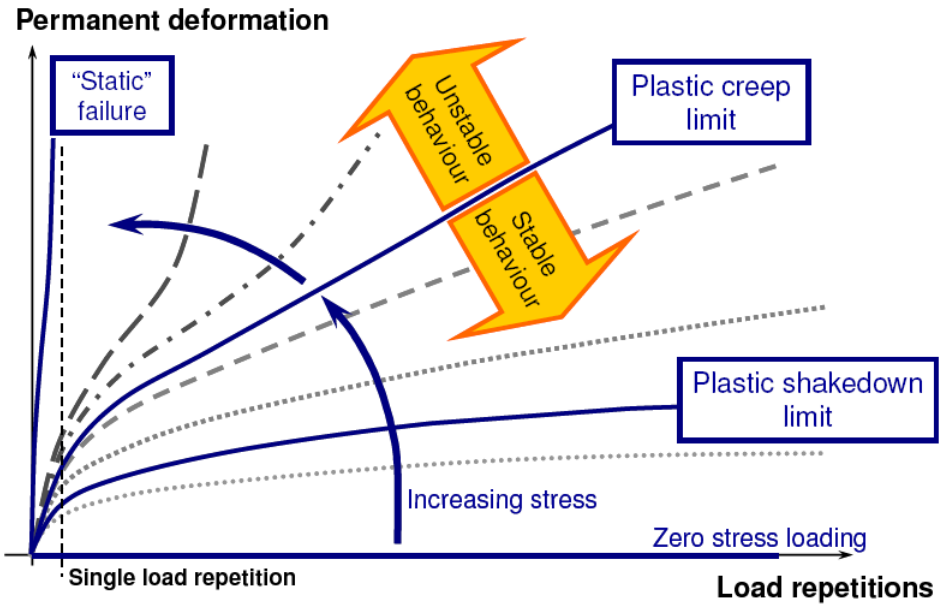


Figure 2.6: Extended Shakedown Theory Proposed by Theyse [32]

### 2.4.1 Permanent Deformation Models for Unbound Granular Materials

Several different characterization models have been proposed by past research studies for permanent deformation response of unbound granular materials. These models typically predict the permanent deformation accumulation in a material by correlating it to one or or more of several different factors such as: number of load applications, applied stress states, ratio of applied stress to aggregate shear strength, etc. Some of the most widely accepted models for predicting permanent deformation in unbound granular materials are summarized below:

#### Barksdale Model

Barksdale in 1972 [34] used standard repeated load triaxial test data to propose a linear relationship between permanent axial strain and the logarithm of number of load applications as shown below:

$$\epsilon_p = a + blog(N) \tag{2.6}$$

where $\epsilon_p$ is the axial permanent strain; N is the number of load applications; a, and b are model parameter estimates from linear regression analysis of laboratory experimental data.

#### Phenomenological Model

Monismith in 1975 [35] proposed a log-log relationship between permanent strain and the number of load applications as shown in Equation 2.7. This model also known as the phenomenological model, is used widely to present permanent deformation test results from laboratory experiments.

$$\epsilon_p = AN^b \tag{2.7}$$

where the definitions of $\epsilon_p$, N, A (or a), and b are the same as given above.

Note that researchers have proposed a value less than unity (1.0) for the regression parameter 'b' for stress conditions significantly below the shear strength of the material [30, 35]. However, a value of 'b' that is less than unity (1.0) would imply a permanent deformation accumulation rate of infinity ($\infty$) for the first load application (N = 1), and zero for large values of N. This also implies that the 'A' parameter represents an asymptote for the accumulated permanent deformation for large values of N. Note that asymptotic permanent deformation response is

typical of range A (plastic shakedown) material behavior as previously discussed. Therefore, the phenomenological model can predict material behavior accurately only for stress levels below the plastic shakedown limit. Thompson and Nauman [36] observed that the 'A' term in the phenomenological model was significantly affected by stress states ('A' values typically increased with increasing stress levels), whereas the 'b' parameter varied in the range between 0.12 and 0.20 for different granular material types.

Wolff Model

Wolff in 1992 developed the following model to predict permanent strain accumulation in aggregate base and subbase layers from Heavy Vehicle Simulator (HVS) test data [37].

$$\epsilon_p = (mN + a)\left(1 - e^{-bN}\right) \tag{2.8}$$

where $\epsilon_p$ is the axial permanent strain; N is the number of load application; and a, b, and m are model parameters. The primary feature of Wolff's model is that it accounts for the initial rapid increase in permanent deformation followed by a linear phase in which the permanent deformation increases at a steady rate. Upon differentiating the above expression to study the rate of accumulation of permanent strain, $\frac{\partial \epsilon_p}{\partial N}$, once can see that the incremental permanent deformation is equal to $a \times b$ for N = 0, and approaches 'm' as $N \to \infty$. It should be noted that in light of the shakedown concept, $m = 0$ and $m > 0$ correspond to plastic shakedown, and plastic creep response ranges respectively [26].

Van Niekerk and Huurman Model

Van Niekerk and Huurman [38] proposed the following relationship between plastic strain and the number of load repetitions for unbound granular materials

$$\epsilon_p = a_1 \left(\frac{\sigma_1}{\sigma_{1,f}}\right)^{a_2} \left(\frac{N}{1000}\right)^{b_1\left(\frac{\sigma_1}{\sigma_{1,f}}\right)^{b_2}} \tag{2.9}$$

where $\epsilon_p$ is the permanent or plastic strain; N is the number of load applications; $\sigma_1$ is the major principal stress; $\sigma_{1,f}$ is the major principal stress at failure; and $a_1, a_2, b_1, and b_2$ are model parameter estimates. Note that as the ratio of $\sigma_1$ to $\sigma_{1,f}$ is kept constant for a particular test, the

above equation is essentially the same as the phenomenological model given by $\epsilon_p = AN^b$.

Hurrman Model

Huurman in 1997 [39] combined stress level and number of load applications into one expression to predict the accumulation of permanent deformation in unbound granular materials.

$$\epsilon_p = A\left(\frac{N}{1000}\right)^B + C\left(exp\left(D.\frac{N}{1000}\right) - 1\right) \tag{2.10}$$

where the parameters A, B, C, and D account for the stress dependency of permanent strains as shown below:

$$X = x_1\left(\frac{\sigma_1}{\sigma_{1,f}}\right)^{x_2} \tag{2.11}$$

where X is a variable representing each parameter A, B, C, or D in Equation 2.10; $x_1$ and $x_2$ are variables representing related coefficients $a_1, a_2, b_1, b_2, c_1, c_2, d_1$, and $d_2$ respectively.

Among the above listed permanent deformation models, the phenomenological model (Equation 2.7) has been selected and used in this study to fit laboratory permanent deformation test results and subsequently for conducting statistical analyses of different aggregate physical properties affecting permanent deformation model parameters.

## 2.5 Design Philosophies for Unsurfaced Pavements and Construction Platforms

The general principles governing the design of unsurfaced pavements is often quite different from those used in the design of conventional flexible pavement systems. In a conventional flexible pavement, most of the stresses imposed by the wheel loads are taken up by the asphalt layer, and hence the underlying layers (base/subbase and subgrade) are not exposed to very high stress levels. Therefore, the stress-strain levels in the unbound pavement layers are often in the plastic shakedown range under normal traffic loading conditions. Such stress-strain tests have been analyzed with reasonable accuracy by adopting "elastic layer theories". However, such elastic layer theories are often not suitable for unsurfaced pavements and construction platforms. Moreover, although "surface treated" pavements do have a thin asphalt coating on top of the aggregate layer, they are primarily for drainage purposes and seldom contribute towards the load

carrying capacity of the pavement structures. The high stress levels experienced by the unbound aggregate layers in such pavements cause the unbound granular materials to undergo non-linear inelastic behavior. Several different approaches have been used for the design of unsurfaced pavements and construction platforms.

### 2.5.1 Methods based on Subgrade Strength

#### The California State Highway Department Method

Some of the most commonly used design methods for unsurfaced pavements and construction platforms are based on the subgrade strength as the primary input parameter, with the "CBR-Method" being the most widely known. Developed by the California Division of Highways in late 1930s through investigation of several in-service pavements at different conditions, this method recommends the required thickness of pavement layers to protect a subgrade of given strength [40, 41, 42]. Figure 2.7 shows the thickness design curves used by the CBR method [40, 42]. Note that the design curves were developed based on subgrade strength and wheel load only, and did not consider the number of load applications or material quality used to construct the overlying layers.

#### The Illinois Department of Transportation Method

The Illinois Department of Transportation (IDOT) uses the subgrade unsoaked CBR (also known as Immediate Bearing Value or IBV) as a primary input for recommending the thickness of pavement construction platforms. Aggregate "cover" layer thicknesses are recommended to protect the subgrade from excessive deformations under the heavy loads imposed by construction vehicles and equipment [6]. This procedure was originally developed by Thompson et al. in 1977 through finite element analyses of unsurfaced pavement sections comprising different aggregate layer thicknesses over varying subgrade conditions [43]. Up to 5,000 passes of a 142-kN (32-kip) tandem axle were considered to calculate the subgrade vertical compressive stress ($\sigma_d$) as the critical pavement response parameter. Rutting potential of the subgrade was assessed by calculating the Subgrade Stress Ratio (SSR), defined as the ratio of $\sigma_d$ and $Q_u$ (SSR = $\sigma_d/Q_u$), where $Q_u$ is the subgrade unconfined compressive strength. Aggregate cover thickness values were recommended by setting a threshold value of SSR as approximately 0.75 to limit the rutting to

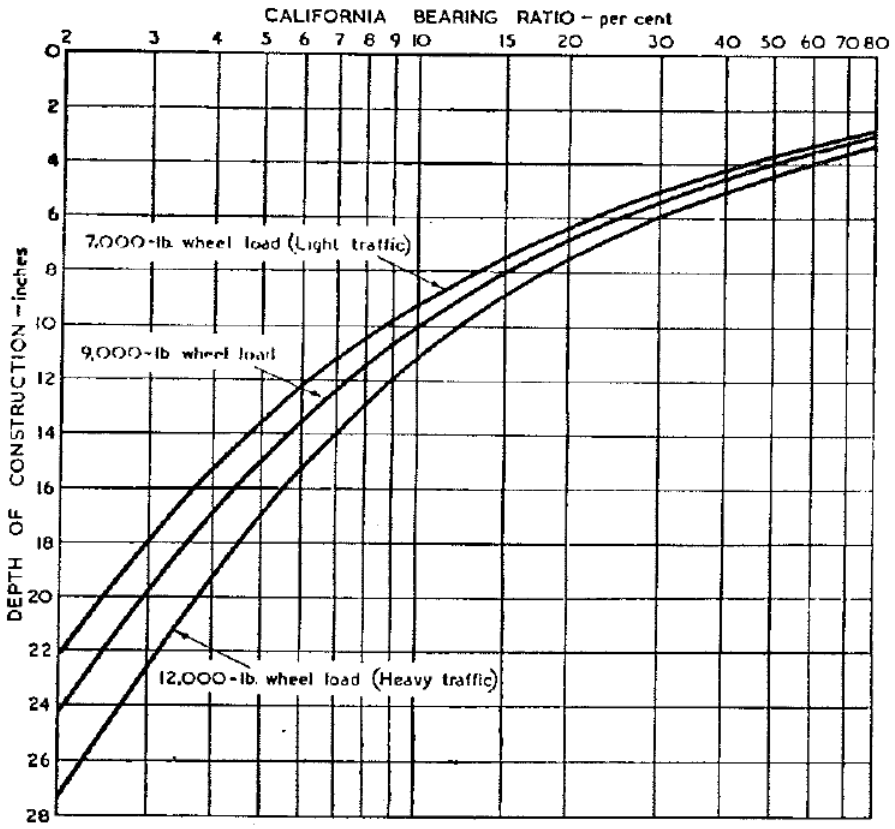


Figure 2.7: Design Curves for the CBR Method [40, 42]

below 0.5 in. [43]. Note, that although the IDOT procedure is not purely empirical like the original CBR-method, the quality of aggregates used in the "cover" layer is not considered, and the same subgrade rutting is assumed to be the only mechanism contributing to pavement failure.

The United Kingdom (UK) Approach

In the United Kingdom, the traditional approach for pavement foundations design has been through the use of established empirical relationships and a recipe specification according to which specified materials are laid and compacted using specified methods. The pavement foundation thicknesses vary from 0 mm to 600 mm (0 in. to 12 in.). However, irrespective of the thickness, the procedure assumes that all foundation layers achieve a similar minimum level of performance, and hence are treated equally [44]. This design followed the HD25/94 [45] manual, which was a recipe approach (see Figure 2.9).

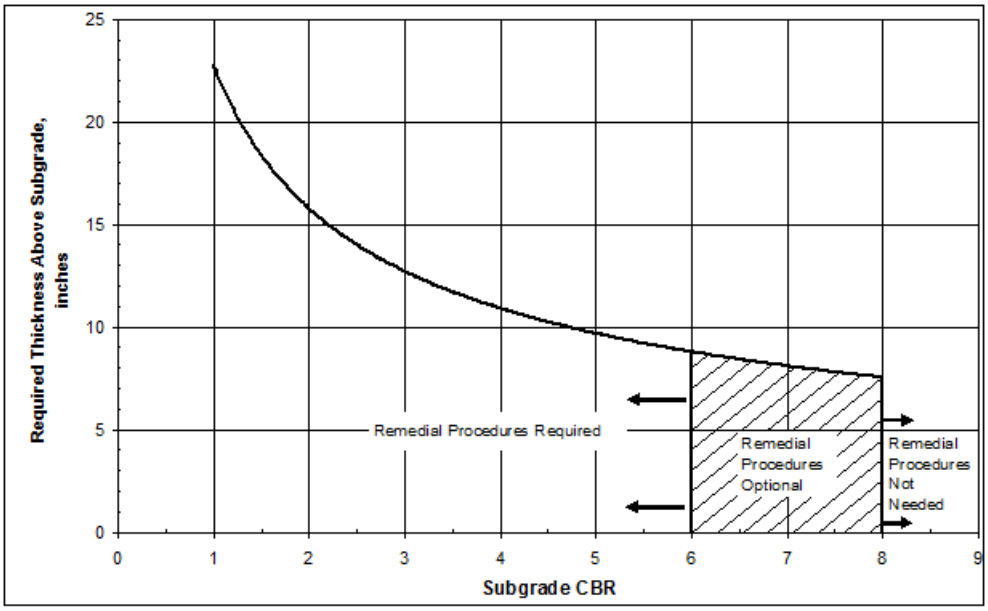


Figure 2.8: The Illinois Department of Transportation Procedure for Determining Aggregate Cover Layer Thickness based on Subgrade Unsoaked CBR (IBV) Values [6]

Although the thickness values recommended by the United Kingdom design recipe were found to perform adequately in the field, one important thing to note is that the procedure was highly empirical. The approach did not distinguish between different types of aggregate materials while recommending the thickness of the capping layer. The allowed granular capping materials could have fines (material passing the 0.075 mm sieve) anywhere in the range of 0% to 12% [46]. As the performances of granular layers are known to be dependent on the amount of fines, the "one thickness for all" approach recommended by the recipe was not likely to work for different conditions. Moreover, the design recipe could not recommend adequate thicknesses for new recycled materials and marginal aggregates.

Recent research in the United Kingdom has resulted in the adoption of a performance-based specification for pavement foundation construction [44, 47]. In a performance-based approach, the material properties are determined in the laboratory before design using representative samples both of the subgrade and of the proposed foundation material tested at anticipated environmental conditions. The same properties are again measured in-situ on the same materials during construction to confirm that the desired properties (in terms of stiffness and resistance to permanent deformation) have been achieved [44, 47]. Figure 2.10 shows the new suggested layer

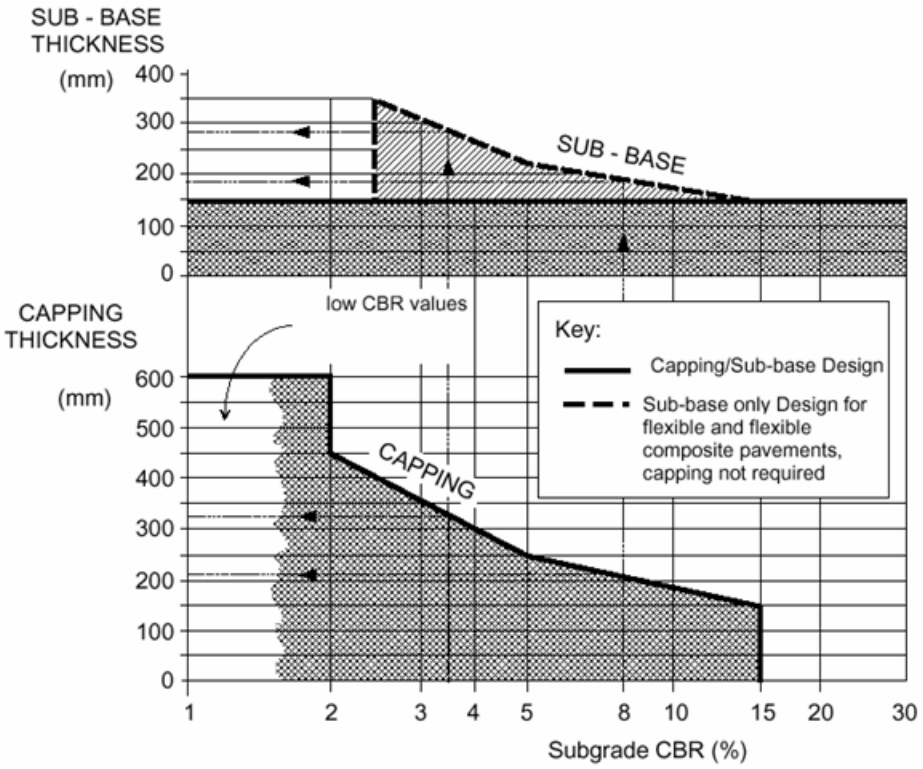


Figure 2.9: Capping and subbase thickness designs in the United Kingdom [45]

thickness design approach, which is based on the layer stiffness (measured in-situ) of the foundation/cover layer. It can clearly be seen that the required thickness of the foundation layer for a given subgrade stiffness (also indicated by CBR value) decreases as the material quality used in the foundation layer becomes better (which is indicated by a higher foundation layer stiffness). Similar curves have been developed for different ranges of foundation layer stiffness. The primary advantage of this approach lies in the consideration of the material quality used to construct the foundation layer.

The AUSTROADS Pavement Design Method

The procedure used in Australia for design of granular pavements with thin (less than 25-mm thick) bituminous surfacing is highly empirical in nature, and is derived from the original CBR-method. As shown in Figure 2.11, the Australian approach to design aggregate layer thickness also does not consider the quality of aggregate material used in construction, and recommends the design thickness values based on subgrade CBR and design traffic volume only.

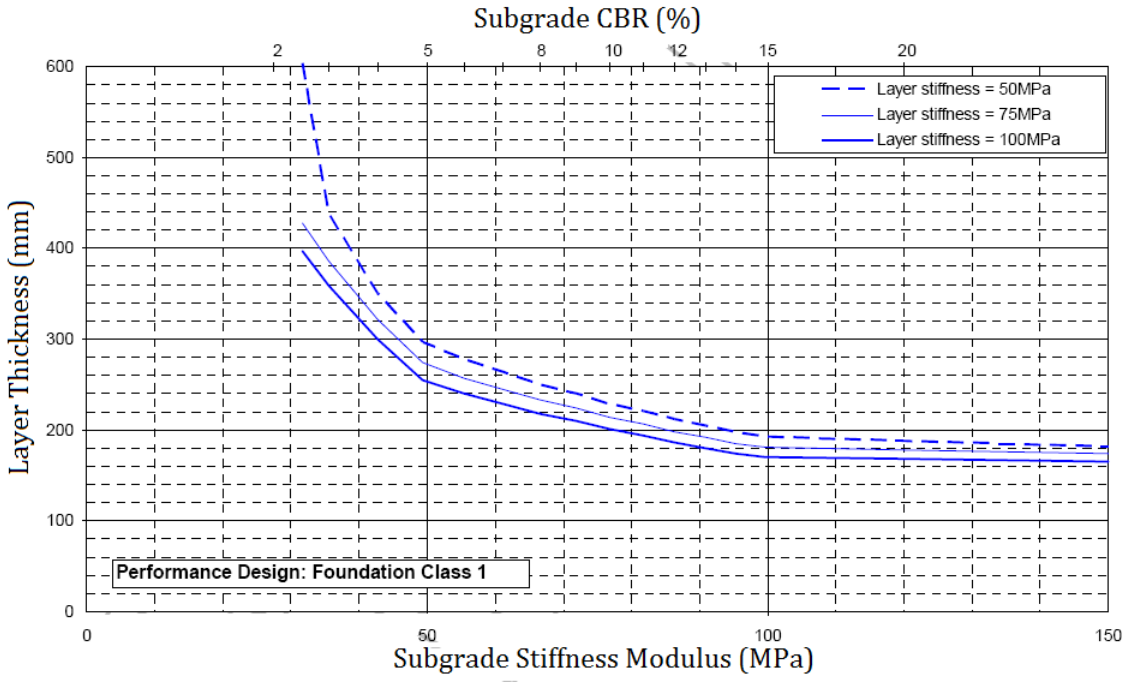


Figure 2.10: Foundation Layer Design Approach Based on Material and Construction Quality used in the United Kingdom [48]

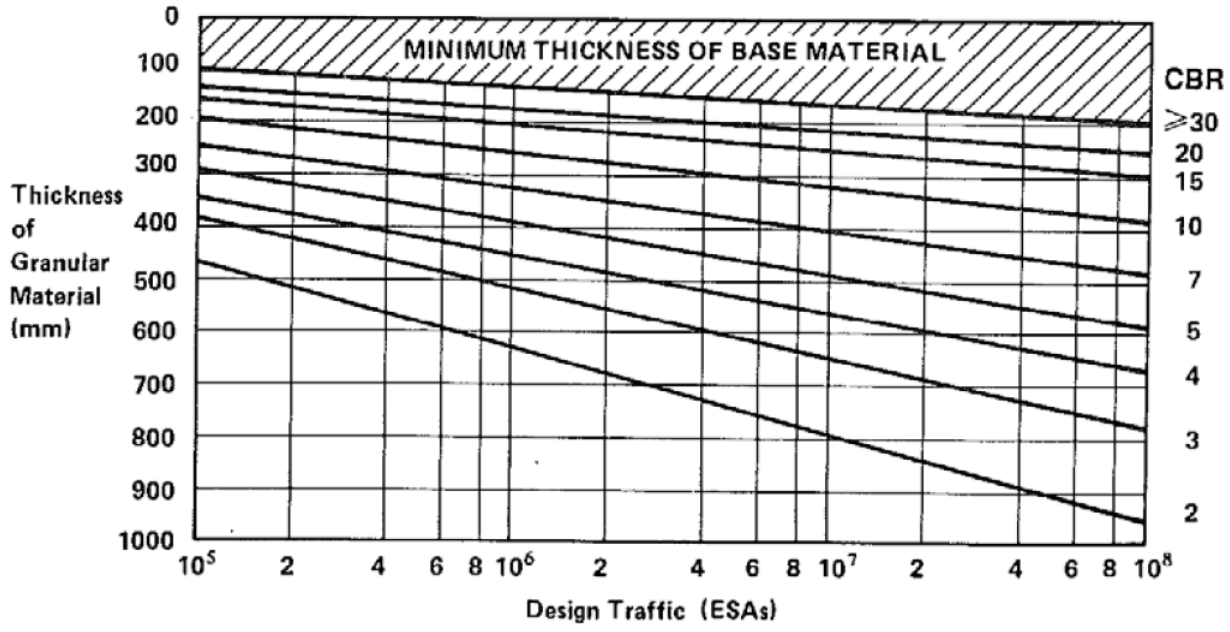


Figure 2.11: AUSTROADS Design Chart for Granular Pavements with thin Bituminous Surfacing [49]

As summarized in this section, the design procedures for unsurfaced pavements and construction platforms have traditionally been based on the principle of "protecting" the subgrade. Aggregate layer thicknesses are recommended based on subgrade strength as the primary input without giving any consideration to the quality of material used for constructing the aggregate layers.

### 2.5.2 Methods based on Bearing Capacity Theory

Due to the high stress levels applied on the unbound aggregate layers in unsurfaced pavements, the use of elastic analysis may not be justified to predict the performance of these pavements under loading. As the stress levels experienced by unsurfaced pavement layers often approach the material shear strength, design procedures based on bearing capacity theory may be more applicable for design of such pavement systems [50, 51].

Several researchers have attempted to extend the traditional bearing capacity theory to the design of unsurfaced pavements. Among the pavement design procedures adopting bearing capacity theory, some focuss on design of unreinforced unpaved roads [52, 53, 54, 55], whereas the others analyze the effects of geosynthetics on unsurfaced pavement performance [56, 57, 58]. Moreover, these design approaches can be broadly classified into the following two categories: (a) methods that consider the base layer as an elastic material designed to distribute the load to the subgrade, and (b) methods that assume a general shear type failure mechanism involving all pavement layers [50].

All the design approaches mentioned above, have several shortcomings related to the prediction of ultimate loads in layered pavements and the inability to incorporate environmental factors like pore water pressure into subgrade performance, etc. Moreover, these design approaches are based on a fixed level of traffic, and do not consider the effect of traffic levels on pavement performance. For example, the design approach proposed by Broms [54, 55] does not consider the contribution of layers above the subgrade to the shear resistance of the pavement, and assumes the shear failure to be located primarily in the subgrade. However, this assumption is not valid for cases where a thick aggregate layer consisting of "poor quality" material is placed on top of the subgrade. The unsurfaced pavement system in such cases may fail primarily due to shear movement within the

aggregate layer. Note that in spite of several different pavement design methods developed based on the bearing capacity theory, their usage in practice is not very common.

## 2.6 Modes of Rutting in Unsurfaced Pavements

As discussed in the previous section, most methods commonly used for the design of unsurfaced pavements are based on the principle of "protecting" the subgrade. These methods assume that subgrade rutting is the primary mechanism contributing to pavement failure, and do not incorporate aggregate material quality into the thickness design procedure. However, researchers in the past [59] have identified several different mechanisms contributing to the failure of unsurfaced pavement systems.

Dawson et al. [59] distinguished between four fundamental mechanisms contributing to the development of rutting in unsurfaced pavements and low volume roads. These four mechanisms, named arbitrarily as Modes 0, 1, 2, and 3 often act simultaneously to result in rut accumulation in a given pavement structure. Figure 2.12 presents the schematics of the first three modes [59]. Mode 0 is primarily caused by initial reorientation of particles achieved during compaction, and hence can be avoided through adequate compaction of the layers during construction. Mode 1 is characterized by local shear within the aggregate layer resulting in heave development adjacent to the wheel path. This mode is predominant in narrow roads where wheel wander and the resulting material "push-back" is absent. The development of Mode 1 rutting in an unsurfaced pavement system is primarily governed by aggregate quality and the relative magnitudes of the applied stresses with respect to aggregate shear strength. Mode 2 rutting primarily originates from subgrade deformation, with the aggregate layer moving with the subgrade like a "flexible mat". Traditional design methods for unsurfaced pavements based on the concept of "subgrade protection" assume Mode 2 rutting to be the only mechanism contributing to pavement failure provided that the subgrade is covered by an aggregate layer of adequate thickness. Mode 3 rutting is attributed to particle crushing and abrasion, and is more prevalent during the placement and compaction stages than due to actual traffic loads.

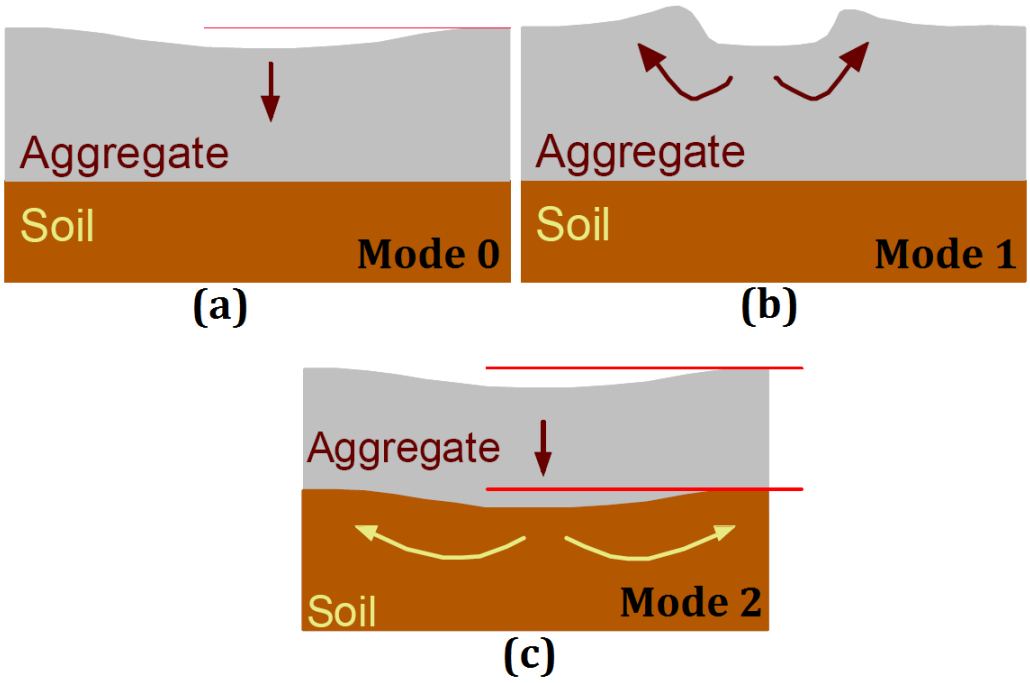


Figure 2.12: Different Rutting Modes in Low Volume Roads [59]

## 2.7 Aggregate Properties Affecting Unbound Granular Layer Behavior

As mentioned in Chapter 1, the primary objective of this research study was to evaluate the effects of aggregate physical properties on unsurfaced pavement performance. Accordingly, extensive review of technical literature was conducted to identify the most important physical properties affecting aggregate behavior in unbound as well as bound pavement layers. A summary of the findings from the literature review is presented below.

### 2.7.1 Particle Size Distribution and Fines Content

Gradation and fines content are interconnected in their effects on strength, modulus and permanent deformation characteristics. For a dense-graded crushed aggregate base material having a 25-mm (1-in.) top size, Gray's pioneering work [60] indicated that maximum strength was achieved at a fines content of about 8%. As the maximum aggregate size increased, the optimum amount of fines that gave the maximum strength typically decreased. Well-graded aggregates have been found to have higher resilient modulus values up to the point where the fines content of the mixture displaces the coarse particles and the properties of the fines

dominates [10, 61, 9]. Barksdale and Itani [62] found a dramatic 60% reduction in the resilient modulus when the fines content was increased from 0 to 10%. Kamal et al. [61] and Dawson et al. [63] found the effect of grading to be more significant than degree of compaction with the densest mix having the highest permanent deformation resistance. Increasing the amount of fines in a mix reduces the permanent deformation resistance [64, 34, 8]. Moreover, the type of fines in an aggregate layer has also been found to affect the performance significantly. The results of a recent IDOT field study, Experimental Feature IL 03-01, indicate that aggregate properties have a significant effect on their performance in subgrade applications [6].

### 2.7.2 Particle Shape and Surface Texture

Particle shape and surface texture have been found by researchers to be significant factors that affect aggregate performance in bound as well as unbound pavement layers. Increasing particle angularity and roughness increases the resilient modulus while decreasing the Poisson's ratio [17, 65, 66, 64, 62]. The reported research indicates that aggregates made with uncrushed or partially crushed particles have a lower resilient modulus than those with angular crushed particles. This effect has been attributed to the higher number of contact points in crushed aggregates which distribute loads better and create more friction between particles [9].

Allen [11] and Barksdale and Itani [62] investigated the effects of the surface characteristics of unbound aggregates and found that angular materials resisted permanent deformation better than rounded particles because of the improved particle interlock and higher angle of shear resistance between particles. Similarly, Thom and Brown in 1989 [67] observed that permanent deformation was primarily affected by visible roughness of particles. Barksdale and Itani [62] concluded that blade shaped crushed particles are slightly more susceptible to rutting than other types of crushed aggregates and that cube-shaped, rounded river gravel with smooth surfaces is more susceptible than crushed aggregates.

More recently, Rao et al. [68] studied the impact of imaging based aggregate angularity index variations on the friction angle of different aggregate types and reported an increase in aggregate performance when the percentage of crushed particles was increased. An increase in crushed materials beyond 50% significantly increased friction angle obtained from rapid shear triaxial tests indicating a higher resistance to permanent deformation accumulation. Later on, Pan et al.

[69] found that increased surface texture and particle angularity as quantified from imaging increased the resilient modulus of asphalt concrete. In another study, Tutumluer and Pan [70] reported that aggregate blends comprising angular, rough particles consistently showed lower permanent deformation accumulations represented by lower values for the A and b parameters as used in the phenomenological model (see Equation 2.7).

### 2.7.3 Degree of Compaction

Density is used in pavement construction as a quality control measure to help determine the compaction level of the constructed layers. Generally, increasing the density of a granular material makes the aggregate layer stiffer and reduces the magnitude of the resilient and permanent deformation response to both static and dynamic loads [71]. While some have found the research on density to be ambiguous in regards to the resilient behavior of soils causing little change in the resilient modulus [72, 73, 9] others have found that there is a general increase in the resilient modulus with increasing density [74, 75].

The impact of density seems to be larger on the permanent deformation behavior of aggregates. Decreased density, as measured by degree of compaction, substantially increases permanent deformation. Barksdale [34] found that decreasing the degree of compaction from 100% to 95% of maximum dry density increased permanent axial strain by 185% (on average). Increasing density from the standard to modified compactive effort maximum density decreased permanent deformation 80% for crushed limestone and 22% for gravel [11]. Moreover, van Niekerk [76] reported that increasing the degree of compaction from 97% to 103% increased the axial stresses required to cause a similar magnitude of permanent axial strain for the investigated specimens. Holubec [77] found that increased density improves properties of unbound aggregates with angular particles more than for aggregates with rounded particles, provided there is no increase in the transient pore pressure during repetitive loading.

### 2.7.4 Moisture Content

Moisture has been widely accepted to adversely affect the performance of unbound aggregate layers in pavement structures, and can affect aggregates in three different ways: (1) make them stronger with capillary suction, (2) make them weaker by reducing causing lubrication between

the soil particles, and (3) reduce the effective stress between particle contact points due to increasing pore water pressure thus decreasing the strength of the soil.

Holubec in 1969 [77] conducted repeated load triaxial tests on crushed aggregates and gravel sands over a range of moisture contents. He reported an increase in permanent deformation by 300% for crushed aggregates and 200% for gravel sands when the moisture content was increased by 2.8% and 3.6%, respectively. Thompson and Robnett [78] and Dempsey [79] found that open graded aggregates did not develop pore pressures, but uniformly graded dense aggregates with higher fines contents did develop pore pressures and resulted in a reduction in resilient modulus values. Thom and Brown [80] found that no noticeable pore water pressures developed below 85% saturation and that most of the reduction in resilient moduli was due to the lubricating effect of the water. It can also be assumed that increasing the water content in a soil reduces the capillary suction between particles thus decreasing the effective stress and the resilient moduli. Therefore, moisture can have a positive effect on unbound granular materials as long as the moisture increases the capillary suction between particles. Once the saturation reaches a point where it reduces the capillary suction, the moisture becomes a detriment to preventing residual deformation and can even cause a lubricating effect. And at even higher saturation levels where excess pore water pressure can develop and reduce the effective stress, the rutting resistance can decrease dramatically resulting in deeper ruts [80]. Maree et al. [81] conducted Heavy Vehicle Simulator (HVS) tests on pavements with untreated granular bases and reported higher permanent deformation for layers with higher moisture contents. Moreover, Maree also observed that "unstable" conditions in unbound aggregates was triggered at lower values of stress ratio (defined as the ratio of applied stress, to aggregate shear strength) when the degree of saturation was increased.

## 2.8 Summary

Findings from an extensive review of technical literature conducted under the scope of the current research study were presented in this chapter. A detailed discussion of granular material behavior under repeated loading was first presented, followed by discussion on commonly used models to predict the resilient and permanent deformation behavior under loading of unbound granular materials. A summary of different methods used for thickness design of unsurfaced pavements

and construction platforms was provided, and the primary features of each design method were discussed. From review of these methods, the need to study the effect of aggregate quality on unsurfaced pavement performance was established. Finally, important aggregate physical properties identified by researchers as governing the behavior of unbound granular layers were listed. Findings from the review of technical literature will be used in Chapter 3 to establish the research framework and identify different research tasks targeted towards accomplishing the ultimate objective of this research.

# CHAPTER 3

# RESEARCH FRAMEWORK, & MATERIALS USED

## 3.1 Introduction

This chapter outlines the scientific approach adopted during the current study to evaluate individual effects of selected aggregate physical properties on behavior. Research framework established to accomplish the ultimate research objective is described in details, followed by selection of important aggregate physical properties (test factors) for laboratory experimentation and field evaluation. Development of a laboratory test matrix is explained, and the importance of using a common engineered gradation for laboratory testing is emphasized. Test methods commonly used to evaluate the mechanical behavior of aggregates in the laboratory are discussed along with relevant information about the test equipment used. Finally, this chapter also presents details on the different aggregate types tested during this research along with results from preliminary material characterization tests conducted in the laboratory.

## 3.2 Research Framework

A research framework was developed to investigate the effects of different aggregate physical properties on unsurfaced pavement performance. To this end, the research scope comprised laboratory testing of aggregates as well as accelerated testing of full-scale unsurfaced pavement sections. Laboratory tests, commonly used to assess unbound granular material behavior were conducted to evaluate the effects of different aggregate physical characteristics governing material quality. Next, full-scale unsurfaced pavement test sections were constructed for verification of the laboratory test results through accelerated pavement testing.

### 3.2.1 Selection of Important Aggregate Physical Properties

Based on extensive review of technical literature (outlined in Chapter 2) the following aggregate physical properties (test factors) were selected for evaluating their effects on aggregate behavior: particle shape, texture and angularity, fines content (material finer than 0.075 mm), plasticity of fines (measured on material finer than 0.425 mm), and compaction (moisture-density) conditions. A controlled particle-size distribution was used to ensure that observed changes in aggregate behaviors could be attributed to the effects of varied aggregate properties (e.g. fines percentage, plasticity of fines, etc.).

## 3.3 Development of Laboratory Test Matrix

First phase of the research scope involved laboratory testing to evaluate individual effects of the test factors on aggregate behavior. The laboratory test results would subsequently be used to identify the minimum variations required in the test factors to affect aggregate behavior significantly. Three different aggregate types commonly used in the state of Illinois for pavement applications were selected for laboratory testing as well as constructing full-scale pavement sections for accelerated testing. The material selection was aimed to adequately encompass extreme aggregate physical property combinations allowed by current and future possible transportation agency specifications while simultaneously considering the time requirements and expenses associated with an extensive laboratory and field testing program.

An experimental test matrix was developed for laboratory assessment of aggregate behavior at different combinations of the aggregate physical properties (test factors). Two different crushed stones (limestone and dolomite) were selected along with one uncrushed "river-run" gravel for laboratory characterization and accelerated testing of full-scale unsurfaced pavement sections. The primary objective was to establish ranges for the test factors that primarily influence strength, modulus and deformation behavior of aggregates, and thus govern the behavior of aggregate layers in a pavement system. The following variations were induced in the test factors to represent different UGM types commonly used in pavement layer construction.

**Particle Shape, Texture and Angularity:** Effect of particle shape, texture and angularity on UGM behavior were studied through comparison of (shear) strength, (resilient) modulus,

and (permanent) deformation characteristics of crushed vs. uncrushed aggregate materials.

**Fines Content:** To study effects of fines on aggregate behavior, laboratory specimens were prepared and tested at four different fines contents, 4%, 8%, 12%, and 16% material by weight passing No. 200 sieve (material finer than 0.075 mm). These values were selected to encompass entire ranges of fines contents that may be allowed by state transportation agencies.

**Type of Fines:** To distinguish between different types of fines, the plasticity index was taken as the indicative parameter, as determined by measuring the Atterberg limits of material passing the No. 40 sieve size (material finer than 0.425 mm). Two different fines types, nonplastic and plastic (with a PI in the range of 10% to 12% obtained by adding clay to nonplastic fines) were used to evaluate the effect of plasticity of fines on aggregate behavior.

**Compaction Conditions:** The effects of compaction conditions on aggregate behavior were studied in the laboratory by testing specimens at three different moisture contents: 90% $W_{opt}$, $W_{opt}$, and 110% $W_{opt}$, where $W_{opt}$is the optimum moisture content (OMC) determined using the standard compaction (ASTM D 698) method [13]. Similarly, the effect of moisture condition on the field performance of unsurfaced pavement sections was evaluated through accelerated pavement testing of the full-scale test sections at near-optimum and flooded aggregate layer moisture conditions.

Varying the test factors within the above specified ranges resulted in a $4 \times 2 \times 3$ factorial laboratory test matrix (4 different fines contents, 2 different types of fines, 3 different moisture contents) for each of the three selected aggregate types.

## 3.4 Preliminary Laboratory Testing of Aggregates

Preliminary laboratory tests were first conducted on the three selected aggregate materials to characterize the original particle size distribution, Atterberg limits, as well as particle shape, texture and angularity parameters. Four samples for each aggregate type were collected from different locations on the stockpiles, and processed through washed sieving to determine the particle size distributions (see Figure 3.1). Note that the crushed limestone and dolomite materials contained significantly higher amounts of fines (material finer than 0.075 mm)

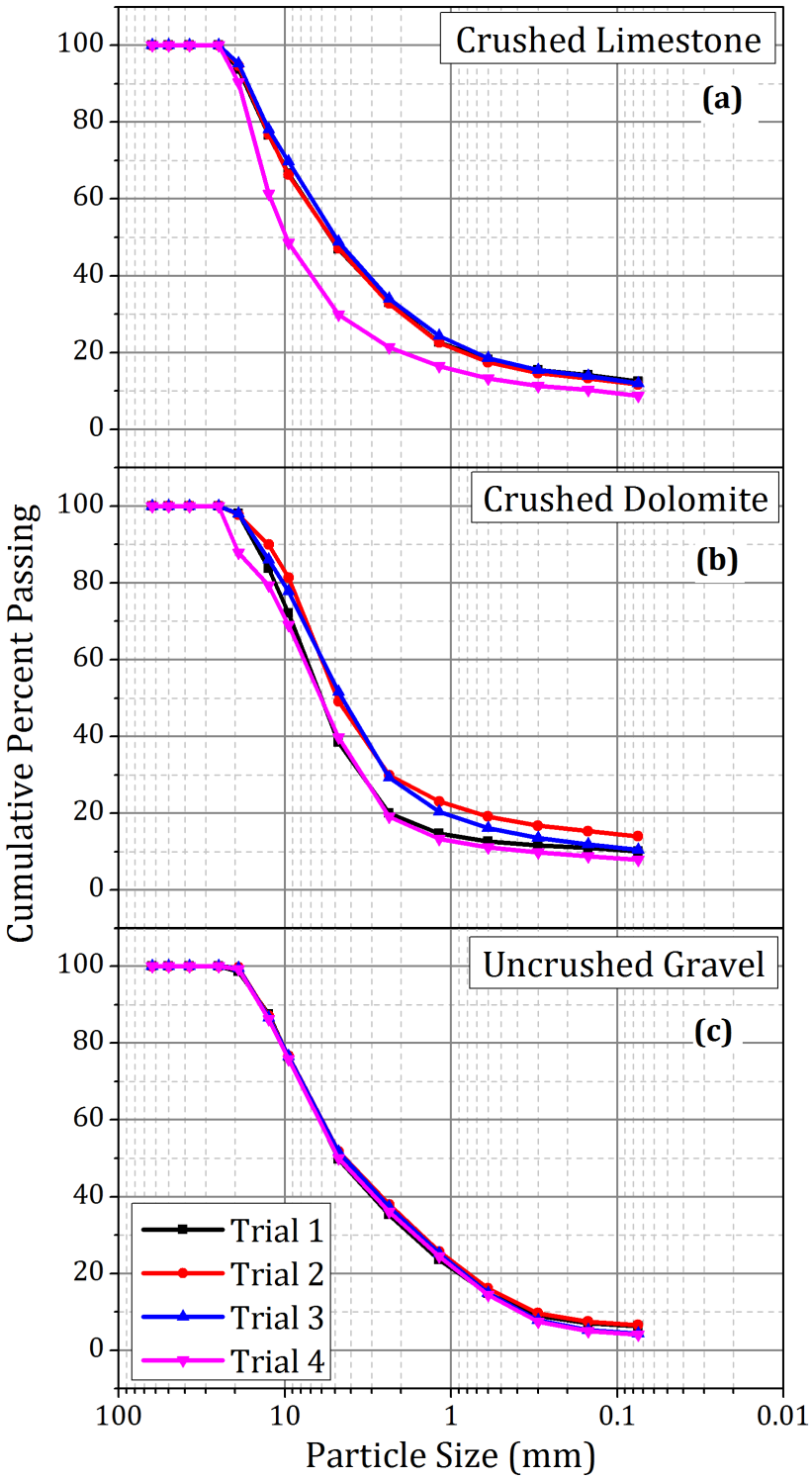


Figure 3.1: Original Gradations of (a) Crushed Limestone, (b) Crushed Dolomite, and (c) Uncrushed Gravel Materials Selected in this Research

compared to the uncrushed gravel. Moreover, gradation curves for these two materials showed significant variations across the four samples tested, whereas the gravel samples showed identical gradations. As particle size distribution or packing order is critical to governing the load distribution pattern in an aggregate matrix, hence affecting behavior under loading, differences in aggregate gradations can lead to significantly different unbound granular layer performance for the same aggregate type. It was therefore decided to use gradation as a control parameter during this research study. The methodology adopted to prepare laboratory specimens at a controlled gradation, is described in Section 3.5.1. Material passing sieve No. 40 (finer than 0.425 mm) for the three aggregate types were tested in the laboratory for Atterberg Limit determination, and were nonplastic in nature (Plasticity Index or PI = 0%).

### 3.4.1 Imaging Based Quantification of Aggregate Morphological Indices

Particle shape, texture and angularity characteristics of the three aggregate types were quantified in the laboratory using a validated image analysis system, the University of Illinois Aggregate Image Analyzer (UIAIA). The UIAIA was identified by the NCHRP project 4-30A as one of the most promising aggregate imaging systems providing automated means to determine coarse aggregate size and shape properties [82, 83]. The UIAIA system (see Figure 3.2) can take images of an individual aggregate particle from three orthogonal views, to reconstruct the three-dimensional (3-D) particle and compute its volume as well as size and shape indices. The UIAIA based image indicial data for coarse aggregates fall into two categories: (i) particle size and volume (including maximum, intermediate and minimum dimensions) [82, 83]; and (ii) particle morphological or shape indices (including Flat and Elongated (F&E) Ratio [84], Angularity Index (AI) [68], and Surface Texture (ST) Index [85]). These two categories of imaging based aggregate shape indices have been validated in the past by successfully linking them to laboratory strength data and field rutting performances of many different types of aggregates [68, 86].

Approximately 250 aggregate particles were selected from each aggregate type and scanned using the UIAIA through three replicate tests. For selecting the particles from each aggregate type, care was taken not to select very small particles as the UIAIA results tend to be more accurate for intermediate to larger size aggregates [83]. For the current study, particles corresponding to material retained on sieves No. 4 and No. 8 (4.75-mm and 2.36-mm opening

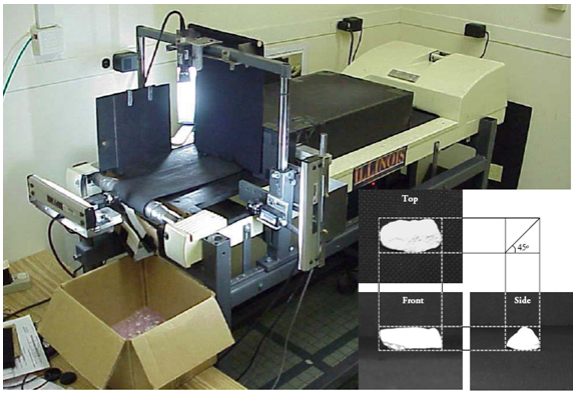


Figure 3.2: The University of Illinois Aggregate Image Analyzer (UIAIA) System

size, respectively) up to 1-in. size were scanned to determine the shape and surface texture indices using automated algorithms [68, 85].

Results and Discussion

Figure 3.3 shows the ST index values graphed with particle number, for the three aggregate types. ST indices for crushed limestone and dolomite were typically greater than those for the uncrushed gravel. Similarly, Figure 3.4 presents the AI values graphed for the three aggregate types and clearly shows higher percentage of crushed limestone and dolomite particles representing higher AI ranges as compared to the uncrushed gravel.

Table 3.1 lists the average particle shape, texture and angularity indices for the three aggregate types studied in this research study. It should be noted that higher AI and ST values indicate more angular and rougher surface textured aggregates, respectively. The uncrushed gravel particles were closer to spherical shapes with the lowest F&E ratios by weight among the three aggregate types. Table 3.1 also lists typical AI and ST index values identified for crushed limestone and uncrushed gravel particles from imaging of 39 different coarse aggregate materials during a recent study [87]. Note that the shape indices for the three aggregates investigated in this research study appropriately fall within the typical ranges shown in Table 3.1.

Different shape and surface texture indices correspond to differences in shear resistance and load spreading abilities of an unbound granular layer, and can be directly linked to aggregate behavior for identifying contributions of crushed and uncrushed particles. This link can be used

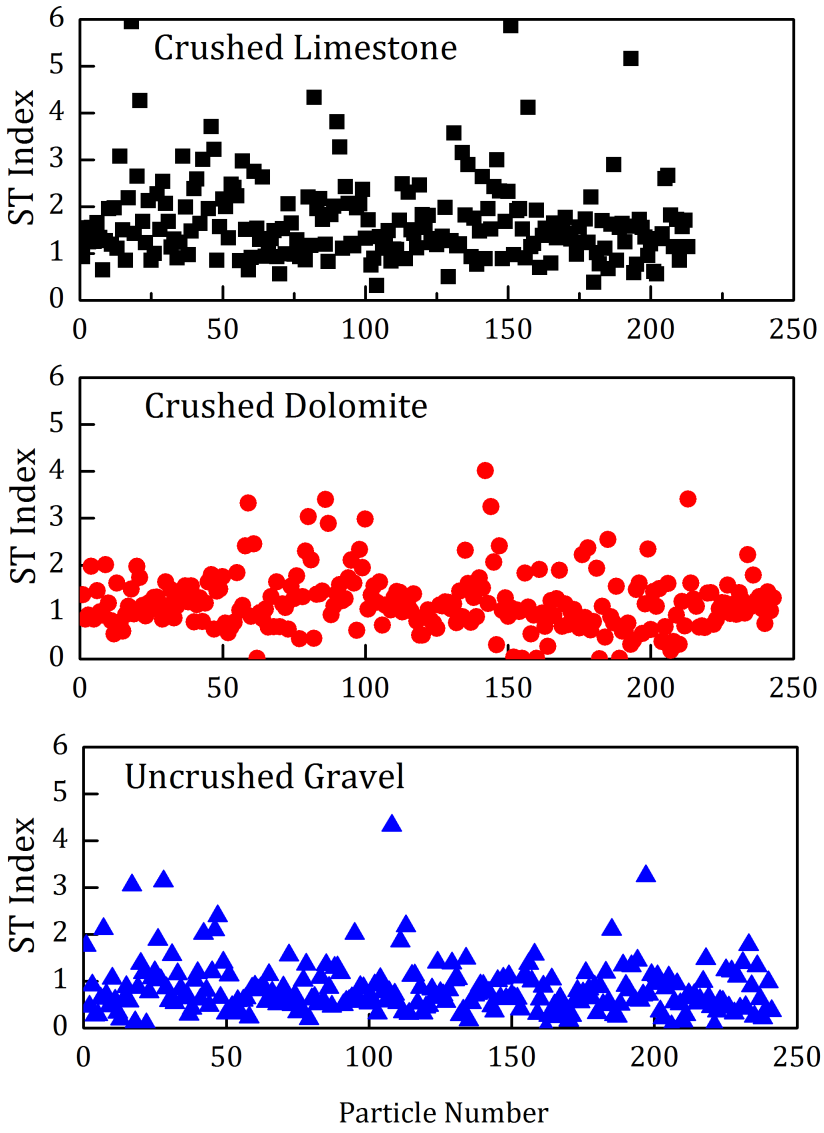


Figure 3.3: Summary of Surface Texture Distribution for the Three Aggregate Types

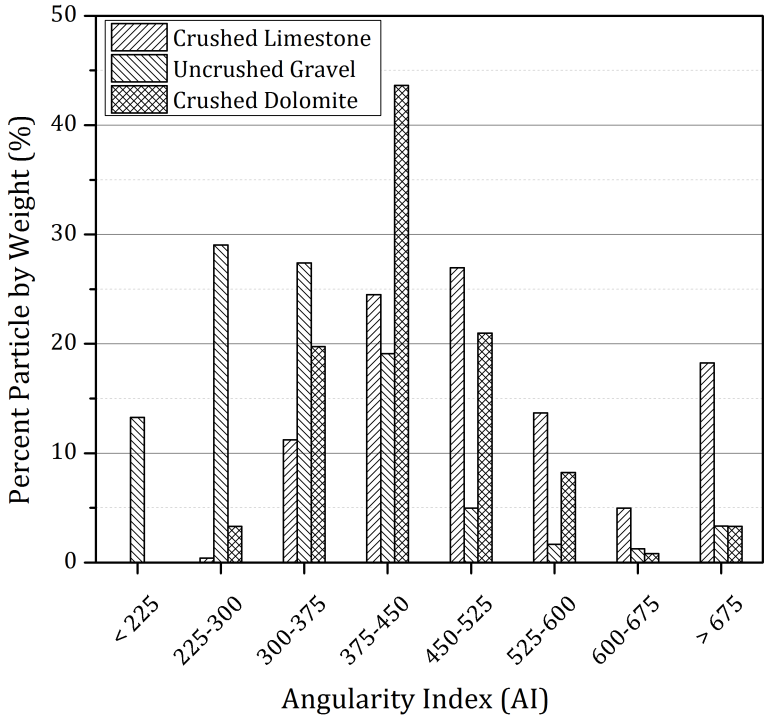


Figure 3.4: Summary of Angularity Indices for the Three Aggregate Types

Table 3.1: Average Aggregate Shape and Surface Texture Indices

| | **Angularity Index (AI)** | | **Surface Texture Index (ST)** | | **Flat & Elongated Ratio (by Weight)** |
|---|---|---|---|---|---|
| | Measured Value | Typical Range[1] | Measured Value | Typical Range[1] | Measured Value |
| Crushed Limestone | 481 | 400-550 | 1.8 | 1.2-1.8 | 2.5 |
| Crushed Dolomite | 428 | N/A[2] | 1.3 | N/A[2] | 3.3 |
| Uncrushed Gravel | 330 | 250-350 | 1.0 | 0.5-1.2 | 1.9 |

[1] Typical values identified from 39 different coarse aggregate materials in a pool fund study [87]
[2] N/A = data not available

as a guideline to select aggregate materials for unsurfaced pavement applications. These indices will later be used to justify trends observed during shear strength (Chapter 4), and repeated load triaxial testing (Chapter 5) of the aggregates.

## 3.5 Laboratory Assessment of Aggregate Behavior

This section describes the development of a controlled particle-size distribution or engineered gradation for all the aggregate materials studied. This is followed by details on different mechanical tests performed to characterize the shear strength, permanent deformation, and resilient modulus characteristics of aggregates at different combinations of the test factors.

### 3.5.1 Common Engineered Gradation for Factorial Study

Before conducting a parametric study of aggregate physical properties affecting behavior, it was important to control the particle-size distributions consistently across different materials tested. A controlled particle-size distribution would help to attribute the observed change in behavior to the effect of the varied aggregate property (e.g., fines percentage, plasticity of fines) only. A typical dense graded aggregate specification (Coarse Aggregate Gradation No. 6 or CA-6) used by the Illinois Department of Transportation (IDOT) served as the reference for developing target gradations for laboratory testing. The primary objective was to have a constant gradation for all test specimens, with only the fines content changed to the four pre-determined target values (4%, 8%, 12%, and 16%). Gradation boundaries for the IDOT CA-6 corresponding to individual sieve sizes were considered for developing the engineered gradations. Figure 3.5 shows the engineered aggregate gradation curves developed for the different target fines contents.

To prepare specimens according to the engineered gradations for laboratory testing, sieving and size separation of the aggregates were first undertaken. Approximately 3.6 tonnes (8,000 lb) of each aggregate material were processed through sieving for amounts retained on individual sieve sizes and collecting them into different barrels. After sorting individual aggregate sizes into separate barrels, the next step was to blend the aggregates as per the engineered gradations shown in Figure 3.5.

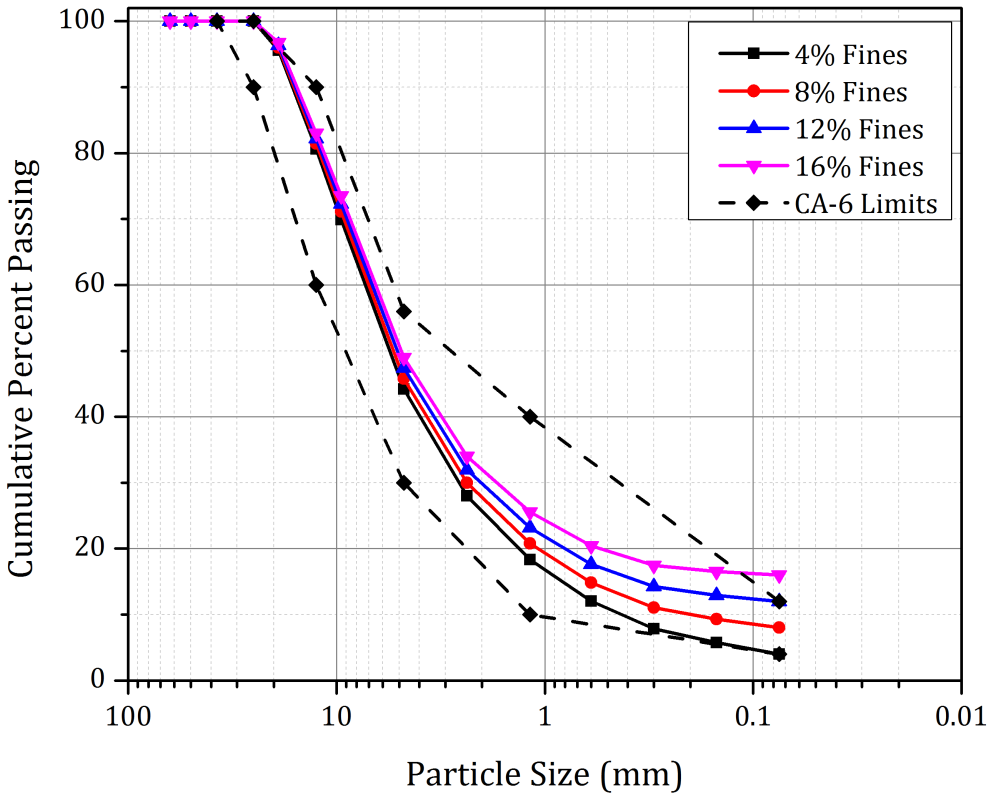


Figure 3.5: Engineered Gradations for Different Target Percent Fines (Passing No. 200 sieve)

Sample Blending and Effect of Fines Sticking to Coarse Particles

Washed sieving of blended aggregate samples was conducted to compare the target and achieved gradations. Washed sieving results showed that the achieved fines contents of blended samples were consistently higher than the target fines contents based on dry blending. This difference was attributed to the significant amount of fines that remained on the surfaces of larger particles during dry sieving and contributed toward the total fines content determined by washed sieve analysis. These fines could considerably influence aggregate behavior and therefore had to be accounted for in preparing laboratory test specimens. Several replicates of washed gradations were conducted on blended samples to quantify the difference between target and achieved fines contents. Table 3.2 summarizes the average differences observed between target and achieved fines contents determined in the blended samples for the three aggregate types.

Table 3.2: Target and Achieved Fines Contents

| **Target Fines Content** (%) **(based on dry sieving)** | **Achieved Fines Content** (%) **(based on wet sieving)** | | |
|---|---|---|---|
| | **Limestone** | **Uncrushed Gravel** | **Dolomite** |
| 0 | 4.4 | 2.9 | 0.7 |
| 4 | 8.1 | 6.8 | 4.7 |
| 8 | 11.8 | 10.6 | 8.7 |
| 12 | 15.5 | 14.5 | 12.6 |
| 16 | 19.2 | 18.3 | 16.6 |

Note that even a sample blended targeting 0% fines (no material passing No. 200 sieve) contained 4.4% fines in the case of limestone, and 2.9% fines for uncrushed gravel. However, the dolomite sample (received as washed material from the quarry) contained less than 1% fines. The limestone and uncrushed gravel stockpiles were received directly from the quarry and hence had a significant amount of fines sticking to larger particles. For both limestone and gravel, the achieved fines were consistently about 2.5% to 4% higher than the target fines. Therefore, it was decided to blend these samples by targeting 0%, 4%, 8%, and 12% fines, to ensure achieved fine contents of the order of 4%, 8%, 12%, and 16%, respectively. Dolomite samples, with negligible amount of fines sticking to larger particles were blended by targeting 4%, 8%, 12%, and 16% actual fines. Figure 3.6 shows the modified engineered gradations (0% target fines curve is added).

Blending of Fines to Achieve Target Plasticity

One of the test factors for this study was the type of fines, characterized by PI values measured on material passing sieve No. 40 (finer than 0.425-mm opening size). Test specimens were prepared at different gradations using nonplastic (PI = 0%) as well as plastic (PI $\sim$ 8-10%) fines to evaluate the effects of fines plasticity on UGM behavior. As already mentioned, the fines portion obtained from size separation of the three aggregate types were nonplastic in nature, and hence were used to blend test specimens with nonplastic fines. Nonplastic fines obtained from aggregate sieving were proportionally blended with a clay soil referred to as “refractory clay”, to engineer a blend PI in range of 8-10% for preparing specimens with plastic fines.

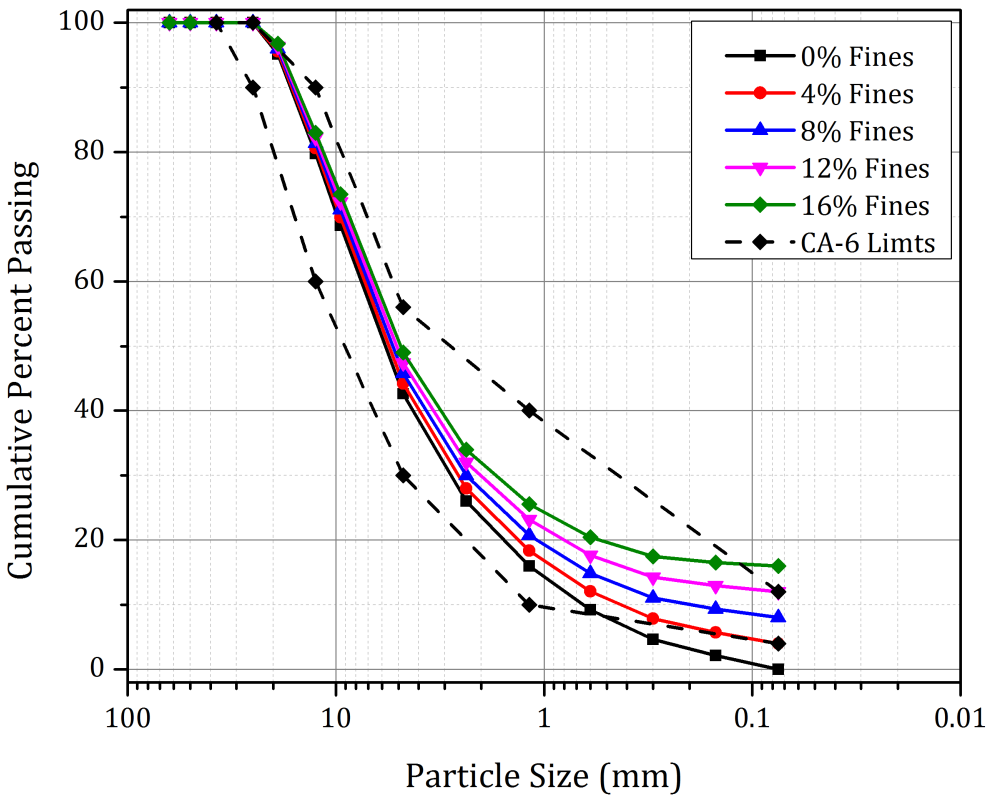


Figure 3.6: Final Engineered Gradations with 0% Target Fines Curve Added

### 3.5.2 Moisture-Density and Unsoaked CBR Tests

Compaction characteristics were established for the three aggregate types at different combinations of the test factors using the standard effort (ASTM D 698, Method C) [13]. A minimum of four points were used for each material combination to establish the optimum moisture content (OMC or $W_{opt}$) and maximum dry density (MDD) values. After compaction, each sample was penetrated by a circular plunger of 19.4 $cm^2$ (3 $in.^2$) area at a rate of 1.27 mm/min. (0.05 in./min.) to determine the unsoaked CBR (AASHTO T 193) values as the expedited shear strength properties from compaction specimens. Important trends observed from the moisture-density and CBR testing of the aggregates are presented in Chapter 4. OMC and MDD values established for each material combination were later used to prepare specimens for triaxial testing.

### 3.5.3 Monotonic Triaxial Tests for Shear Strength Characterization

The effects of individual test factors on aggregate shear strength were evaluated through a test procedure referred to here, as the University of Illinois Rapid Shear Strength Test. Cylindrical specimens, 305-mm (12-in.) high and 152 mm (6 in.) in diameter, were tested under strain controlled monotonic loading conditions to determine the shear strength properties of different aggregate material combinations. Compared to conventional triaxial shear tests, the rapid shear test punches the loading ram into the specimen at a much higher loading rate of 38 mm (1.5 in.) per second, subjecting the specimen to 12.5% strain in one second. This deformation rate corresponds to a 5% failure strain in a 305-mm (12-in.) high sample, in around 400 msec. Because of the high loading rate, the rapid shear strength test produces slightly higher peak stress values compared to conventional shear strength tests. However, it is believed to better simulate any possible failure condition of an in-service pavement layer under the dynamic application of a moving wheel load [12, 88]. Moreover, the recent NCHRP Project 4-23 has listed the University of Illinois Rapid Shear Test as a fairly simple and precise test method for accurate quantification of aggregate shear strength [89].

#### Test Equipment Description

The test setup used for conducting the rapid shear strength tests consists of a Material Testing System (MTS) closed-loop servo hydraulic system. The main part of the system includes a controller (MTS Model-407), a loading frame, and a hydraulic power supply. The system is fitted with a 44.5-kN (10-kip) hydraulic actuator. The loading ram of the actuator is fitted with an internal Linear Variable Differential Transducer (LVDT) for displacement-controlled applications. The MTS-407 controller provides the electronics for closed-loop controls and system operations. The applied force is measured with an external load cell of 44.5-kN (10-kip) capacity placed directly over the specimen. Force and displacement data during the test were recorded using a data acquisition interface written in LabView$^{TM}$. Figure 3.7 shows a picture of the test setup.

Three different specimens were tested at confining pressures of 34.5, 69.0, and 103.5 kPa (5, 10, and 15 psi respectively) to determine the cohesion ($c$) and friction angle ($\phi$) values as shear strength properties of each aggregate material combination. This resulted in a total of 216 aggregate specimens (3 aggregate types $\times$ 4 fines contents $\times$ 2 fines of fines $\times$ 3 moisture

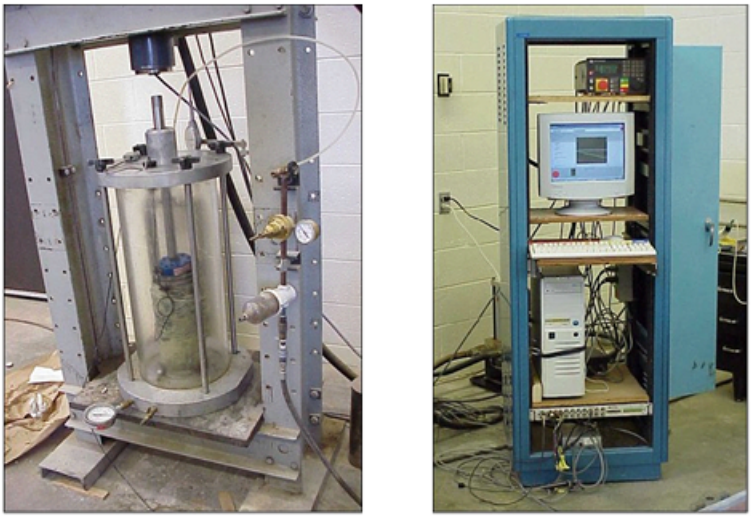

Figure 3.7: MTS 407 Servo-Hydraulic System Used for Rapid Shear Testing of Aggregate Specimens

conditions × 3 confining pressures) compacted and tested for shear strength characterization. Important test results from the shear strength tests are presented in Chapter 4.

### 3.5.4 Repeated Load Triaxial Tests for Permanent Deformation and Directional Modulus Characterization

To evaluate the effects of individual aggregate physical properties on resilient modulus ($M_R$) and permanent deformation behavior, the three aggregate types were tested in the laboratory at different test factor combinations. Cylindrical test specimens (152 mm or 6 in. in diameter and 152 mm or 6 in. in height) were prepared and tested under repeated loading, using an advanced triaxial testing equipment, referred to as the University of Illinois FastCell (UI-FastCell), capable of switching and pulsing the major principal stresses both in the axial and radial directions by the use of two independently controlled pneumatic actuators.

The samples were first tested for permanent deformation behavior during the conditioning phase of the AASHTO T 307 resilient modulus test procedure by applying 1,000 repetitions of a maximum axial deviator stress of 103 kPa (15 psi) using a haversine-shaped load pulse (pulse duration of 0.1 seconds and rest period of 0.9 seconds), at a confining pressure of 103 kPa (15 psi). Directional modulus tests were subsequently performed on the same specimens through pulsed load application in the axial (direction 1), followed by radial (direction 3) directions. The

stress states specified in the AASHTO T 307-99 procedure [90] were used for calculating the vertical (from axial pulsing) and horizontal (from radial pulsing) $M_R$values. Accordingly, the pulsed deviator stresses ($\sigma_{nd}$) ranged from approximately 21 to 276 kPa (3 to 40 psi) in both axial and radial directions whereas the hydrostatic pressures ($\sigma_S$) ranged from about 21 to 138 kPa (3 to 20 psi). One hundred load repetitions were applied at each stress state. Table 3.3 lists the different stress states used during resilient modulus testing of the specimens, in both axial and radial directions.

Table 3.3: Stress States Applied for Directional Resilient Modulus Testing (after AASHTO T 307-99)

| Sequence Number | Confining Pressure,$\sigma_{ns}$ (kPa) | Pulsed Deviator Stress, $\sigma_{nd}$(kPa) |
|---|---|---|
| 1 | 20.7 | 20.7 |
| 2 | 20.7 | 41.4 |
| 3 | 20.7 | 62.1 |
| 4 | 34.5 | 34.5 |
| 5 | 34.5 | 68.9 |
| 6 | 34.5 | 137.9 |
| 7 | 68.9 | 68.9 |
| 8 | 68.9 | 137.9 |
| 9 | 68.9 | 206.8 |
| 10 | 103.4 | 68.9 |
| 11 | 103.4 | 103.4 |
| 12 | 103.4 | 206.8 |
| 13 | 137.9 | 103.4 |
| 14 | 137.9 | 137.9 |
| 15 | 137.9 | 275.8 |

The directional modulus testing approach was successfully applied by Seyhan and Tutumluer [91] who studied thirteen aggregates with varying material properties and applied the concept of anisotropic modulus ratio (ratio of horizontal to vertical $M_R$values) as a material quality indicator. Figure 3.8 shows the consistent trend of increasing directional modulus ratios for "Good Quality" materials with the shear stress ratios [91]. Tutumluer and Seyhan [92] concluded that directional dependency or anisotropy of aggregate stiffness can be successfully used to quantify maximum allowable fines content (minus 0.075 mm or No. 200 sieve) in a given aggregate gradation, and recommended an optimum fines content of 7% for a crushed limestone aggregate base material having the IDOT CA-6 gradation. Comparative analyses of permanent

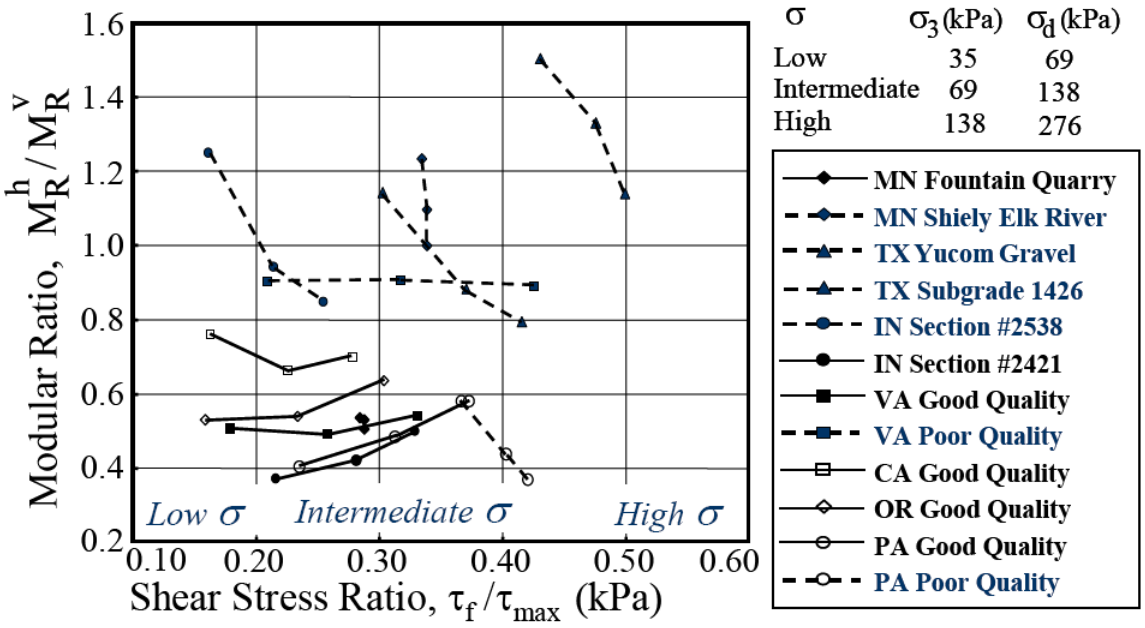


Note: Horizontal modulus ($M_R^h$) was obtained with pulsed horizontal stresses;
Vertical modulus ($M_R^v$) was obtained with pulsed vertical stresses.

Figure 3.8: Variations of Horizontal to Vertical Modulus Ratios with Failure Surface Shear Stress Ratios [91]

deformation, and directional modulus behaviors of the three aggregate types tested at different combinations of the test factors are presented in Chapter 5.

Test Equipment Description

The UI-FastCell is a Universal Testing Machine (UTM), closed-loop servo control material testing set-up. The main part of the system consists of a loading frame, the triaxial cell, compressed air supply, Control and Data Acquisition System (CDAS), and a personal computer with an integrated software package. The CDAS directly controls the servo valves to apply the desired loading rates or waveform and captures data from the transducers and transfers these data to the personal computer via a standard serial communication port.

An air actuator applies the axial pressure, whereas the confining pressures are applied through a hydraulic fluid within the rubber membrane. A fluid/air interface, which provides "fast" application and switching of the dynamic loading in the confinement "cell" is used to minimize

compressibility effects when radial stresses on a specimen are cycled. Pulsed load application in the radial direction is used for investigating anisotropic effects and the response to loading in which a 90° rotation of planes of principal stress is important. As it is not feasible to reorient unbound granular material specimens in a triaxial cell, the UI-FastCell incorporates switching the direction of pulsed load application for the same sample orientation. Figure 3.9 shows a picture of the UI-FastCell with the confinement cell lowered down on the specimen for the testing position. Sample preparation details, and test results from the repeated load triaxial testing are presented in Chapter 5.

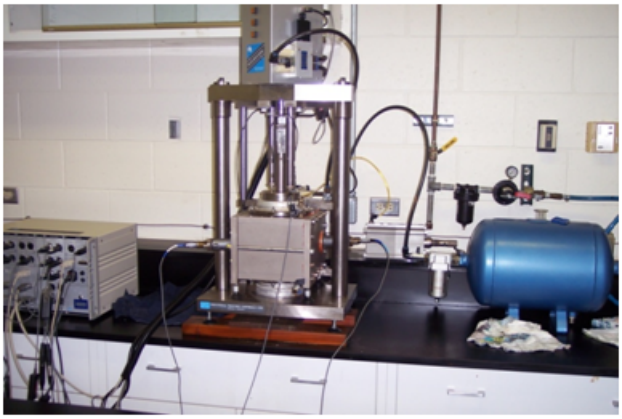

Figure 3.9: The University of Illinois FastCell

## 3.6 Accelerated Testing of Full-Scale Unsurfaced Pavement Sections

Phase II of the current research study comprised accelerated testing of full-scale unsurfaced pavement sections for verifying laboratory research findings through field performance evaluations. To this end, field test sections were constructed at the University of Illinois Advanced Transportation Research and Engineering Laboratory (ATREL) using different aggregate types, and were loaded to failure using an Accelerated Transportation Loading Assembly (ATLAS). The primary objective was to use a controlled environment for constructing similar test sections using the same, consistent construction techniques and procedures. Material selection, and cross sectional design of the full-scale test sections were based on laboratory established aggregate behavior trends, and are discussed in Chapter 6.

The number of test sections constructed for full-scale testing was decided based on equipment, space, construction, and cost constraints. The three aggregate types commonly found and utilized in Illinois for pavement applications, were used in the laboratory experimentation as well as for constructing the test sections. Field evaluation of test section performance also involved: (1) Dynamic Cone Penetrometer (DCP) tests for measuring in-place subgrade CBR, (2) nuclear density tests for moisture-density measurements, and (3) In-situ modulus measurements using a Dynatest® Light Weight Deflectometer (LWD) model 3031 and a Humboldt® Soil Stiffness Gauge (GeoGauge™). Moreover, the use of Ground-Penetrating Radar (GPR) scanning was also pursued for subsurface deformation assessment. Results from the in-place modulus measurements and GPR scanning, are presented in Chapter 7. Results from additional laboratory tests conducted on the aggregate materials used for constructing the test sections are presented in Chapter 6.

The ATLAS machine is approximately 37.8-m (124-ft) long, 3.7-m (12-ft) high, and 3.7-m (12-ft) wide with a loading length of 25.9 m (85 ft) and transmits a load up to 356 kN (80,000 lbs) to the pavement through a hydraulic ram attached to a wheel carriage. The wheel carriage assembly can accommodate different tire configurations and a lateral wander of up to 91 cm (3 ft). Individual test sections constructed in this research study were loaded to failure through unidirectional application of a 44.5-kN (10-kip) wheel load using a super-single tire. Pavement performance was monitored through surface profile measurements and GPR scanning after different number of load applications. Comparative analyses of different test section performance trends are presented in Chapter 8.

## 3.7 Summary

This chapter outlined the research framework development for fulfilling the ultimate research objective of evaluating individual effects of aggregate physical properties on behavior. The research work was primarily divided into two phases, namely: laboratory experimentation, and accelerated testing of full-scale unsurfaced pavement sections. Findings from an extensive review of technical literature were used to identify the most important physical properties (test factors) influencing unbound aggregate behavior. Three different aggregate types, namely crushed limestone, crushed dolomite, and uncrushed "river-run" gravel, commonly used in the state of

Illinois for pavement applications, were selected for investigation in the laboratory experimentation and construction of full-scale test sections. Development of a laboratory test matrix to encompass different test factors that may be allowed by different transportation agency specifications was outlined. A common particle size distribution was engineered to eliminate the influence of gradation differences on aggregate behavior.

Commonly used laboratory tests performed in this study for shear strength, permanent deformation, and resilient modulus characterization of the aggregates at different combinations of the test factors were described, and salient features of the test equipment were presented. Imaging based indices quantifying the shape, texture and angularity of the three aggregate types were presented from preliminary laboratory testing. The next chapter will present compaction and shear strength characteristics of the three aggregate types at different combinations of the test factors.

# CHAPTER 4

# AGGREGATE COMPACTION & SHEAR STRENGTH CHARACTERISTICS

## 4.1 Introduction

This chapter presents laboratory test results from compaction and shear strength characterization of the three aggregate types during phase I of the current study. Moisture-density curves were first established for the three aggregate types at all possible combinations of the test factors. The effects of individual test factors on compaction characteristics, and unsoaked California Bearing Ratio (CBR) tests (conducted on individual compaction specimens) are discussed. The unsoaked CBR values are presented as expedited shear strength indices obtained from the compaction specimens. Finally, results from strain controlled monotonic triaxial testing of the aggregates are presented to analyze the effects of selected aggregate physical properties on shear strength.

## 4.2 Moisture-Density and Unsoaked CBR Testing

Most construction specifications for unbound granular layers are designed by referencing the maximum dry density (MDD) and optimum moisture content (OMC) values as determined from laboratory testing of aggregate specimens using the standard or modified compactive effort (ASTM D 698 or ASTM D 1557). Thus, it was important to first study the compaction characteristics of the aggregate materials at different combinations of the test factors. As mentioned in Chapter 3, the optimum moisture content ($w_{opt}$) was taken as the basis to study the effect of moisture variation on aggregate behavior. Moreover, the compaction curves were

This chapter includes results already reported in the following publication. Contribution of the coauthors is sincerely acknowledged:

1. *Mishra, D., Tutumluer, E., and Butt, A. A.; "Quantifying Effects of Particle Shape and Type and Amount of Fines on Unbound Aggregate Performance Through Controlled Gradation"; In Transportation Research Record 2167, Journal of the Transportation Research Board, Transportation Research Board of the National Academies, Washington, D.C., 2010, pp. 61-71 (Voted "Practice Ready" Paper).*

later used to determine target densities on the dry or wet side of $w_{opt}$ to prepare test specimens for strength, modulus, and deformation characterization.

Compaction characteristics of the aggregates were established using the standard compactive effort specified in ASTM D 698 [13]. A minimum of four points were used to develop the curve and establish the OMC and MDD values for each individual combination of the test factors. It is important to note that the standard compactive effort [13] maximum dry density (MDD) values were used as references for preparing the laboratory specimens as well as for constructing full-scale pavement sections (see Chapter 6) during this research. This selection was based on the fact that unsurfaced pavements and pavement working platforms are often constructed over weak subgrade layers that cannot support extensive compaction of the overlying unbound granular layer (UGL). Density-based compaction specifications for such pavements therefore primarily target certain percentages of the standard compaction MDD values. Table 4.1 presents a summary of the standard compaction optimum moisture content (OMC) and maximum dry density (MDD) values for different combinations of the test factors determined.

### 4.2.1 California Bearing Ratio Tests

Unsoaked California Bearing Ratio (CBR) tests were conducted following ASTM D 1883 [93] on the same specimens used to develop the compaction curves. The CBR value thus determined, is referred to as the Immediate Bearing Value (IBV) as per IDOT specifications, and is an expedited method of determining the strength index at different moisture contents. All the CBR tests reported in this thesis were conducted under "unsoaked" conditions unless otherwise specified. The variations in CBR values with moisture were analyzed for the individual engineered gradations and discussions on important observed trends are presented below. It should be noted that the actual fines contents determined from washed gradations have been used as legends in the compaction and CBR figures. However, the approximate gradation terminologies (e.g. 4%, 8%, 12%, and 16% target fines content) are used for presenting the shear strength (Section 4.4), as well as repeated load triaxial test results (Chapter 5).

Table 4.1: Compaction Characteristics of the Three Aggregate Types with Different Type and Amount of Fines Determined using the Standard Compactive Effort (ASTM D 698)

| | Crushed Dolomite | | | | Crushed Limestone | | | | Uncrushed Gravel | | | |
|---|---|---|---|---|---|---|---|---|---|---|---|---|
| | Nonplastic | | Plastic | | Nonplastic | | Plastic | | Nonplastic | | Plastic | |
| **Target Fines** (%) | OMC (%) | MDD (kN/m$^3$) | OMC (%) | MDD (kN/m$^3$) | OMC (%) | MDD (kN/m$^3$) | OMC (%) | MDD (kN/m$^3$) | OMC (%) | MDD (kN/m$^3$) | OMC (%) | MDD (kN/m$^3$) |
| **4** | 10.6 | 20.8 | 10.4 | 21.2 | 10.5 | 20.8 | 9.3 | 21.3 | 9.2 | 20.8 | 8.0 | 21.1 |
| **8** | 8.5 | 21.7 | 7.4 | 21.7 | 8.4 | 21.4 | 8.0 | 21.3 | 8.1 | 21.1 | 7.3 | 21.3 |
| **12** | 6.8 | 21.2 | 6.6 | 22.0 | 7.6 | 22.0 | 7.6 | 21.9 | 7.1 | 21.6 | 7.1 | 21.5 |
| **16** | 6.6 | 22.5 | 6.6 | 22.2 | 6.8 | 22.3 | 7.1 | 22.3 | 7.1 | 21.7 | 6.9 | 21.4 |

## 4.3 Aggregate Physical Properties Affecting Compaction and CBR Characteristics

The effects of selected aggregate physical properties (test factors) on compaction and CBR characteristics of the three aggregate types are evaluated in this section. Significant trends in CBR values (shear strength indices) are analyzed to highlight the relative importance of individual test factors in governing aggregate behavior.

### 4.3.1 Effect of Nonplastic Fines

Standard compaction and CBR tests were conducted on specimens containing different percentages of nonplastic fines, and the changes in aggregate behavior with amount of nonplastic fines were studied.

Figure 4.1 presents the standard compactive effort moisture-density and unsoaked CBR test results for crushed limestone specimens containing different amounts of nonplastic fines. The upper part of Figure 4.1 shows the compaction curve, whereas the lower part shows the unsoaked CBR values for each of the compaction specimens. Typically, the maximum dry density values increased as the percentage of fines in the sample increased, with the highest maximum dry density obtained at a fines content of 19.2%. As the addition of fines gradually filled the voids, the aggregate matrix grew denser, thus making the 19.2% sample the densest. The change in unsoaked CBR value (see lower part of Figure 4.1) with moisture content was erratic at low fines contents (i.e. 4.4%, and 8.1%). At higher fines contents, however, the CBR value decreased rapidly with increase in moisture content. The rate of decrease in the CBR value with moisture was higher at higher fines contents. A similar trend was observed for dolomite samples (shown in Figure 4.2), with the density of dolomite specimens increasing with increasing amounts of fines, and the highest density achieved at a fines content of 15.9%.

Figure 4.3 shows a similar plot for uncrushed gravel specimens blended with different amounts of nonplastic fines. Initially as the fines content increased from 2.9% to 14.5%, the MDD also increased. However, as the fines content further increased to 18.3%, the MDD value decreased. This can be explained by considering the packing characteristics and void structure of crushed and uncrushed aggregates. The uncrushed gravel matrix, which comprises rounded aggregate

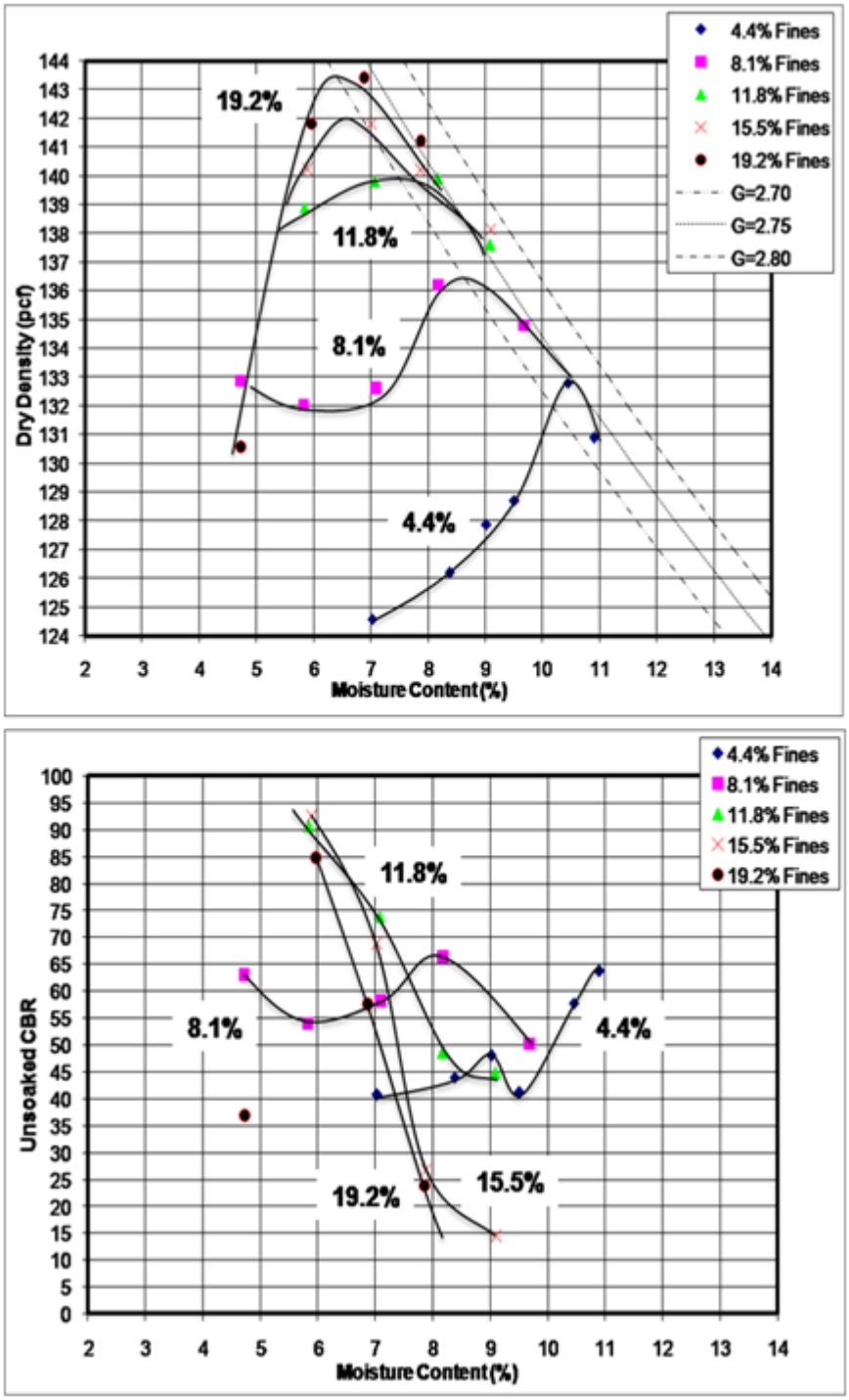


Figure 4.1: Effect of Nonplastic Fines on Crushed Limestone Moisture-Density and CBR Characteristics (1 pcf = 0.157 kN/m$^3$)

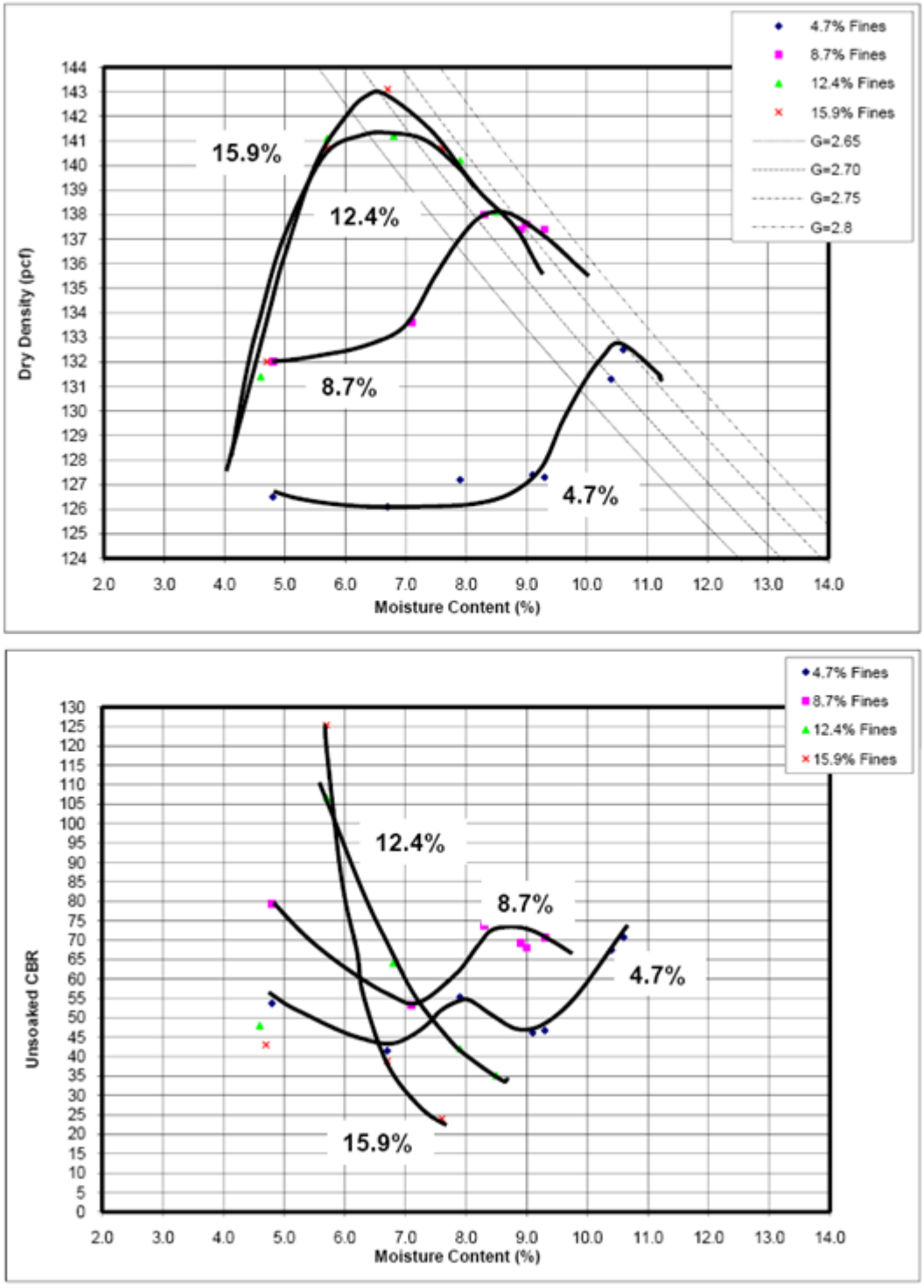


Figure 4.2: Effect of Nonplastic Fines on Crushed Dolomite Moisture-Density and CBR Characteristics (1 pcf = 0.157 kN/m$^3$)

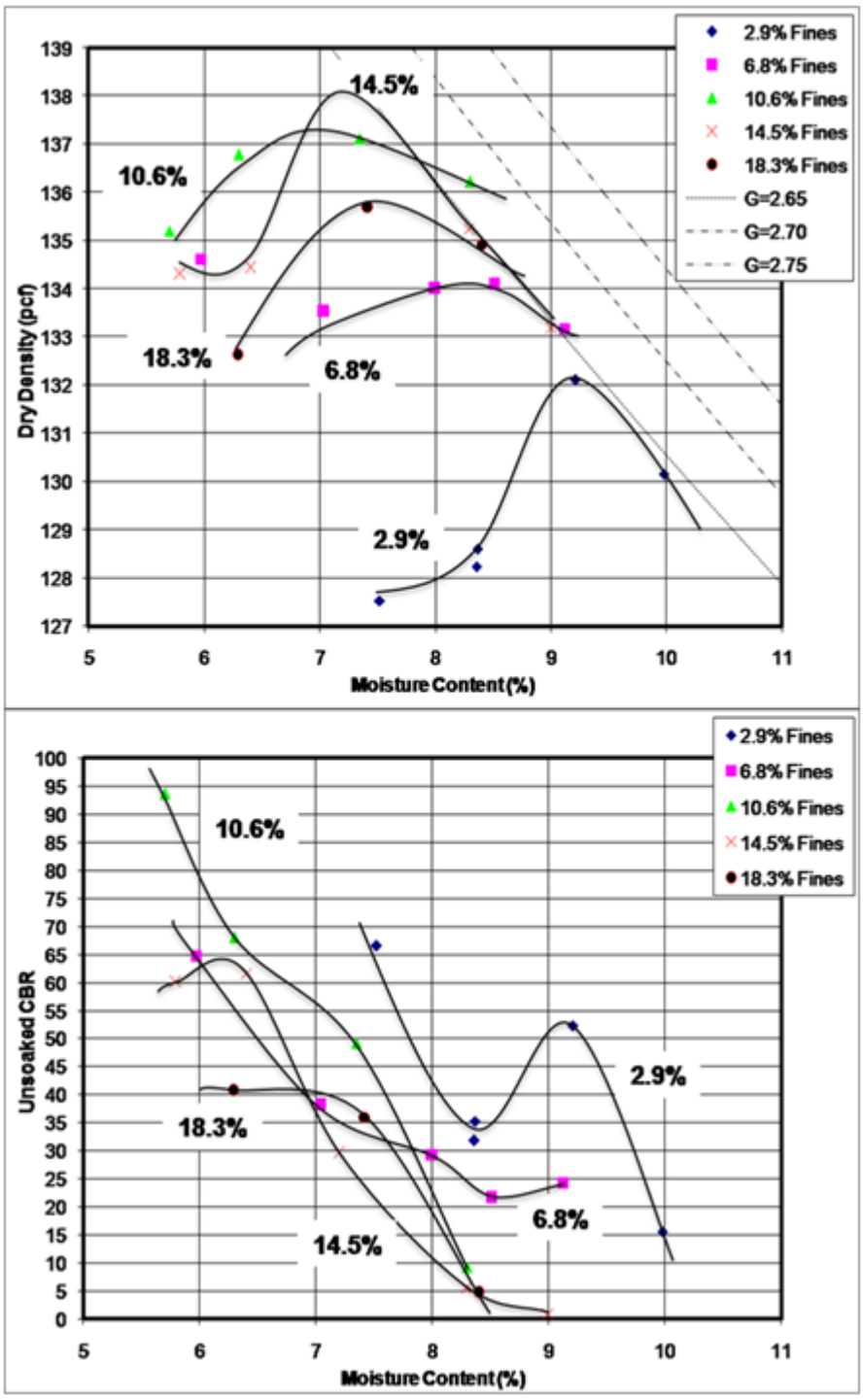


Figure 4.3: Effect of Nonplastic Fines on Uncrushed Gravel Moisture-Density and CBR Characteristics (1 pcf = 0.157 kN/m$^3$)

particles, has a lower amount of total voids than that of crushed limestone or dolomite matrices. As the fines content is increased beyond a certain point, all the voids in the uncrushed gravel matrix get filled, and the coarse particles start to float in the matrix (transition from state (b) to state (c) as shown in Figure 4.4). This results in a reduction in dry density, due to the lower

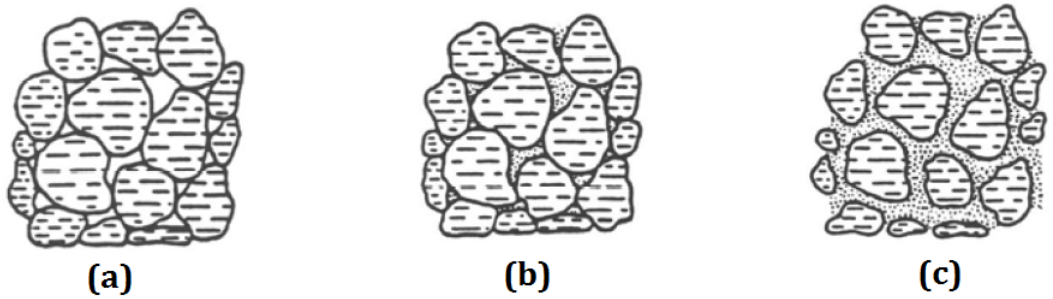


Figure 4.4: Aggregate Void Structure at Different Amounts of Fines: (a) No Fines Content, (b) Optimum Fines Content, (c) Excessive Fines Content

specific gravity of fines compared to that of the coarse particles. For limestone specimens even the presence of 19.2% fines did not completely fill the voids. Similar to the case of limestone, the unsoaked CBR relationship of gravel with moisture content was erratic at low fines contents. However, as the fines content increased, a rapid decrease in CBR with increasing moisture content was observed.

### 4.3.2 Effect of Plastic Fines

To study the effect of plastic fines on aggregate behavior, test specimens were prepared at different percentages of plastic fines. The plastic fines used in this study were engineered to have plasticity index (PI) values in the range of 8% to 14% through proportional blending of a refractory clay (PI = 18) with nonplastic fines. Figure 4.5 shows the overall impact of plastic fines on the behavior of the limestone samples. The moisture-density behavior shows a pattern similar to that observed with the nonplastic fines. The attained maximum dry density values increase with increasing fines content from 6.6% to 15.3%.

The lower part of Figure 4.5 clearly captures the different influences of plastic and nonplastic fines. Unlike in the case of nonplastic fines, the CBR value decreases rapidly with increasing moisture content even at low percentages of plastic fines. Moreover, it should be noted that the

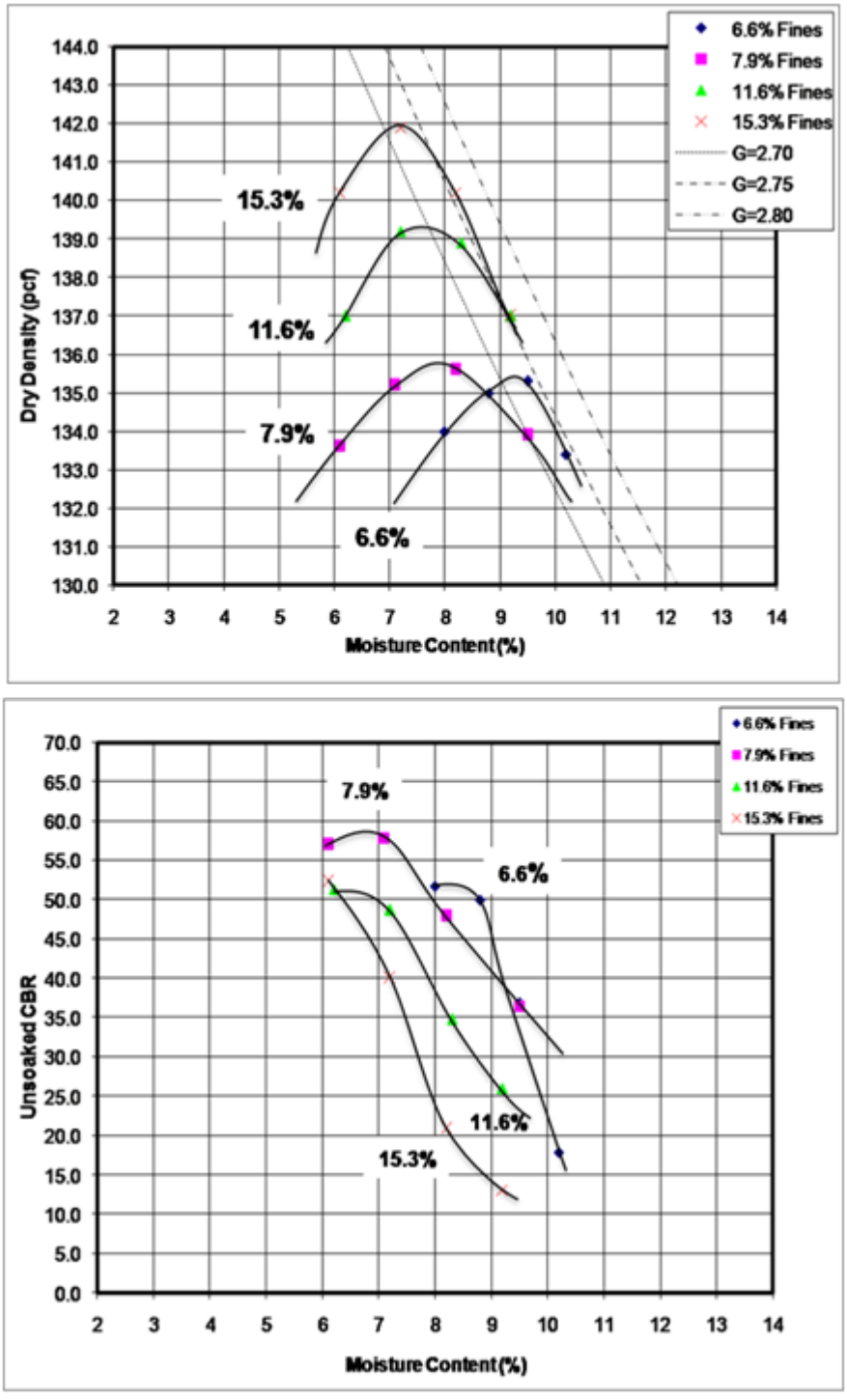


Figure 4.5: Effect of Plastic Fines on Crushed Limestone Moisture-Density and CBR Characteristics (1 pcf = 0.157 kN/m$^3$)

CBR values for samples with plastic fines were appreciably lower than those with nonplastic fines, even at the same moisture contents. The findings outlined here support the common observation that plastic fines deteriorate aggregate performance significantly. Moreover, the rapid fall in CBR value on the wet side of OMC highlights the drastic reduction in the overall material quality caused by the combined action of plastic fines and moisture. Attention needs to be paid, therefore, to the type of fines when one determines the maximum amount of fines allowed in any aggregate layer. Specifying one limit for both nonplastic and plastic fines may lead to poor performance, particularly in cases where plastic fines are introduced with high-moisture contents. Figure 4.6 shows a similar plot for dolomite samples.

The effect of plastic fines on uncrushed gravel is shown in figure 4.7. The moisture density curves exhibit similar trends to those observed with nonplastic fines (MDD decreases at very high % fines). However, the CBR-moisture relationship exhibits a stronger effect of plastic fines on the aggregate strength characteristics when compared to nonplastic fines.

### 4.3.3 Comparing Effects of Plastic and Nonplastic Fines

To compare and better evaluate the effects of type and amount of fines on aggregate strength, the unsoaked CBR values of the three aggregate types at OMC were compared at different fines contents. Figure 4.8 shows that for all aggregate types, CBR values for samples with plastic fines were lower than those with nonplastic fines at high fines contents. For limestone and dolomite samples, the same trend was observed even at low fines contents. The effect of plastic fines on gravel, however, was not as pronounced at low fines contents. From the CBR results, it appears that the effect of fines plasticity on aggregate behavior is significant only at high amounts of fines. Therefore for unbound granular layers constructed with aggregate materials with low amount of fines, no distinction needs to be drawn based on fines plasticity.

### 4.3.4 Comparing Effects of Crushed and Uncrushed Aggregates

Figure 4.8 also illustrates the contribution of particle shape and angularity on CBR behavior. For the same fines percentage, the crushed stones (limestone and dolomite) exhibited higher unsoaked CBR values than uncrushed gravel. This observation correlates to the ST and AI values reported in Chapter 3. Limestone and dolomite, each of which comprised crushed particles with a rough

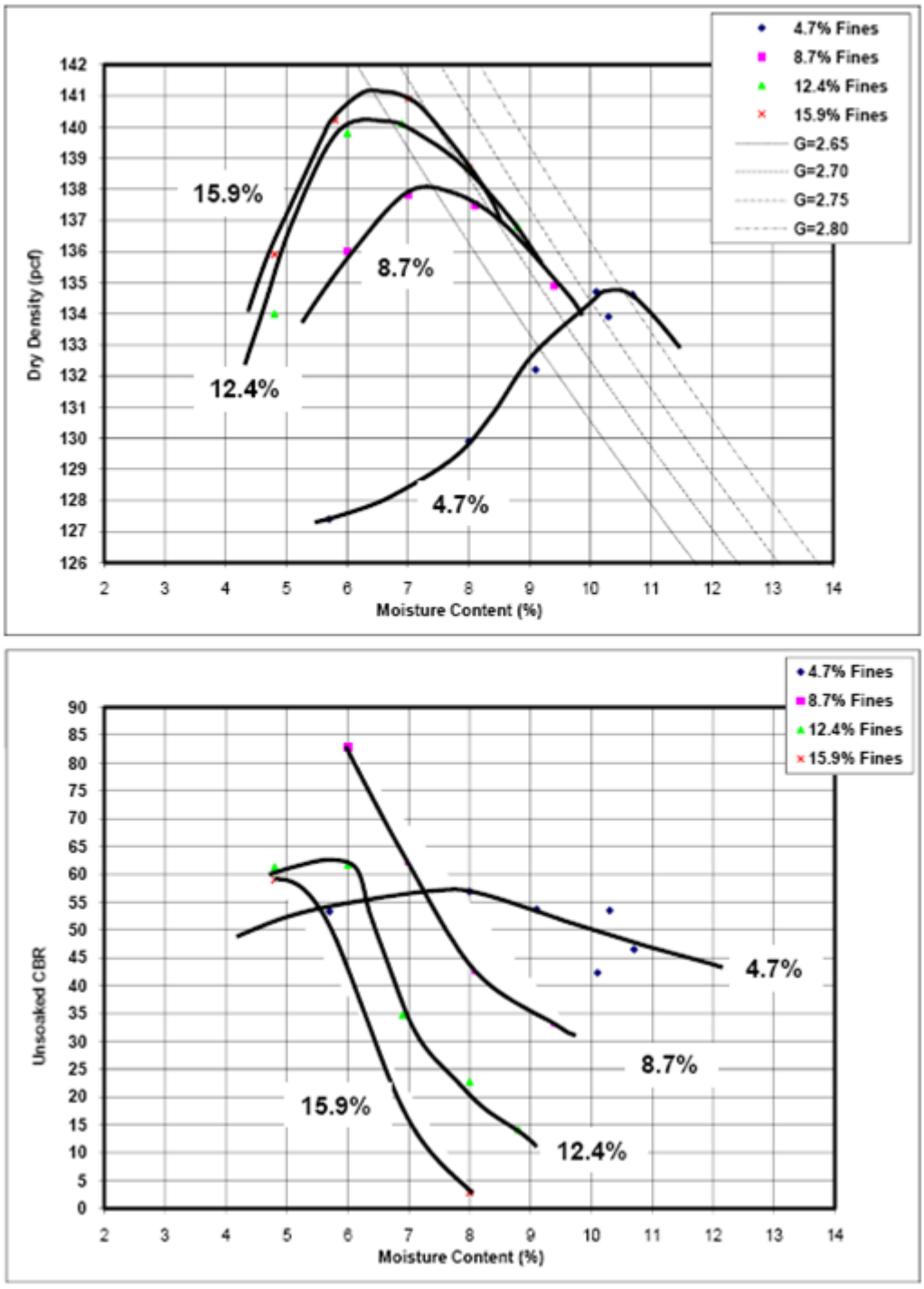


Figure 4.6: Effect of Plastic Fines on Crushed Dolomite Moisture-Density and CBR Characteristics (1 pcf = 0.157 kN/m$^3$)

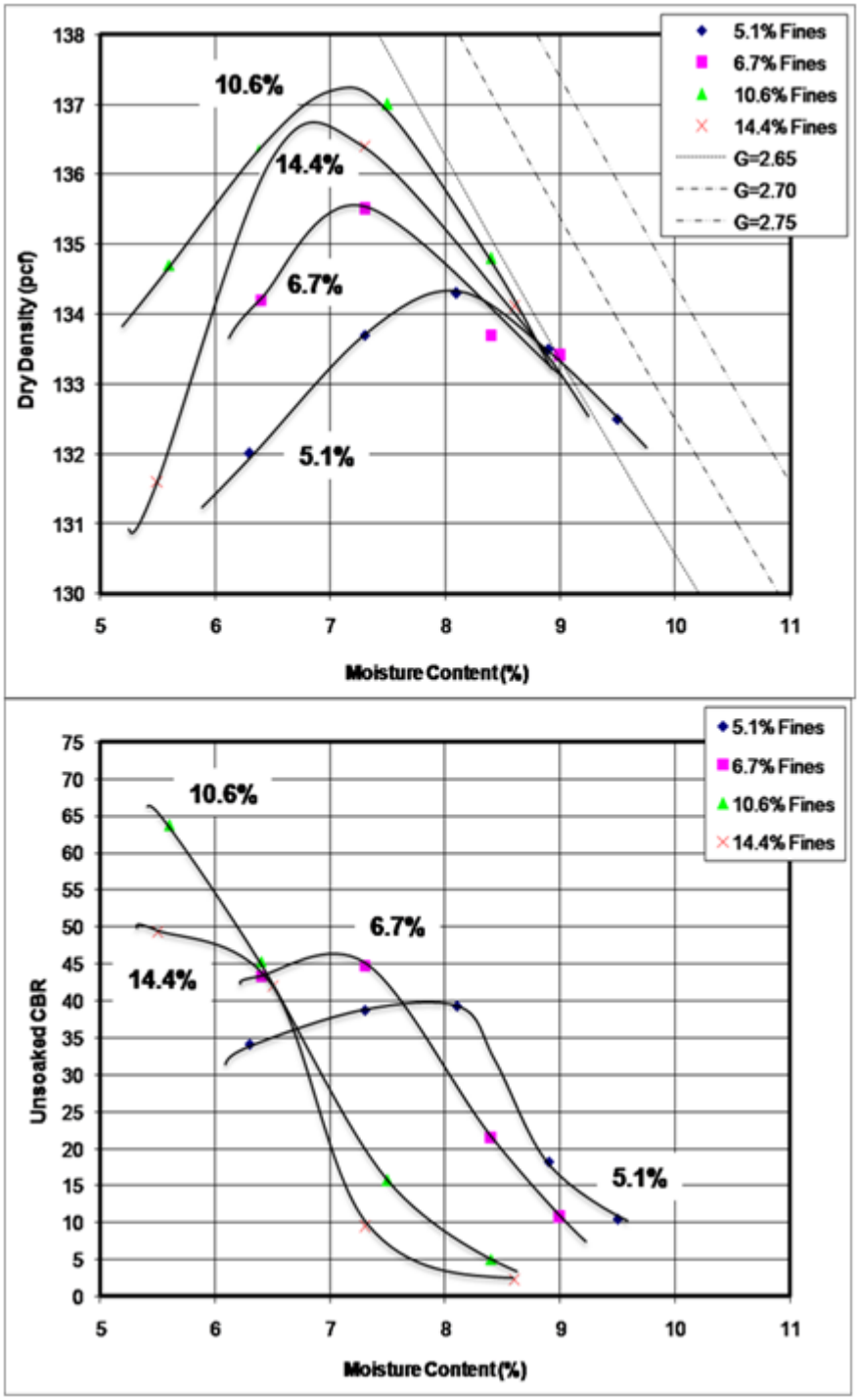


Figure 4.7: Effect of Plastic Fines on Uncrushed Gravel Moisture-Density and CBR Characteristics (1 pcf = 0.157 kN/m$^3$)

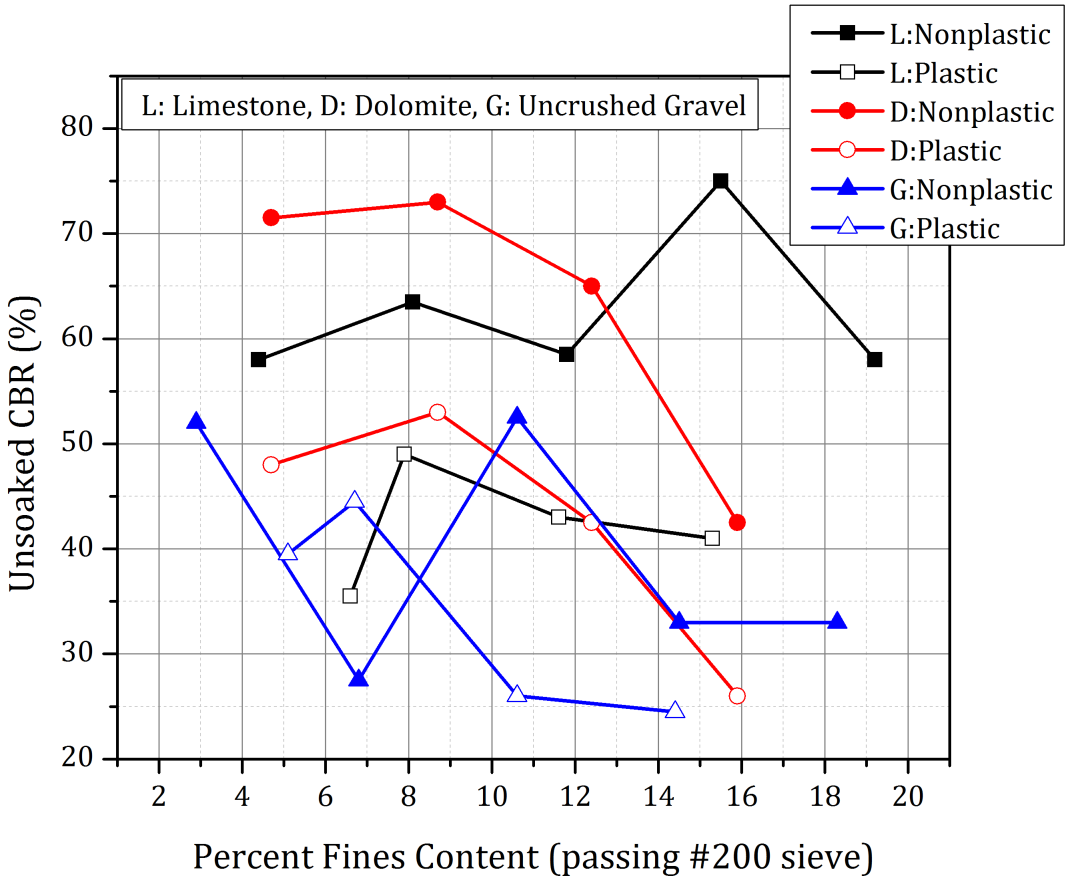


Figure 4.8: Variations of Unsoaked CBR with Fines Content at $W_{opt}$ for the Three Aggregate Types

surface texture, demonstrated better particle-to-particle contact in the aggregate skeleton. The better interlock manifested itself in higher CBR values, which could be an indicator of the shearing resistance of the material. This also reinforced the common observation that crushed aggregate particles perform better in pavement systems than uncrushed particles as far as shear-related failure is concerned. Limestone surpassed dolomite in CBR values attained beyond a fines content of 13% (Figure 4.8). This may be explained by the slightly higher AI and ST indices for limestone than for dolomite (Table 3.1). For limestone, higher angularity corresponded to higher voids and greater tolerance to accommodate increased amounts of fines beyond 13% without compromising aggregate-to-aggregate contact, which is essential for maintaining high CBR values.

### 4.3.5 Effect of Moisture Content

The effect of moisture content on CBR was studied by analyzing the change in CBR with fines content for the three aggregate types tested at 90% $w_{opt}$, 100% $w_{opt}$, and 110% $w_{opt}$, where $w_{opt}$represents the optimum moisture content determined using the standard compaction method [13]. These values for the limestone material are presented in Figure 4.9 which shows that the CBR value at a given fines content is typically the lowest when the moisture content is at 110% of $w_{opt}$. Moreover, the figure also shows that samples having plastic fines at 110% of $w_{opt}$had the lowest CBR values. Thus for any pavement layer, the combination of plastic fines and high moisture content will result in the lowest shear strength properties. Similar trends were observed for the crushed dolomite and uncrushed gravel materials, and the test results are presented in Figures 4.10, and 4.11,respectively.

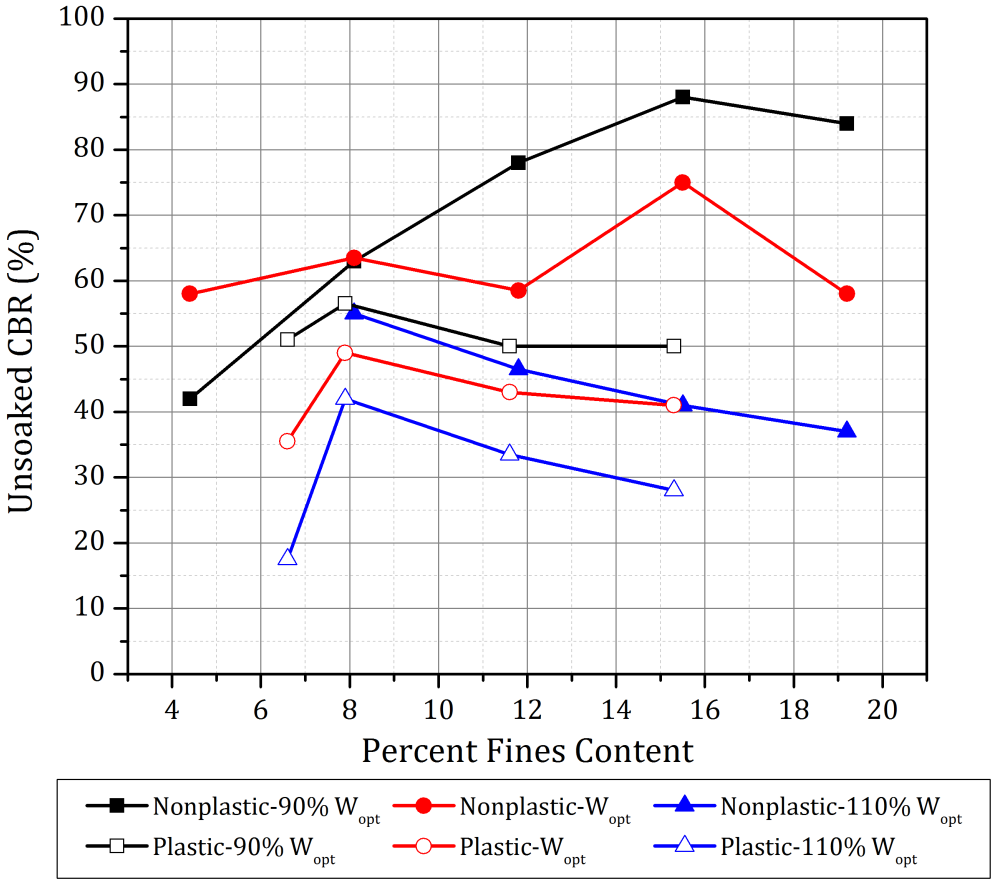


Figure 4.9: Relationship between Unsoaked CBR and Percent Fines for Crushed Limestone

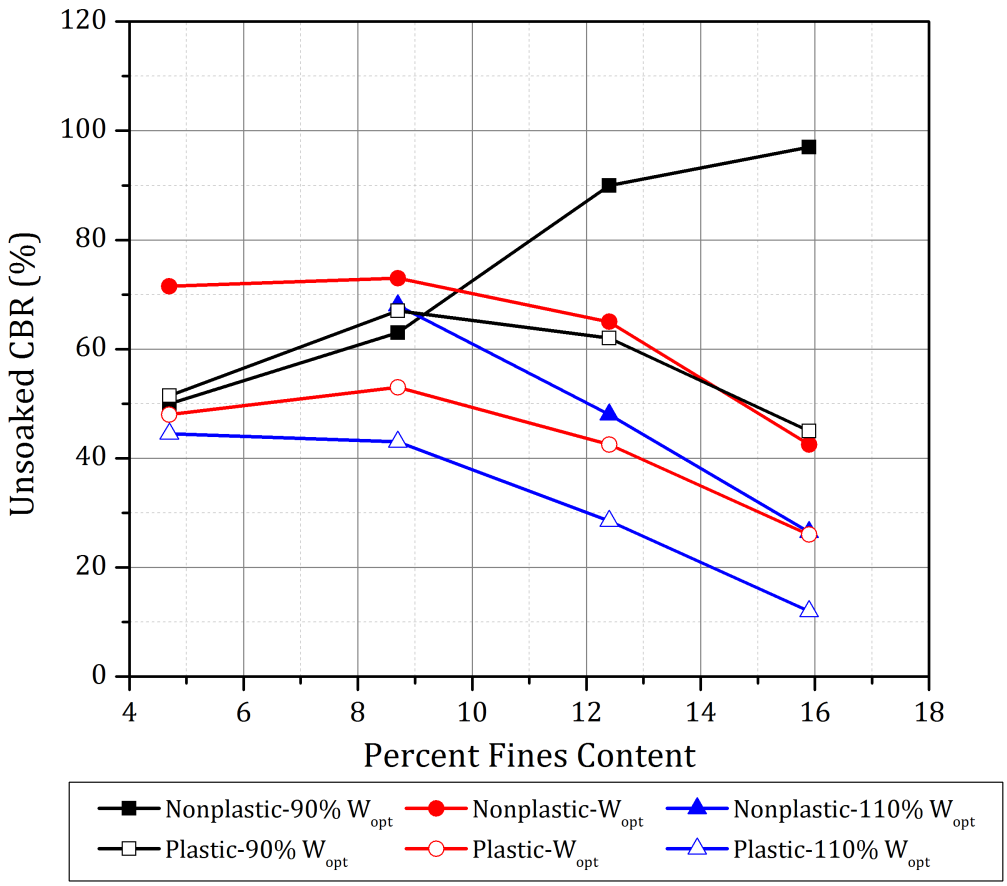


Figure 4.10: Relationship between Unsoaked CBR and Percent Fines for Crushed Dolomite

### 4.3.6 Important Observations from Compaction and CBR Characterization

The following observations can be made from moisture-density and unsoaked CBR test results for the three aggregate types at all possible combinations of the selected aggregate physical properties.

1. Crushed aggregates exhibited higher tolerance to the amount of fines, and showed lower moisture sensitivity even at high fines contents.

2. For nonplastic fines, the variation of CBR with moisture content was erratic and did not indicate any significant trends at low fines contents. However at higher fines contents, CBR values decreased rapidly with the increasing moisture.

3. The effect of fines plasticity on aggregate behavior was not very clear at low fines contents. However, as the amount of fines in a matrix was increased, specimens with plastic fines

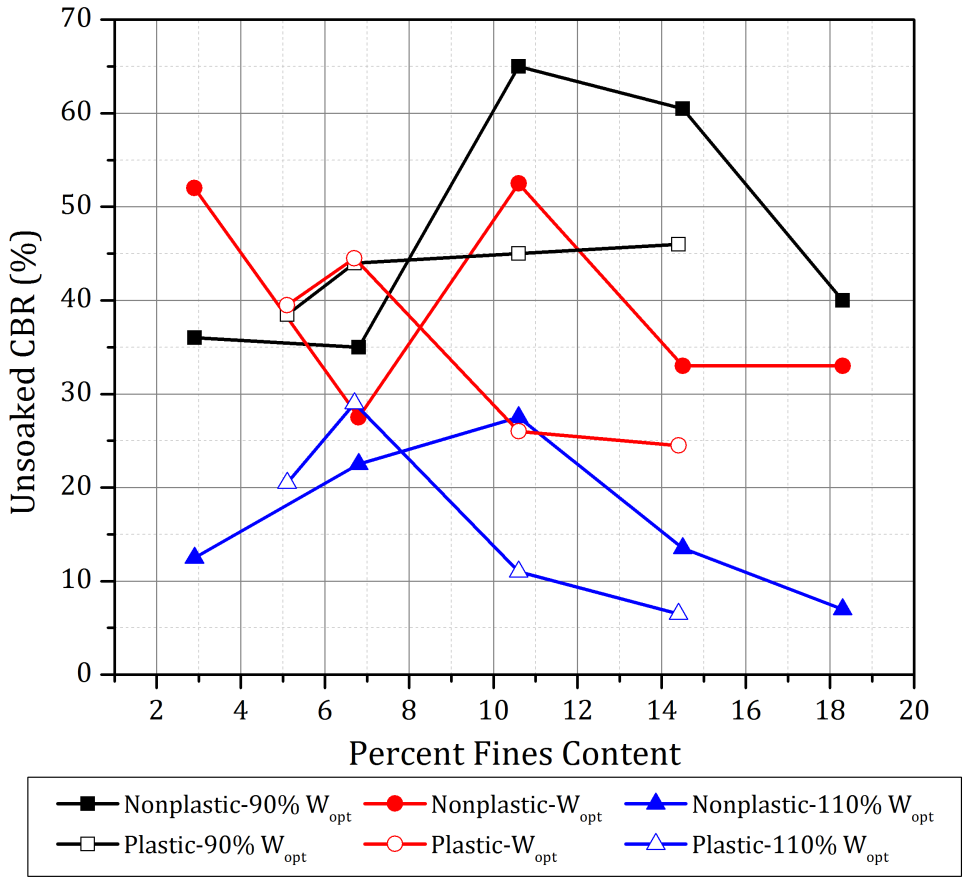


Figure 4.11: Relationship between Unsoaked CBR and Percent Fines for Uncrushed Gravel

clearly showed poor performance compared to those with nonplastic fines.

4. The effect of moisture on aggregate behavior was clearly apparent for aggregates with high fines. Specimens with high amounts of plastic fines showed the lowest inter-particle friction in the presence of excess moisture.

5. Aggregate specifications currently used by transportation agencies therefore need to be modified to consider the effect of the fines plasticity, and set different threshold limits for nonplastic and plastic fines, as far as maximum allowable fines content in an aggregate matrix is concerned.

The following section presents results from triaxial shear strength tests conducted on the three aggregate types to quantify the change in aggregate shear resistance with induced changes in the selected aggregate physical properties.

## 4.4 Rapid Shear Strength Testing of Aggregates

To better evaluate the effects of different aggregate physical properties on shear strength behavior, triaxial shear strength tests were conducted on the three aggregate materials. As mentioned in Chapter 3, the test procedure followed, was that of "Rapid Shear Strength Test", commonly performed at the University of Illinois on pavement geomaterials. Three different specimens were tested at confining pressures of 34.5, 69.0, and 103.5 kPa (5, 10, and 15 psi), respectively to determine the shear strength properties at different combinations of the test factors. The maximum deviator stress at failure, or the peak deviator stress value was used as an indicator of aggregate shear strength. Detailed description of the test set-up used for shear strength testing of the aggregates was presented in Chapter 3.

### 4.4.1 Sample Preparation and Test Procedure

The rapid shear strength tests were conducted on cylindrical specimens, 152 mm (6 in.) in diameter by 305 mm (12 in.) in height, prepared using a split aluminum compaction mold. A latex membrane was attached to the bottom platen and was folded over the split mold before placing of the aggregate. The aggregate mixed with required amount of water, was compacted in three equal lifts. Figure 4.12 shows the aluminum split mold as well as the assembled mold with membrane ready for sample placement and compaction. A pneumatic vibratory compactor was


Figure 4.12: Split Mold Assembly Used Aggregate in Sample Preparation and Compaction

originally used for compacting the individual layers. However as the optimum moisture contents

for the specimens were usually high (often as high as 10%), the vibratory compaction caused excessive splashing of water, and resulted in free standing water on top of the specimen (see Figure 4.13). To avoid such excessive moisture loss and subsequent effects on aggregate behavior, the specimens were compacted using an impact hammer similar to the one used during the standard compaction procedure [13]. It should be noted that such similarity between the specimen preparation procedures would better correlate the moisture-density behavior with strength and modulus results.

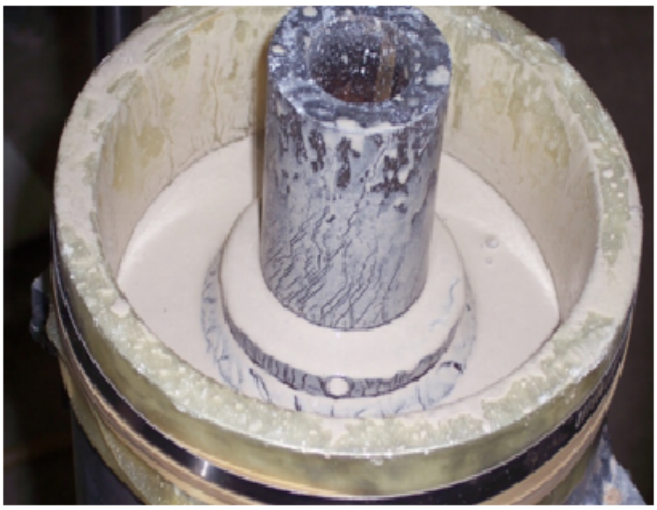

Figure 4.13: Free Standing Water on Top of Compaction Plate for Specimens at $W_{opt}$and 110% $W_{opt}$

Specimen density was calculated by measuring the weight of material and the compacted thickness of each lift referenced to the top of the mold. Each lift was then scarified up to a depth of approximately 12 mm (0.5 in.) before placing the next lift to ensure adequate interlayer bonding. After compaction a second membrane was placed on the specimen to facilitate application of vacuum and prevent air leakage in and out of the specimen. The load cell was then placed on top of the specimen with the specimen sitting in the upright position in the acrylic confining chamber of the triaxial setup. Before connecting the confining pressure, proper sealing of the acrylic chamber wall was maintained with vacuum grease. Extreme care was taken to reduce the time lag between removal of the compaction mold and testing of the specimen. This was done to reduce the amount of moisture lost due to free drainage through the specimen. Figure 4.14 shows some water lost from the specimen after the compaction mold was removed.

Through extreme care, it was possible to reduce the amount of water loss, and to control the difference between compaction water content and water content during the test. Figure 4.15 shows the deformed shape of the specimen after completion of the test.

Figure 4.14: Moisture Loss from Specimen upon Removal of Compaction Mold

Figure 4.15: Deformed Specimen after Completion of the Shear Strength Test

### 4.4.2 Analyses of Triaxial Rapid Shear Strength Results

Table 4.2 lists the friction angle ($\phi$) and cohesion intercepts (C) determined from rapid shear strength testing of the three different aggregate types under different combinations of the test factors. Although small changes induced in the test factor combinations were not directly reflected from the shear strength parameter (C, $\phi$) values, effects of drastic differences in material quality were clearly apparent. For example as shown in Table 4.2, uncrushed gravel specimens with high amounts of plastic fines resulted in the lowest friction angle ($\phi$) values, particularly at high moisture contents. Note that due to the "free-draining" nature of aggregate specimens with low amounts of fines and associated variabilities induced in the shear strength properties, the friction angle ($\phi$) and cohesion intercepts (C) determined from the three specimens (tested at confining pressures of 34.5, 69.0, and 103.5 kPa, respectively) were not always consistent. It was therefore decided to use the average peak deviator stresses corresponding to the three confining pressures to consistently compare strength characteristics and draw conclusions regarding the effects of material type, amount of fines, type of fines, and moisture content on aggregate shear strength. Significant trends observed in the strength behavior of the three aggregate materials are presented below.

Table 4.3 lists the average peak deviator stress values for dolomite specimens with nonplastic and plastic fines tested under optimum moisture conditions. The specimens with plastic fines showed steady decrease in the average peak deviator stress at failure as the fines content increased. However, an increase in nonplastic fines generally resulted in higher average peak deviator stresses. The exception was between 8% and 12% fines content, where the shear strength did not change considerably. These results were similar to the unsoaked CBR results presented in Figure 4.2. For the dolomite specimens with nonplastic fines, even the unsoaked CBR value did not change significantly when the fines contents changed from 8% to 12% (CBR value changed from 73 to 65). At very low fines contents, there was no significant difference between the peak deviator stresses for specimens that contained nonplastic fines and those that contained plastic fines. As the fines content increased beyond 8%, however, the average peak deviator stress values for the specimens with plastic fines became significantly lower than those with nonplastic fines. These results will later be referred to in Chapter 5 while presenting the effects of type and amount of fines on permanent deformation behavior. The effect of fines plasticity on shear

Table 4.2: Shear Strength Properties for the Three Aggregate Types Tested in Rapid Shear Strength Tests at Different Combinations of the Test Factors

| Fines Plasticity | Fines Content (%) | Moisture Condition | Limestone | | Dolomite | | Gravel | |
|---|---|---|---|---|---|---|---|---|
| | | | C (kPa) | $\phi$ (deg) | C (kPa) | $\phi$ (deg) | C (kPa) | $\phi$ (deg) |
| Nonplastic | 4 | Dry | 126.9 | 29.0 | 105.5 | 27.2 | 0.0 | 45.0 |
| | | Optimum | 97.9 | 35.6 | 55.2 | 46.7 | 39.3 | 35.9 |
| | | Wet | 57.9 | 41.8 | 117.2 | 30.8 | 48.3 | 34.0 |
| | 8 | Dry | 35.2 | 47.0 | 13.8 | 47.3 | 11.0 | 40.5 |
| | | Optimum | 118.6 | 34.4 | 57.2 | 49.7 | 29.6 | 39.7 |
| | | Wet | 48.3 | 46.9 | 0.0 | 55.0 | 15.2 | 43.5 |
| | 12 | Dry | 112.4 | 29.9 | 142.0 | 34.1 | 64.1 | 37.8 |
| | | Optimum | 35.2 | 47.0 | 44.1 | 51.2 | 8.3 | 42.7 |
| | | Wet | 0.0 | 51.7 | 84.1 | 42.6 | 51.0 | 32.9 |
| | 16 | Dry | 140.0 | 32.6 | 122.0 | 39.1 | 44.1 | 40.5 |
| | | Optimum | 97.2 | 34.0 | 112.4 | 41.2 | 68.9 | 35.8 |
| | | Wet | 144.8 | 15.7 | 569.5 | -34.2 | 0.0 | 39.7 |
| Plastic | 4 | Dry | 42.7 | 40.8 | 215.8 | 19.2 | 0.0 | 48.2 |
| | | Optimum | 101.4 | 37.0 | 116.5 | 33.2 | 14.5 | 34.2 |
| | | Wet | 100.7 | 35.3 | 73.8 | 43.0 | 39.3 | 38.3 |
| | 8 | Dry | 0.0 | 52.2 | 83.4 | 38.8 | 38.6 | 38.5 |
| | | Optimum | 66.2 | 42.6 | 114.5 | 24.0 | 61.4 | 30.7 |
| | | Wet | 80.0 | 40.0 | 159.3 | 28.7 | 68.3 | 28.1 |
| | 12 | Dry | 105.5 | 25.0 | 104.1 | 33.5 | 48.3 | 45.1 |
| | | Optimum | 36.5 | 43.6 | 192.4 | 0.6 | 103.4 | 16.9 |
| | | Wet | 62.1 | 33.9 | 43.4 | 42.7 | 38.6 | 34.0 |
| | 16 | Dry | 48.3 | 49.3 | 66.2 | 39.6 | 51.7 | 42.1 |
| | | Optimum | 82.7 | 34.4 | 65.5 | 34.0 | 85.5 | 24.5 |
| | | Wet | 55.2 | 33.1 | 22.8 | 45.7 | 71.0 | 19.7 |

strength was therefore not pronounced at low fines contents (about 4%). As the amount of fines increased, however, the type of fines tended to play a dominant role in governing aggregate behavior. Large amounts of plastic fines, when combined with high moisture contents, would no doubt result in the worst combination.

Table 4.4 lists the average peak deviator stresses for uncrushed gravel and crushed dolomite specimens, all of which contained nonplastic fines and were tested on the dry side of optimum moisture conditions. The crushed dolomite specimens had consistently higher strength values than the uncrushed gravel specimens (similar to the results for unsoaked CBR). The differences became even more pronounced as the fines percentage varied with the dolomite specimen

Table 4.3: Effect of Fine Types on Peak Deviator Stress of Dolomite at $W_{opt}$

| **Target Fines Content (%)** | **Average Peak Deviator Stress (kPa) Tested @ 100% $W_{opt}$** | |
|---|---|---|
| | Nonplastic Fines | Plastic Fines |
| 4 | 566.1 | 584.0 |
| 8 | 675.0 | 440.6 |
| 12 | 648.1 | 390.9 |
| 16 | 765.3 | 400.6 |

becoming almost twice as strong at 8% fines. It is also important to note that for uncrushed gravel as the fines content increases beyond 12%, the shear strength started decreasing. However for the crushed dolomite, there was an increase in shear strength even while going from 12% to 16% fines. This observation could be related to the compaction characteristics discussed earlier to emphasize that crushed aggregates with high amount of voids in the matrix show higher tolerance to change in fines contents. Irrespective of the type and amount of fines, aggregate shape and angularity consistently played an important role in governing shear strength behavior (crushed aggregates showed consistently higher shear strength compared to the uncrushed gravel).

Table 4.4: Effect of Aggregate Type on Average Peak Deviator Stress 90% $W_{opt}$

| **Nonplastic Fines Content (%)** | **Average Peak Deviator Stress (kPa) Tested @ 90% $W_{opt}$** | |
|---|---|---|
| | Uncrushed Gravel | Crushed Dolomite |
| 4 | 271.7 | 439.9 |
| 8 | 277.2 | 551.6 |
| 12 | 499.9 | 688.8 |
| 16 | 411.6 | 723.3 |

Similar to the observations made from the unsoaked CBR test results, the worst impact of adding plastic fines at high moisture contents could be clearly seen from the shear strength test results. Table 4.5 lists the average peak deviator stress values for the uncrushed gravel specimens tested under wet of optimum conditions. For the nonplastic fines, the peak deviator stress started to decrease once the fines content increased beyond 8%, and became more noticeable beyond 12% fines. However for plastic fines, as the fines content increased from 4% to 8%, the average peak

deviator stress, i.e. shear strength, dropped immediately.

Table 4.5: Effect of Fines Type on Gravel Peak Deviator Stress 110% $W_{opt}$

| **Target Fines Content (%)** | **Average Peak Deviator Stress (kPa) Tested @ 110% $W_{opt}$** | |
|---|---|---|
| | Nonplastic | Plastic |
| 4 | 307.5 | 365.4 |
| 8 | 377.8 | 328.2 |
| 12 | 348.9 | 280.6 |
| 16 | 279.9 | 267.5 |

Table 4.6 captures the effect of moisture content on shear strength for limestone specimens with nonplastic fines. Interestingly at low fines contents (4% and 8%), there was an apparent increase in the average peak deviator stress values towards $w_{opt}$and a further decrease at 110% of $w_{opt}$. At 12% fines content, the peak deviator stress values under dry of optimum and optimum moisture conditions were similar, and were higher than that for wet of optimum moisture conditions. Finally for the specimens with 16% fines, the peak deviator stress value was highest under dry of optimum conditions, and showed a continual decrease as the moisture content was increased. This trend is often common with silty soils which exhibit a tremendous change in strength from dry to wet of optimum conditions. It was obvious that for the specimens with 16% fines, the effect of moisture was more significant as the fines occupied a significant portion of the void structure, and reduced the inter particle friction in the presence of excessive moisture. Therefore, combined presence of excess moisture and high fines deteriorates aggregate shear strength significantly, even for crushed aggregates with nonplastic fines.

## 4.5 Summary

This chapter evaluated the effects of individual aggregate physical properties (test factors) on the moisture-density, CBR and shear strength characteristics of the three aggregate types. On the basis of the unsoaked CBR and shear strength tests, the most significant factor affecting aggregate behavior was the aggregate type that governed angularity (i.e., crushed or uncrushed particles). Unless all voids in aggregate matrix were completely filled with fines, particle angularity typically

Table 4.6: Effect of Moisture Content on the Shear Strength of Crushed Limestone Specimens with Nonplastic Fines

| **Nonplastic Fines Content (%)** | **Average Peak Deviator Stress (kPa)** | | |
|---|---|---|---|
| | 90% $W_{opt}$ | 100% $W_{opt}$ | 110% $W_{opt}$ |
| 4 | 544.7 | 641.2 | 519.9 |
| 8 | 456.4 | 596.4 | 554.3 |
| 12 | 526.1 | 528.8 | 406.8 |
| 16 | 666.0 | 601.9 | 431.6 |

governed the shear strength, and aggregates with crushed particles showed consistently higher shear strength compared to the uncrushed gravel. Moreover, crushed aggregates showed higher tolerance to changes in fines content owing to the higher amount of voids in the matrix.

The difference between nonplastic and plastic fines was not clear when the aggregate matrix comprised low amount of fines. However as the amount of fines in the matrix was increased, the effect of fines plasticity on aggregate behavior became more apparent. For example, high amounts plastic fines had a drastic effect on aggregate shear strength, whereas increased amounts of nonplastic fines did not cause significant reduction in aggregate shear strength. Therefore, the distinction between nonplastic and plastic fines needs to be emphasized when the aggregate matrix comprises significant amount of fines.

The effect of excess moisture on aggregate behavior was not very clear at low fines contents. This was primarily due to the free draining nature of the aggregate matrix that was not capable of retaining the excessive moisture. However at higher fines contents, the effect of moisture became clearly evident. High amounts of plastic fines with excessive moisture presented the worst combination as far as the effect on aggregate shear strength was concerned. However, even specimens with high amounts of nonplastic fines showed rapid reduction in shear strength in the presence of excessive moisture.

From the compaction and shear strength test results presented above, it was clear that careful attention should be given to particle shape and to the types and amounts of fines when selecting aggregate materials for unsurfaced pavement applications. The use of crushed aggregates should

always be encouraged irrespective of the type and amount of fines. At low fines contents, the type of fines is not likely to play an important role. However as the amount of fines increases, plastic fines found in nature may cause aggregate performance to deteriorate much faster than nonplastic fines. High percentages of plastic fines combined with greater than optimum moisture contents should therefore be avoided to prevent excessive rutting and shoving of unsurfaced pavements under traffic.

# CHAPTER 5

# REPEATED LOAD TRIAXIAL TESTING

## 5.1 Introduction

Repeated load triaxial testing of pavement geomaterials plays an important role in evaluating modulus-deformation characteristics in the laboratory. Both the resilient and permanent deformation behavior of pavement geomaterials can be quantified in the laboratory from appropriate repeated load testing data. Resilient behavior is typically realized after the specimen is shaken down during the conditioning stage, which may be used to generate the permanent deformation evaluation data for the materials tested. Note that in a well-designed pavement system, the permanent strain accumulated per load cycle is usually very small compared to the total strain.

This chapter presents results from repeated load triaxial tests conducted in the laboratory to characterize the permanent deformation and directional modulus behavior of aggregates at different combinations of aggregate physical properties (test factors). Test results are interpreted for significant trends identified in aggregate permanent deformation and resilient modulus characteristics and possible causes for differences in aggregate behavior are investigated. Commonly used models to characterize the resilient and permanent deformation behavior of aggregates were fitted to the laboratory test results, and the model parameter values were calculated for different combinations of the test factors. Analysis of Variance (ANOVA) on the

This chapter includes results already reported in the following publications. Contribution of the coauthors is sincerely acknowledged:

1. *Mishra, D., and Tutumluer, E.;"Aggregate Physical Properties Affecting Modulus and Deformation Characteristics of Unsurfaced Pavements"; Accepted for Publication in the ASCE Journal of Materials in Civil Engineering (Manuscript Submission: March-2011).*
2. *Mishra, D., Tutumluer, E. Butt, A. A., and Kern, J.; "Characterizing Aggregate Permanent Deformation Behavior based on Types and Amounts of Fines"; In Proceedings of the 8th International Conference on Bearing Capacity of Roads, Railways and Airfields, Champaign, IL, 2009, pp. 237-246.*

model parameters was conducted to identify significant effects of variations in the test factors. The applicability of anisotropic modulus ratio (defined as the ratio of horizontal to vertical resilient modulus values) as a material quality indicator is evaluated using directional modulus test results. Finally, the effect of compaction conditions on anisotropic modulus ratios is analyzed to establish a link with aggregate performance under loading.

## 5.2 Characterization of Permanent Deformation and Directional Modulus Behavior

As already discussed in Chapter 3, permanent deformation trends in the aggregate materials were evaluated using 1,000 load applications during the conditioning phase specified in the AASHTO T 307 [90] resilient modulus test protocol. The aggregate specimens were subsequently tested for directional modulus behavior through independent pulsed load applications in the vertical and horizontal directions, each applied at 15 different stress states specified in AASHTO T 307 [90]. This chapter first presents details on the specimen preparation procedure for repeated load triaxial testing of the aggregates at different combinations of the test factors. This is followed by analyses of permanent deformation and resilient modulus test results.

## 5.3 Specimen Preparation and Test Procedures

The University of Illinois FastCell (UI-FastCell) device was used for conducting repeated load triaxial testing on aggregates at different combinations of the test factors under investigation. Cylindrical specimens, 150 mm in diameter by 150 mm in height ($\sim$ 6 in. $\times$ 6 in.), were prepared in a split mold to be tested in the confinement chamber of the UI-FastCell under repeated loading. A latex membrane attached to the bottom platen with an o-ring was folded over the top of the split mold, and secured with a second o-ring. A vacuum line was used to hold the membrane tight against the mold. A non woven geofabric was placed on top of the bottom platen to prevent clogging of the drainage port. The aggregate material, mixed with required amounts of water was placed in the mold in three (for standard compaction conditoins) or five (for modified compaction condition) lifts, and compacted using both an impact and vibratory hammer. Specimen density was calculated by measuring the weight of material and the compacted thickness of each lift referenced to the top of the mold. Each lift was then scarified up to a depth

of approximately 12 mm ($\sim$ 0.5 in.) before placing the next lift. After compaction, the vacuum was removed from the split mold and applied to the bottom of the platen to create suction through the specimen, thereby causing a confinement by the membrane.

The loading platen was then placed on top of the specimen and a second latex membrane (0.3-mm thick) was placed on the specimen and secured to the top and bottom platens with o-rings. The second membrane was required because the first membrane was often punctured during compaction of the specimen. Next, the specimen was placed under the loading ram and the confining cell was lowered around the specimen. Figure 5.1 shows pictures of (a) sample compaction within the split mold, (b) compacted specimen in place for testing with the loading ram lowered, and (c) the confining chamber lowered around the specimen ready for testing. Important trends observed from permanent deformation and directional modulus testing of the aggregate materials, are presented in the sections below.

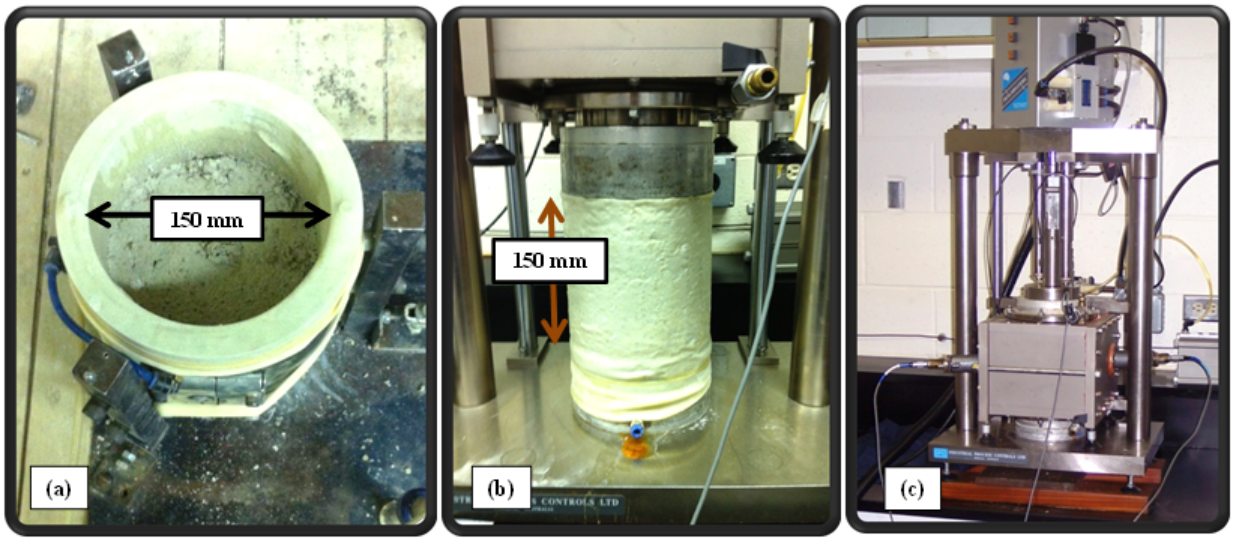


Figure 5.1: (a) Specimen Preparation; (b) Specimen in Place for Testing; and (c) Assembled UI-FastCell Repeated Load Triaxial Test Device

## 5.4 Permanent Deformation Test Results

As mentioned in Chapter 3, permanent deformation tests were conducted on triaxial cylindrical specimens through the application of 1,000 cycles of haversine dynamic pulse loading applied at 0.1 seconds with a 0.9 seconds rest period at a confining stress level of 103 kPa (15 psi) and an

axial deviator stress of 103 kPa (15 psi) similar to AASHTO T 307 [90]. The accumulation of permanent deformation was recorded for each load cycle. Note that permanent deformation behavior of an unbound aggregate layer is the most important performance indicator in the field, as it plays a significant role in governing the mobility of construction equipment (for construction platforms) and performance under heavy traffic (for unsurfaced road).

As observed from the moisture-density and unsoaked CBR test results reported in Chapter 4, the crushed limestone and dolomite materials performed similar in most of the cases. Moreover, the imaging based aggregate shape, texture and angularity indices (reported in Chapter 3), also showed significantly higher values for the crushed aggregates compared to the uncrushed gravel. Based on these observations, it was predicted that the permanent deformation characteristics for limestone and dolomite would also be somewhat similar. This was verified by first comparing the permanent deformation behavior of crushed dolomite and limestone specimens at different test factor combinations.

Figures 5.2 and 5.3 compare the permanent deformation trends of crushed dolomite and limestone specimens tested under two different test factor combinations. Figure 5.2 shows the comparative behavior for specimens with 4% nonplastic (target) fines tested at 90% of standard compactive effort optimum moisture content ($W_{opt}$), while Figure 5.3 shows the same for specimens containing 8% nonplastic fines tested at 100% $W_{opt}$. Interestingly, both figures indicate similar permanent deformation trends for the two aggregate types with dolomite giving slightly higher permanent deformations, which may be attributed to the slightly lower angularity and surface texture AI and ST indices reported in Chapter 3. Although the magnitudes of permanent deformation were slightly different for the two aggregate types, the trends in behavior with change in different aggregate properties were similar. Therefore, to present more conservative results of crushed aggregate materials and for the sake of brevity, test results for dolomite samples will only be presented in this chapter. Note that since the dolomite aggregates were received as washed materials from the quarry, the amount of fines during specimen preparation could be controlled very accurately for comparison across specimens.

Figure 5.4 shows the effect of increasing amounts of nonplastic fines on the permanent deformation behavior of crushed dolomite specimens tested under dry of optimum moisture

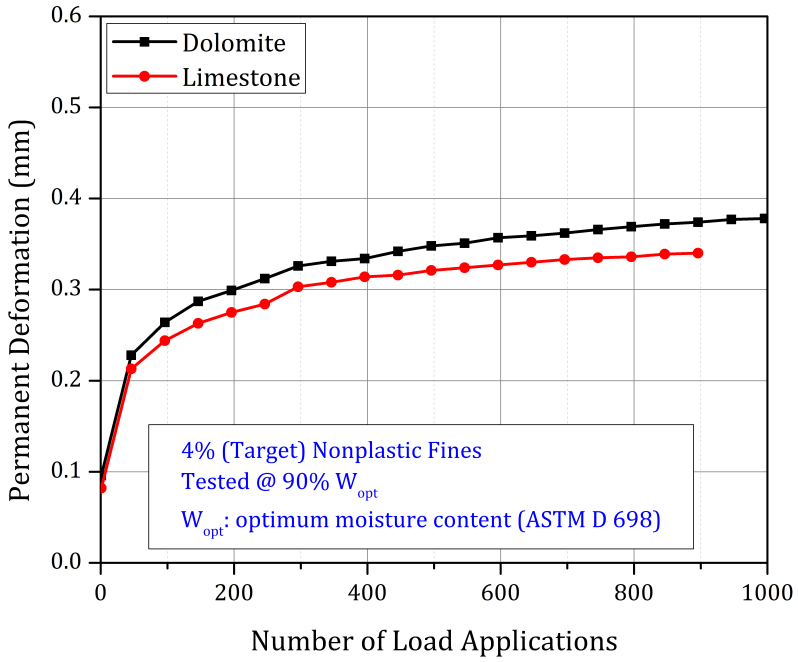


Figure 5.2: Comparing Permanent Deformation Trends in Limestone and Dolomite Materials with 4% Nonplastic Fines Tested at 90% of $W_{opt}$

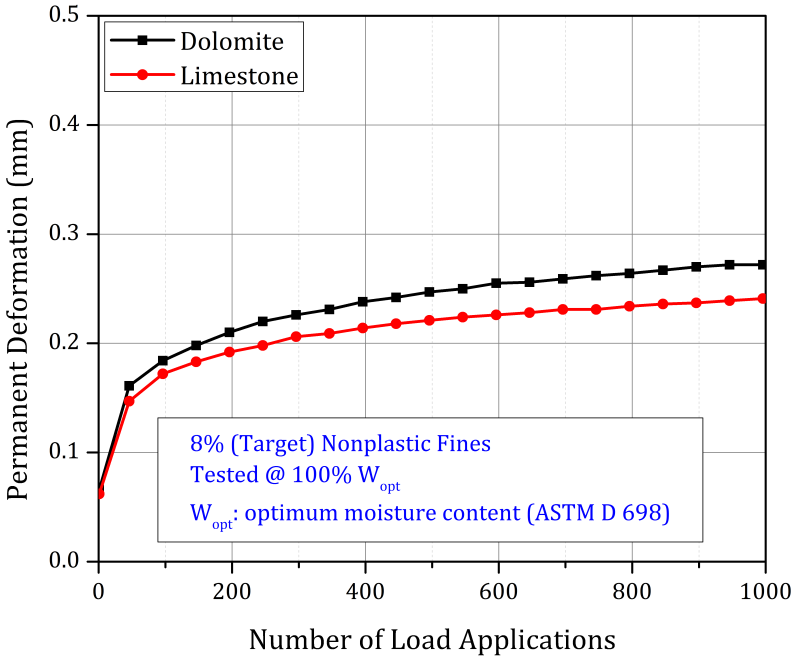


Figure 5.3: Comparing Permanent Deformation Trends in Limestone and Dolomite Materials with 8% Nonplastic Fines Tested at 100% $W_{opt}$

conditions (90% $W_{opt}$). Note that the permanent deformation values recorded for the specimen with 8% fines were lower than those for the specimen with 4% fines. However as the fines content increased from 8% to 12% and then subsequently to 16%, the permanent deformation values increased significantly. The exact same trend was observed for the dolomite specimens with nonplastic fines tested under optimum ($W_{opt}$) as well as at wet of optimum (110% $W_{opt}$) moisture conditions (see Figures 5.5 and 5.6). This behavior at relatively low fines contents was attributed to the unstable aggregate matrix and the presence of high void space in crushed dolomite specimens. As the amount of fines increased, the voids were gradually filled up to provide better packing of particles. However as the fines content was increased beyond 8%, the fines occupied a significant portion of the total void space and started affecting aggregate behavior through reduction of inter-particle contact. This resulted in the permanent deformation value at 12% fines becoming higher than that at 8% fines. Moreover, the permanent deformation at 16% fines was drastically higher and might lead to failure of such an aggregate layer in the field. These preliminary observations suggested 8% fines as the optimum fines content for crushed aggregates, and were in agreement with the recommendation made by Tutumluer and Seyhan [92] that an acceptable limit for nonplastic fines should be set around 7 to 8% for crushed aggregate layers. Moreover, better performances of specimens with 8% fines compared to those with 4% fines emphasized the role of fines in an aggregate matrix. Aggregate materials with very-low to no fines can exhibit unstable behavior and undergo significant permanent deformation due to particle movement and rearrangement.

Figure 5.7 presents the permanent deformation test results for uncrushed gravel specimens with nonplastic fines tested under dry of optimum moisture conditions. From the figure, the permanent deformation values increased consistently when the amount of fines was increased. Unlike in the case of the crushed dolomite, the uncrushed gravel aggregate matrix did not show lower permanent deformation values at 8% fines when compared to the case at 4% fines. The exact same trend was observed for uncrushed gravel specimens with plastic fines.

Figure 5.8 compares the permanent deformation trends of uncrushed gravel and crushed dolomite specimens. Both dolomite and gravel permanent deformation curves are plotted for specimens with 4% and 8% nonplastic fines tested under dry of optimum moisture conditions. Note that at 4% fines content, the crushed dolomite specimen accumulated much higher

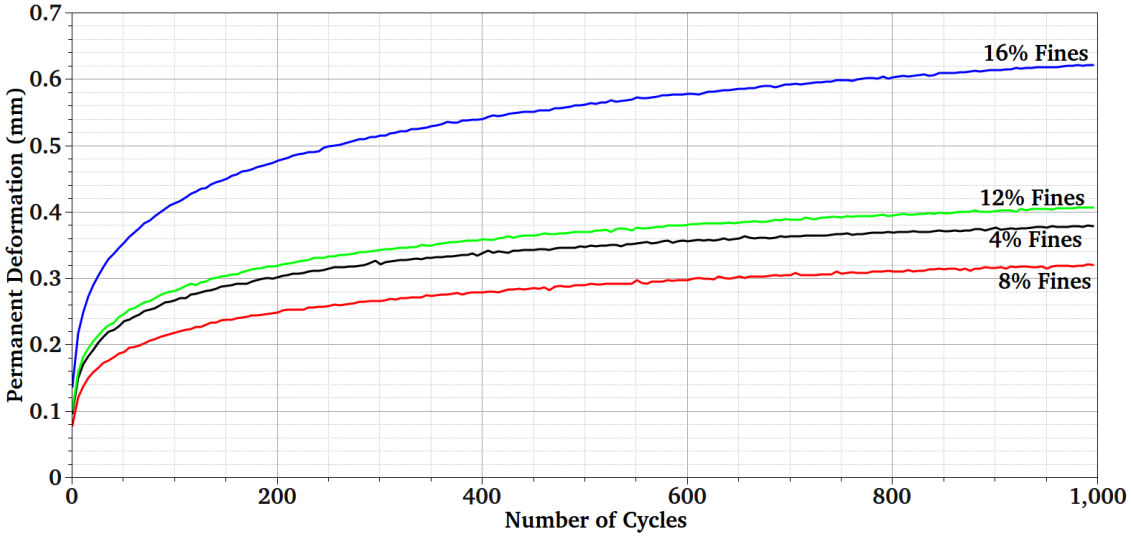


Figure 5.4: Percent Nonplastic Fines Affecting Permanent Deformation Behavior of Crushed Dolomite Specimens Tested at 90% of $W_{opt}$

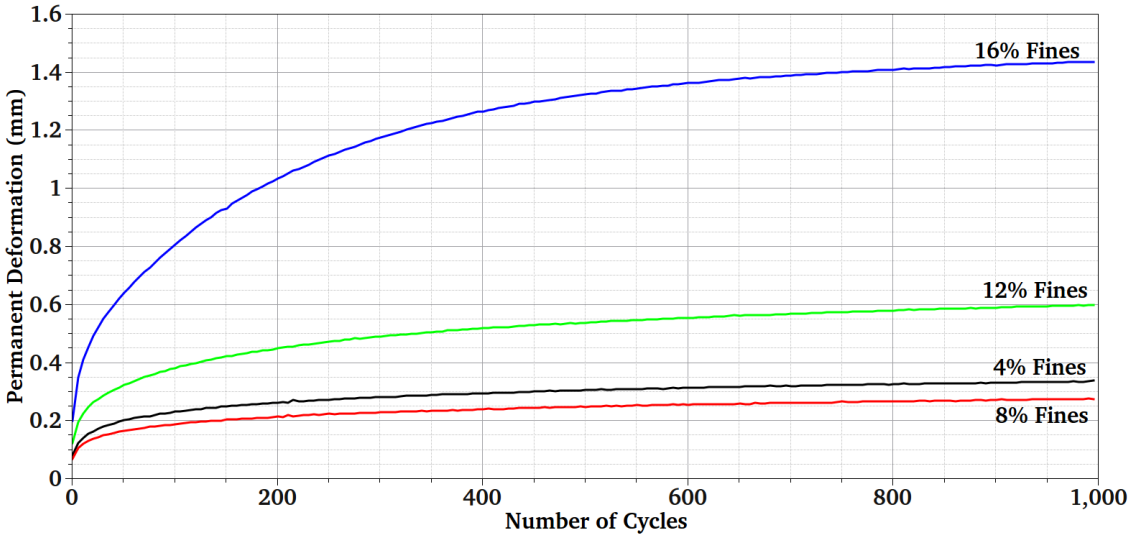


Figure 5.5: Percent Nonplastic Fines Affecting Permanent Deformation Behavior of Crushed Dolomite Specimens Tested at 100% $W_{opt}$

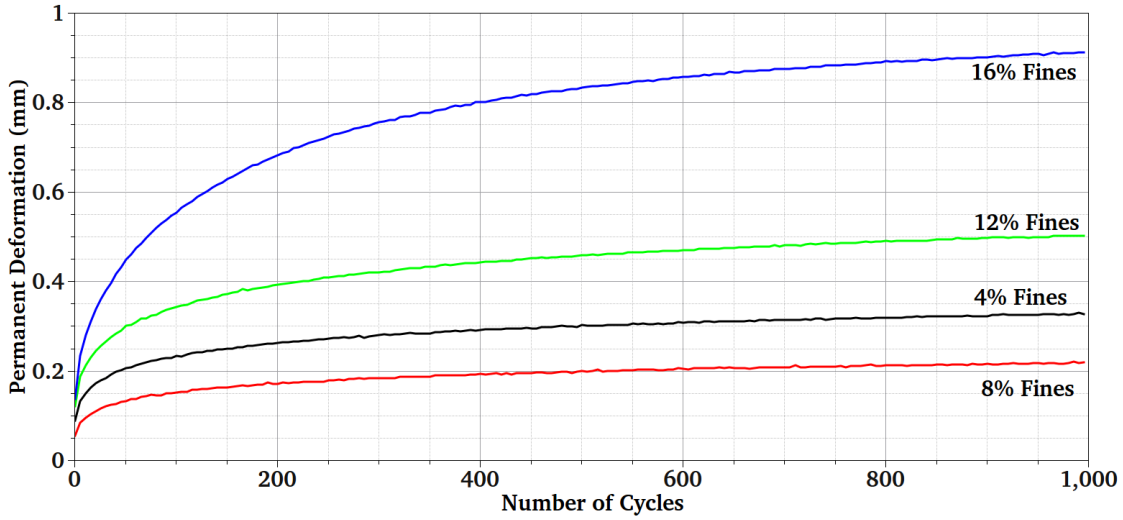


Figure 5.6: Percent Nonplastic Fines Affecting Permanent Deformation Behavior of Crushed Dolomite Specimens, Tested at 110% of $W_{opt}$

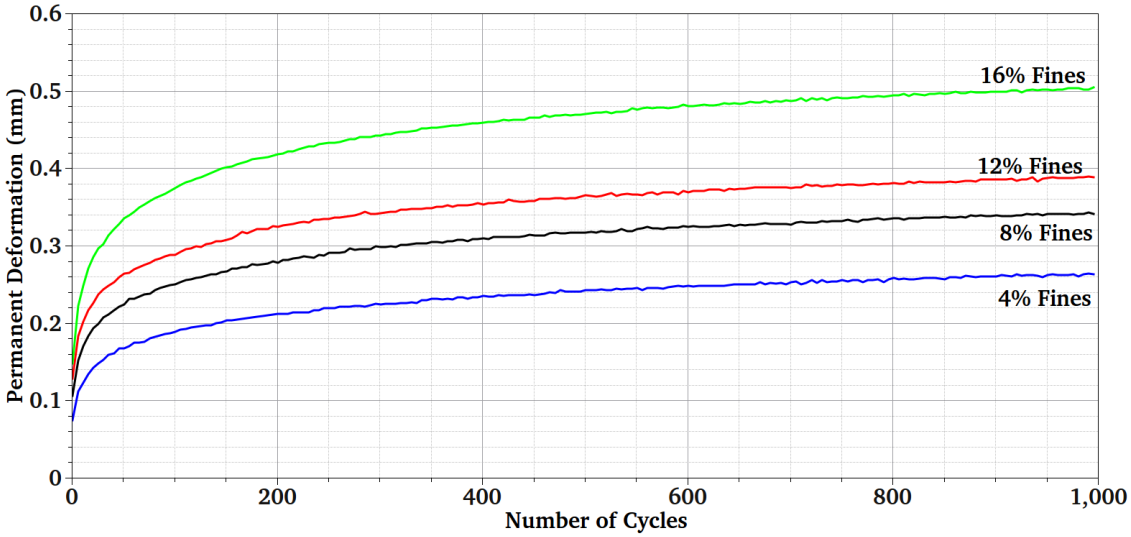


Figure 5.7: Percent Nonplastic Fines Affecting Permanent Deformation of Uncrushed Gravel at 90% of $W_{opt}$

permanent deformations when compared to the uncrushed gravel specimen. The interpretation of results shown in Figure 5.8 was that at 4% fines, the crushed dolomite aggregate matrix contained higher void space, and therefore the aggregate particles rearranged themselves to achieve a more stable configuration. As the amount of fines increased to 8%, permanent deformation values for the uncrushed gravel specimen became higher than those for the crushed dolomite. This implies that when the amount of fines is somewhat low, crushed aggregates may show higher permanent deformation values than uncrushed aggregates due to lower packing orders. Standard compactive efforts are often unable to bring the crushed aggregate matrix to the densest configuration at low fines contents. Therefore, some rearrangement may take place under the application of traffic and as such, aggregate layers containing crushed particles should be better shaken down under construction equipment and traffic.

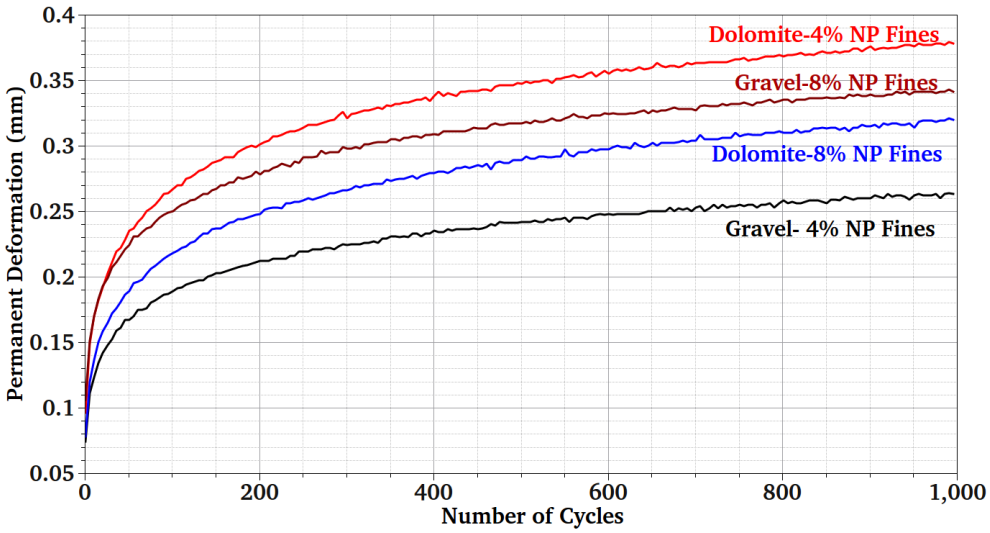


Figure 5.8: A Comparison of the Permanent Deformation Trends of Uncrushed Gravel and Crushed Dolomite Specimens Tested at 90% of $W_{opt}$

By comparing the dry of optimum and optimum curves given in Chapter 4, it can be clearly seen that when the fines contents were in a range such that most of the voids in the aggregate matrix were not filled with fines, the effect of moisture was not as significant and therefore the permanent deformation values were not affected as much. However as the amount of fines was increased, the effect of moisture became much more apparent. This was particularly noticeable for the specimen with 16% fines. Although the optimum moisture condition corresponds to the

maximum dry density from the compaction curves, the most resistance to permanent deformation may not necessarily be at the optimum moisture condition. Often, granular materials compacted on slightly dry side of optimum have higher shear strength properties and therefore, attaining a certain compaction such as maximum density alone may not always be a sufficient performance indicator in the field.

### 5.4.1 Effects of Aggregate Angularity and Plasticity of Fines

To better understand the suitability of different aggregate types for unsurfaced pavement applications, it was important to evaluate the relative impacts of the different test matrix variables on the permanent deformation behavior of the three aggregate types. For this purpose, Figure 5.9 compares the relative impact levels of aggregate angularity and plasticity of fines on permanent deformation behavior. The crushed dolomite specimen with 8% nonplastic fines tested under dry of optimum (90% $W_{opt}$) moisture conditions was considered here as the reference curve. To compare the effect of aggregate type or angularity on permanent deformation behavior, test results for the uncrushed gravel were also plotted under the same conditions. Note that the uncrushed gravel specimen showed higher permanent deformation accumulations compared to the crushed dolomite indicating that particle angularity was an important factor governing aggregate behavior. On the other hand, for the dolomite specimen also tested with plastic fines under the exact same conditions, the test results clearly showed that plastic fines resulted in the highest permanent deformations. This implied that in the presence of moderately high amounts of fines, the type of fines may play a more significant role compared to aggregate angularity or type as far as governing the permanent deformation behavior is concerned.

Figure 5.10 shows a similar comparison for aggregate specimens with 12% target fines tested on the wet side (110% $W_{opt}$) of optimum moisture conditions. A drastic deterioration in aggregate performance could be clearly seen when excess moisture was introduced in the specimen with high amounts of plastic fines. The gravel specimen with 12% nonplastic fines tested at 110% of optimum moisture content was used here as the reference curve. As the aggregate type was changed to crushed dolomite (all the other parameters remaining the same), there was no significant change in the permanent deformation behavior. However as the type of fines was changed from nonplastic to plastic (curve plotted for gravel with 12% target plastic fines tested at

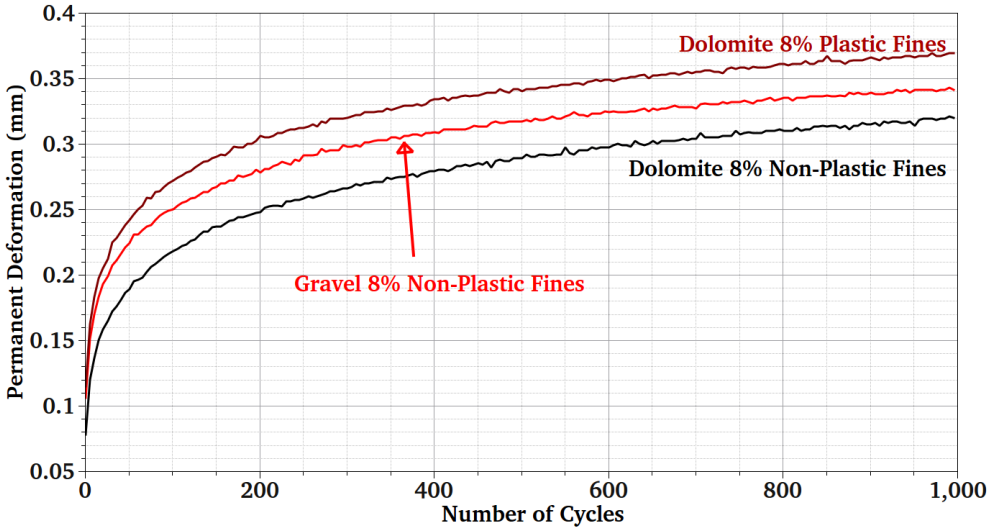


Figure 5.9: Relative Effects of Particle Angularity and Plasticity of Fines Evaluated at 90% of $W_{opt}$through Comparison of Uncrushed Gravel and Crushed Dolomite Specimens

110% of $w_{opt}$), there was a significantly higher rate of permanent deformation accumulation.

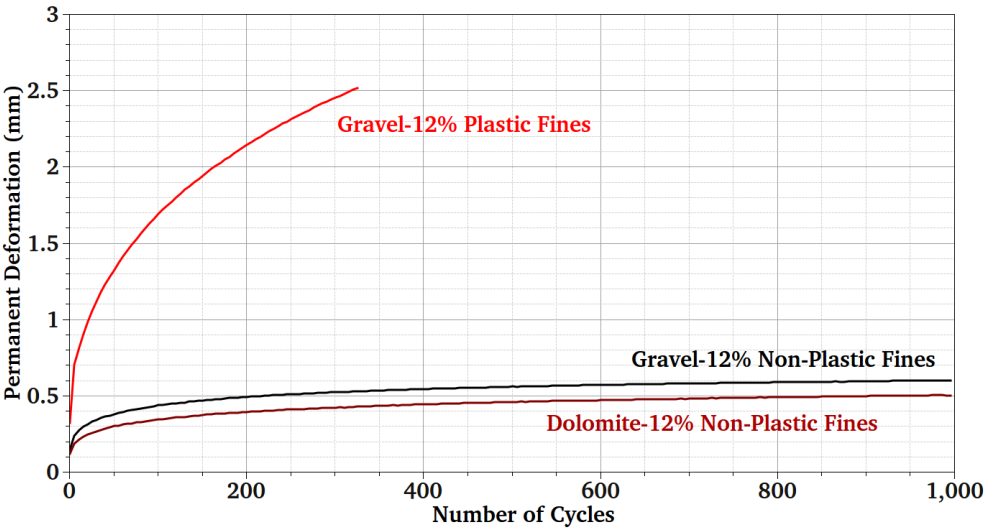


Figure 5.10: Relative Effects of Angularity and Plasticity of Fines Evaluated at 110% of $W_{opt}$

The effects of increasing percent fines on the permanent deformation behavior can be quite different depending on the void structure of the aggregate matrix and whether the aggregate particles are crushed or uncrushed. As for the implications of these experimental findings, the amount of fines may often vary in actual aggregate mixes delivered to construction sites.

Accordingly, different limits may need to be set for the maximum amount of fines permitted in the gradation depending on whether the aggregate material is crushed or uncrushed for the best field performance. When plastic fines are introduced with excessive moisture, the aggregate layer strength may be dramatically reduced. Further, when high amounts of fines (whether nonplastic or plastic) are considered at elevated moisture levels, the angular particles alone can no longer govern the behavior, i.e. both uncrushed and crushed aggregates may behave similarly. Then, the types and amounts of fines and the moisture conditions may primarily dictate the behavior.

### 5.4.2 Effects of Moisture Content and Plasticity of Fines

Figure 5.11 compares the relative impacts of moisture content and plasticity of fines on aggregate permanent deformation behavior. The comparisons are presented for crushed dolomite specimens with 12% fines and the reference curve is for nonplastic fines tested at 90% of $W_{opt}$. As the moisture content was increased to 110% of $W_{opt}$, the permanent deformation values increased by approximately 25%. This showed the adverse effect of moisture even on nonplastic fines at relatively high fines contents. However, if the type of fines was changed from nonplastic to plastic (represented by curves of dolomite with 12% plastic fines tested at $W_{opt}$and 90% of $W_{opt}$), the permanent deformation values increased even more dramatically. This clearly indicated that increase in moisture content was not as critical for nonplastic fines when compared to the case of plastic fines. These results combined with the previously reported ones in Figure 5.10 indicated that the control of moisture is much more important for aggregate layers containing plastic fines than for those containing nonplastic fines. Moreover as previously mentioned, optimum moisture conditions may not always lead to better performance in aggregate materials comprising high amounts of fines. The amount of moisture plays a more important role for such materials, and better performance is almost always realized for specimens with lower amount of moisture accessible to the fine particles. Moisture control and drainage provisions become critical aspects for unsurfaced pavement performance, especially in the presence of plastic fines.

### 5.4.3 Summary of Findings from Permanent Deformation Testing

From the permanent deformation tests conducted on the three aggregate types at different combinations of the aggregate physical properties (test factors) of interest, it appears that the most important parameter at low fines (passing No. 200 sieve size or smaller than 0.075 mm)

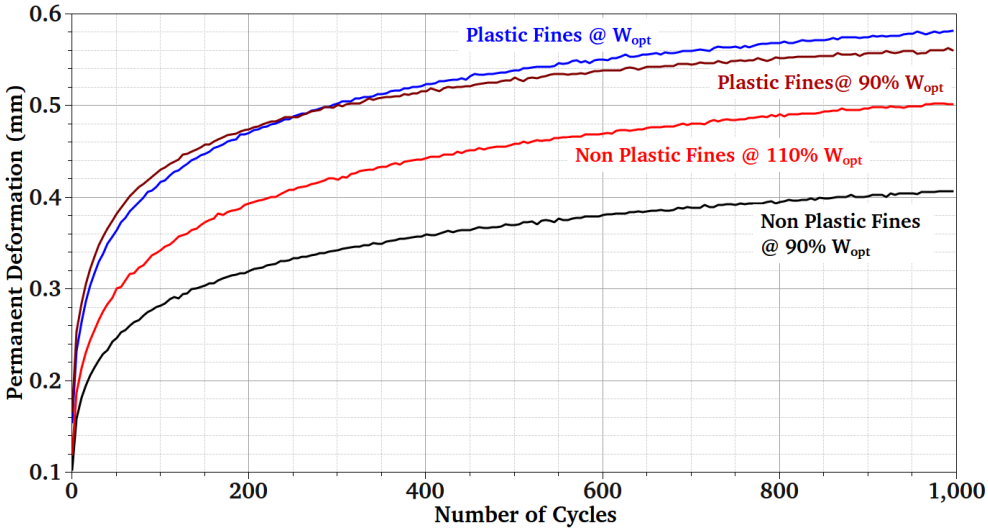


Figure 5.11: Relative Effects of Varying Moisture Content and Plasticity of Fines at 12% Fines Content Presented for Crushed Dolomite

contents was the aggregate type governing the angularity, i.e. crushed or uncrushed particles. Unless all voids in aggregate matrix were completely filled with fines, particle angularity, i.e. crushed or uncrushed particles, typically governed the permanent deformation behavior. The second most important parameter that affected aggregate behavior was the plasticity of fines. High amounts of plastic fines, at wet of optimum moisture conditions were found to quickly deteriorate the aggregate load transfer matrix thus resulting in excessive permanent deformations.

The effect of moisture content on aggregate performance varied significantly depending on the amount and plasticity of fines. For low percentages of nonplastic fines, moisture content did not have a significant effect on aggregate performance, and often aggregate type or angularity was the most important factor. However, for aggregates with plastic fines, moisture became the most important factor that governed aggregate behavior.

## 5.5 Directional Modulus Testing of Aggregates

Starting with the 1986 AASHTO Pavement Design Guide [94], resilient modulus has been used to characterize the stiffness behavior of subgrade soil and granular base/subbase layers subjected to repeated traffic loading. With the routine use of resilient modulus as a primary input into mechanistic-empirical pavement design procedures, many state highway agencies are now making

an effort to establish the appropriate "resilient modulus" inputs for granular materials and subgrade soils. It should be noted that rutting is primarily controlled by shear strength, and therefore, resilient modulus is not a performance indicator of an aggregate layer. However as a measure of a material's ability to withstand repeated loading and protecting the subgrade from excessive stress levels, resilient modulus plays an integral part in the thickness design and long term performance of a pavement.

The directional modulus testing using the UI-FastCell under vertical or horizontal dynamic (pulsed) loads was successfully applied in the past to evaluate aggregate response and performance [91, 95]. Horizontal to vertical directional modulus ratios (Modulus Ratio = $M_R^h/M_R^v$) are determined by applying horizontal pulsing only to determine horizontal modulus and vertical pulsing only to determine vertical modulus, respectively. Detailed analyses of the test data by Seyhan and Tutumluer [91] indicated that these modulus ratios could serve as aggregate performance indicators for determining the quality and strength properties of aggregates under various field-loading conditions and hence could be used to predict rutting potentials of aggregates.

After initial conditioning, directional resilient modulus tests were performed by independent pulsed load application on the specimens first in the axial direction followed by pulsing in the radial directions [95]. The 15 stress states specified in AASHTO T 307 were used for pulsing in the axial as well as radial directions. The vertical and horizontal moduli values were calculated from the independent pulsing tests using the following set of isotropic stress-strain equations.

**Vertical Pulsing Only**

$$\epsilon_1 = \frac{1}{M_R^v} \times \sigma_{1d} \tag{5.1}$$

$$\epsilon_3 = \frac{1}{M_R^v} \times (-\nu\sigma_{1d}) \tag{5.2}$$

**Horizontal Pulsing Only**

$$\epsilon_1 = \frac{1}{M_R^h} \times (-2\nu\sigma_{3d}) \tag{5.3}$$

$$\epsilon_3 = \frac{1}{M_R^h} \times [\sigma_{3d} \times (1-\nu)] \tag{5.4}$$

where $\epsilon_1$ = Recorded axial strain;

$\epsilon_3$= Recorded radial strain;

$\nu$ = Poisson's ratio;

$\sigma_{1d}$ = Applied axial (pulsed) deviator stress;

$\sigma_{3d}$ = Applied radial (pulsed) deviator stress;

$M_R^v$ = Resilient modulus in vertical direction;

$M_R^h$ = Resilient modulus in horizontal direction.

Note that for an isotropic material, $M_R^v = M_R^h = M_R$

## 5.6 Effect of Aggregate Physical Properties on Resilient Modulus

### 5.6.1 Effect of Particle Shape and Angularity

Figure 5.12 shows the effect of aggregate type or angularity on laboratory-determined resilient modulus characteristics. The resilient moduli were computed at the applied 15 stress states with pulsed deviator stresses applied in the axial direction for the dolomite and gravel both containing 8% plastic fines and tested under dry of optimum moisture conditions. The crushed dolomite specimen showed consistently higher resilient modulus values when compared to the uncrushed gravel. Moreover, at low values of bulk stress ($\theta$, or first stress invariant), there were no significant differences between the resilient moduli obtained for the crushed and uncrushed aggregate particles. However as the bulk stress value increased, the differences in the resilient response became more apparent. The crushed dolomite material exhibited higher stress hardening behavior compared to the uncrushed gravel. The exact same trend can be seen in Figure 5.13, which shows the crushed limestone and uncrushed gravel materials containing 12% target nonplastic fines tested under dry of optimum conditions.

### 5.6.2 Effect of Fines Content

Figure 5.14 shows the effect of fines content on the resilient behavior of the crushed dolomite material tested with plastic fines under dry of optimum moisture conditions. Note that an increase in the amount of fines from 8% to 12% did not cause any significant difference in the resilient modulus behavior. However when higher bulk stress levels were applied, the specimen with 12% fines resulted in slightly lower modulus values compared to the one with 8% fines. This showed that the slight increase in fines content did not have a noticeable effect on the resilient

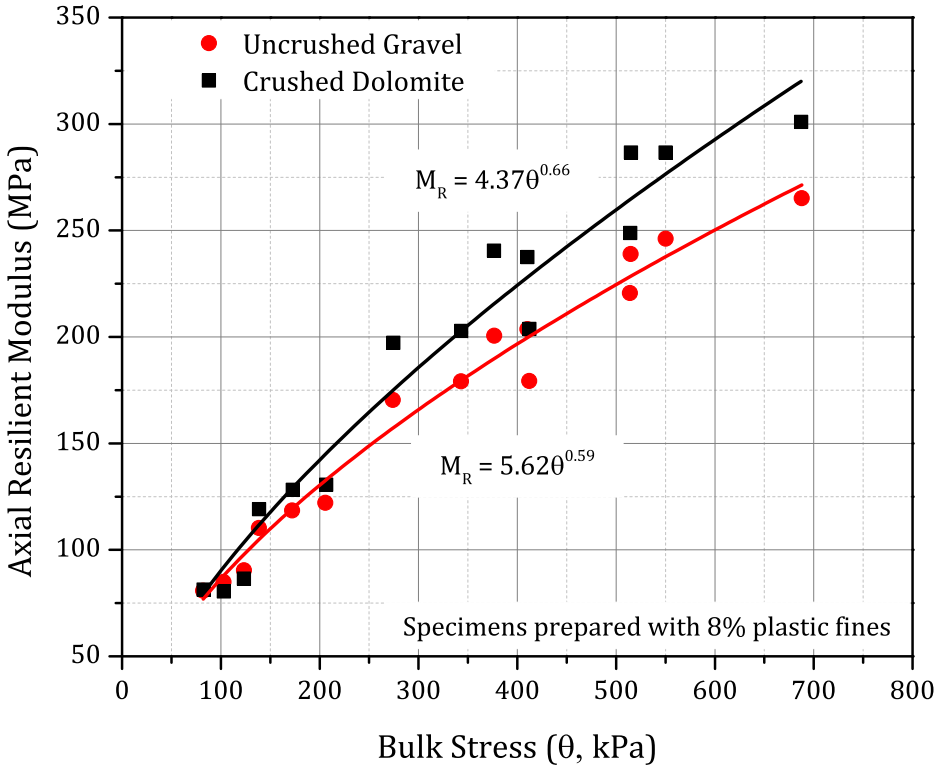


Figure 5.12: Compared Resilient Responses of Uncrushed Gravel and Crushed Dolomite Materials with 8% Plastic Fines Tested at 90% of $W_{opt}$

modulus values. However when the amount of fines was changed drastically, the resilient behavior underwent significant changes. This can be clearly shown by plotting the resilient modulus curves for the uncrushed gravel material (see Figure 5.15) tested with 4% and 16% plastic fines under optimum moisture conditions. From Figure 5.15, it can be clearly seen that increasing the fines percentage drastically did have a significant damaging effect on the load dissipating ability of aggregates. Therefore as far as resilient behavior is concerned, the impact of fines was noticeable only when the fines content was changed by a significant percentage.

## 5.7 Modeling Repeated Load Behavior of Aggregates

To compare the resilient responses of the three aggregate types at different combinations of the test factors numerically, two different models commonly used to characterize the nonlinear stress dependent resilient behavior of unbound aggregates were fitted to the $M_R$ test results. Resilient modulus model parameters serve as essential layer inputs for mechanistic-empirical (M-E)

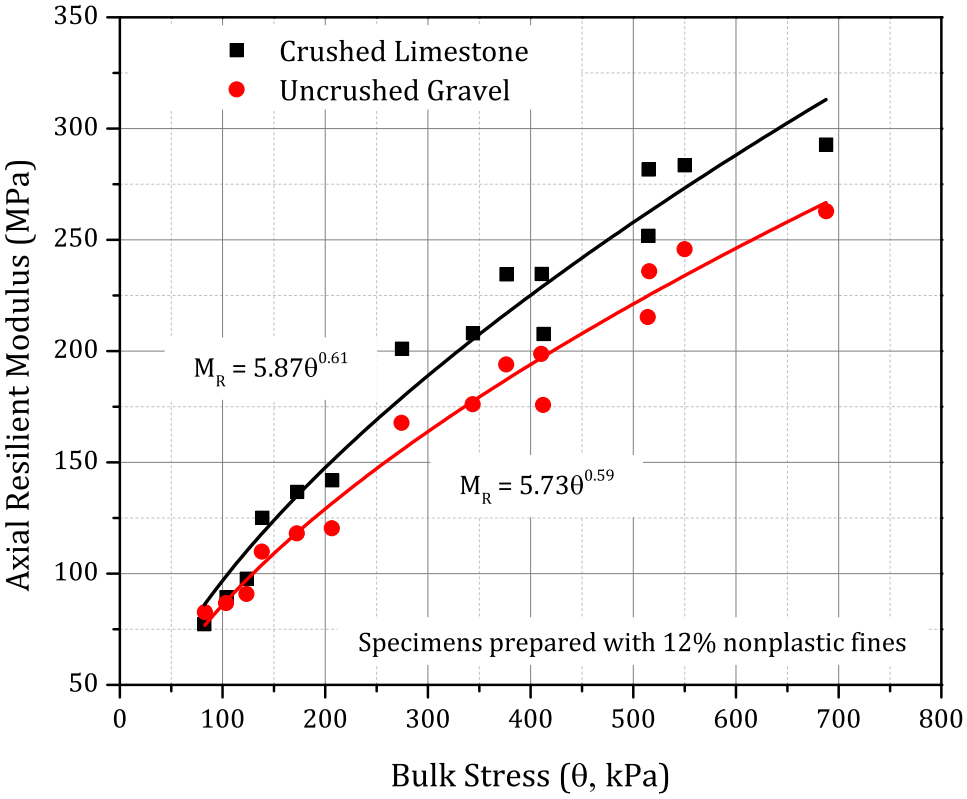


Figure 5.13: Compared Resilient Responses of Uncrushed Gravel and Crushed Limestone Materials with 12% Nonplastic Fines Tested at 90% $W_{opt}$

pavement analysis and design procedures, such as in the Level 1 analysis of the hierarchical MEPDG material property assignments, and they can be linked to aggregate physical properties. The models selected in this research study were: K-$\theta$ [17] and the MEPDG [24] models. As discussed in Chapter 2, the K-$\theta$ model simply correlates the resilient modulus to bulk stress (first stress invariant) without considering the applied shear stress levels, and can be used to model the stress hardening behavior of unbound aggregate materials. The MEPDG model on the other hand, incorporates shear stress effects, and can model the stress hardening as well as stress softening behavior of geomaterials [24]. Equations 5.5 and 5.6 show the K-$\theta$ and MEPDG resilient modulus models, respectively.

$$M_R = K\left(\frac{\theta}{p_0}\right)^n \tag{5.5}$$

$$M_R = k_x p_a \left(\frac{\theta}{p_a}\right)^{k_y} \left(\frac{\tau_{oct}}{p_a} + 1\right)^{k_z} \tag{5.6}$$

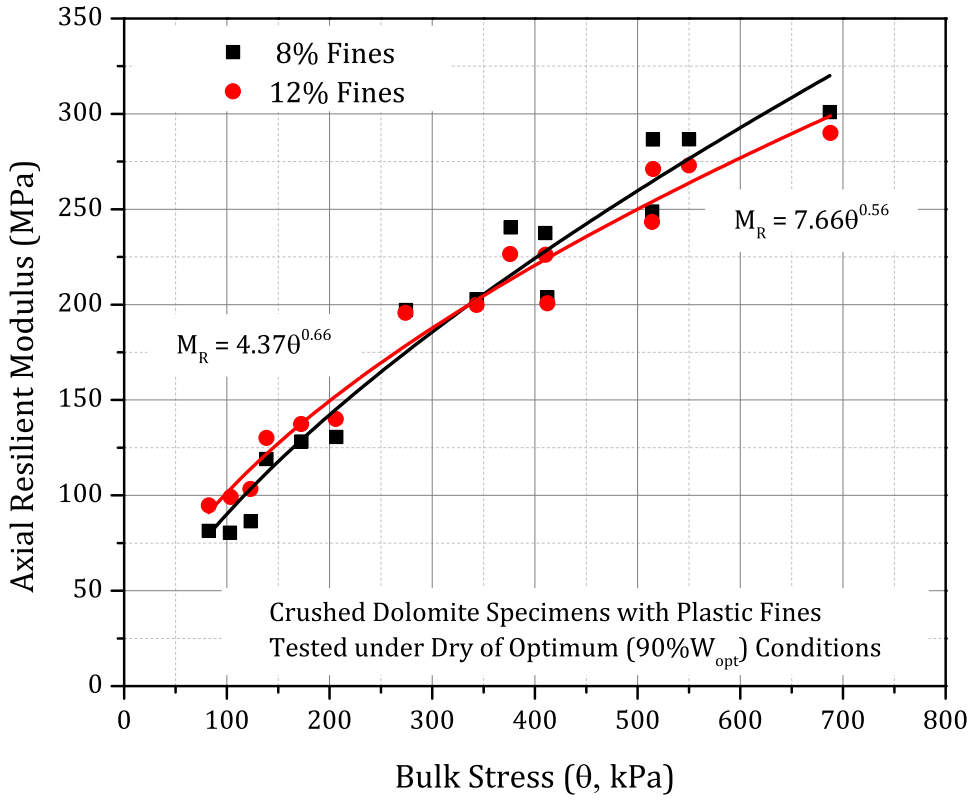


Figure 5.14: Amount of Fines Affecting Resilient Response of Crushed Dolomite Specimens under Dry of Optimum Moisture Conditions

where $M_R$= Resilient modulus;

$\theta = \sigma_d + 3\sigma_3$ = Bulk stress or First Stress Invariant;

$\sigma_d$ = Deviator stress;

$\sigma_3$ = Confining stress;

$\tau_{oct} = \frac{1}{3}\sqrt{(\sigma_1 - \sigma_2)^2 + (\sigma_2 - \sigma_3)^2 + (\sigma_3 - \sigma_1)^2}$ = Octahedral shear stress;

$\sigma_1$ = Major principal stress;

$\sigma_2, \sigma_3$ = Intermediate and Minor principal stresses;

$p_a$= Atmospheric pressure (101.3 kPa, or 14.7 psi);

$p_0$ = Unit pressure;

$K, n$ = Model parameters obtained from linear regression;

$k_x, k_y, k_z$= Model parameters obtained from multiple linear regression

Moreover, permanent deformation test results from the initial conditioning stage of the $M_R$tests were used to develop the commonly used phenomenological model, $\epsilon_p = AN^b$ proposed

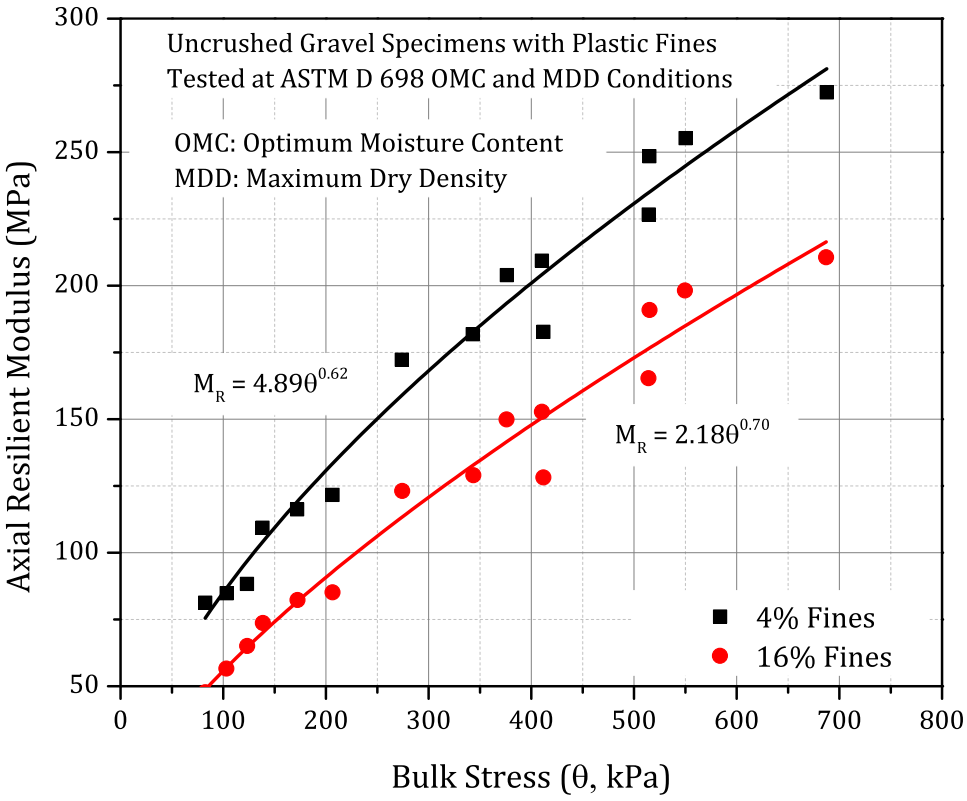


Figure 5.15: Percentage of Fines Affecting Resilient Response of Gravel Material

by Monismith [35], where: $\epsilon_p$ is the permanent strain; N is the number of load applications; A and b are linear regression parameters.

Table 5.1 lists the $M_R$ and $\epsilon_p$ characterization model parameters determined from laboratory testing of the three aggregate types under optimum moisture ($W_{opt}$) conditions. As listed in Table 5.1, the effects of type and amount of fines were different on different material characterization model parameters. The most significant effect was noticed on the $K$ parameter of the K-$\theta$ model, with the value ranging from 1766 kPa to 14,679 kPa. The $n$ parameter varied between 0.464 and 0.767. High values for the $K$ parameter usually corresponded to low values for the $n$ parameter. These results were in agreement with findings by Rada and Witczak [18], who reported an inverse power relationship between $K$ and $n$, where an increase in the $K$ parameter was often accompanied by a reduction in the $n$ parameter. In their comprehensive study of granular material $M_R$ test results, Rada and Witczak [18] reported higher $K$ values of the K-$\theta$ model for "higher quality" granular materials such as crushed stone. As given in Table 5.1, the

highest values for the $K$ parameter (at $W_{opt}$) were obtained for the crushed dolomite with 8% nonplastic fines, whereas the two lowest $K$ values were determined for the uncrushed gravel with 12% nonplastic (1766 kPa) and plastic (1816 kPa) fines. As a crushed dolomite with 8% fines is usually expected to perform better than an uncrushed gravel with 12% fines, the laboratory test results confirmed the trend of higher $K$ values for "better quality" aggregates. Variation in the $k_1$ parameter (MEPDG model) was not as pronounced as the $K$ parameter (K-$\theta$ model).

Table 5.1: Material Characterization Model Parameters under Standard Compactive Effort (ASTM D 698) OMC and MDD Conditions

| Aggregate Type | Aggregate Properties | | Resilient Modulus | | | | | Perm. Deformation | |
|---|---|---|---|---|---|---|---|---|---|
| | Plasticity Index (PI) | Target Fines (%) | K-$\theta$ Model | | MEPDG Model | | | $AN^b$ Model | |
| | | | $K$ (kPa) | $n$ | $k_1$ | $k_2$ | $k_3$ | $A$ (x $10^{-3}$) | $b$ |
| Dolomite | Nonplastic | 4 | 11217 | 0.529 | 1339 | 0.622 | -0.359 | 0.631 | 0.187 |
| | | 8 | 14679 | 0.490 | 1475 | 0.598 | -0.418 | 0.526 | 0.183 |
| | | 12 | 11772 | 0.493 | 1188 | 0.586 | -0.364 | 0.924 | 0.216 |
| | | 16 | 2217 | 0.767 | 814 | 0.908 | -0.550 | 1.483 | 0.281 |
| | Plastic | 4 | 11704 | 0.532 | 1438 | 0.654 | -0.472 | 0.959 | 0.150 |
| | | 8 | 13070 | 0.498 | 1349 | 0.587 | -0.348 | 0.740 | 0.156 |
| | | 12 | Specimen Failed During Testing | | | | | | |
| | | 16 | 5634 | 0.562 | 758 | 0.595 | -0.129 | 1.922 | 0.252 |
| Limestone | Nonplastic | 4 | 12658 | 0.522 | 1455 | 0.609 | -0.340 | 0.454 | 0.172 |
| | | 8 | 11003 | 0.533 | 1343 | 0.639 | -0.416 | 0.507 | 0.171 |
| | | 12 | 12495 | 0.508 | 1345 | 0.591 | -0.322 | 0.552 | 0.180 |
| | | 16 | 11559 | 0.508 | 1239 | 0.581 | -0.283 | 0.860 | 0.174 |
| | Plastic | 4 | Specimen Failed During Testing | | | | | | |
| | | 8 | 11724 | 0.523 | 1380 | 0.640 | -0.455 | 0.640 | 0.168 |
| | | 12 | 13449 | 0.464 | 1182 | 0.547 | -0.322 | 1.104 | 0.163 |
| | | 16 | 11000 | 0.502 | 1151 | 0.585 | -0.323 | 1.093 | 0.170 |
| Gravel | Nonplastic | 4 | 7852 | 0.547 | 1001 | 0.608 | -0.236 | 0.013 | 0.582 |
| | | 8 | 6616 | 0.552 | 874 | 0.634 | -0.317 | 0.953 | 0.149 |
| | | 12 | 1766 | 0.759 | 611 | 0.857 | -0.380 | 1.503 | 0.187 |
| | | 16 | Specimen Failed During Testing | | | | | | |
| | Plastic | 4 | 4880 | 0.620 | 893 | 0.727 | -0.414 | 0.944 | 0.149 |
| | | 8 | 3591 | 0.660 | 788 | 0.761 | -0.392 | 1.077 | 0.154 |
| | | 12 | 1816 | 0.743 | 584 | 0.841 | -0.380 | 1.463 | 0.167 |
| | | 16 | 2185 | 0.703 | 591 | 0.825 | -0.473 | 2.051 | 0.156 |

Figure 5.16 shows the functional relationship between K and n, with a coefficient of determination ($R^2$) value of 0.68, proposed by Rada and Witczak from statistical analyses of

laboratory $M_R$ test results on various aggregate materials [18]. In comparison, the K-n relationship obtained from the current laboratory study can be seen in Figure 5.17 with a coefficient of determination ($R^2$) of 0.92. The significant increase in $R^2$ value over that reported by Rada and Witczak [18] was primarily achieved through elimination of inter-laboratory, inter-equipment and inter-operator variabilities. Existence of such a strong K-$\theta$ model parameter relationship can be particularly useful in pavement structural evaluation and layer moduli estimation through Falling Weight Deflectometer (FWD) based backcalculation algorithms [96]. The functional relationship between model parameters can be used to reduce the number of variables in the backcalculation scheme and thus will enhance the practicality and efficiency of the algorithm. Further, development of such functional relationships for locally available materials can greatly assist transportation agencies in pavement structural condition assessment and design of overlays.

## 5.8 Analyses of Variance on Material Behavior Model Parameters

The previous sections presented the effects of different aggregate physical properties on permanent deformation and resilient modulus behavior of the aggregates tested under the scope of the current research study. A statistical approach for checking the significance of these different aggregate properties on mechanistic response and performance is by conducting Analyses of Variance (ANOVA) on the $M_R$ and $\epsilon_p$ material characterization model parameters. Effects of each of the four classification variables in ANOVA, i.e., aggregate angularity, amount of fines, type of fines, and moisture condition were individually studied on the following model parameters: K, n (K-$\theta$ model), $k_1$, $k_2$, $k_3$ (MEPDG model), and A, b (phenomenological permanent strain model). The statistical software package SAS$^{TM}$ was used for analyzing the data. The effects of individual aggregate properties on any given model parameter were found to be interacting with each other. For example, the effect of amount of fines on the model parameters changed depending on the moisture condition, as well as the type of fines. This is in agreement with some of the results established in the previous sections. Therefore to identify the individual effects of material physical properties on the $M_R$ and $\epsilon_p$ model parameters, each factor was considered separately as classification variables and averaged over all possible combinations of the other properties. The significance of each classification variable was checked at a type-I error level ($\alpha$) of 0.05. Table 5.2 summarizes the findings from the ANOVA results. A cell marked

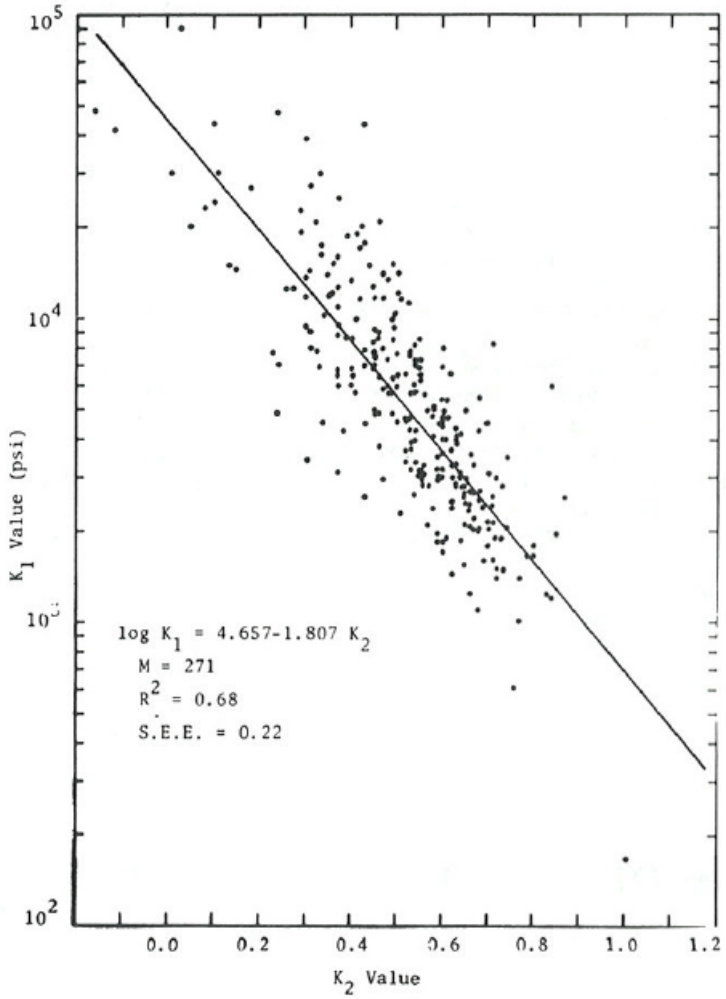


Figure 5.16: Relationship between K and n Parameters of the K- $\theta$ Model Reported by Rada and Witczak [18]

by $\surd$ means that a particular aggregate property had a significant effect on the model parameter in question, whereas a cell marked by '–' means, the effect was insignificant at $\alpha = 0.05$. Main findings from the ANOVA results are discussed below.

### 5.8.1 Particle Shape

ANOVA results for particle shape (crushed vs. uncrushed) showed that both K and $k_1$ parameters are affected significantly by particle shape. In other words, the K and $k_1$ values for crushed aggregates were significantly different (higher in this case) than those for the uncrushed gravel. This observation was in agreement with previously reported research findings [11, 62, 68].

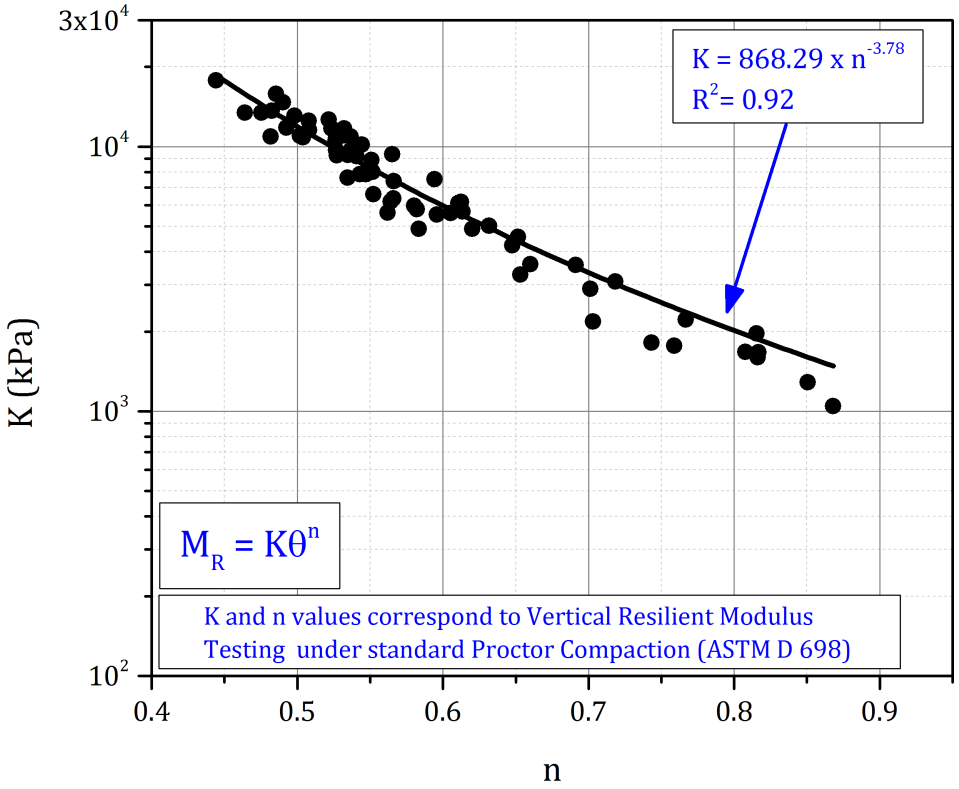


Figure 5.17: Relationships between K and n Parameters of the K- $\theta$ Model Developed from the Laboratory Test Results on Uncrushed Gravel, and Crushed Limestone and Dolomite Materials

Table 5.2: Significance of Aggregate Properties Affecting Resilient Modulus and Permanent Deformation Model Parameters

| | $M_R = K\left(\frac{\theta}{p_0}\right)^n$ | | $M_R = k_1 p_a \left(\frac{\theta}{p_a}\right)^{k_2} \left(\frac{\tau_{oct}}{p_a} + 1\right)^{k_3}$ | | | $\varepsilon_p = AN^b$ | |
|---|---|---|---|---|---|---|---|
| Aggregate Property | K | n | $k_1$ | $k_2$ | $k_3$ | A | b |
| Particle Shape | √ | — | √ | — | — | — | — |
| Compaction Moisture Condition | — | — | — | — | √ | — | √ |
| Fines Content | — | — | — | — | — | √ | — |
| Plasticity of Fines | — | — | — | — | — | √ | √ |
| Low vs. High Fines | — | — | √ | — | — | √ | — |

√: Significant Effect at $\alpha = 0.05$

Unbound aggregate layers having crushed particles have been consistently found to perform superior compared to those with uncrushed particles in terms of providing a stiffer layer for load distribution. However, particle shape was not found to have a significant effect on the permanent deformation model parameters (A and b).

### 5.8.2 Fines Content

The effect of fines content (4%, 8%, 12%, and 16%) on $M_R$ model parameters was found to be insignificant from the ANOVA results. However, fines content did have a significant effect on the "A" parameter used to characterize permanent deformation. This was in agreement with the permanent deformation results presented earlier in this chapter; a drastic change in permanent deformation accumulation occurred with changes in fines contents. The ANOVA results emphasize the point that although an increase in fines content may not lead to significant differences in the resilient modulus behavior (and hence the layer's ability to protect the subgrade), it can still lead to unacceptable permanent deformation within the aggregate layer leading to internal shear failure [88, 97].

### 5.8.3 Plasticity of Fines

Similar to the amount of fines, plasticity of fines did not have a significant effect on the $M_R$ model parameters. However, its effect on permanent deformation model parameters (both A and b in this case) was found to be quite significant. This means, although plastic fines may not influence the stiffness of an aggregate layer significantly, they will lead to high shear deformations within the aggregate layer, resulting in excessive rutting and potential bearing capacity type shear failures at extreme conditions.

### 5.8.4 Low vs. High Fines

Based on the laboratory test results, different threshold values for the amount of fines were set for crushed and uncrushed aggregates to define "low" and "high" fines contents. For crushed aggregates (dolomite and limestone), specimens with up to 8% fines were categorized as having "low" fines, whereas for the uncrushed gravel, specimens with only up to 4% fines was categorized as "low" fines. This was based on the apparent stabilization effect around 8% fines for crushed

materials, and the absence of such effect in uncrushed gravel as shown in Figures 5.4 and 5.7. ANOVA results showed that materials with "low" vs. "high" fines exhibited significantly different $k_1$ and A values. This means, based on the stability of the aggregate matrix, unbound aggregate layers in the field would show significantly different modulus and permanent deformation trends. Such a classification to distinguish between aggregate matrices with "low" vs. "high" fines can be used in the development of material quality specifications used by state and national transportation agencies.

## 5.9 Aggregate Physical Properties Affecting Modulus Anisotropy

This section investigates the effects of aggregate physical properties (test factors) on modulus anisotropy of the aggregate materials. As already mentioned in Section 5.5, directional modulus tests were successfully used in the past to develop horizontal to vertical modulus ratios for different qualities of aggregates and relate them to strength characteristics [91, 92, 95].

### 5.9.1 Effect of Particle Shape and Angularity

Figures 5.18 and 5.19 show the vertical and horizontal directional modulus values for the crushed dolomite and uncrushed gravel materials respectively, both containing 8% (target) nonplastic fines tested under optimum moisture ($W_{opt}$) conditions. The vertical moduli are indicated with solid lines and the horizontal moduli with dashed lines at each of the 5 AASHTO T 307 [90] confining pressure values (all around hydrostatic pressure, $\sigma_s$). From the figures, it can be seen that for both the materials, the vertical modulus values were consistently higher than the horizontal ones. Moreover, the modulus values for the crushed dolomite material were consistently higher than those for the uncrushed gravel. The horizontal modulus values for the uncrushed gravel with 8% nonplastic fines decreased with increasing deviator stresses (stress-softening behavior), whereas no such significant decrease in horizontal moduli was observed for the crushed dolomite (see Figure 5.18). This behavior may be attributed to the low amount of voids in the uncrushed gravel matrix thus showing low tolerance to fines contents. Note that permanent deformation test results reported earlier in Section 5.4 showed that increasing fines content from 4% to 8% had detrimental effects on performance of the uncrushed gravel material. However, both the dolomite and gravel specimens showed higher vertical moduli compared to the horizontal ones, which has

been established in literature, as an indicator of material quality [91]. From Figures 5.18 and 5.19, it was apparent that crushed aggregates with "low" fines showed consistently higher vertical moduli and non-decreasing horizontal moduli with increasing deviator stress levels, compared to uncrushed aggregates with the same amount of fines.

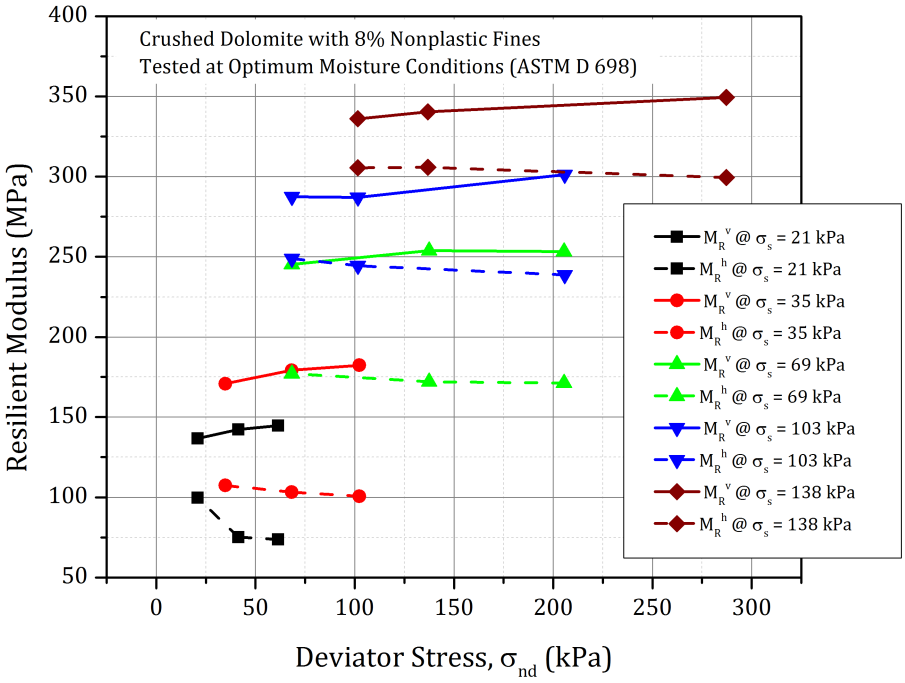


Figure 5.18: Vertical and Horizontal Modulus Results for the Crushed Dolomite Material with 8% Target Nonplastic Fines Tested at $W_{opt}$(Solid Lines: $M_R^v$; Dashed Lines: $M_R^h$)

### 5.9.2 Effect of High Amounts of Plastic Fines

Figures 5.20 and 5.21 show the directional moduli determined for the crushed dolomite and uncrushed gravel specimens respectively, this time both containing 16% plastic fines tested at dry of optimum. Both Figures 5.20 and 5.21 show the horizontal modulus values (dashed lines) consistently decreasing with an increase in deviator stress, which is a typical stress-softening modulus behavior of fine-grained soils or poor quality aggregate materials with excessive fines. This emphasizes the detrimental effect of high amounts of plastic fines on aggregate performance. Comparing Figures 5.18 and 5.20, the detrimental effect of high amounts of plastic fines on aggregate behavior can be clearly deduced. Note that for the crushed dolomite specimen with 8% nonplastic fines tested at optimum moisture contents (see Figure 5.18), the horizontal modulus

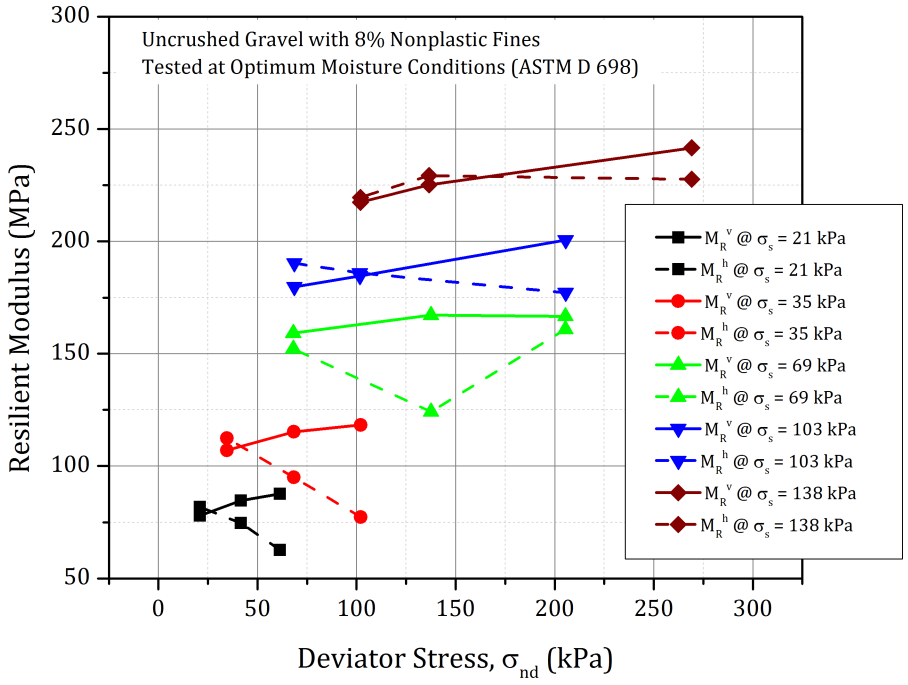


Figure 5.19: Vertical and Horizontal Modulus Results for the Uncrushed Gravel Material with 8% Target Nonplastic Fines Tested at $W_{opt}$(Solid Lines: $M_R^v$; Dashed Lines: $M_R^h$)

values did not show significant stress-softening behavior.

For the uncrushed gravel specimen with 16% plastic fines (see Figure 5.21), the horizontal modulus values showed clear stress-softening behavior. Moreover as shown in Figure 5.21, the horizontal moduli were consistently higher than the vertical ones. Note that Seyhan and Tutumluer [91] suggested higher vertical moduli than horizontal moduli as an indicative trend for identifying "good quality" aggregate materials. Higher horizontal moduli reported for the uncrushed gravel specimen in Figure 5.21 therefore illustrates "poor" aggregate matrix behavior.

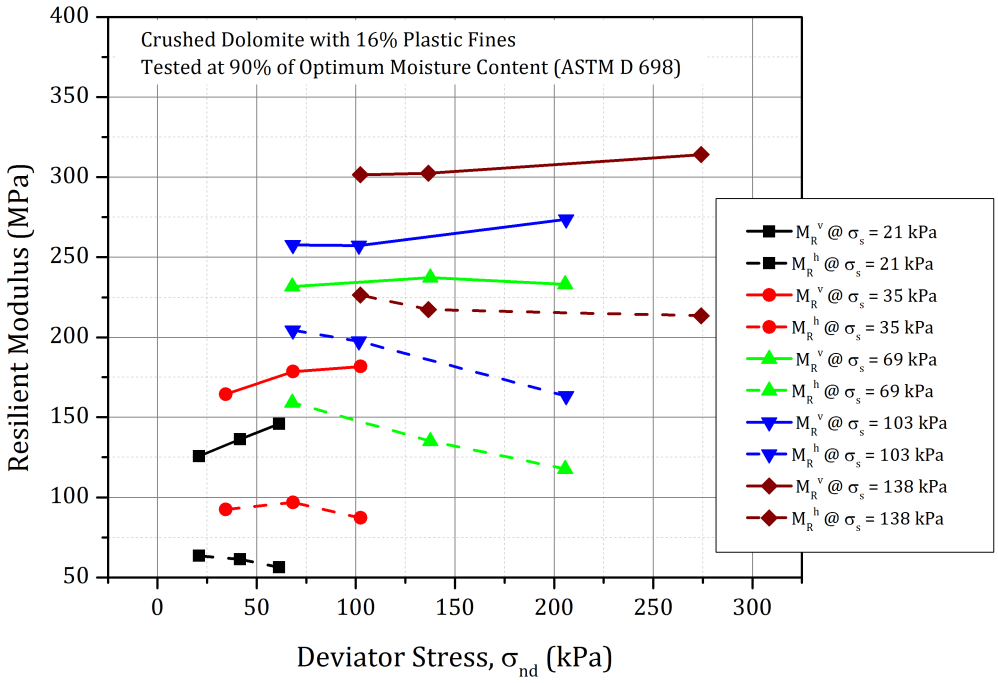


Figure 5.20: Vertical and Horizontal Directional Modulus Results for Dolomite with 16% Target Plastic Fines Tested at 90% $W_{opt}$(Solid Lines: $M_R^v$; Dashed Lines: $M_R^h$)

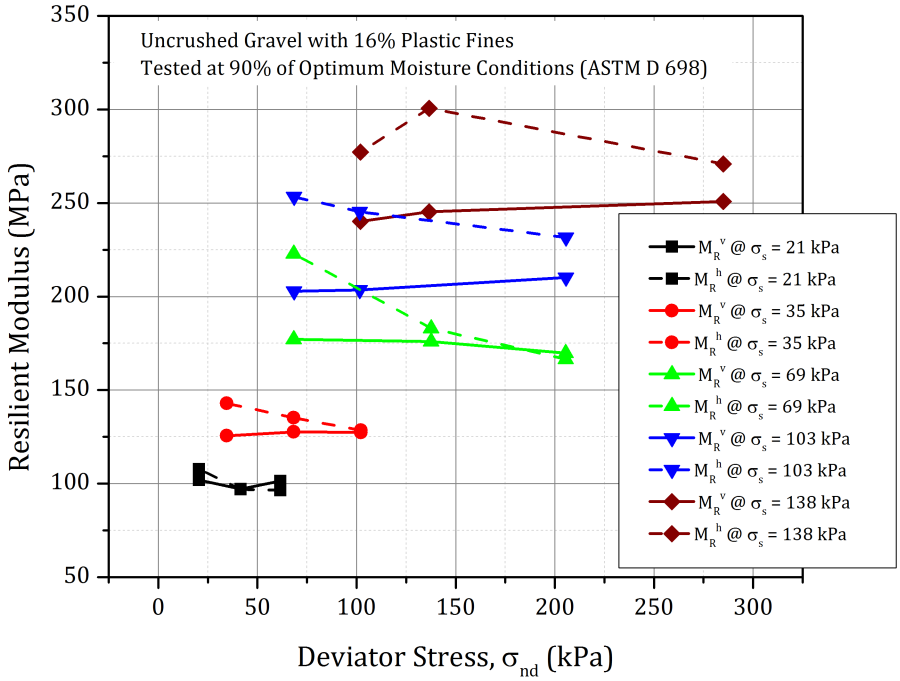


Figure 5.21: Vertical and Horizontal Directional Modulus Results for Gravel with 16% Target Plastic Fines Tested at 90% $W_{opt}$(Solid Lines: $M_R^v$; Dashed Lines: $M_R^h$)

## 5.10 Effect of Compactive Effort on Modulus Anisotropy

A secondary objective of this research study was to evaluate the effects of compactive effort on anisotropic modulus ratios. Accordingly, four different aggregate materials were tested for directional modulus characteristics under different compaction conditions to establish a link between anisotropic modulus ratios and compactive energy levels. Note that the first task to achieve this objective involved development of compaction curves for different aggregate types using both standard as well as modified compactive efforts. As previously mentioned, laboratory testing of aggregates at different combinations of the test factors under the scope of this research study only focussed on standard compaction (ASTM D 698) conditions. Developing new sets of compaction curves using the modified compactive effort for all the different test factor combinations was not feasible as far as time and testing effort requirements were concerned since it required extensive effort in the laboratory to prepare specimens through engineered gradations. It was therefore decided to study the effect of compaction levels on modulus anisotropy using four representative dense graded aggregates. Table 5.3 presents the fines contents and compaction characteristics of the four different aggregate materials.

Table 5.3: Aggregate Materials Tested in the Laboratory for Evaluating the Effects of Compaction Conditions on Anisotropic Modulus Ratio

| Material Description | Fines Content (%) | Compaction Characteristics | | | |
|---|---|---|---|---|---|
| | | Standard Compaction | | Modified Compaction | |
| | | OMC (%) | MDD ($kN/m^3$) | OMC (%) | MDD ($kN/m^3$) |
| Crushed Limestone (L1) | 12 | 6.2 | 22.3 | 5.3 | 23.0 |
| Crushed Dolomite | 13 | 7.7 | 22.2 | 5.5 | 22.4 |
| Uncrushed Gravel | 12 | 8.6 | 21.4 | 8.2 | 22.0 |
| Crushed Limestone (L2) | 10 | 8.1 | 22.1 | 5.7 | 22.6 |

Three of the four materials listed in Table 5.3 (except for the crushed limestone with 12% fines, designated as 'L1') were used in the construction of full-scale unsurfaced pavement sections for accelerated testing. Directional modulus tests were conducted on triaxial specimens prepared using the four aggregate material types compacted to different densities. Note that the crushed limestone (L1) and uncrushed gravel materials, both with 12% fines, showed unstable matrix behavior under standard compactive effort (ASTM D 698) optimum moisture content (OMC or $W_{opt}$) and maximum dry density (MDD) conditions. Therefore, the effect of compactive effort

on modulus anisotropy was studied for these two materials by testing specimens under modified and intermediate (in between standard and modified) compaction conditions.

Figure 5.22 shows the effect of compactive effort on the anisotropic modulus ratios of the crushed limestone (L1) with 12% fines. The intermediate compaction conditions for this material were selected from the "line of optimums" obtained from the standard and modified compaction curves. The anisotropic modulus ratio trends at different compaction levels were compared at three representative stress states applied on the specimen during resilient modulus testing following the AASHTO T 307 test protocol. Based on the stress levels applied on the specimens, the three stress states were termed as "Low" ($\sigma_s = 35$ kPa; $\sigma_{nd} = 69$ kPa), "Intermediate" ($\sigma_s = 69$ kPa; $\sigma_{nd} = 138$ kPa) and "High" ($\sigma_s = 138$ kPa; $\sigma_{nd} = 276$ kPa) respectively, where $\sigma_s$ is the all-round hydrostatic confining pressure, and $\sigma_{nd}$ is the pulsed deviator stress (n = 1 for vertical pulsing, and 3 for horizontal pulsing).

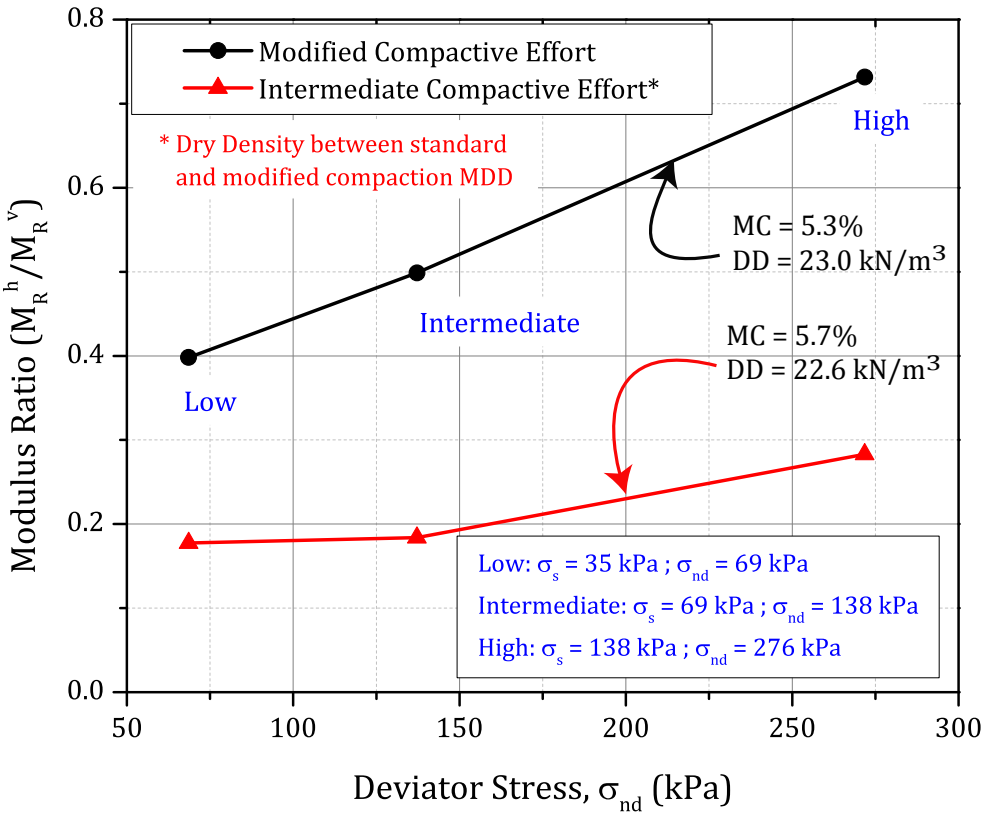


Figure 5.22: Effect of Compactive Effort on Anisotropic Modulus Ratio of the Crushed Limestone Material (L1) with 12% Fines

From Figure 5.22, the anisotropic modulus ratios clearly increased as the compactive effort was increased from intermediate to modified compaction conditions. Moreover for a given compactive effort, the modulus ratio showed an increasing trend with increase in the deviator stress values. Seyhan and Tutumluer [91] reported increasing modulus ratio trends with increase in stress levels for good quality materials, whereas poorer quality materials showed an overall decrease in modulus ratios with increasing deviator stress levels. It is also important to note that the modulus ratios for both the intermediate and modified compactive efforts showed values less than unity, which has also been established in the literature as a threshold value separating "good" and "poor" quality materials [92].

Figure 5.23 shows a similar trend for the crushed dolomite material with 13% nonplastic fines (modulus ratios increased as the compaction level was increased). This was particularly apparent for the intermediate and high stress states. Moreover, it is important to note that the modulus ratios did not increase significantly with increasing deviator stress levels for the specimen compacted to standard compactive effort maximum dry density. Higher modulus ratios and a higher rate of increase in modulus ratio with increasing stress levels illustrated better performance of the specimen prepared using the modified compactive effort.

As already mentioned, the uncrushed gravel material with high fines showed unstable matrix behavior under standard compaction conditions, and therefore could not be tested for directional modulus characteristics. As permanent deformation test results reported earlier in this chapter clearly established the detrimental effects of moisture on the behavior of uncrushed gravel specimens with high fines, it was decided to prepare specimens targeting the standard compactive effort maximum dry density, but at reduced moisture contents. Several specimens were prepared at the standard compaction (ASTM D 698) MDD (21.4 kN/m$^3$or 136.4 pcf), with progressively lower moisture contents. Stable behavior for the matrix was observed at a moisture content equal to 60% of the standard compaction OMC value of 8.6%.

As the objective was to evaluate the effects of compactive effort on anisotropic modulus ratios, it was decided to compare the resilient response of specimens at the following compaction conditions: Dry density equal to 22.0 kN/m$^3$(140.3 pcf) at a moisture content of 8.2% (modified compactive effort OMC and MDD), and Dry density equal to 21.4 kN/m$^3$(136.4 pcf) at a moisture

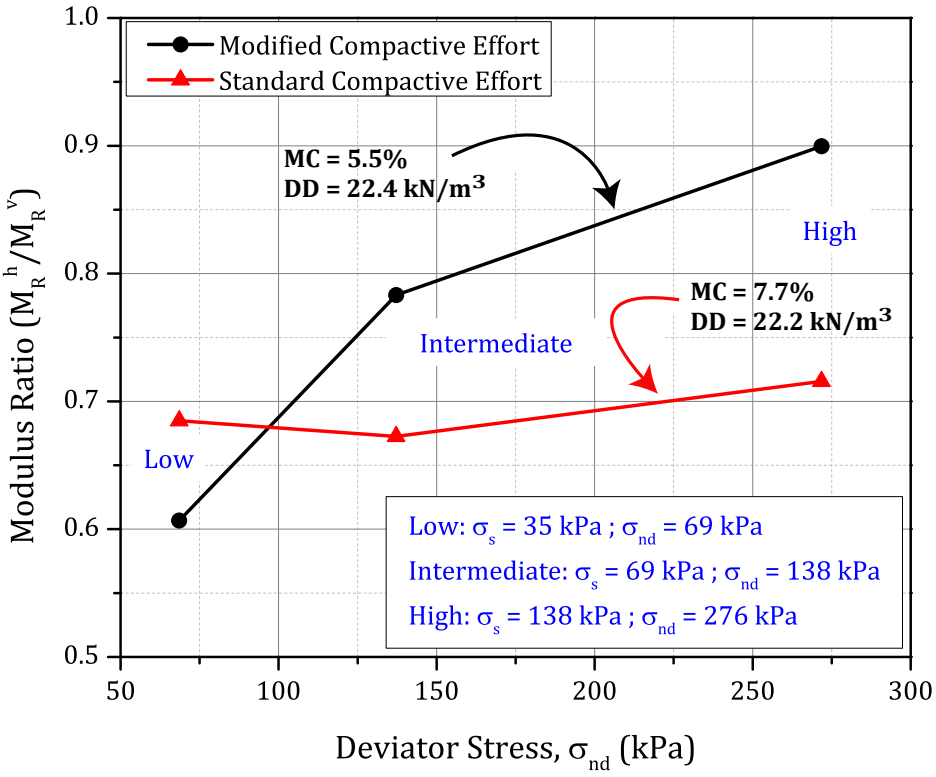


Figure 5.23: Effect of Compactive Effort on Anisotropic Modulus Ratio of the Crushed Dolomite Material with 13% Fines

content of 5.2% (standard compaction MDD, at 60% OMC). Figure 5.24 illustrates the effect of compaction conditions on anisotropic modulus ratios for the uncrushed gravel with 12% fines. As shown in the figure, the specimen compacted to modified compactive effort MDD had lower modulus ratios compared to the one compacted to standard compaction MDD. Both specimens showed increasing trends for the modulus ratios with increase in the deviator stress level.

One important observation needs to be made from the trends shown in Figure 5.24. Although the specimen compacted to modified compactive effort MDD had a higher density, it showed lower modulus ratios than the specimen at standard compaction MDD. This was was attributed to the higher moisture contents corresponding to the former (8.2% compared to 5.2%). Although higher compaction densities usually lead to better performance under loading, moisture content plays a critical role in governing the behavior of uncrushed gravel materials with high fines. Therefore among the specimens compared for directional modulus characteristics, amount of moisture in the matrix was the primary factor governing aggregate behavior. As a result, the

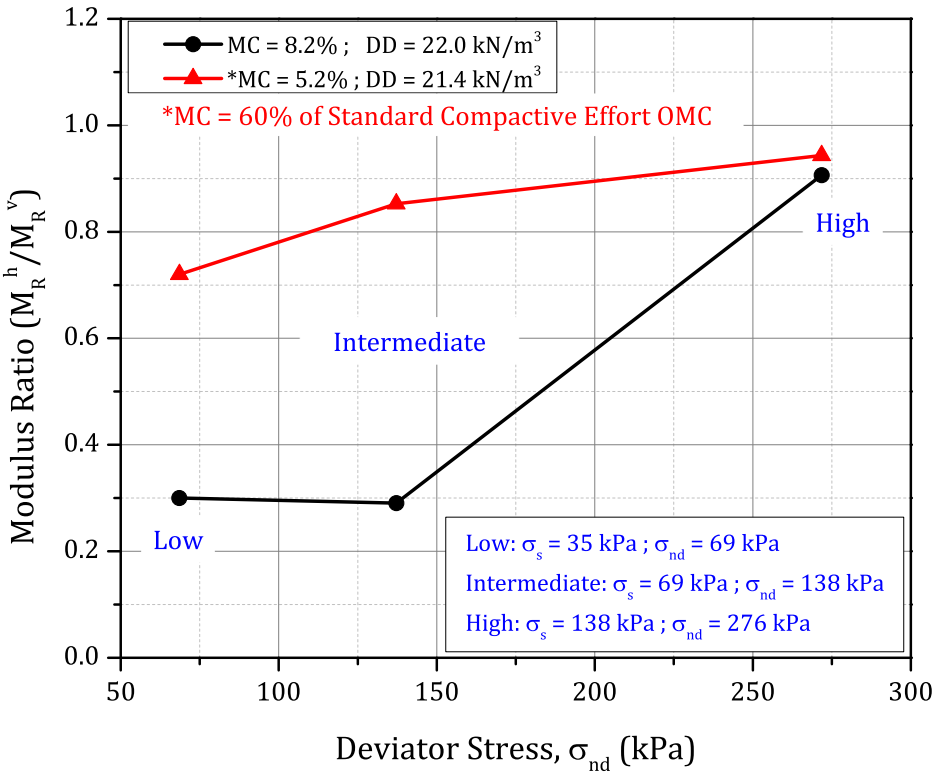


Figure 5.24: Effect of Compactive Effort on Anisotropic Modulus Ratio of the Uncrushed Gravel Material with 12% Fines

specimen at standard compactive effort MDD and a moisture content of 5.2% indicated higher modulus ratios than the other.

As permanent deformation behavior is often considered the primary indicator of aggregate performance under loading, the permanent deformation trends of the two uncrushed gravel specimens obtained from the conditioning phase of AASHTO T 307 procedure were next compared (see Figure 5.25). As shown in the figure, the specimen with lower amount of moisture in the matrix accumulated significantly lower permanent deformations, which could be directly linked to the reported trends in anisotropic modulus ratios.

Figure 5.26 shows the effect compactive energy on the crushed limestone (L2) material with 10% fines. An interesting trend was observed upon comparing the modulus ratios of specimens compacted to standard and modified compactive effort (ASTM D 698 and ASTM D 1557, respectively) maximum dry densities (MDD). The specimen tested at standard compaction

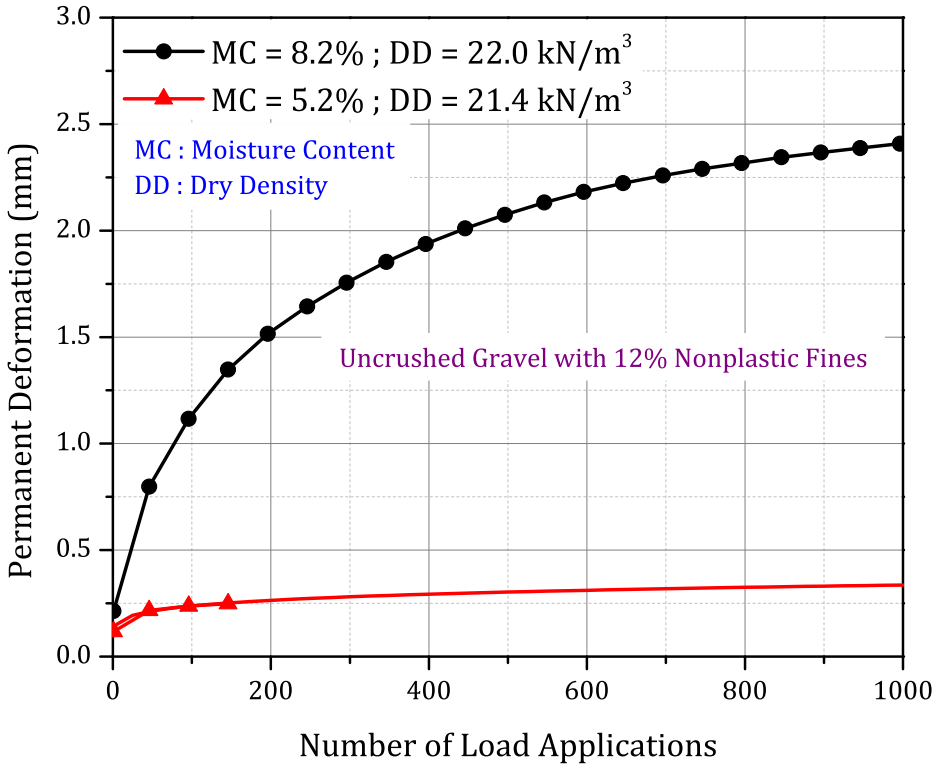


Figure 5.25: Permanent Deformation Trends of Uncrushed Gravel Material with 12% Fines at Different Compaction Conditions

maximum dry density showed consistently higher modulus ratios compared to the one at modified compaction MDD (see Figure 5.26). As higher modulus ratios usually correspond to "better" quality aggregates, this would indicate that for the crushed limestone (L2) with 10% fines, specimens under standard compactive effort MDD should perform "better" than specimens under modified compaction MDD. This was verified by comparing permanent deformation trends for specimens compacted to standard as well as modified compactive effort optimum moisture content and maximum dry densities (see Figure 5.27). As shown in Figure 5.27, the specimen tested under standard compaction OMC and MDD conditions showed lower permanent deformation accumulation than the one compacted to modified compaction OMC and MDD conditions. This could be the result of some dilative behavior within the aggregate matrix. Nevertheless, combined analyses of Figures 5.26 and 5.27 illustrate the link between anisotropic modulus ratio and performance (permanent deformation) trends.

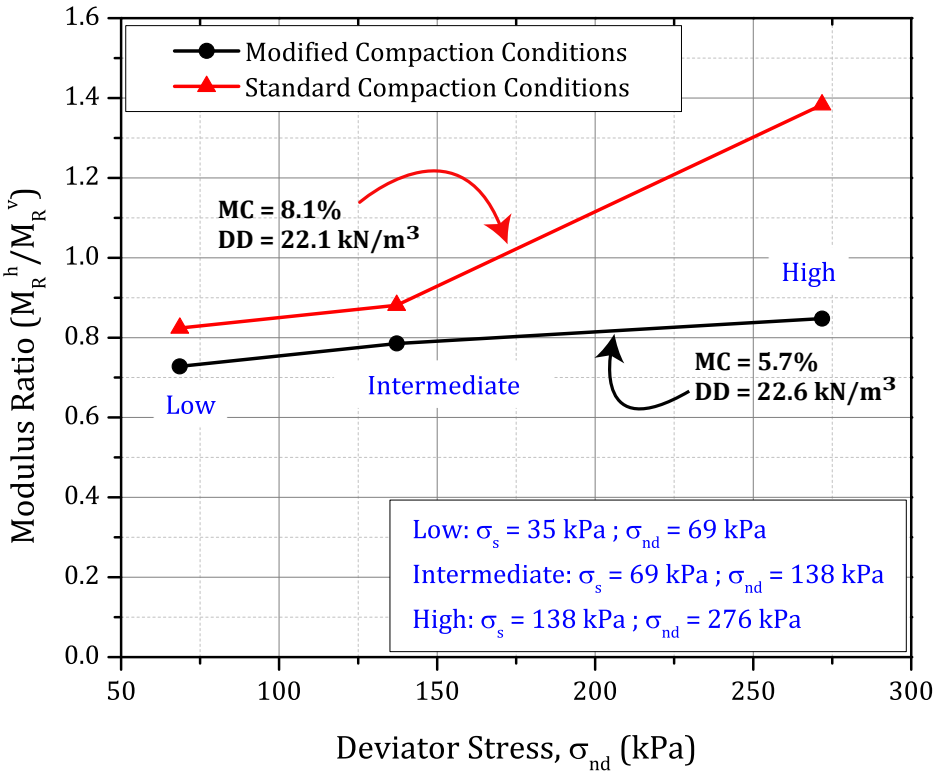


Figure 5.26: Effect of Compactive Effort on Anisotropic Modulus Ratio of the Crushed Limestone Material (L2) with 10% Fines

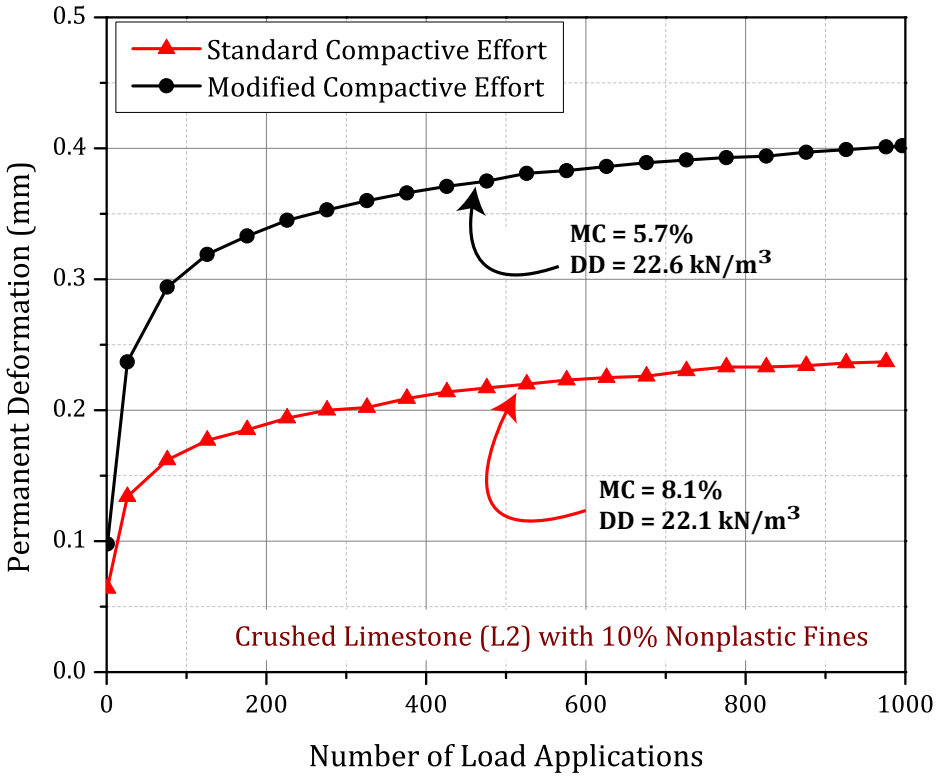


Figure 5.27: Permanent Deformation Trends of the Crushed Limestone Material (L2) with 10% Fines under Different Compaction Conditions

## 5.11 Summary

This chapter reported results from repeated load triaxial tests conducted on the three aggregate materials to characterize their permanent deformation and directional modulus behaviors under different combinations of the test factors. From the permanent deformation and directional modulus results, it appeared that the most important test factor governing aggregate behavior at low fines contents was the aggregate type governing the angularity, i.e. crushed or uncrushed particles. Unless all voids in aggregate matrix were completely filled with fines, particle angularity, i.e. crushed or uncrushed particles, typically governed the modulus and deformation behavior. This pattern was the most noticeable from permanent deformation tests. The second most important parameter that affected aggregate behavior was the plasticity of fines. High amounts of plastic fines at wet of optimum moisture conditions were found to quickly destroy the aggregate load transfer matrix thus resulting in excessive permanent deformations.

As far as resilient behavior was concerned, the crushed aggregates performed better than the uncrushed gravel. However at very low values of applied bulk stress, there was not much difference between crushed and uncrushed aggregates. Increasing the amount of fines did not result in significant decreases in aggregate modulus and deformation behavior in the case of nonplastic fines. However for plastic fines, the amount of fines had a drastic effect on aggregate performance. Moreover, small changes in the amount of fines did not affect the resilient modulus behavior significantly, although there were often significant differences in the modulus values when very low and very high, i.e. extreme, fines contents were evaluated.

The effect of moisture content on aggregate performance varied significantly depending on the amount and plasticity of fines. For low percentages of nonplastic fines, moisture content did not have a significant effect on aggregate performance, and often aggregate type or angularity was the most important factor. However, for aggregates with plastic fines, moisture was the most important factor governing aggregate behavior. Moisture when combined with plastic fines created the worst effect.

The horizontal to vertical modulus ratios determined from directional resilient modulus tests adequately indicated the excessive amount of fines affecting aggregate quality. Anisotropic modulus ratios for "good quality" materials typically showed increasing trends with increasing

deviator stress levels, and the horizontal moduli were consistently lower than vertical moduli. Combined analyses of permanent deformation and directional modulus test results established the applicability of anisotropic modulus ratio as a material quality indicator.

# CHAPTER 6

# DESIGN & CONSTRUCTION OF FULL-SCALE TEST SECTIONS

## 6.1 Introduction

This chapter describes the design and construction of full-scale unsurfaced pavement sections for accelerated pavement testing and verification of the laboratory test results presented in Chapters 4 and 5. Full-scale unsurfaced pavement sections were constructed over a weak subgrade of controlled strength through field CBR checks to evaluate the effects of different aggregate physical properties (test factors) on performance. Selection of aggregate types representing different combinations of the test factors under investigation is discussed and followed by laboratory characterization of individual aggregate types used for constructing the test sections. Typical trends observed in the material behavior during laboratory experimentation are used later in Chapter 8 to justify the test section performance under loading. The use of finite element analysis for thickness design of typical unsurfaced pavement sections is explained along with the effect of different aggregate physical characteristics (test factors) on critical pavement response parameters. Details of test section layout and construction procedure are subsequently reported along with subgrade characterization and engineering through moisture addition.

## 6.2 Experimental Design through Material Selection

To verify the laboratory test results reported in Chapters 4 and 5, full scale unsurfaced pavement sections were constructed with aggregate types representing different combinations of the test

This chapter includes results already reported in the following publication. Contribution of the coauthor is sincerely acknowledged:

1. *Mishra, D., and Tutumluer, E.;"Aggregate Physical Properties Affecting Modulus and Deformation Characteristics of Unsurfaced Pavements"; Accepted for Publication in the ASCE Journal of Materials in Civil Engineering (Original Submission: March-2011).*

factors over a weak subgrade of controlled strength. As described in Chapter 3, the test factors selected for investigation in this research study were: (1) Particle shape, texture and angularity, (2) fines content (defined as material finer than 0.075 mm), (3) plasticity of fines (measured on material finer than 0.425 mm), and (4) compaction (moisture-density) conditions.

The number of full-scale pavement sections needed for a complete factorial evaluation of the aggregate characteristics of interest was not feasible as far as space requirements and construction costs were concerned. It was therefore decided to construct a limited number of full-scale test sections using aggregate materials representing extreme boundaries of the test factors. For example, the effect of fines content on aggregate behavior was significant only when two aggregate types representing extreme boundaries of the allowable fines contents were compared. Similarly, the behavior of crushed limestone and dolomite were similar, and showed significant difference only when compared to uncrushed gravel. Therefore small differences in aggregate shape, texture and angularity characteristics (limestone showed slightly higher AI and ST values) were not clearly reflected from the strength, permanent deformation, and resilient modulus test results. Moreover, the effect of moisture on aggregate behavior was significant only when moisture content of the samples varied significantly. Based on the above observations, the following material types were selected for constructing the full-scale test sections.

**Material No. 1** Uncrushed "river-run" gravel with high amounts of nonplastic fines

**Material No. 2** Crushed limestone with high amounts of plastic fines

**Material No. 3** Crushed dolomite with high amounts of nonplastic fines

**Material No. 4** Crushed limestone with low amounts of nonplastic Fines

Selection of the above four materials ensured comparison of the following test factors affecting aggregate behavior. The effect of aggregate angularity could be studied through comparison of materials 1 with 2 and/or 3. The effect of fines content could be studied by comparing materials 3 and 4. Similarly, the effect of type of fines on aggregate behavior could be studied by comparing materials 2 and 3. Moreover, the effect of moisture on aggregate behavior was evaluated by testing each of the four aggregate types under two different moisture conditions.

Table 6.1: Type and Amount of Fines in the Four Aggregate Materials Received for use in Construction of the Test Sections

| **Material Number** | **Material Description** | **Fines Content** (%) **(Sample 1 & Sample 2)** | **Plasticity Index (%)** |
|---|---|---|---|
| 1 | Uncrushed Gravel | 11.7 & 12.9 | 0.0 |
| 2 | Crushed Limestone | 5.0 & 5.3 | 5.7 |
| 3 | Crushed Dolomite | 11.5 & 14.0 | 0.0 |
| 4 | Crushed Limestone | 9.0 & 10.9 | 0.2 |

## 6.3 Laboratory Characterization of Aggregates used in Test Sections

Based on a preliminary survey of potential aggregate sources around the state of Illinois, the four aggregate types listed above were identified and obtained for laboratory characterization and field construction. Upon receiving the materials from the respective sources, the first task involved in-depth laboratory characterization of each aggregate type for determination of their physical and mechanical properties. Preliminary tests were conducted on each material type to determine its particle size distribution (AASHTO T 11), Atterberg limits (ASTM D 4318), compaction characteristics (ASTM D 698, ASTM D 1557), and unsoaked CBR (ASTM D 1883). Repeated Load Triaxial (RLT) tests were conducted following the AASHTO T 307 test protocol to characterize their permanent deformation and resilient modulus behavior. Findings from laboratory testing of the four aggregate materials are reported in the following sections along with figures highlighting important trends. Additional figures and test results are presented in Appendix B.

### 6.3.1 Particle Size Distribution, Atterberg Limits and X-Ray Diffraction

Washed sieve analysis (AASHTO T 11) and Atterberg limit (ASTM D4318) tests were first conducted on the four aggregate materials and a summary of the results is provided in Table 6.1. The most significant difference between "quarry reported" and "actual" fines contents was observed for material no. 2 which had significantly lower fines (5.2%) as compared to the initially reported value (∼12%). Moreover, material no. 4 had approximately 10% fines, which was higher than the threshold value of 8% recommended in Chapter 5 and reported in literature [60, 91] as the boundary to separate "high fines" from "low fines" for crushed aggregates. It was therefore decided to categorize materials 2 and 4 as "low fines" and "high fines", respectively. Table 6.2 lists the final designations of the materials used in construction of the test sections. It should be

Table 6.2: Material Specifications for the Four Aggregate Types used to Construct the Full-Scale Test Sections

| **Material Number** | **Aggregate Material Type** |
|---|---|
| 1 | Uncrushed Gravel with High Amounts of Nonplastic Fines |
| 2 | Crushed Limestone with Low amounts of Plastic Fines |
| 3 | Crushed Dolomite with High Amounts of Nonplastic Fines |
| 4 | Crushed Limestone with High Amounts of Nonplastic Fines |

noted that the "as-constructed" designations for materials 2 and 4 listed in Table 6.2 are different from those originally identified in Section 6.2. Because of the difference in material classification of the actual aggregates used in construction from those listed in Section 6.2, the effect of aggregate angularity was now evaluated through comparison of materials 1 and 3. Materials 3 and 4 were both classified as "high fines", and therefore any difference in aggregate behavior was attributed to the slight difference (∼2%) in fines contents. Material no. 2 (crushed limestone with ∼5% fines) was the only aggregate type received with plastic fines (PI = 5.7). However, as observed from laboratory testing of aggregates during the first phase of the study (refer to Chapters 4 and 5), the effect of plasticity of fines on crushed aggregate behavior was significant only at high fines contents; crushed aggregate specimens with nonplastic and plastic fines showed similar behavior at fines contents below 8%. Therefore, it would appear that the low amount of plastic fines would not have a significant effect on performance of the crushed limestone (material no. 2). Therefore, no two material types used for constructing the full-scale test sections could be compared to assess the effect of fines plasticity on unsurfaced pavement performance.

X-ray diffraction (XRD) tests were conducted on the fine fraction (passing No. 200 sieve, or finer than 0.075 mm) of the four aggregate materials to determine the predominant mineral type in each. This was particularly important to account for trends in aggregate layer performance that could be affected by differences in aggregate mineralogy. XRD scan results showed that materials 1 and 3 were predominantly dolomite, whereas materials 2 and 4 primarily comprised limestone (calcite) minerals. Individual XRD test results for the four aggregate types are presented in Appendix B. Note that the presence of quartz in all the four aggregate materials was a common feature.

Table 6.3: Compaction Characteristics of Aggregates used for Constructing the Full-Scale Test Sections

| **Material Number** | **Standard Compactive Effort** | | **Modified Compactive Effort** | |
|---|---|---|---|---|
| | OMC (%) | MDD (kN/m$^3$) | OMC (%) | MDD (kN/m$^3$) |
| 1 | 8.6 | 21.4 | 8.2 | 22.0 |
| 2 | 6.5 | 18.1 | 7.3 | 21.5 |
| 3 | 7.7 | 22.2 | 5.5 | 22.4 |
| 4 | 8.1 | 22.1 | 5.7 | 22.6 |

### 6.3.2 Compaction Characteristics and Unsoaked CBR

The four aggregate materials were tested in the laboratory for compaction characteristics using both standard (ASTM D 698) and modified (ASTM D 1557) compactive efforts. A summary of the optimum moisture content (OMC) and maximum dry density (MDD) values determined from both methods is presented in Table 6.3. After compaction, each specimen was penetrated by a circular plunger of 19.4 cm$^2$ (3 in$^2$) area at a rate of 1.27 mm/min (0.05 in./min) to determine the unsoaked CBR (ASTM D 1883) values. Individual curves showing the variation of dry density and unsoaked CBR with moisture content are presented in Appendix B.

As shown in Table 6.3, the OMC for material 2 (crushed limestone with low fines) under modified compaction conditions was higher than that determined using the standard compactive effort (7.3% compared to 6.5%). This was in contradiction with commonly observed trends for compaction curves which show a decrease in OMC with increased compactive effort. This discrepancy was primarily attributed to the low fines content ($\sim$ 5%) in the material which resulted in a free-draining aggregate matrix not capable of retaining moisture. Therefore, obtaining consistent compaction curves for this material was not possible, and the OMC and MDD values were determined from the best possible smooth curve joining individual data points. At this point, it is important to emphasize the inadequacy of the "impact hammer" method for determining the compaction characteristics of open graded and uniformly graded materials.

Two important observations can be made from Figure 6.1 that shows the change in unsoaked CBR values of the four aggregate materials with moisture content under standard compaction conditions. Firstly, for the uncrushed gravel with 12% fines (material 1), the CBR value decreased rapidly with increase in moisture even on the dry side of OMC. This reinforces findings from the laboratory tests reported in Chapter 5 regarding the high moisture sensitivities of

uncrushed aggregates with high fines. Secondly, material no. 2 (crushed limestone with 5% fines) did not show any significant change in CBR values with increasing moisture content. This was attributed to the free-draining nature of the material, and will be used later in Chapter 8 to analyze the effect of flooding on the performance trends of unsurfaced pavement sections constructed using this material. Moreover, the lack of fines in material no. 2 resulted in an unstable aggregate matrix under standard compaction conditions. This is clearly apparent from the low CBR values (14-19%) as shown in Figure 6.1.

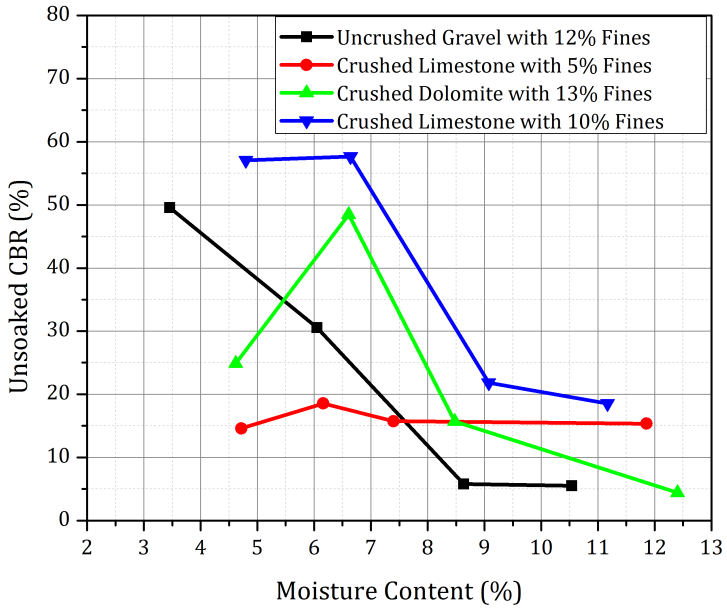


Figure 6.1: Variations in Unsoaked CBR Values with Moisture Content under Standard Compaction (ASTM D 698) Conditions

### 6.3.3 Resilient Modulus and Permanent Deformation Characteristics

The effect of aggregate quality on resilient modulus and permanent deformation behavior was studied by conducting repeated load triaxial tests on each of the four aggregate materials compacted using both the standard and modified (ASTM D 698 and ASTM D 1557, respectively) methods. Cylindrical triaxial specimens (150 mm Φ, 150 mm height) were prepared at the OMC and MDD values listed in Table 6.3 and were tested using the University of Illinois FastCell for permanent deformation and directional modulus characteristics. As discussed in Chapter 5, the first 1,000 cycles (conditioning phase) of the resilient modulus test (AASHTO T 307) were used

as an indicator of the permanent deformation susceptibility of the material. Resilient modulus tests were subsequently conducted on the specimens through pulsed load application at 15 different stress states specified in the AASHTO T 307 protocol. Anisotropic modulus properties were determined through independent pulsed load application in the vertical, followed by the horizontal directions. The anisotropic modulus ratios ($M_R^h/M_R^v$) thus determined, were analyzed to evaluate their applicability as material quality indicators.

It should be noted that materials 1 and 2 (uncrushed gravel with high fines, and crushed limestone with low fines) both exhibited unstable matrix behavior under standard compaction conditions, and sustained excessive bulging under the seating load (2.1 kPa) applied prior to repeated load triaxial testing. Therefore, the resilient modulus and permanent deformation behavior of these two materials could not be characterized under standard compaction (ASTM D 698) conditions. However, specimens prepared with materials 3 and 4 showed stable behavior even under standard compaction conditions, and could be tested for permanent deformation and resilient modulus characteristics. Comparisons of the permanent deformation and resilient modulus trends for materials 3 and 4 are presented in Figures 6.2 and 6.3, respectively . As shown in Figure 6.2, material 3 showed higher accumulation of permanent deformation under standard compaction conditions than material 4. This was attributed to the higher fines content in the material 3 (13%) compared to material 4 (10%). Similarly, material 4 showed higher modulus values compared to material 3, due to lower amount of fines in the matrix (see Figure 6.3).

The effect of aggregate quality on modulus and deformation characteristics was further investigated by testing specimens compacted using the modified compactive effort (ASTM D 1557). Figure 6.4 shows the permanent deformation trends in the four aggregate types as determined from the conditioning phase of AASHTO T 307 test protocol. From the figure, it is clearly apparent that the uncrushed gravel with 12% fines (material no. 1) showed significantly higher permanent deformation accumulation as compared to the crushed aggregates. This was consistent with the findings from laboratory testing aggregates at engineered gradations reported in Chapter 5. Figure 6.4-b shows the non-stabilizing behavior (non-decreasing permanent strain rates) of the uncrushed gravel material even after the accumulation of high permanent strain values.

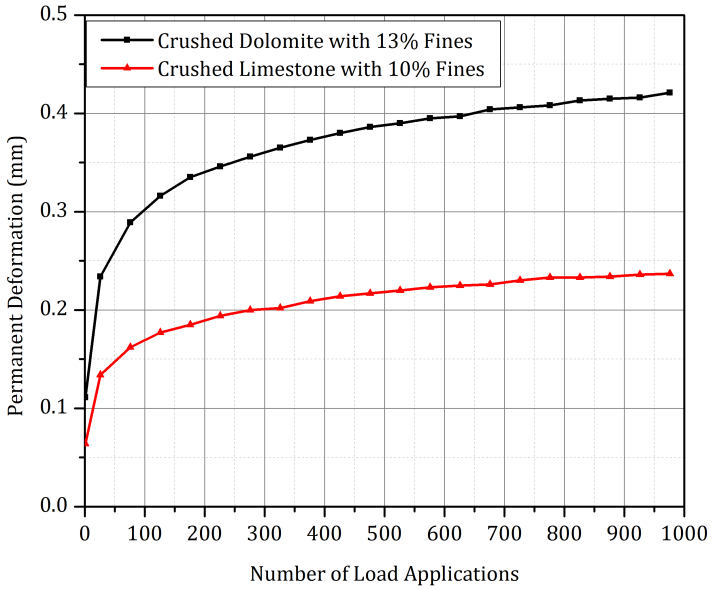


Figure 6.2: Effect of Material Quality on Permanent Deformation Behavior under Standard Compactive Effort (ASTM D 698) Optimum Moisture Conditions

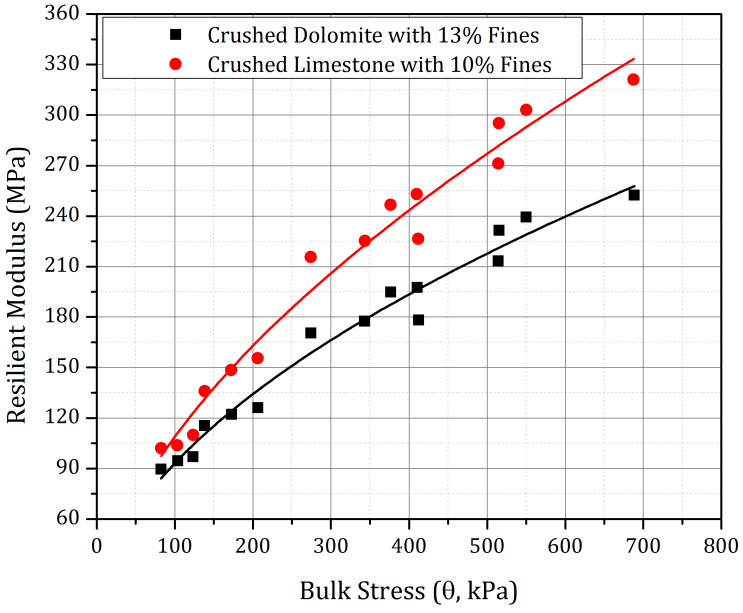


Figure 6.3: Effect of Material Quality on Resilient Modulus Behavior under Standard Compactive Effort (ASTM D 698) Optimum Moisture Conditions

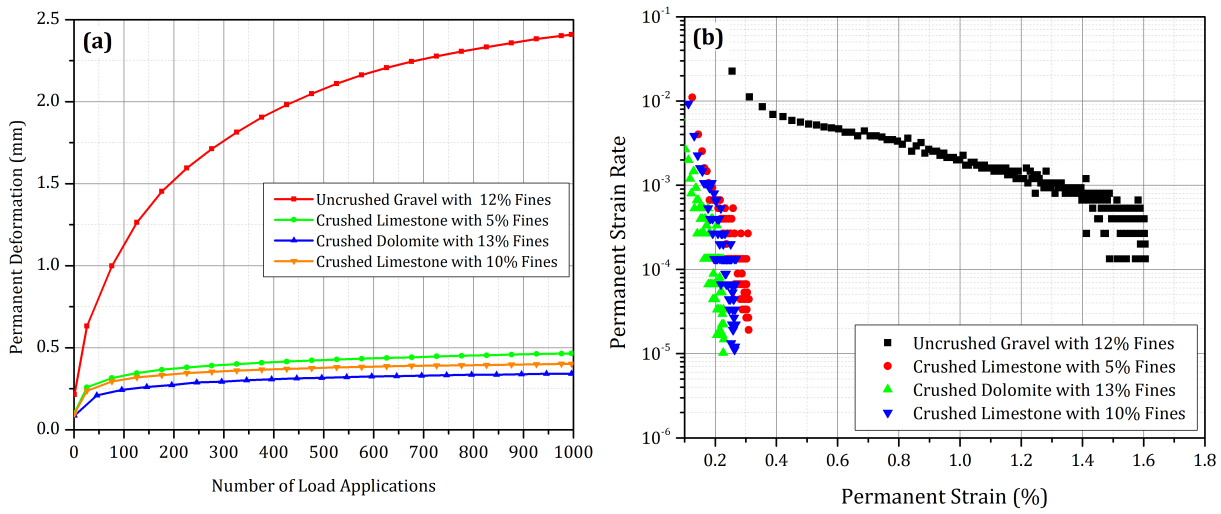


Figure 6.4: Permanent Deformation Trends for Different Aggregate Types under Modified Compactive Effort (ASTM D 1557) Optimum Moisture Conditions

It is important to note from Figure 6.4 that material no. 2 showed similar permanent deformation values as the other two crushed aggregate types (materials 3 and 4). Although material no. 2 consisted of moderately plastic fines (PI = 5.7), the effect of plasticity of fines on aggregate behavior was not significant at such low fines contents (5.2% for material no. 2). However, note that due to the lack of fines material 2 showed unstable matrix behavior under standard compaction conditions. This observation will be used later in Chapter 8 to explain the performance of test sections constructed using this material.

Although materials 3 & 4 both had "high" fine contents (13 % and 10% respectively), neither showed progressive collapse during the permanent deformation testing due to the low OMC values corresponding under the modified compactive effort. The response of both materials can be said to fall under the "plastic shakedown" range as defined by Werkmeister [15]. As reported in Chapter 5, the amount of moisture plays a critical role in governing aggregate behavior at high fines contents. In wet of optimum conditions, the fines and moisture form a "slurry" that reduces the particle interlock significantly leading to rapid accumulation of permanent deformation.

Figure 6.5 shows the resilient modulus values for the four aggregate materials under modified compaction (ASTM D 1557) conditions plotted against the bulk stress ($\theta = \sigma_1 + \sigma_2 + \sigma_3$). The consistently higher moduli values for crushed aggregates (materials 2, 3 & 4) as compared to the

uncrushed gravel (material 1) are clearly apparent from Figure 6.5. Moduli values for materials 1 and 3 can be directly compared to assess aggregate angularity effects on stiffness characteristics of unbound granular layers.

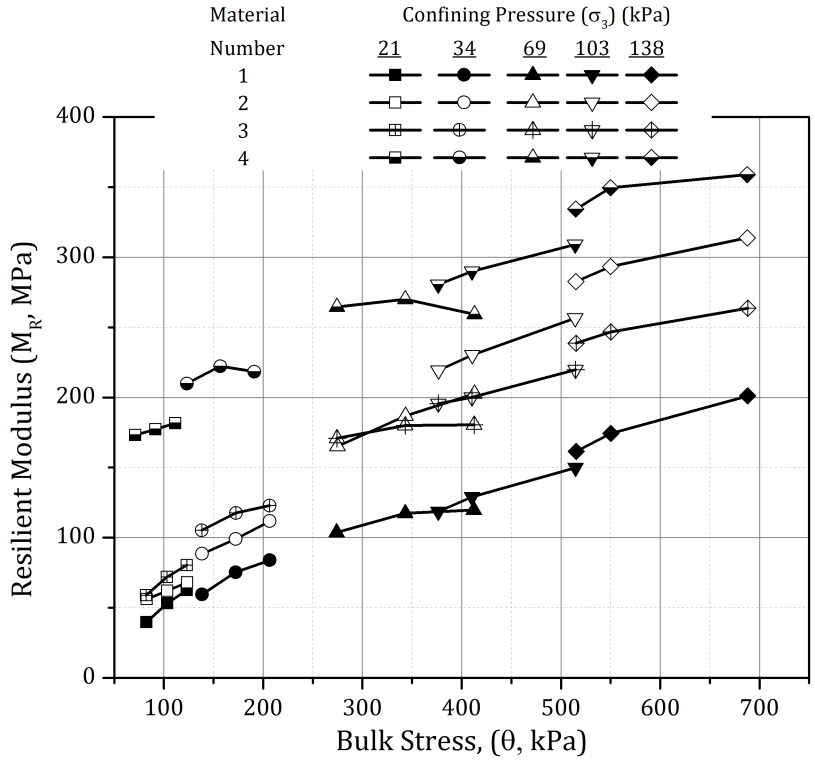


Figure 6.5: Resilient Modulus Trends for Different Aggregate Types under Modified Compactive Effort (ASTM D 1557) OMC and MDD Conditions

Similarly, the effect of fines content on resilient modulus can be studied by close inspection of materials 2, 3 & 4. A direct comparison of materials 3 and 4 highlights the detrimental effect of excessive fines on resilient modulus behavior (reflected by lower moduli for material 3). Stress softening behavior of the excess fines in material 3 resulted in the lower resilient modulus values when compared to those of materials 2 and 4. Although material 2 showed unstable matrix behavior under standard compaction, its performance at modified compaction was significantly better (higher moduli values than material 3) due to increased particle interlock. Material 4 contained 10% fines, and showed slightly higher moduli values than material 2. However, the change in moduli values was insignificant as the fines content increased from 5% (material 2) to 10% (material 4).

### 6.3.4 Summary of Findings from Laboratory Characterization of Aggregates used in Field Sections

The four aggregate types received for use in construction of the full-scale test sections, were characterized in the laboratory for strength, permanent deformation, and resilient modulus behavior. The uncrushed gravel with high fines (material 1) showed very high moisture sensitivity, whereas the crushed limestone with low fines (material 2) did not show any moisture sensitivity due to its free-draining open graded matrix. While compacted using the standard compactive effort (ASTM D 698), both these materials showed unstable matrix behavior and therefore could not be tested for resilient modulus, and permanent deformation characteristics. Modified compaction (ASTM D 1557) conditions were therefore used to compare the mechanical behavior of the four aggregate types and establish links with material quality aspects. The uncrushed gravel material showed significantly higher permanent deformation and lower resilient modulus values, compared to the three crushed aggregates. Although the crushed limestone with low fines (material 2) showed unstable behavior under standard compaction conditions, it showed significantly better performance under modified compactive effort OMC and MDD conditions. The crushed dolomite with 13% nonplastic fines (material 3) showed the lowest resilient modulus among the crushed aggregates. This was attributed to the stress-softening nature of the high amount of fines in the aggregate matrix. The high amount of fines in material 3 combined with high moisture contents, resulted in higher permanent deformation and lower resilient modulus values compared to material 4 under standard compactive effort OMC and MDD conditions. These laboratory test results will be used in Chapter 8 to justify performance trends observed under loading for unsurfaced pavement sections constructed using these materials.

## 6.4 Thickness Design of Unsurfaced Pavement Sections using Finite Element Analysis

This section describes the approach used for thickness design of unsurfaced pavement sections during the course of this research study using a nonlinear axisymmetric finite element program, GT-PAVE [21]. Unbound aggregate material characterization models developed from the laboratory phase of the study were used in a nonlinear, stress-dependent, isotropic analysis to evaluate the effects of the varying $M_R$ behavior on mechanistic response of typical two-layered unsurfaced pavement sections. The GT-PAVE FE program utilizes isoparametric 8-node

quadrilateral elements to analyze flexible pavement structures consisting of linear or nonlinear elastic layers. Details on the nonlinear solution technique used in GT-PAVE are described elsewhere [21, 98]. All aggregate materials tested during the laboratory phase of the research established the FE analysis inputs for GT-PAVE runs. The unsurfaced pavement sections analyzed, consisted of aggregate layers with thicknesses 203, 305, and 356 mm (8, 12, and 14 in., respectively) placed over a soft subgrade soil of California Bearing Ratio (CBR) = 3%. These layer configurations were selected based on commonly encountered unsurfaced pavement sections constructed in the state of Illinois. For the purpose of analysis, the subgrade was assigned a constant modulus of 31 MPa (4.5 ksi), which corresponded to an unconfined compressive strength ($Q_u$) of approximately 158 kPa (23 psi) based on data from typical fine-grained soils in the state of Illinois. Figure 6.6 represents a schematic of typical two-layer unsurfaced pavement structures analyzed during this task.

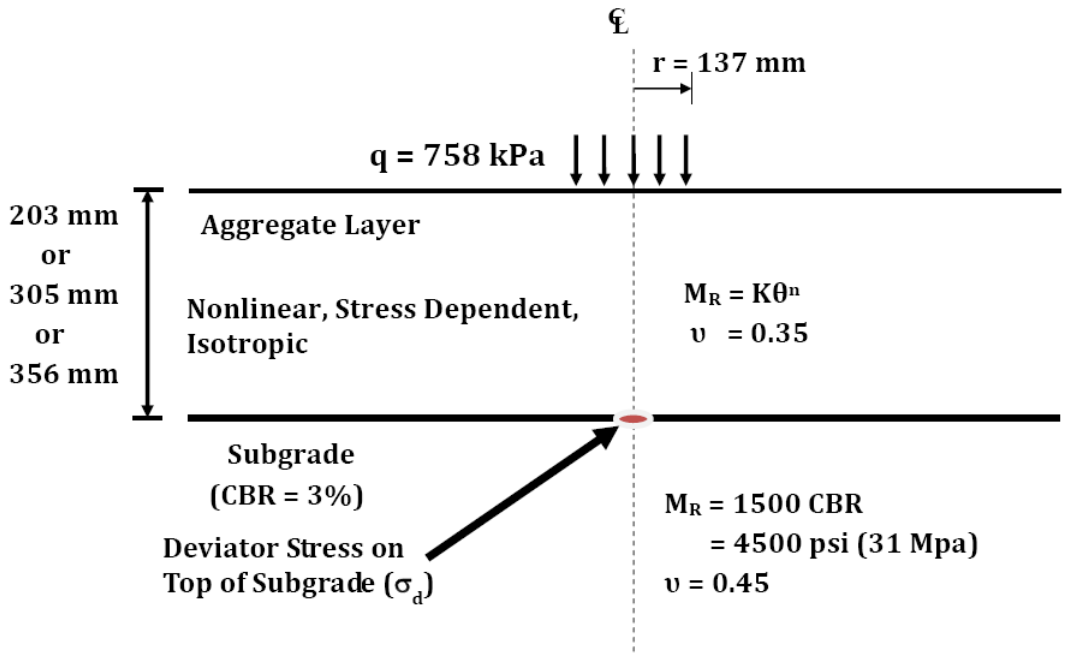


Figure 6.6: Schematic of a Typical Two-Layer System Analyzed using GT-PAVE

The GT-PAVE FE mesh included 600 elements (30 rows and 20 columns) to model the two layer pavement structure with proper consideration given to boundary conditions in the selection of mesh size [21, 98]. A single wheel load of 44.5 kN (10 kip) was applied at a uniform pressure of 758 kPa (110 psi) over a circular area of radius 137 mm (5.4 in.). The Poissons ratios for

unbound aggregate and subgrade layers were taken as 0.35 and 0.45, respectively. Note that the wheel load used during analysis was higher than the typical equivalent single-axle load (ESAL) of 40 kN (9 kip). This was done to simulate the movement of heavy trucks, and construction equipment on the unsurfaced pavements and construction platforms. Figure 6.7 shows the finite element mesh used for analyses of typical unsurfaced pavement structures.

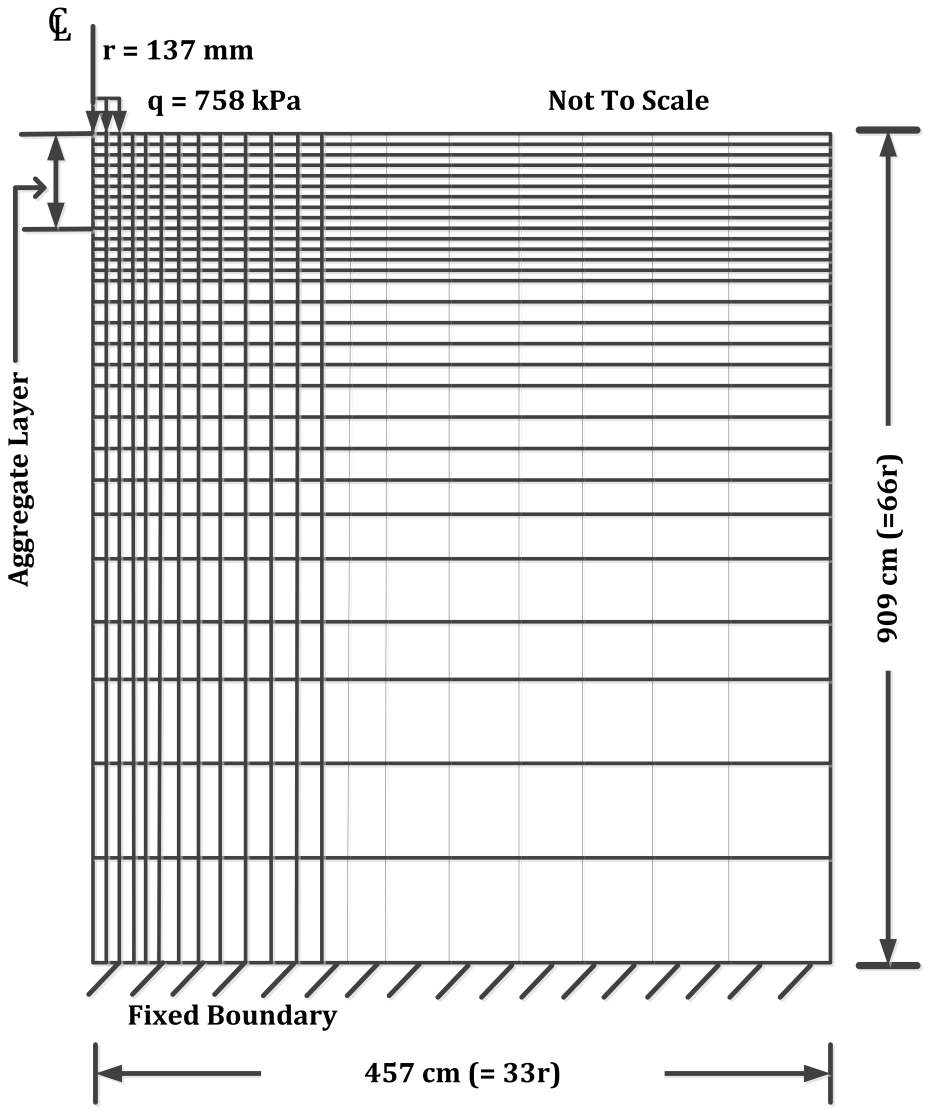


Figure 6.7: Finite Element Mesh for Typical Unsurfaced Pavement Structure Analyzed

Vertical deviator stress on top of the subgrade ($\sigma_d$) was taken as the critical pavement response of interest. Rutting potential of the subgrade was assessed by calculating the Subgrade Stress Ratio (SSR), defined as the ratio of vertical deviator stress on the subgrade ($\sigma_d$) and the subgrade unconfined compressive strength ($Q_u$). The SSR value was established by Thompson et al. [43] as a more robust and better indicator of subgrade rutting potential in comparison to using vertical strain on top of the subgrade as the critical pavement response associated with subgrade rutting. Accordingly, the approach for designing unsurfaced pavements in the state of Illinois is based on limiting the allowable SSR to 0.6-0.7 in order to prevent excessive rutting of the subgrade [46]. For unsurfaced pavements and construction platforms that are characterized by lower number of load applications and lower serviceability standards, the threshold value of SSR can be set to a higher value (of the order of 0.75) [43]. The SSR values calculated from GT-PAVE analyses of the pavement sections were used to assess the adequacy of the aggregate layer for limiting subgrade rutting. The effects of individual aggregate physical properties (test factors) on the computed SSR values were studied to identify factors that govern the load spreading ability of aggregate layers and their effects on subgrade rutting potential.

Figure 6.8 shows the change in the SSR values with nonplastic fines content for a 305-mm (12-in.) thick crushed dolomite layer on top of the soft subgrade. The dark solid line in Figure 6.8 shows the main regression trend line while the dashed lines show the typical upper and lower data scatter. It should be noted that the upper and lower dashed lines in subsequent figures are for visual demonstration of data scatter for a particular fines content only, and are not intended to suggest the SSR values for a particular fines content. As discussed later, the upper and lower dashed boundaries can be used to highlight the effect of moisture on SSR values at different fines contents. As shown in Figure 6.8, there was a clear trend of increasing SSR values when the fines content in the aggregate matrix was increased; this may, for example relate to aggregate material degradation due to intrusion of subgrade soil fines in the field. Since a higher SSR value indicates greater stress levels applied on top of the subgrade, increase in amount of fines clearly had a detrimental effect on the load spreading ability of the aggregate layer. Another interesting observation from Figure 6.8 is the slight reduction in the SSR values while going from 4% to 8% fines, which may be linked to the optimum fines content as reported by researchers in the past [91]. However as the fines content subsequently increased beyond 8%, the SSR values increased, showing greater susceptibility of the pavement structure to undergo subgrade rutting.

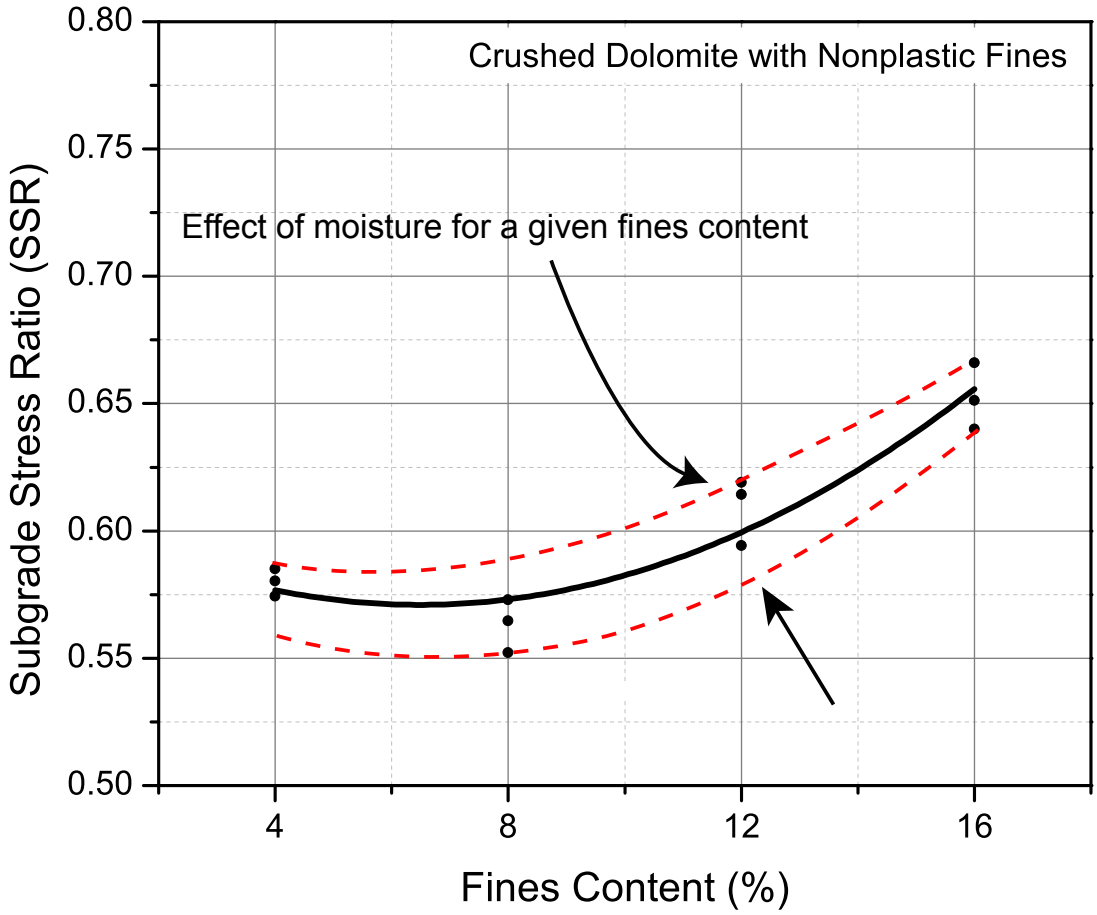


Figure 6.8: Subgrade Stress Ratios (SSRs) due to 305-mm Thick Crushed Dolomite Layer with Nonplastic Fines

Interestingly, the exact same trend was found from permanent deformation testing of the crushed dolomite samples as reported in Chapter 5.

The trend in SSR values is a reflection of the effect of fines content on the modulus of the aggregate, which results in different degrees of stress reduction at the aggregate-subgrade interface. The change in behavior while going from 4% to 8% was explained in Chapter 5 by the fact that at 4% fines the crushed dolomite matrix structure was not stable, and there was sufficient room for the particles to move and rearrange, therefore leading to higher deformation and lower moduli values. However, as the fines content was increased to 8%, the aggregate matrix gradually stabilized and presented better resistance to particle movement and rearrangements. As the fines content increased beyond 8%, all the voids in the aggregate matrix were filled, and the

fines started governing the aggregate material behavior leading to higher deformation and lower moduli values. These results can be used to establish a threshold value of allowable fines in aggregate layers. As the reduction in material quality is apparent (shown by higher deformations and lower moduli values) beyond a fines content of 8%, this value seems to serve as the boundary between "low" and "high" fines categories. This observation was in complete agreement with findings by Tutumluer and Seyhan [91] who suggested 7-8% as the limit for allowable fines in unbound aggregate layers comprising crushed particles.

A distinction between crushed and uncrushed aggregate materials can be made by comparing the above findings with similar results for uncrushed gravel presented in Figure 6.9 which indicated no evidence of matrix stabilization when the fines content was increased from 4% to 8%. In other words, the uncrushed gravel matrix showed deterioration in load carrying ability as the

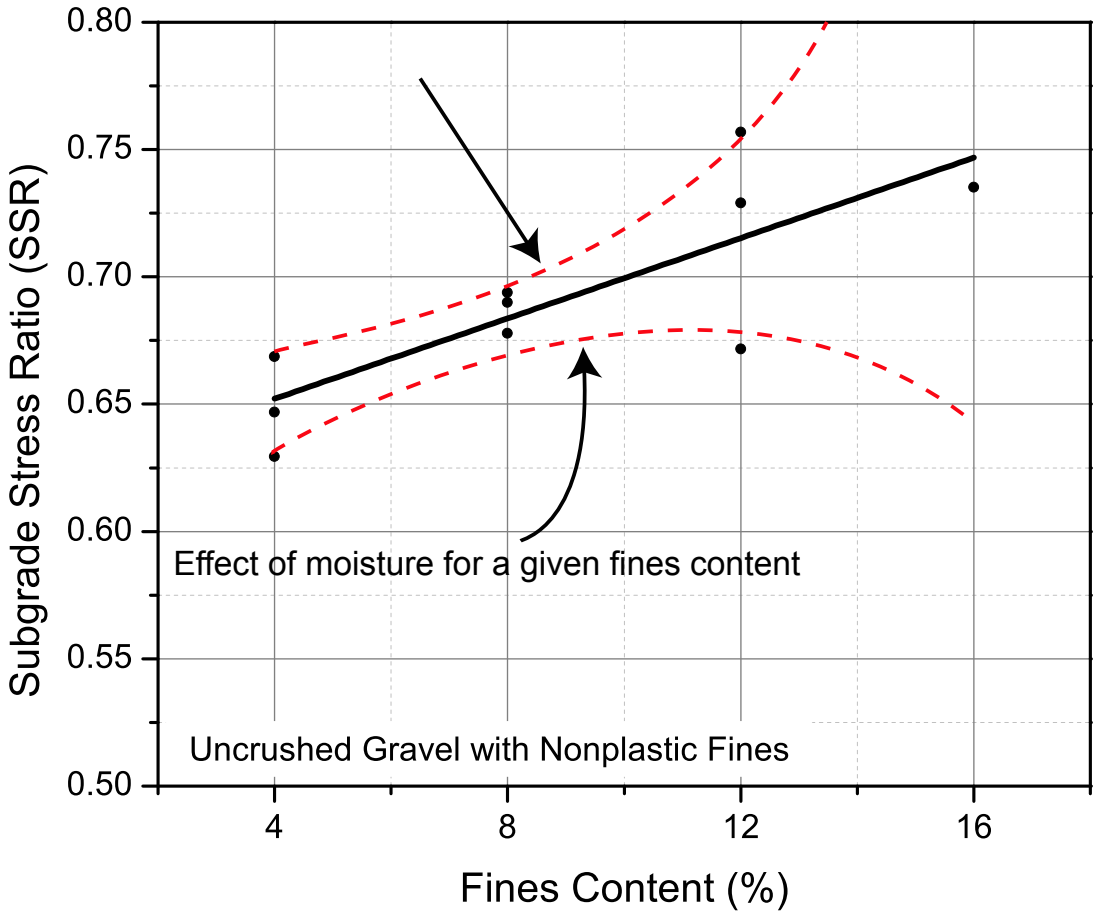


Figure 6.9: Subgrade Stress Ratios (SSRs) due to the 12-in. (305-mm) Thick Uncrushed Gravel Layer with Nonplastic Fines

fines content was increased beyond 4%. The exact trend was observed from permanent deformation test results presented in Chapter 5 and was explained by the lower voids content in the uncrushed gravel matrix that could attain a "stable configuration" at relatively lower fines contents (less than 8%). This observation was subsequently used to recommend different threshold values for allowable fines contents in crushed and uncrushed aggregates in Chapter 5.

Figures 6.8 and 6.9 can also be analyzed together for the effect of change in aggregate layer moisture content on its adequacy for subgrade protection. Both Figures 6.8 and 6.9 showed that the effect of moisture content (represented by the three data points corresponding to each fines content) on aggregate modulus (and hence SSR) varied depending on whether the aggregate was crushed or uncrushed. For example, in case of the crushed dolomite with nonplastic fines (see Figure 6.8), the data points corresponding to different moisture contents at individual fines contents were consistently close to each other. Therefore, change in moisture did not have a significant effect on the load-spreading ability irrespective of the amount of fines. However in the case of the uncrushed gravel (see Figure 6.9), the scatter became wider as the fines content increased (particularly visible at 12% fines). As already discussed in Chapter 5, aggregate specimens with 16% fines became unstable at wet of optimum moisture conditions and could not be tested for modulus and permanent deformation properties.

The scatter in the SSR values at high fines contents was even more pronounced in the case of uncrushed gravel with plastic fines (see Figure 6.10). This clearly proved that the effect of moisture on the load carrying capacity of an unbound aggregate layer is dependent on particle shape (crushed or uncrushed), fines content, as well as plasticity of fines. Therefore to quantify the effect of moisture content change on aggregate behavior, consideration must also be given to these other aggregate physical properties.

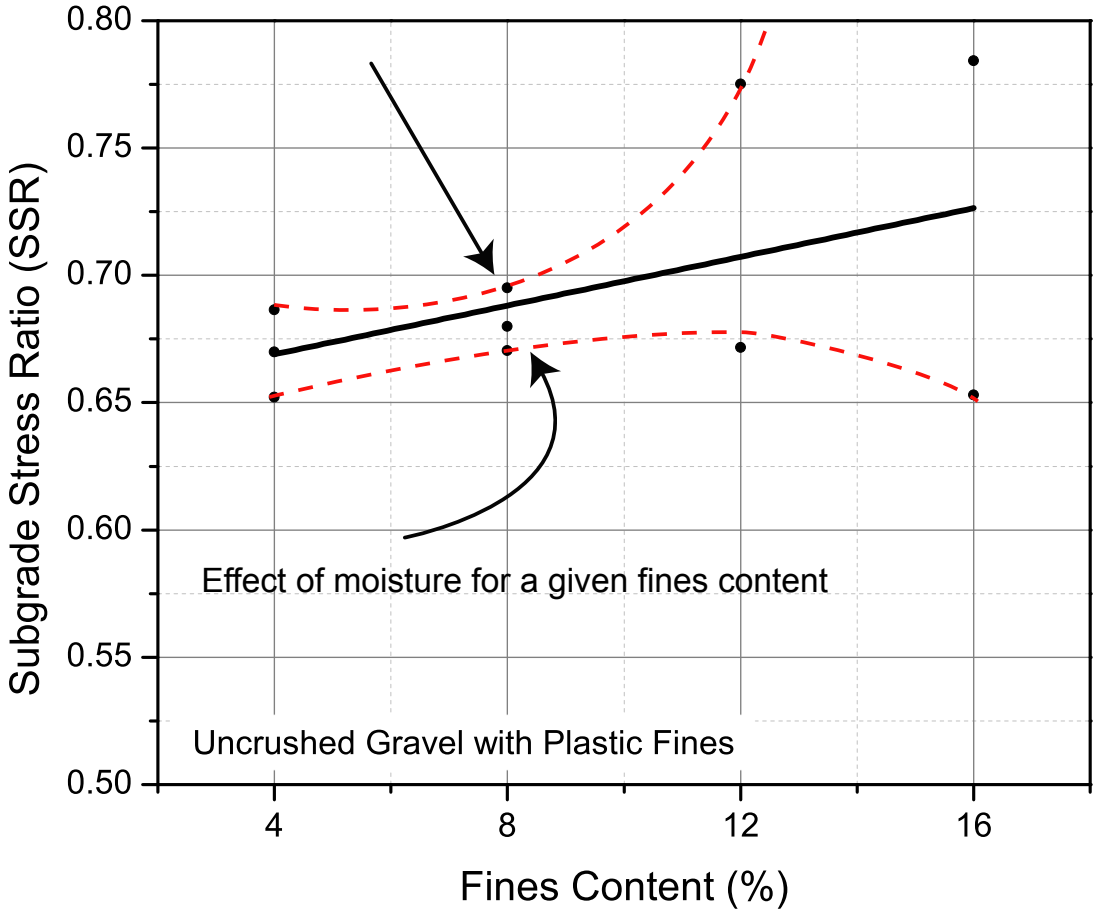


Figure 6.10: Subgrade Stress Ratios (SSRs) due to the 305-mm (12 in.) Thick Uncrushed Gravel Layer with Plastic Fines

### 6.4.1 Importance of Considering both Modulus and Deformation Characteristics

The previous section highlighted some of the similarities in the change in modulus and permanent deformation behavior of aggregates with change in physical properties. However, designing unbound aggregate layers based solely on the concept of subgrade protection can often be misleading. The effects of aggregate properties on modulus and deformation behavior are not necessarily proportional. This can be noted by simply contrasting Figures 6.11 and 6.12. Figure

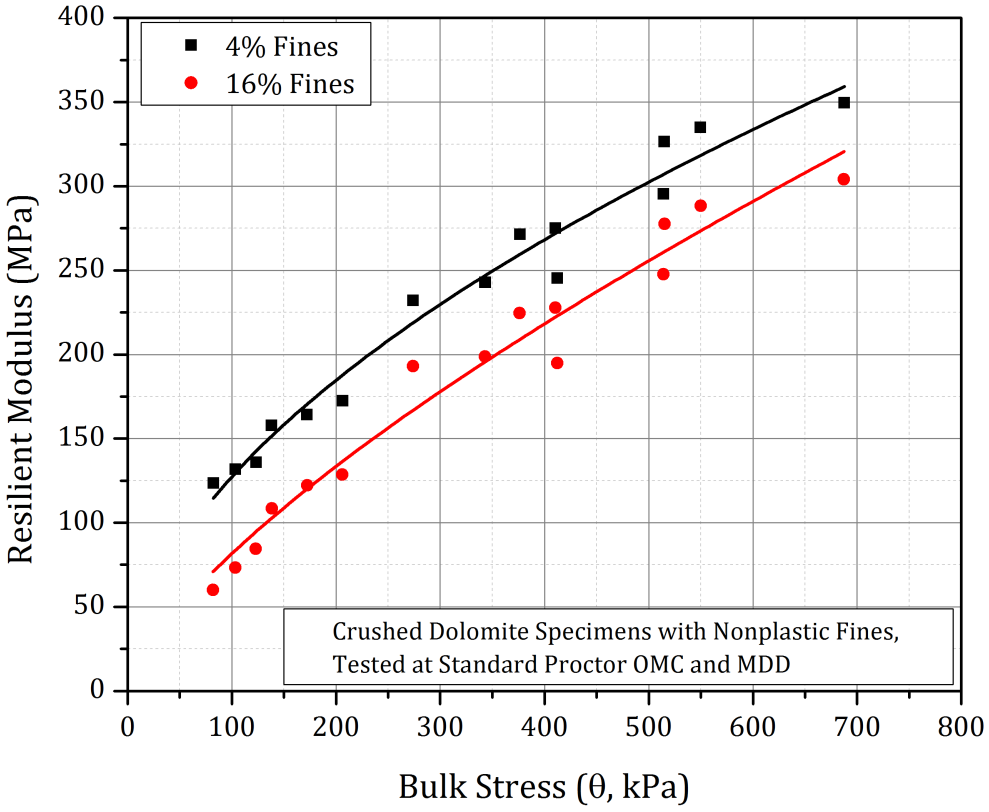


Figure 6.11: Resilient Modulus Test Results for Crushed Dolomite with Nonplastic Fines at $W_{opt}$

6.11 shows $M_R$ curves for crushed dolomite specimens with 4% and 16% nonplastic fines compacted to standard compactive effort optimum moisture content and maximum dry density conditions. Figure 6.12 on the other hand, shows the permanent deformation test results for the same two specimens. It can be seen that as fines content was increased from 4% to 16%, its effect on permanent deformation (increase by 400%) was much more severe than the effect on resilient modulus (decrease by 20-25%). This issue was further investigated by contrasting the design aspects emphasizing subgrade protection and aggregate layer rutting or shear failure. Figure 6.13

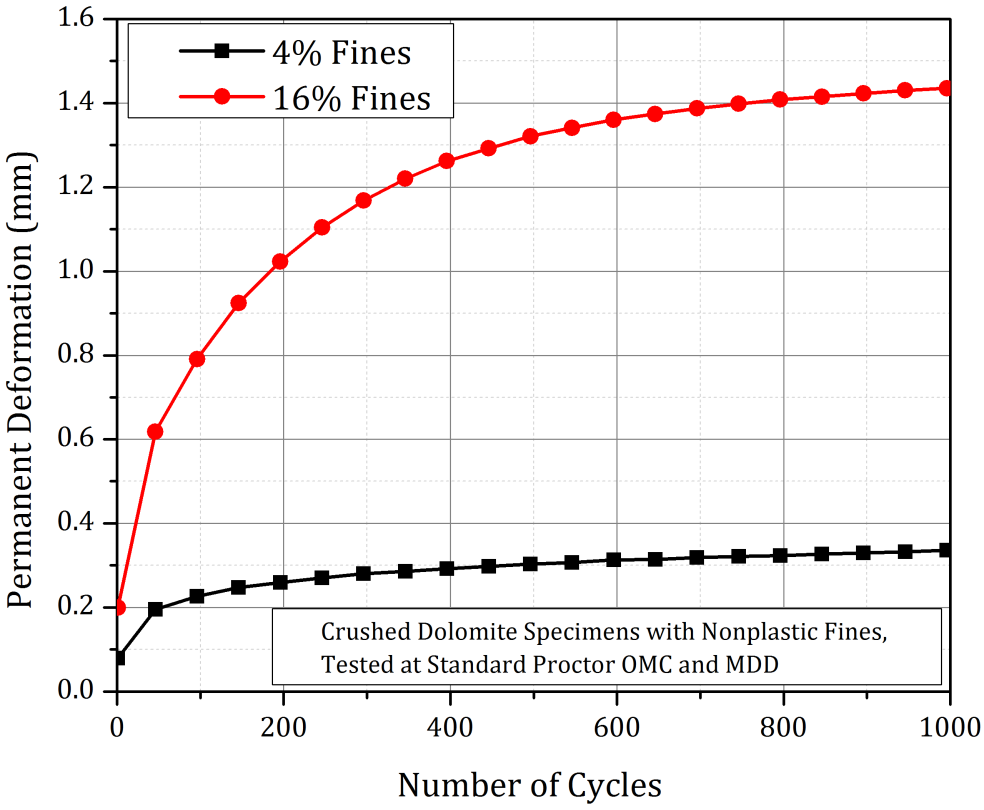


Figure 6.12: Permanent Deformation Behavior of Crushed Dolomite with Nonplastic Fines at $W_{opt}$

shows the change in SSR values with increasing unbound aggregate layer thickness for typical unsurfaced pavement sections constructed using crushed dolomite with 12% nonplastic fines and uncrushed gravel with 12% plastic fines, respectively. As expected, a reduction in the subgrade stress ratio values was observed with increase in the aggregate cover layer thickness. However for a 356-mm (14-in.) thick aggregate layer, pavement sections constructed using the crushed dolomite with 12% nonplastic fines as well as the uncrushed gravel with 12% plastic fines, both exhibited acceptable SSR values (0.55 and 0.6, respectively). Therefore, judging by the criteria of subgrade protection, it would appear that both pavement structures would perform adequately under loading by limiting the subgrade rutting potentials. However, comparing the permanent deformation behavior of the two materials revealed significantly different results (see Figure 6.14). As shown in Figure 6.14, the uncrushed gravel with 12% plastic fines experienced progressive shear failure during the permanent deformation testing after approximately 300 load applications. A pavement structure constructed with this material would undergo shear failure due to excessive

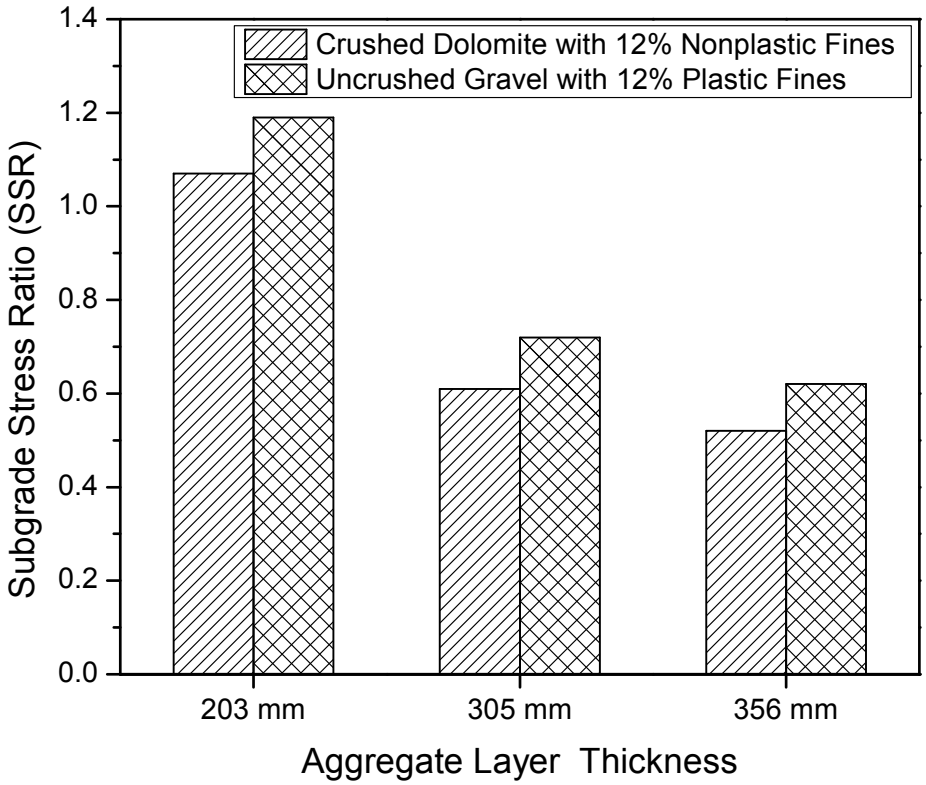


Figure 6.13: Subgrade Stress Ratios (SSRs) for Crushed Dolomite with 12% Nonplastic Fines Compared to SSRs for Uncrushed Gravel with 12% Plastic Fines (1 in. = 25.4 mm)

particle movement within the aggregate layer. Therefore, "protecting" the subgrade is not the only factor that influences the performance of unsurfaced pavement systems, and due consideration should be given to aggregate type and quality and their effects on both modulus and permanent deformation behavior of the aggregate layer.

### 6.4.2 Conclusions from Finite Element Analysis of Unsurfaced Pavement Sections

The relative effects of aggregate physical properties under investigation on the resilient modulus ($M_R$) and permanent deformation behavior of unbound aggregate layers for use in unsurfaced pavement systems were studied through finite element analyses of typical unsurfaced pavement sections. Material characterization model parameters developed from the laboratory phase of the research study (refer to Section 5.7) were used in a nonlinear axisymmetric finite element based pavement analysis program (GT-PAVE) to predict vertical subgrade deviator stresses as the critical pavement response assuming isotropic aggregate layer behavior. The concept of Subgrade

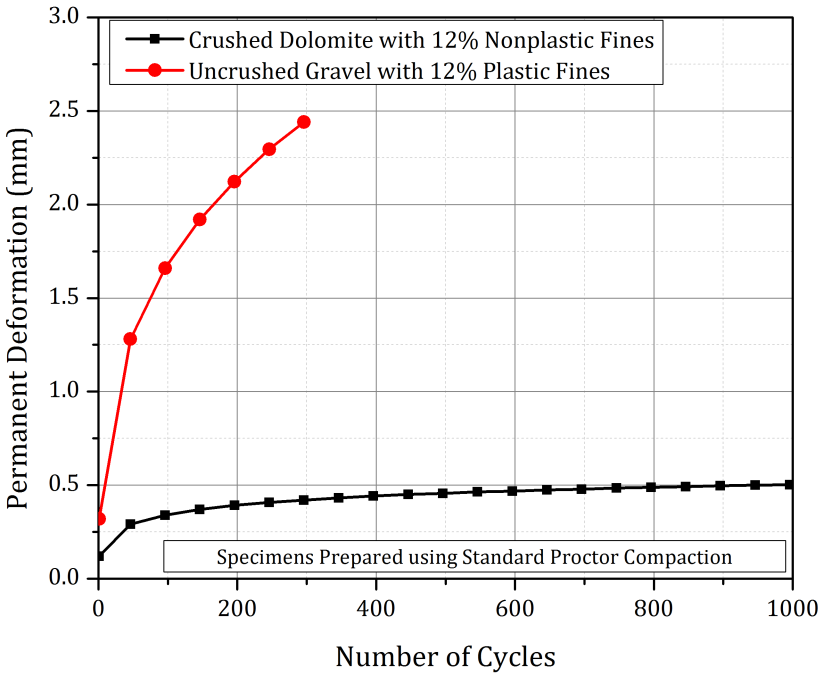


Figure 6.14: Permanent Deformation Trends of Crushed Dolomite with 12% Nonplastic Fines and Uncrushed Gravel with 12% Plastic Fines

Stress Ratio (SSR) was used to assess the adequacy of the aggregate layers for subgrade protection. Although the change in SSR values for different combinations of the test factors was not significant for a given aggregate layer thickness, aggregate layer permanent deformation trends were significantly affected by the aggregate type and quality. The SSR values calculated from the analyses of unsurfaced pavements of three different thicknesses (356 mm, 305 mm, and 203 mm) for all possible material combinations are shown in Figure 6.15. As shown in the figure, the 356-mm and 305-mm aggregate layers consistently resulted in acceptable SSR values (0.5-0.7), whereas the 203-mm aggregate layer reflected SSR values corresponding to subgrade shear failure. This indicates that based on the principle of subgrade protection, unsurfaced pavement sections with at least 305-mm thick aggregate layer should perform adequately over a subgrade of CBR = 3% irrespective of the aggregate material quality. To verify these findings and better understand the effect of aggregate quality on mechanisms of rut accumulation, unsurfaced pavement sections with 356-mm, 305-mm and 203-mm thick aggregate layers were constructed using the four selected aggregate materials over a weak subgrade of CBR $\approx$ 3%.

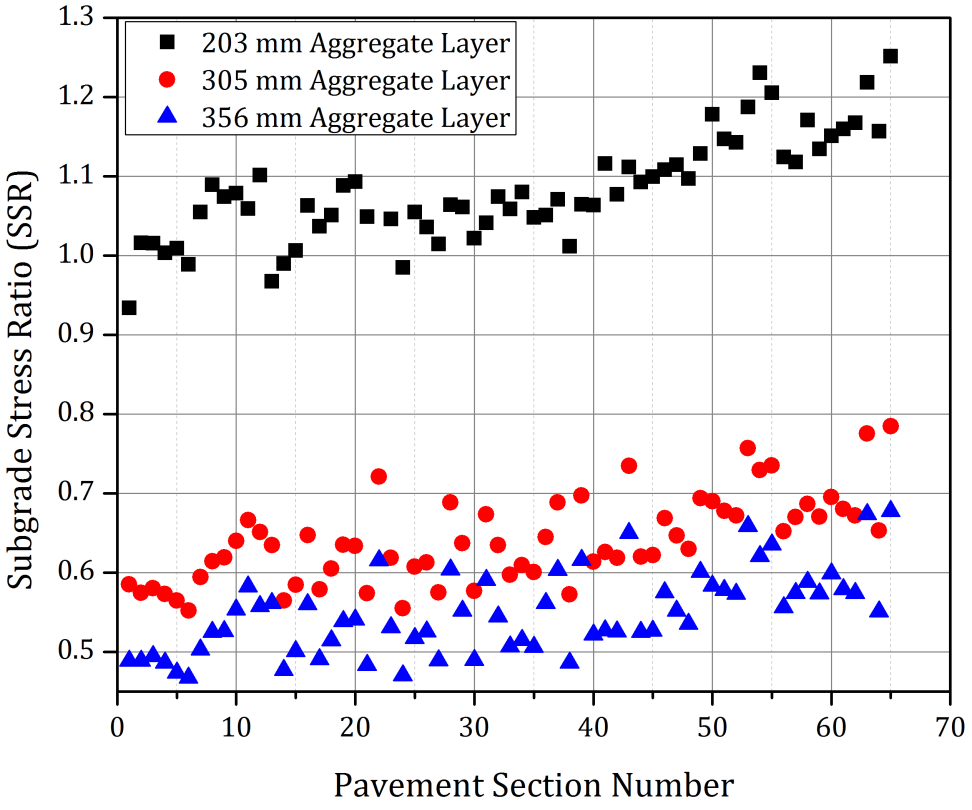


Figure 6.15: Subgrade Stress Ratios Corresponding at Factorial Combinations of the Test Factors for Three Different Aggregate Layer Thicknesses

## 6.5 Layout and Cross-Sectional Profile of Full Scale Test Sections

Six test "cells" (numbered 1 through 6) were constructed along three longitudinal strips using the four aggregate types listed in Table 6.2 to evaluate the effect of aggregate quality on unsurfaced pavement performance. This thesis focusses on the performance of five test cells (1 through 5) constructed at different combinations of aggregate type, properties, and subgrade strength. The sixth cell (Cell 6) was constructed to investigate a secondary objective, and its performance evaluation is not covered in this PhD thesis. Cells 1 through 4 were constructed with the four selected aggregate materials over a weak subgrade of CBR = 3%. Identical subgrade conditions and aggregate layer thicknesses ensured differences in pavement performance to be directly linked to differences in aggregate quality. Cell 5 was constructed using material No. 2 (same as Cell 2) over a stronger subgrade of CBR = 6%. The main purpose was to evaluate the effect of subgrade strength on unsurfaced pavement performance and mechanisms contributing to rut accumulation.

Figure 6.16 shows the layout of the test cells along three longitudinal strips 72.4-m (237.5- ft.) long and 5.5-m (18-ft.) wide separated by 3.7-m (12-ft.) wide access roads for construction equipment operation. Longitudinal edge drains were constructed along the North side of each cell and were connected to transverse drains near the West end of the cell. The edge drains sloped from east to west, and the discharge was carried by the long transverse drain along the west boundary to a sump pit. Water was continually pumped out from the sump pit to prevent accumulation of water in the drain pipes.

Figure 6.17 presents a schematic of the layout and cross-sectional details of individual test cells, that were constructed 39.6-m (130-ft) long and comprised of three test "sections" with aggregate layers of thicknesses 356 mm (14 in.), 305 mm (12 in.) and 203 mm (8 in.), respectively. Each cell was separated from the adjacent cell (longitudinally) by a 6.9-m (22.5-ft.) long transition section for placement of the Accelerated Transportation Loading Assembly (ATLAS) tracks. From West to East, the 356-mm (14-in.) thick aggregate section was named "Section 1" whereas the 203-mm (8-in.) thick aggregate section was named "Section 3" consistently. Each section was 4.57-m (15-ft.) long and was separated from adjacent sections by 3.05-m (10-ft.) long transition zones. At either end of the cell 3.1-m (10-ft.) long speed stabilization zones were constructed to ensure uniform speed of loading on each section. As already mentioned, Cell 5 was constructed over a subgrade of CBR = 6% and therefore the aggregate layer thicknesses for the three sections were

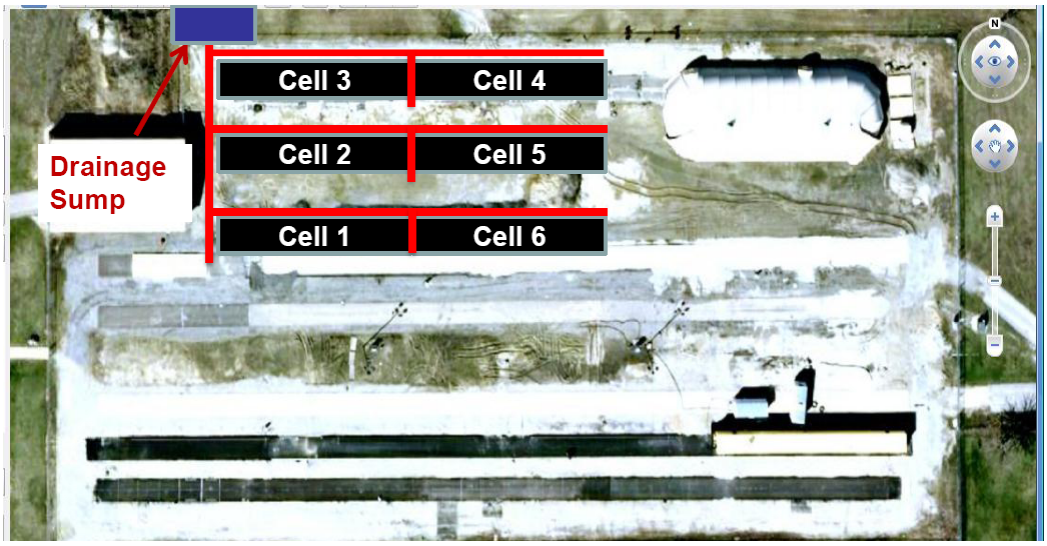


Figure 6.16: Aerial View of Test Section Layout

254 mm, 203 mm and 152 mm (10, 8 & 6 in.), respectively.

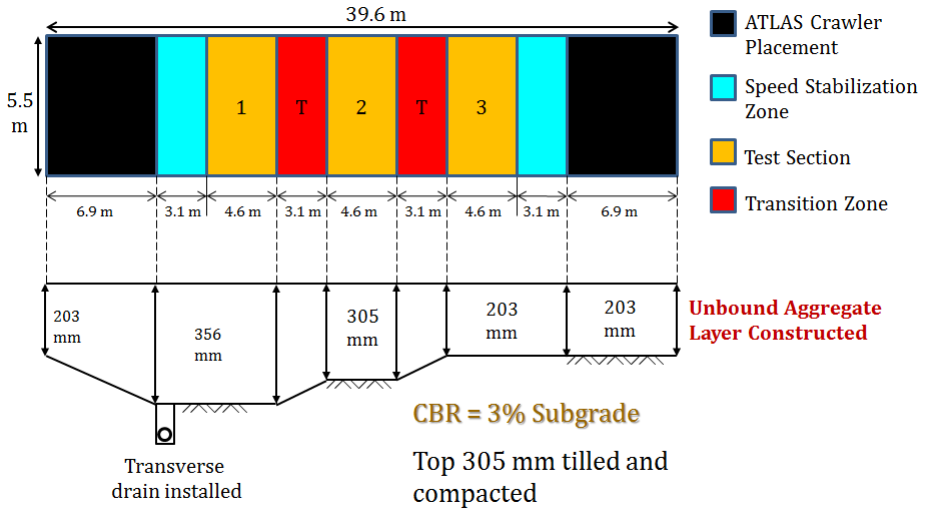


Figure 6.17: Plan View (on Top) and Cross Sectional Details of the Full-Scale Unsurfaced Pavement Test Sections

## 6.6 Subgrade Characterization

The first step in construction of the full-scale test sections involved laboratory characterization of the subgrade soil to quantify the change in CBR with moisture content, and ultimately determine

Table 6.4: Laboratory Classifications of Preliminary Subgrade Soil Groups Identified

| | **Group 1** | **Group 2** | **Group 3** | **Group 4** |
|---|---|---|---|---|
| **Unified Classification** | CL-ML | CL-ML | CL-ML | CL-ML |
| **AASHTO Classification** | A-4 | A-4 | A-4 | A-4 |
| **Liquid Limit (%)** | 21 | 22 | 20 | 22 |
| **Plasticity Index (%)** | 6.0 | 7.0 | 5.0 | 6.0 |
| **Optimum Moisture Content (%)** | 10.5 | 10.5 | 10.2 | 11.6 |
| **Maximum Dry Density (kN/m$^3$)** | 19.6 | 19.4 | 19.9 | 18.8 |

the target moisture content in the field to achieve an engineered subgrade of desired CBR. This was particularly important as the primary objective was to evaluate the effects of aggregate physical properties on unsurfaced pavement performance over a uniformly weak, prepared subgrade. This would be possible only by eliminating subgrade variability to the maximum possible extent. Twelve (12) boreholes, each 1.2-m (48-in.) deep were dug covering the entire area of the test strips, and soil samples were collected using plastic bags at 15-cm (6-in.) intervals to assess variability in the subgrade profile.

Visual classifications of the soil samples were first conducted, and four sub-groups were developed by merging samples with similar color, texture, and odor. Later, each sub-group was classified in the laboratory following the Unified [99] as well as AASHTO [100] classification methods. Several laboratory tests were then conducted to characterize the physical, and mechanical behavior of individual sub-groups. All the four sub-groups were classified as low plasticity clayey silt (CL-ML) following the Unified classification system. Table 6.4 summarizes the soil classification, Atterberg limits, and moisture-density characteristics of the individual sub-groups using the standard compaction method (ASTM D 698). Due to similar physical and mechanical characteristics the four sub-groups were merged together, and a representative group (Group 3) was used as the reference for moisture adjustment during the field construction. Note that selection of Group 3 as the representative soil group was primarily based on the relative frequency of collected soil samples belonging to this group. Figure 6.18 shows the moisture-density and CBR characteristics of the representative soil group as determined in the laboratory.

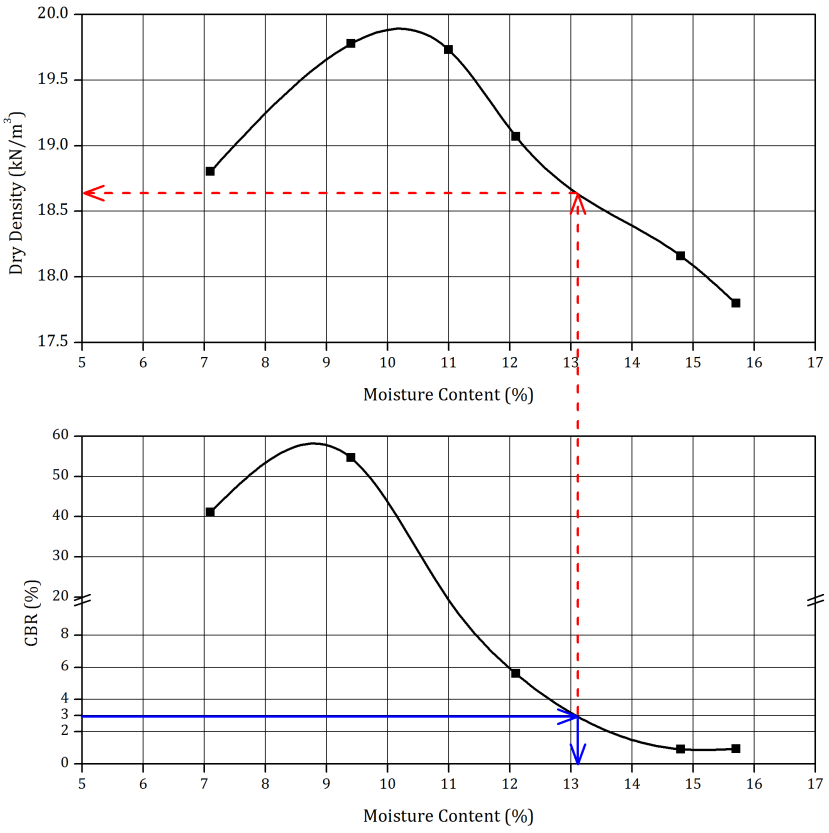


Figure 6.18: Subgrade Moisture-Density and CBR Characteristics (with CBR = 3% Conditions Highlighted)

## 6.7 Engineering Subgrade Strength through Moisture Adjustment

As the goal was to evaluate unsurfaced pavement performance over weak subgrades, the top 305 mm (12 in.) of the subgrade layer was engineered through tilling and moisture addition to achieve a uniform CBR value of 3% (6% for Cell 5). The moisture content corresponding to the target CBR (as illustrated in Figure 6.18) value was used as a starting point to determine the quantity of water to be added to the test cells. In-place CBR values were determined using the empirical relationship proposed by Kleyn et al. [101] (see Equation 6.1) correlating CBR with the penetration rate of a Dynamic Cone Penetrometer (DCP).

$$LOG(CBR) = 2.62 - 1.27 * LOG(PR) \tag{6.1}$$

where:PR is the DCP penetration rate (mm/blow).

This procedure was repeated until the in-place CBR value for the top 305 mm of the subgrade (as determined from Equation 6.1) was reasonably close to the target value (3% or 6%). Figure 6.19 shows the process of (a) subgrade tilling, (b) moisture addition, (c) compaction, and (d) DCP testing on the engineered subgrade layer. Figure 6.20 shows an example in-place subgrade CBR profile determined from DCP testing, for a test cell subgrade of target CBR = 3%. As seen from Figure 6.20, the subgrade tilling and moisture addition proved to be an effective procedure for achieving a uniform subgrade of controlled CBR. After final compaction of the layer,

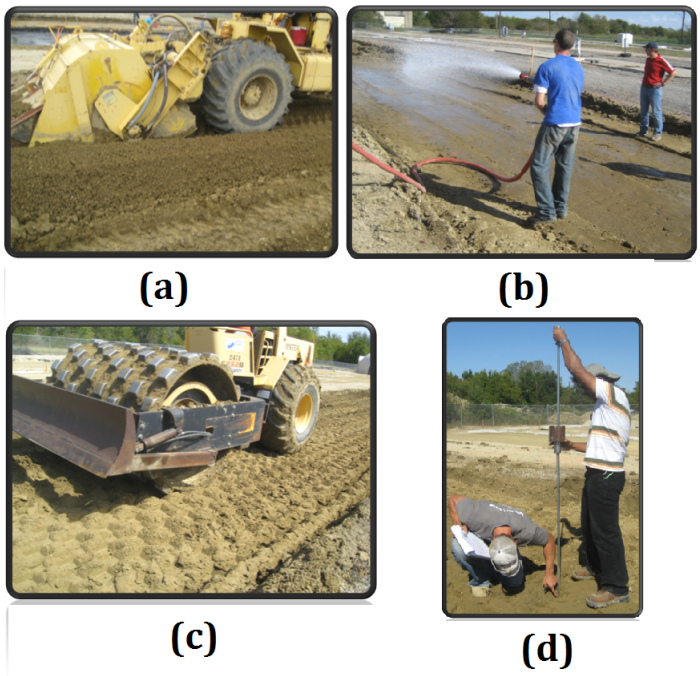


Figure 6.19: Subgrade Tilling and Moisture Control

uniformity of subgrade compaction was verified using different devices such as the Dynatest® Light Weight Deflectometer (LWD), Humboldt® Soil Stiffness Gauge (GeoGauge™), as well as a Troxler® Nuclear Density Gauge. Details on operation of these equipment and important test results will be presented in Chapters 7 and 8.

## 6.8 Earth Pressure Cells to Measure Subgrade Vertical Compressive Stress

To evaluate the effects of aggregate material type and quality on the dissipation of traffic-induced stresses with depth, earth pressure cells were installed on top of the subgrade at the aggregate-subgrade interface along the North wheel path of individual test cells for monitoring

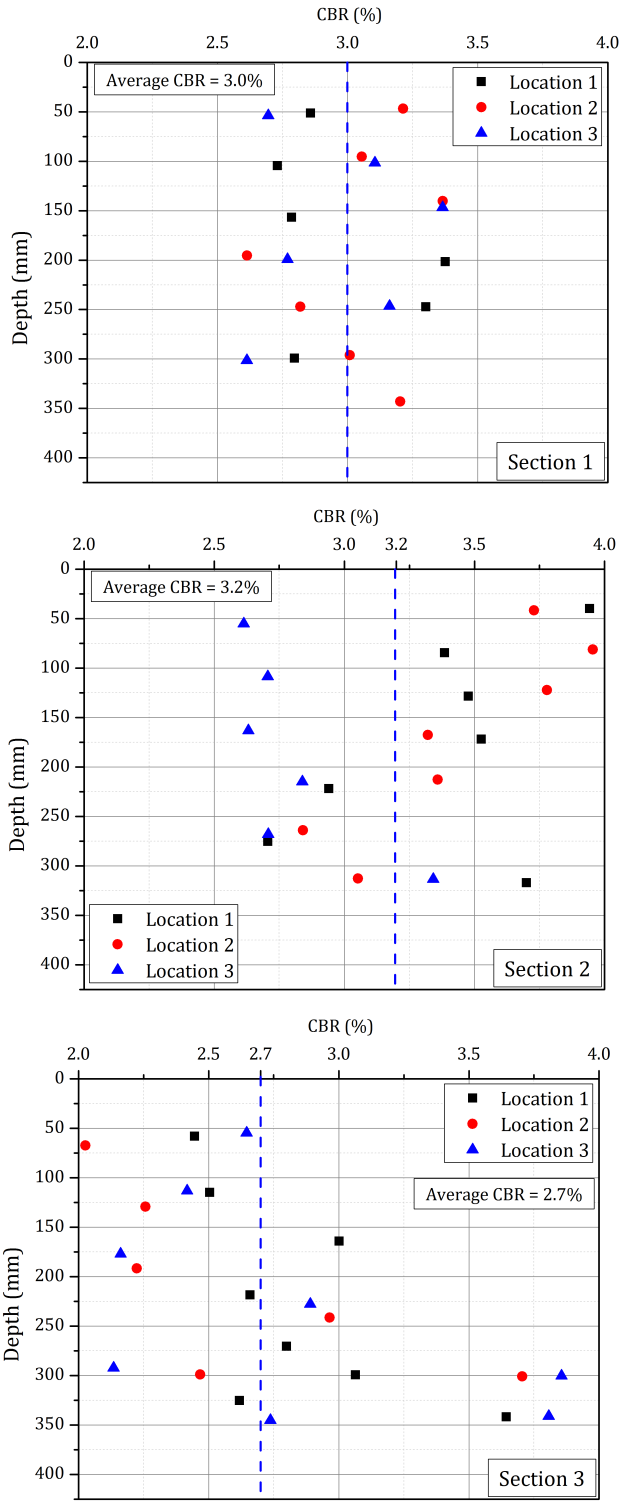


Figure 6.20: Example of In-Place Subgrade CBR Profile Determined from DCP Testing for a Pavement Test Cell with Target CBR = 3%

the subgrade vertical compressive stresses. Two earth pressure cells (one each in Sections 2 and 3) were installed in each pavement test cell along the centerline of the North wheel path. Accordingly for Cells 1 through 4, pressure cells were installed at the aggregate-subgrade interface underneath the sections with 305-mm and 203-mm thick aggregate layers. For Cell 5, however, pressure cells were installed underneath the 203-mm and 152-mm thick aggregate sections.

The earth pressure cells, manufactured by Geokon$^{TM}$(model 3500), were rated for a full-scale range of 400 kPa (58 psi) with an accuracy of 1 kPa (0.15 psi). Each pressure cell consisted of two circular stainless steel plates welded together around their periphery to create a cell approximately 230 mm (9 in.) in diameter and 12-mm (0.5-in.) thick, spaced apart by a narrow cavity filled with de-aired hydraulic oil. Changing earth pressure squeezes the two plates together causing a corresponding increase in fluid pressure inside the cell. A semi-conductor type transducer, which enables the measurement of dynamic pressure, converts this pressure into an electrical signal which is transmitted via cable to the readout location. The cell is designed to accept an input pressure at one end and provide an electrical output voltage ranged 0-5 volts. Pressure data during test section loading was acquired through a LabView$^{TM}$virtual instrument at a frequency of 500 Hz.

### 6.8.1 Earth Pressure Cell Installation Procedure

A small circular hole, approximately 25-mm (1-in.) deep, was first dug in the subgrade and the pressure cell was placed inside it. A circular fabric was placed on top of the pressure cell to protect its surface from sharp aggregate particles. A thin layer of sand was placed underneath the pressure cell to make its surface completely horizontal. Additionally, a trench approximately 75-mm wide by 127-mm deep was excavated to accommodate the transducer housing as well as the cables transmitting the signal to the data acquisition setup. The cable trenches were filled with a thin layer of sand and were thoroughly tamped to protect the cables from splicing during laying and compaction of the aggregate layer. Figure 6.21 shows the process of pressure cell installation at the aggregate-subgrade interface. Note that six of the ten pressure cells installed in the test sections were damaged during compaction of the overlying aggregate layers. Only the pressure cells installed in Cells 1 and 2 functioned properly to record the subgrade vertical stress levels under loading. These measured stress values are used in Chapter 8 to justify observed

trends in the test section performances of Cells 1 and 2.


Figure 6.21: Pressure Cell Installation on Top of the Subgrade at the Aggregate-Subgrade Interface: (a) Excavated Circular Hole and Trench for Placement of Pressure Cell and Cable; (b) Filling of Trench with Bedding Sand; (c) Covering the Excavated Trench with Soil; and (d) Tamping of the Filled Trench

## 6.9 Aggregate Placement and Compaction

After engineering the subgrade to target CBR values, aggregate sections were constructed by placing the material in two lifts and targeting a relative compaction of 95% with respect to the MDD values determined using the standard compaction (ASTM D 698) method. Compaction of each layer was checked using a nuclear gauge, and moisture was added to the aggregate as

Table 6.5: In-Place Moisture-Density Values for Compacted Aggregate Layers

| | Section 1 | | Section 2 | | Section 3 | |
|---|---|---|---|---|---|---|
| Cell Number | Moisture Content (%) | Dry Density ($kN/m^3$) | Moisture Content (%) | Dry Density ($kN/m^3$) | Moisture Content (%) | Dry Density ($kN/m^3$) |
| 1 | 7.6 | 20.4 | 7.3 | 20.3 | 6.9 | 20.6 |
| 2 | 3.6 | 18.8 | 3.5 | 19.3 | 3.0 | 19.7 |
| 3 | 6.1 | 20.4 | 6.1 | 19.8 | 5.8 | 20.4 |
| 4 | 3.6 | 20.0 | 4.2 | 20.4 | 4.1 | 20.8 |
| 5 | 3.6 | 19.6 | 4.0 | 20.3 | 3.6 | 19.5 |

necessary, to aid the compaction process. It should be noted that due to the weak subgrade conditions, it was not always possible to achieve the target value of 95% relative compaction. In such cases, the compaction process was continued until no significant increase in density was noticed from 3 consecutive passes of a vibratory compactor. The "as-constructed" moisture contents and dry densities of compacted aggregate layers, determined from nuclear gauge testing, are summarized in Table 6.5. Figure 6.22 shows the achieved relative compaction values for individual test sections in each of the five pavement test cells.

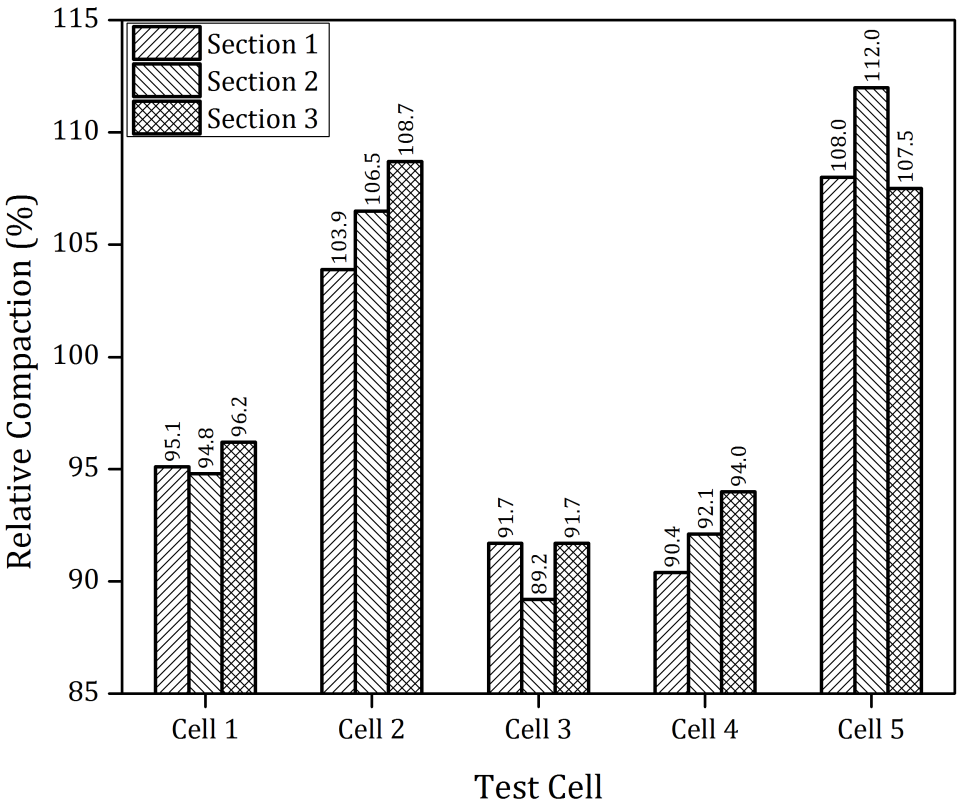


Figure 6.22: Constructed Aggregate Layer Relative Compaction (ASTM D 698) Levels in the Full-Scale Unsurfaced Pavement Test Sections

## 6.10 Summary

This chapter summarized the design and construction of full-scale unsurfaced pavement sections for accelerated pavement testing. Selection of aggregate materials for constructing the test sections was described, followed by laboratory characterization of the selected materials. Two of the aggregate materials (materials 2 and 4) had different fines contents compared to the initially reported values from the quarries, which resulted in a modification of the originally planned material comparisons to evaluate the effects of individual test factors. Results from repeated load triaxial testing of the aggregates were presented, and will be used later in Chapter 8 to explain trends observed in unsurfaced pavement section performance under loading. The use of finite element analysis for thickness design of typical unsurfaced pavement sections was discussed, and the effects of individual test factors on critical pavement response (subgrade vertical deviator stress) were analyzed. Finally, this chapter presented details on the subgrade characterization, moisture control, and aggregate placement for construction of the full-scale test sections for accelerated pavement testing. Chapter 7 will present details on different non-destructive field modulus measurement techniques used in the current study for construction quality assurance, and performance assessment of test sections under loading. The use of Ground-Penetrating Radar (GPR) for assessment of subsurface deformations in unsurfaced pavements will also be discussed in Chapter 7.

# CHAPTER 7

# FIELD MODULUS MEASUREMENT AND SUBSTRUCTURE VISUALIZATION

## 7.1 Introduction

This chapter first presents details on the field modulus measurement and substructure visualization approaches used in the current study to establish links between aggregate quality and performance of unsurfaced pavement sections under loading. The effectiveness of field modulus based assessment of constructed pavement foundation geomaterials is highlighted by presenting results of light weight deflectometer (LWD) and soil stiffness gauge type field devices. The applicability of these two devices for identifying material quality aspects based on field measured moduli is discussed, and influences of achieved moisture-density conditions in the constructed layers on the measured field moduli are investigated. Finally, field and laboratory measured moduli values for the different aggregate types are compared, and the effects of material quality on both are highlighted.

The use of Ground Penetrating Radar (GPR) technology for subsurface deformation assessment in unsurfaced pavements is also described in this chapter. Thin aluminum foil strips were installed at the aggregate-subgrade interface of the constructed full-scale test sections to serve as pure reflectors of GPR electromagnetic waves, and clearly mark the boundary between the two layers. The fundamental principle behind GPR operation is discussed, followed by typical GPR scan results for unsurfaced pavements. Results from the field modulus measurements, and GPR scans of full-scale unsurfaced pavement sections will be used in Chapter 8 to better explain

This chapter includes results already reported in the following publication. Contribution of the coauthors is sincerely acknowledged:

1. *Mishra, D., Tutumluer, E., Moaveni, M. and Xiao, Y.; "Laboratory and Field Measured Moduli of Unsurfaced Pavements on Weak Subgrade"; Accepted for Presentation and Publication at ASCE Geo-Congress 2012-State of the Art and Practice in Geotechnical Engineering, March 25-29, 2012, San Francisco Bay Area, California, USA.*

trends in performance under accelerated pavement testing.

### 7.1.1 Importance of Field Modulus Measurement

Quality control and quality assurance (QC/QA) of pavement layer construction using unbound materials has traditionally been based on target density values, expressed with respect to the maximum achievable densities in the laboratory through commonly used compaction tests (e.g. standard and modified compaction methods). Although past research has successfully correlated higher densities to unbound aggregate layer stiffness or resilient modulus improvements [74, 75], mechanistic-empirical (M-E) pavement design methods do not consider aggregate layer density as an input into pavement thickness design. The resilient modulus on the other hand, governs the nature of stress dissipation in an aggregate layer under loading, and is therefore an essential input for mechanistic analysis of layered pavement structures. This fact alone has made the alternative of measuring in-situ layer modulus very attractive for pavement designers although the development of modulus-based construction control specifications still remains a challenge.

Growing interest in modulus-based compaction control procedures has led to the development of several different alternatives for non-destructive field modulus measurement of pavement layers. The Light Weight Deflectometer (LWD) and the Humboldt® Soil Stiffness Gauge (GeoGauge™) are two such devices that facilitate in-place pavement layer modulus measurement without imposing excessive delays on construction activities. In spite of significant differences in the operating principles, both devices apply a certain load on the pavement surface, and use the resulting deflections to estimate the in-place layer modulus.

In-situ modulus measurements were carried out in this research study using a Dynatest® LWD (model 3031) and a Humboldt® GeoGauge™. Tests were conducted on the engineered subgrade as well as on the finished aggregate layer surface with data collected for the primary objective of analyzing the differences in reported moduli values by the two devices. Rather than comparing the numerical results, the primary focus was to compare the relative trends in the measured moduli from the two devices.

## 7.2 The Light Weight Deflectometer (LWD)

The Light Weight Deflectometer (LWD), also known as a Portable Falling Weight Deflectometer (PFWD) in the United States, is a portable, lightweight device that uses impact loads to estimate the stiffness of pavement layers. A load pulse, generated by dropping a fixed mass through a certain height onto a set of rubber buffers (for damping of the load, and controlling load pulse period), is used for estimating the stiffness of underlying layers. In the Dynatest® LWD (model 3031) used in the current research, the force is transmitted to the ground through a circular plate, typically 300 mm in diameter (but interchangeable to 150 mm). Applied load levels are measured using a load cell, whereas the induced surface deflections are measured by a geophone (velocity transducer) extending through a hole at the center of the base plate. Relative velocities between the pavement surface and the base plate are measured by the geophone, and are subsequently integrated to calculate the surface deflections. Besides the geophone at the center of the base plate, this device also has the capability to measure deflections using two other geophones located at different offsets from the base plate, in a user-defined pattern. Deflection and load time history data are transferred to a Personal Digital Assistant (PDA) device using Bluetooth connection for real time data processing. Relevant technical specifications of the Dynatest® 3031 LWD are presented in Appendix C. Figure 7.1 shows a schematic of different components of a light weight deflectometer assembly equipped with two radial geophone configuration [102].

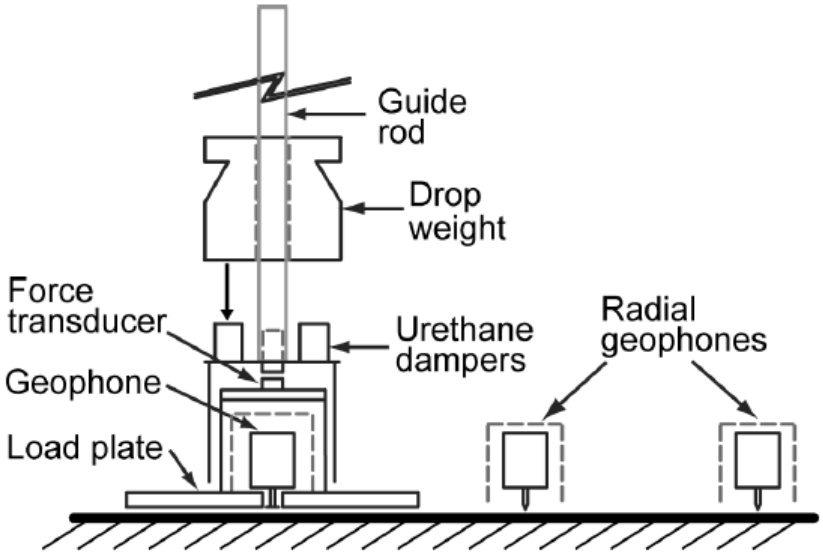


Figure 7.1: Schematic of a Light Weight Deflectometer with Additional Sensors [102]

### 7.2.1 LWD Types and Capabilities

Although the Falling Weight Deflectometer (FWD) is more commonly used for in-place stiffness evaluation of pavement layers, it has several limitations as far as testing on weak subgrades, and unsurfaced pavements constructed over weak subgrade, is concerned. Several portable alternatives have therefore been developed for in-place stiffness estimation of pavement layers under such conditions. Examples of such portable falling weight deflectometers (PFWD) are: Loadman [103], German Dynamic Plate Bearing Test (GDP) [104], TRL Foundation Tester (TFT) [105], and Prima 100 [106]. Several researchers [107, 108, 109] have compared important features of commercially available LWD models, and have highlighted their relative advantages and disadvantages. Although earlier versions of LWDs used the same velocity transducer (geophone) for both deflection (through single integration of the velocity) as well as force measurements, improvements over the years have introduced the use of separate load cells for direct measurement of applied force [107]. Table 7.1 compares important features of the Dynatest® 3031 LWD used in this research to other LWD models.

Table 7.1: Comparison of Commercially Available LWD Models (Modified from [108])

| **Characteristic** | **GDP** | **Prima** | **Loadman** | **TFT** | **Dynatest** |
|---|---|---|---|---|---|
| Plate Style | Solid | Annulus | Solid | Annulus | Annulus |
| Plate Dia (cm) | 15/20/30 | 10/20/30 | 13/20/30 | 10/15/20/30 | 10/15/20/30 |
| Plate Mass (kg) | 15 | 12 | 6 | Variable | 12 |
| Drop Mass (kg) | 10 | 10/15/20 | 10 | 10/15/20 | 10/15/20 |
| Drop Height (kg) | 0.72 | Variable | 0.8 | Variable | Variable |
| Damper | Steel Spring | Rubber | Rubber | Rubber | Rubber |
| Force Measurement | No | Yes | Yes | Yes | Yes |
| Plate Resp. Sensor | Accelerometer | Geophone | Accelerometer | Geophone | Geophone |
| Impulse Time (ms) | 18 ±2 | 15-20 | 25-30 | 15-25 | 15-30 |
| Max Load (kN) | 7.07 | 1-15 | 20 | 1-15 | 1-25 |
| Contact Stress | Uniform | User def. | Rigid | User def. | User def. |
| Poisson's Ratio | 0.5 | User def. | 0.5 | User def. | User def. |

From Table 7.1 it can be seen that the Dynatest® 3031 has several features that make it a versatile tool to be used on different material types, applying different levels of peak loads. It should be noted that the latest version of Prima™100 has essentially the same capabilities as the Dynatest® 3031 [110].

### 7.2.2 Theory of Operation

Layer stiffness estimation using LWD is typically based on the principle of conventional static elastic theory by assuming the pavement system to behave as a homogeneous, isotropic, linear elastic semi-infinite halfspace. Contact stress distribution between the bearing plate and the ground is assumed as uniform or similar to that between a rigid plate on an elastic medium based on different combinations of layer and plate rigidity [111]. For an LWD equipped with one geophone only (to measure center deflection), Boussinesq elastic half space theory can be used to estimate the composite stiffness (E) of the underlying layers, as shown in Equation 7.1.

$$E = \frac{K.p.r.\left(1-\upsilon^2\right)}{d} \tag{7.1}$$

where: E is the composite stiffness (also known as surface modulus), K is a stress distribution factor (depends on layer and base plate rigidity), p is the applied contact pressure, r is the plate radius, d is the deflection, and $\upsilon$ is Poisson's ratio.

For multi-layer systems, the use of Odemark's layer transformation is made along with Boussinesq's equations to calculate deflections in a forward calculation approach.

Careful consideration needs to be given to the interpretation of deflections measured by LWDs. Commercially available LWD software packages usually integrate the geophone signal to determine the peak deflection value. However, due to dynamic effects, the peak deflections measured by geophones do not always occur at the same instant as the peak load (particularly for weak materials). Moreover, deflections induced by the dropping weight comprise both recoverable (elastic) and non-recoverable (plastic) components, and therefore the measured stiffness values are not strictly "elastic" [112]. It is therefore important to practice caution, while using LWD-measured layer modulus values in pavement design packages based on linear-elastic theory. To avoid interpretation of LWD-measured moduli as "elastic", the term "Stiffness Modulus" is used in the UK for presenting LWD measured moduli. The terms "Field Modulus" and "Surface Modulus" are used in this PhD thesis to present layer stiffnesses measured by different devices. Analyses of elastic and plastic components of the induced deflections, are beyond the scope of this research.

### 7.2.3 LWD Testing on Pavement Foundations

Flemming et al. [112] conducted site trials for construction quality assurance using light weight deflectometers, and have reported relatively larger variability in stiffness results on subgrade, compared to well-controlled subbase materials. Moreover, issues with the consistency of good plate to ground contact, and variation in operator test methodologies and basic operator errors have also been reported as sources of inconsistent data [112, 113]. Flemming et al. [113] reported varying success from using a fine sand to smoothen the contact between the loading plate and the ground. Although a small amount of sand was found to improve the contact significantly, a reduction in the measured moduli was observed when excessive sand was used.

During the current research, proper contact between the bearing plate and pavement layer surface was ensured either by placement of a rubber pad (for testing on compacted subgrade), or a thin layer of fine sand (for testing on compacted aggregate layer) underneath the plate. Using at least three seating drops in each test location ensured proper seating of the plate and contact of the geophone with the pavement layer surface. Typical peak stress levels recommended by the manufacturer [114] were followed in this research to ensure operation of the geophones within the calibrated range, and are shown in Table 7.2.

Table 7.2: Recommended Stress Levels for LWD Testing on Unbound Granular Layers

| **Layer Type** | **Stress Range (kPa)** |
|---|---|
| Granular Base | 200-300 |
| Subbase | 100-200 |
| Solid Subgrade | 50-100 |
| Soft Subgrade | 10-60 |

## 7.3 Humboldt® Soil Stiffness Gauge (GeoGauge™)

The Soil Stiffness Gauge or GeoGauge™, manufactured by Humboldt®, is a portable instrument for measuring in-place moduli and load carrying abilities of compacted soil and aggregate layers in a simple, rapid, and precise way [115]. The GeoGauge™ is 28 cm in diameter and 25.4 cm in height and weighs approximately 10 kg. An annular ring, with 114-mm outer diameter and 89-mm inner diameter contacts the soil and supports the weight of the device. Figure 7.2 presents

a schematic of different components of the GeoGauge™ [115].

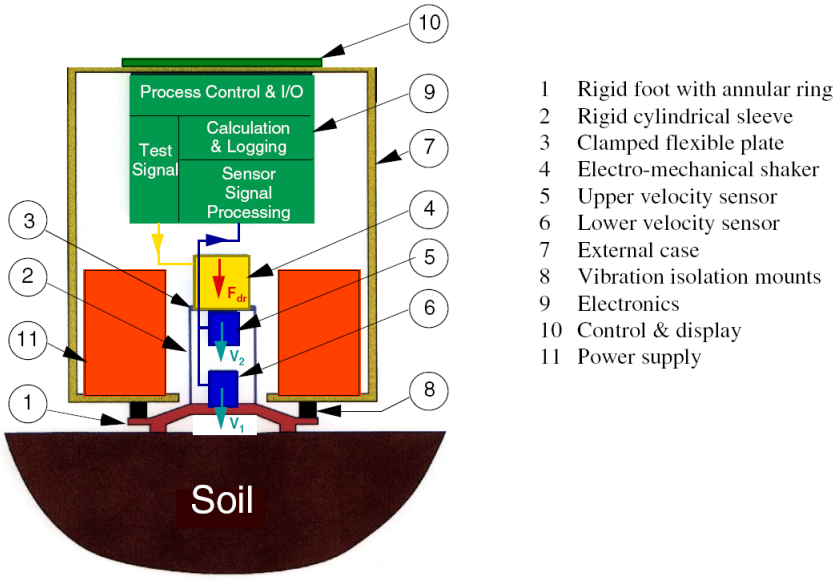


Figure 7.2: Schematic Diagram of the Humboldt® Soil Stiffness Gauge (GeoGauge™)[115]

### 7.3.1 Theory of Operation

Contrary to commonly used deflection based modulus measurement methods, i.e. Falling Weight Deflectometer (FWD) and LWD, that apply large impact forces to produce measurable deflections in a pavement layer, the GeoGauge™ imparts a very small dynamic force of approximately 9-N magnitude [116] at 25 steady state frequencies ranging from 100 to 196 Hz. The force is transmitted to the ground by an annular ring attached to foot of the device, and induces surface deflections, often smaller than $1.27 \times 10^{-6}$ m in magnitude. The surface deflections are used to calculate the layer stiffness value (ratio of applied force to resulting deflection) corresponding to each frequency. Ultimately an average stiffness value is calculated by considering the 25 steady state frequencies. With an assumed Poisson's ratio, the Young's modulus (E) and shear modulus (G) of the material can be determined using the equations given below:

$$E \approx \frac{P}{1.77 \times R \times \delta}\left(1-\nu^2\right) \tag{7.2}$$

$$G \approx \frac{P}{3.54 \times R \times \delta}\left(1-\nu\right) \tag{7.3}$$

where P is the applied load, R is outer radius of the annular ring, $\delta$ is the induced surface deflection, and $\nu$ is Poisson's ratio of the elastic medium. The GeoGauge™ modulus was reported to be influenced by density, moisture content, boundary conditions, and stiffness of the underlying layers [116, 117].

Figure 7.3 shows the LWD and GeoGauge™ testing conducted consistently at the same locations on the compacted subgrade and aggregate layers. In-place moisture-density conditions were also measured using a Troxler® 3450 nuclear density gauge. For analysis of the LWD and GeoGauge™ test results, Poisson's ratio values of 0.35 and 0.45 were assumed for the aggregate and subgrade layers respectively. Moreover, a uniform stress distribution was assumed underneath the LWD base plate (K = 2).

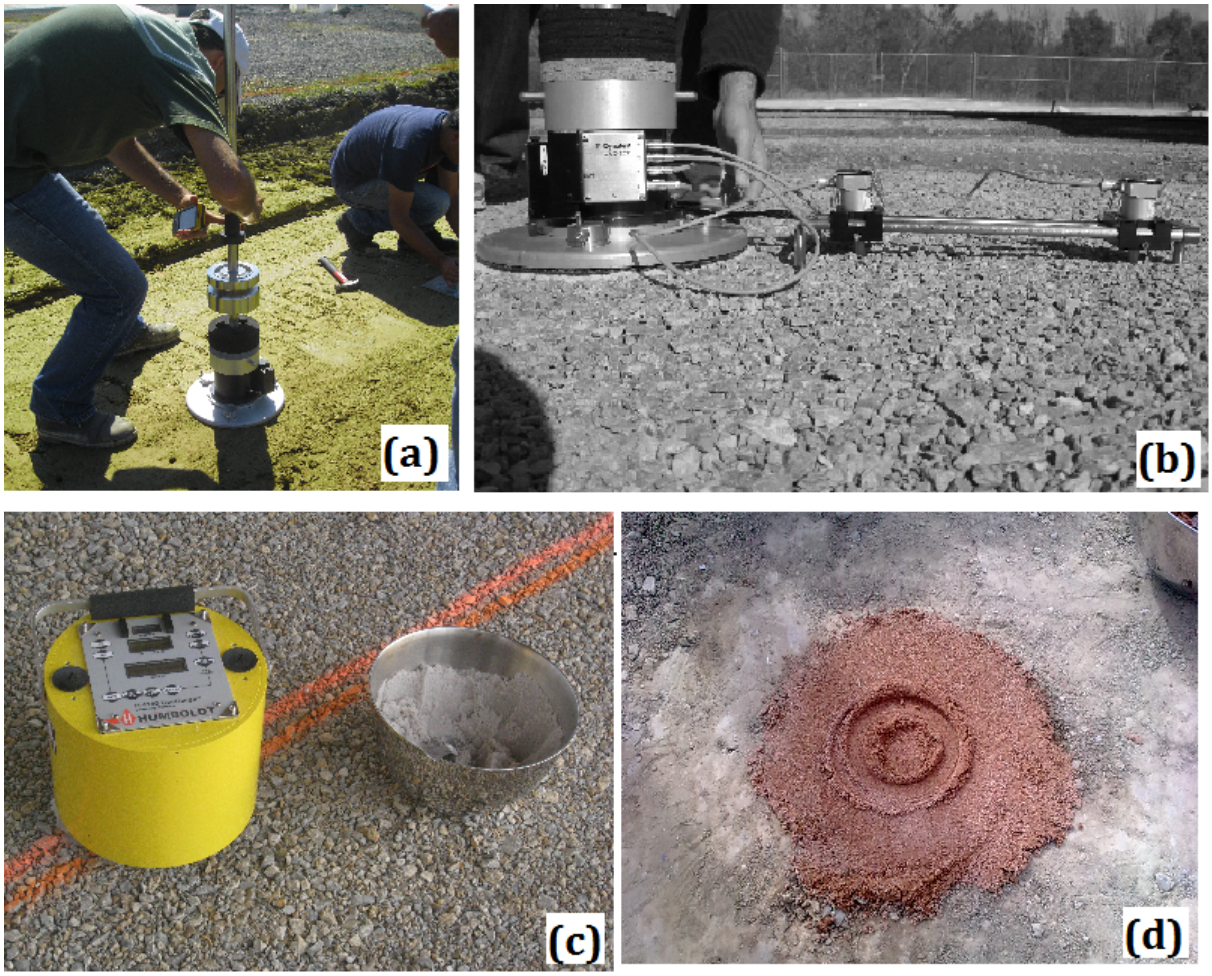


Figure 7.3: (a) LWD Testing on Compacted Subgrade, (b) LWD Testing on Aggregate using the 3-Sensor Assembly, (c) GeoGauge™ Testing on Aggregate, and (d) Bedding Sand Layer Prepared on Aggregate for GeoGauge™ Testing

## 7.4 Analysis of Field Modulus Test Results

### 7.4.1 Field Modulus Measurements on Engineered Subgrade

Results from in-place modulus measurements on top of the subgrade layer are presented in this section. As described in Chapter 6, test section subgrades were prepared in the field by adjusting the moisture contents to achieve target CBR values of 3% (Cells 1 through 4), and 6% (Cell 5). Figure 7.4 presents the subgrade modulus properties measured on Cell 1, which was constructed to a target engineered CBR value of 3%. As shown in Figure 7.4, the modulus values reported by the GeoGauge™ were consistently higher than those measured by the LWD for all three test sections. This was expected, as the strain amplitudes imposed by the GeoGauge™ are significantly lower than those imposed by the LWD. Ryden and Mooney [118] extracted low-strain modulus values from seismic waves during LWD tests, and highlighted the effect of strain levels on field-measured modulus values. Regardless, both devices reported consistent trends in the relative modulus values for the three sections (significantly higher modulus for Section 3 compared to Sections 1 and 2). The higher moduli for Section 3 were primarily due to non-uniform moisture distribution during subgrade preparation in this section. In-place CBR measurements using a Dynamic Cone Penetrometer (DCP) confirmed the non-uniform moisture distribution across the three sections (Section 3 had an average CBR value of 3.9%, compared to 3.0% and 2.7% for Sections 1 and 2, respectively as shown in Figure 7.5).

Figure 7.6 shows subgrade modulus values measured on a significantly stronger subgrade (Cell 5) with a target engineered CBR value of 6%. Note that both the LWD and the GeoGauge™ reported significantly higher modulus values for the stronger subgrade in Figure 7.6 when compared to the values shown in Figure 7.4. The GeoGauge™ measured moduli were slightly higher than those measured with the LWD. The consistent subgrade conditions across the three sections in Figure 7.6 were properly captured by both devices, and were confirmed through DCP testing.

Although the actual magnitudes of moduli reported by the two devices were different from each other, both the LWD and the GeoGauge™ successfully identified the anomaly in construction quality, which was the non-uniform moisture distribution in Cell 1 leading to higher strength for Section 3. This reinforced the findings from the recent NCHRP 10-65 study [119] which reported

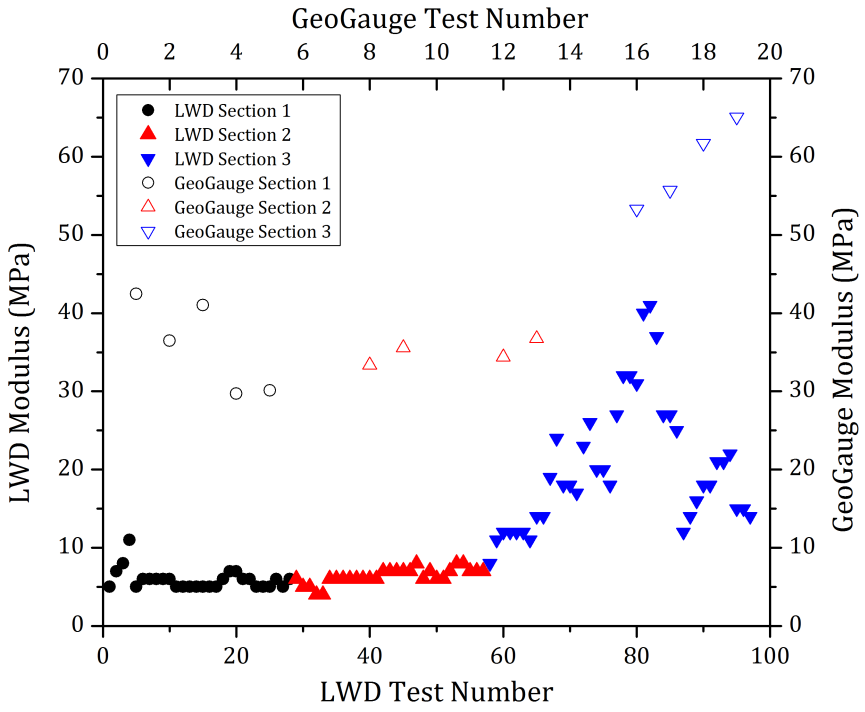


Figure 7.4: Field Modulus Values by LWD and GeoGauge™ Showing Similar Trends but Different Magnitudes on a Compacted Subgrade of Target CBR = 3%

that these field modulus measurement devices consistently identified differences in construction conditions, irrespective of the magnitudes of measured moduli. Further, the study reported a higher success rate (79%) for the GeoGauge™ compared to the LWD (64%) for effectiveness in identifying differences in construction conditions [119].

### 7.4.2 Modulus Measurements on Compacted Aggregate Layers

Field modulus measurements on compacted aggregate layers were also carried out using the LWD and the GeoGauge™ to get a comparative idea about the moduli values associated with different aggregate qualities. Testing always at the same location facilitated such comparison of modulus trends measured with each device. Moisture-density conditions of the aggregate layers were also measured using a nuclear gauge to analyze the trends in field modulus values with traditional compaction QC/QA results. Figure 7.7 shows the moduli values measured on the compacted aggregate layer constructed over Cell 1 (over the subgrade tested in Figure 7.4). As already mentioned in Chapter 6, the aggregate layers in Cell 1 were constructed using an uncrushed "river-run" gravel with high amounts of nonplastic fines, and were compacted targeting 95% of

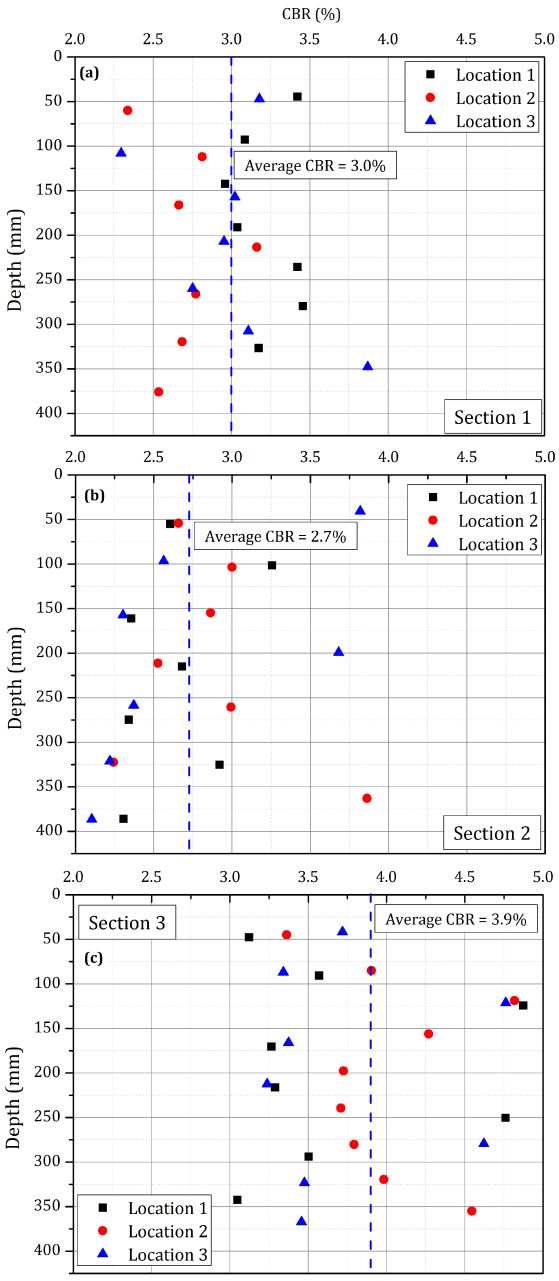


Figure 7.5: CBR Profiles in Engineered Subgrade of Target CBR = 3%

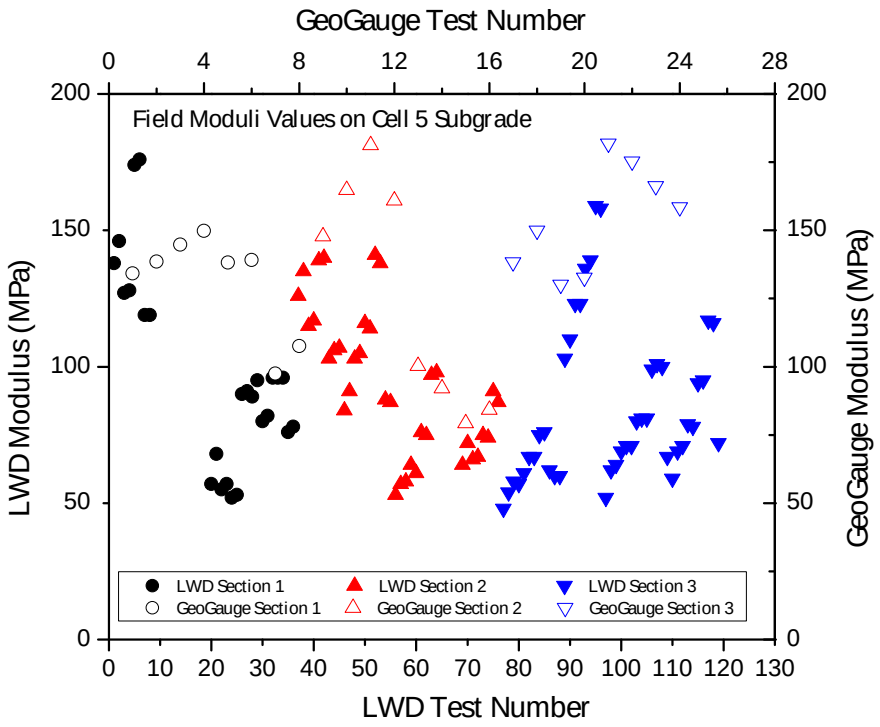


Figure 7.6: Field Modulus Values by LWD and GeoGauge™ Showing Similar Trends and Magnitudes on a Compacted Subgrade of Target CBR = 6%

standard compaction maximum dry density.

For Sections 1 and 2 (356-mm and 305-mm thick aggregate layers, respectively) presented in Figure 7.7, the field moduli reported by the two devices were reasonably close to each other. However, for Section 3 (203-mm thick aggregate layer), the modulus values from LWD were significantly lower than those measured with the GeoGauge™. Note that the Section 3 subgrade for Cell 1 had significantly higher modulus/stiffness properties compared to Sections 1 and 2 (see Figure 7.4). Moreover from Figure 7.7, the achieved compaction level for the aggregate layer in Section 3 was higher than those for the other two sections. As higher degree of compaction usually corresponds to higher modulus values [74, 75], the aggregate layer in Section 3 would then be expected to have higher moduli compared to Sections 1 and 2. Although the GeoGauge™ results followed this same trend, the LWD measured significantly lower modulus values for the aggregate layer in Section 3, which may be explained based on the depth of influence of the two devices. The depth of influence for LWD reported in literature is between 270 to 280 mm [120, 121], deeper than the 203-mm thick aggregate layer in Section 3. According to

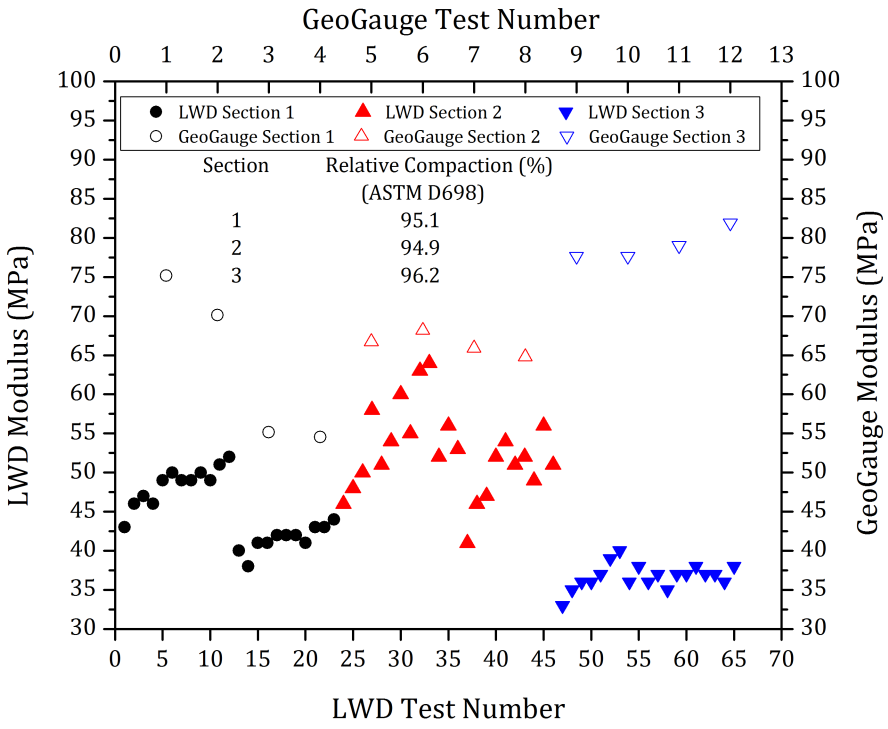


Figure 7.7: Field Modulus Values by LWD and GeoGauge™ Showing Different Trends and magnitudes on Compacted Uncrushed Gravel Layer

Von Quintus et al. [119], LWD tests on thin pavement layers were significantly influenced by the underlying layer, and therefore the results were consistently higher or lower than laboratory measured modulus values for those particular materials. Moreover, Mooney and Miller [108] reported a depth of influence for LWD between 0.9-1.1 times the plate diameter. Therefore for the given study, the depth of influence for the LWD would be between 270-300 mm. Accordingly, the lower LWD-measured modulus values corresponding to the 203-mm thick aggregate layer in Section 3 were probably due to the influence of the weak underlying subgrade layer.

### 7.4.3 Effect of Moisture-Density Conditions

Figure 7.8 shows together the nuclear gauge-determined moisture content and dry density values with the field-measured modulus values for all compacted aggregate layers tested in this field study. Note that both the LWD and the GeoGauge™ show decreasing modulus values with increasing moisture contents for the different test sections highlighted. However, the effect of dry density on layer modulus was not as clear from Figure 7.8 although Von Quintus et al. [119] reported a strong correlation between GeoGauge™ moduli and achieved dry densities in

compacted pavement layers.

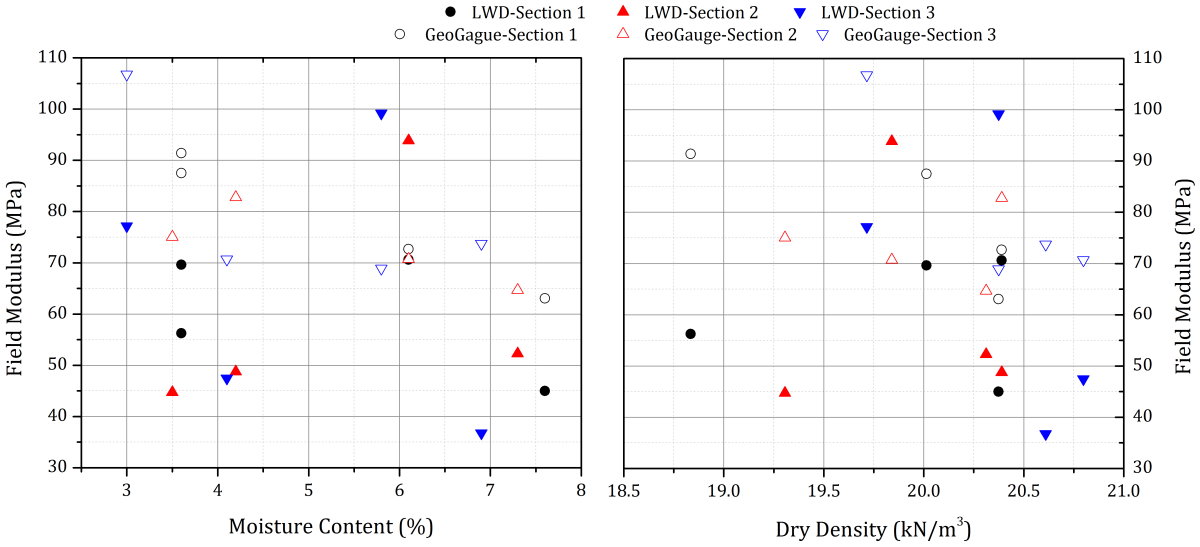


Figure 7.8: Field Moduli Vs. Achieved (a) Moisture Contents and (b) Dry Densities

### 7.4.4 Aggregate Quality Linked to Laboratory and Field-Measured Moduli

As described in Chapter 6, laboratory repeated load triaxial tests were conducted on the four different aggregate materials used in construction of the full-scale tests sections, following the AASHTO T 307 [90] test procedure. Figure 7.9 shows the stress dependent resilient modulus values graphed against the bulk stress (first stress invariant) for the four aggregate types. Note that the uncrushed gravel with 12% fines, corresponding to Cell 1 (tested in Figure 7.7), had significantly lower laboratory-measured modulus values when compared to the other three crushed aggregates. The crushed limestone with 10% fines showed the highest modulus values. Figure 7.9 clearly highlights the detrimental effects of higher fines contents in an aggregate matrix on resilient modulus properties.

Figure 7.10 summarizes the field modulus values measured on all unsurfaced pavement sections constructed using the four aggregate materials. Although the goal was to establish possible linkages between aggregate type and/or fines percentage and field-measured modulus values, no significant effects of aggregate material quality on field moduli were apparent from Figure 7.10. Furthermore in contrast with the laboratory-measured results, the crushed limestone with 10% fines was not indicated to have highest field modulus values. Similarly, the much lower

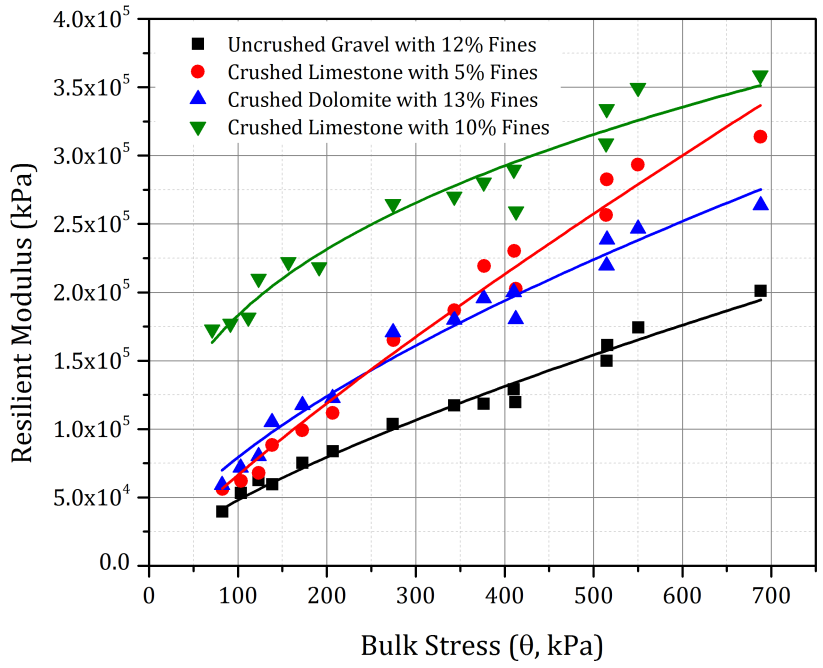


Figure 7.9: Effects of Aggregate Type and Fines Content on Laboratory-Measured Resilient Modulus Properties

laboratory-measured moduli associated with the uncrushed gravel material were not reflected from the field measurements (see Figure 7.10). From field modulus measurements using the LWD and the GeoGauge™ on the subgrade and compacted aggregate layers, it was evident that although both devices were successful in identifying non-uniform construction conditions, no significant effect of aggregate material quality on field modulus was observed. The GeoGauge™ reported more consistent results compared to the LWD primarily due to different depths of influence for the two devices.

## 7.5 Subsurface Visualization using Ground Penetrating Radar

This section covers the application of Ground-Penetrating Radar (GPR) for distinguishing between aggregate and subgrade rutting in unsurfaced pavements. Transverse scanning of the full-scale unsurfaced pavement sections constructed during this research was carried out using GPR to evaluate the effect of aggregate quality on subsurface deformation accumulation. Strips of aluminum paint and thin aluminum strip foils were placed at the aggregate-subgrade interface to function as a pure reflector for electromagnetic (EM) GPR and clearly identify the layer

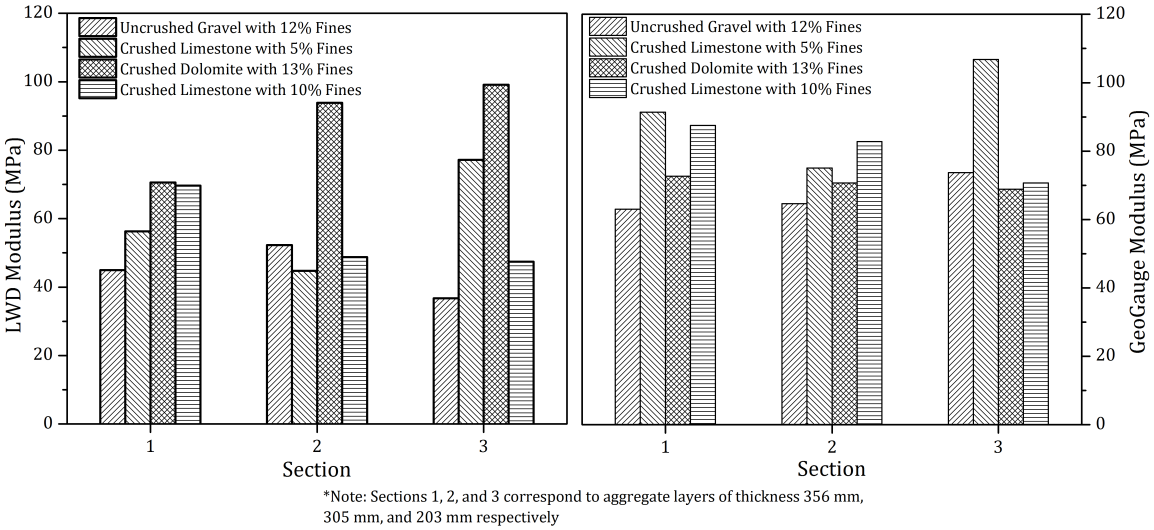


Figure 7.10: Effect of Aggregate Quality on Field Modulus

boundaries.

### 7.5.1 GPR Principles and Data Reduction

The application of GPR is based on transmission of electromagnetic (EM) pulses into the ground and collection of reflected pulses from interfaces corresponding to dielectric contrast. The application of GPR in pavement engineering was first initiated in the 1970's by the Federal Highway Administration (FHWA) for tunnel applications [122] and has since been extended to a wide range of applications, the most common being pavement layer thickness measurement [123, 124, 125, 126, 127], detection of pavement distresses [128, 129], determination of depth and alignment of steel bars [130, 131], and estimation of density and air void content [132, 133, 134].

Depending on the way antennae are deployed, GPR systems are classified into air-coupled (or launched), or ground-coupled systems. Air-coupled antennae are typically mounted 150 to 500 mm (5.9 to 19.7 in.) above the surface (see Figure 7.11a). These systems produce a clean radar signal at the pavement surface and allow for highway speed surveys (up to 100 km/h or 62.5 mph). The drawback of these systems lies in the low depths of penetration as part of the EM energy is reflected back by the pavement surface. In contrast, a ground-coupled GPR antenna is in full contact with the ground (see Figure 7.11b), which gives a deeper penetration at the same frequency but limits the speed of the survey (usually less than 8 kmph or 5 mph). Depending on the requirement of signal resolution and penetrating depth, various antenna frequencies can be

selected for each type of antennae [135]. A general rule of thumb is: a higher antenna central frequency provides a better signal resolution but lower penetrating depth.

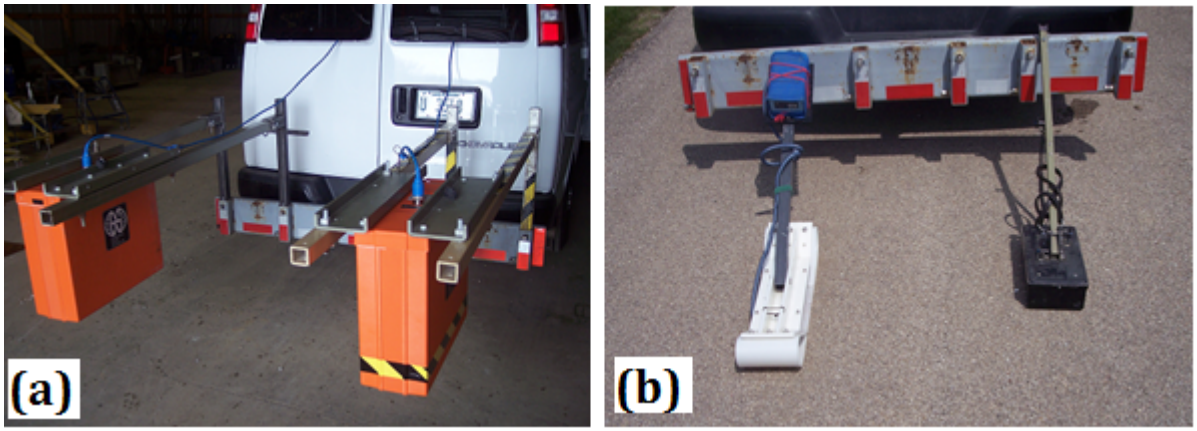


Figure 7.11: Types of GPR Antennae: (a) Air-coupled and (b) Ground-coupled

In this study, a 2GHz air-coupled antenna system, manufactured by Geophysical Survey Systems, Inc. (GSSI), was used to differentiate subgrade rutting from shear flow within the UGL. An air-coupled system was selected to track the deformation of both the aggregate surface and the subgrade interface. The maximum penetrating depth of the 2GHz air-coupled system is approximately 610 mm (24 in.), which is sufficient to penetrate the thickest aggregate section (356 mm or 14 in.) constructed in this study.

Figure 7.12a shows an example single-scan (A-scan) GPR signal collected from an unsurfaced pavement system. The vertical axis in the figure represents GPR signal two-way travel time and the horizontal axis represents reflected signal amplitude. As illustrated in the figure, the first pulse (on the top) corresponds to the coupling between the transmitting and receiving antennae; the second pulse corresponds to the signal reflected from the aggregate surface whereas the third (bottom most) pulse represents the signal reflected from the subgrade interface. A B-scan GPR image (see Figure 7.12b) can be obtained by stacking multiple single-scan GPR signals collected at different locations and using different colors or grey scales to represent different signal reflection amplitudes. In a B-scan GPR image, the horizontal axis represents the GPR survey distance whereas the vertical axis represents GPR signal two-way travel time. The white color shown in the image (see Figure 7.12b) marks the maximum signal reflection amplitude whereas the black color marks the minimum reflection amplitude. From Figure 7.12b, the pavement

structure profile can be clearly visualized. In this study, the B-scan images of the cross sections of each test section at different loading cycles were used to distinguish between rut accumulations in the aggregate and subgrade layers.

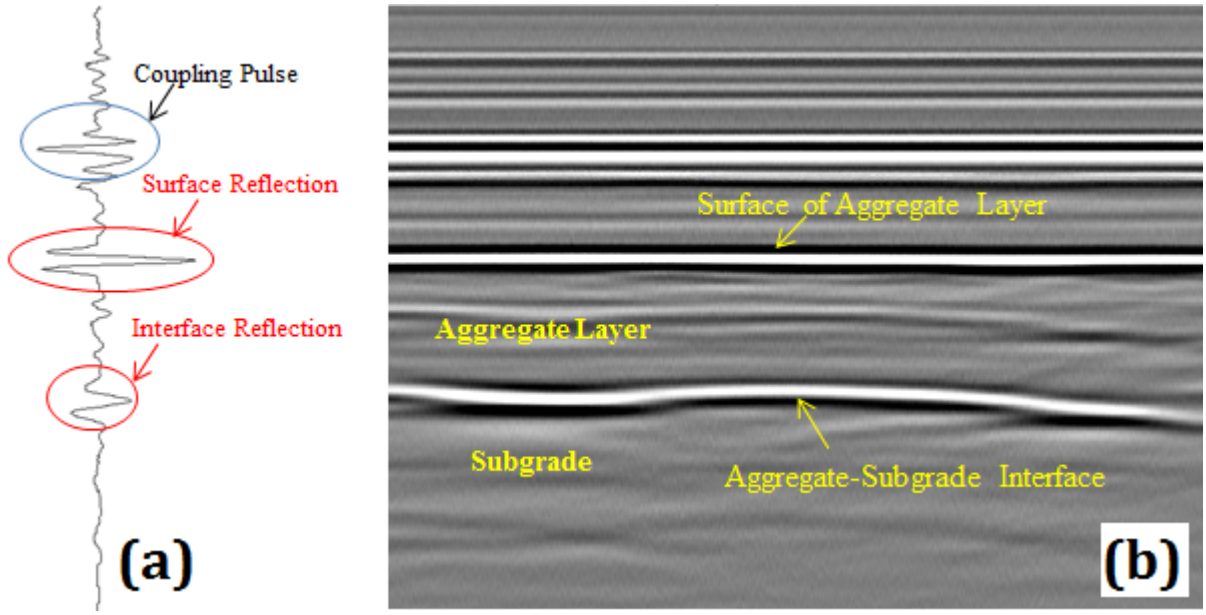


Figure 7.12: Example GPR Data from an Unsurfaced Pavement: (a) Single Scan (A-scan); (b) B-scan Image of the Cross Section

### 7.5.2 Transverse Scanning of Unsurfaced Pavement Sections

After compaction of the engineered subgrade, thin aluminum foil strips were installed at locations corresponding to positions where surface profile measurements would be taken. The aluminum strip was installed to serve as a reflector for the GPR's EM waves to identify the aggregate-subgrade interface. The aluminum strip was sufficiently thin (foil) to ensure it did not have any effect on the pavement rutting performance. Moreover, the subgrade underneath the aluminum strip was coated with aluminum paint to present another reflective surface in case the aluminum strip was ruptured during construction.

Following placement of the aluminum strips, the aggregate was hand-placed on top of the aluminum to prevent rupture from construction equipment. Figures 7.13a and 7.13b show installation of aluminum strip, and hand placement of aggregate on top of the strip. Figure 7.13c shows a custom-built GPR track to facilitate transverse scanning of the pavement sections. The

track was built by assembling two long wooden beams to accommodate a set of plastic wheels mounted on a 2GHz air-coupled GPR antenna system. Care was taken to not use any metallic components in the construction of the GPR tracks to avoid interference with the GPR waves. Figure 7.13d shows GPR scanning of the pavement sections by pulling the antenna along the track at a uniform rate. Note, that scanning with a vehicle mounted antenna was not feasible because of the positioning of ATLAS on top of the pavement sections.

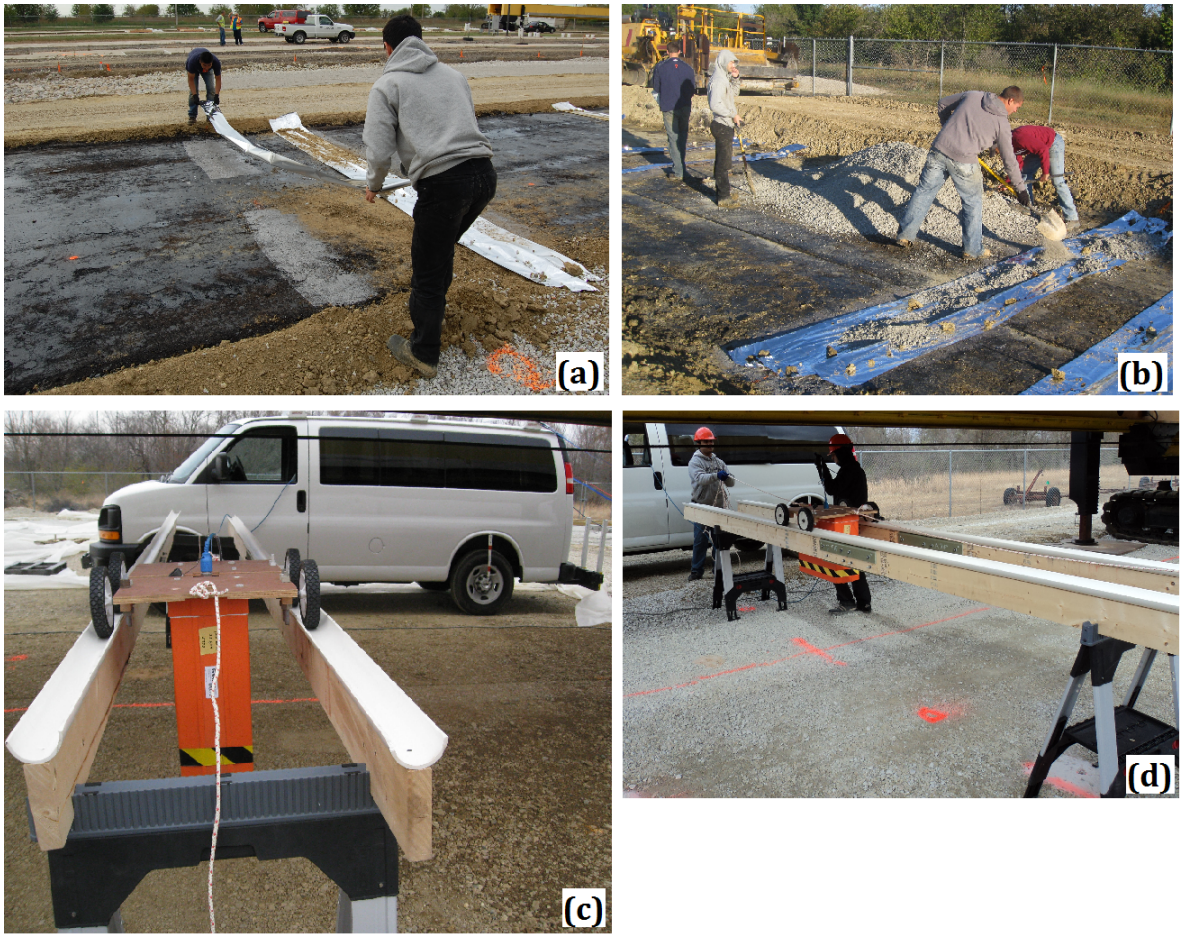


Figure 7.13: Aluminum Foil Installation (a), Aggregate Placement (b), Customized GPR Track for Transverse Scanning of Aggregate Sections (c), GPR Scanning to Measure Rut Development (d)

### 7.5.3 GPR Quantification of Rutting in Subsurface Layers

It is worth noting that the GPR scanning of unsurfaced pavements presented in this PhD work are qualitative and visual in nature. These preliminary findings can further be extended to

quantify the rut accumulation in individual layers. This can be done through the estimation of dielectric constants of individual layers, and the overall concept is presented in this section for further application to unsurfaced pavements.

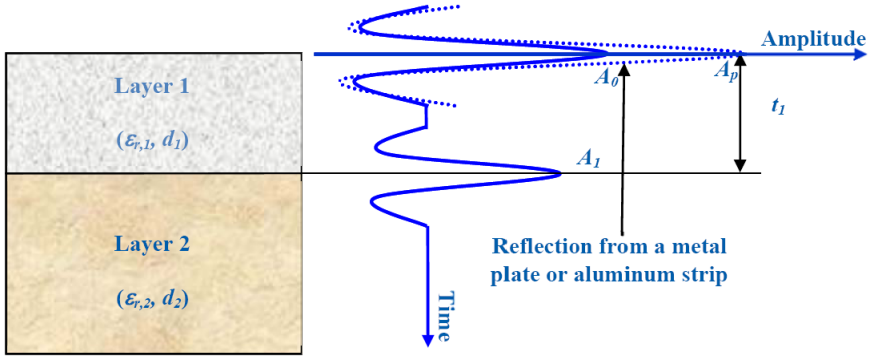


Figure 7.14: Typical Reflections from Interfaces in Unsurfaced Pavements

For a layered structure as shown in Figure 7.14, the thickness of the surface layer, $d_1$, can be calculated using the following equation when its dielectric constant $\epsilon_{r,1}$ is known:

$$d_1 = \frac{ct_1}{2\sqrt{\epsilon_{r,1}}} \tag{7.4}$$

In Equation 7.4, c is the speed of light in vacuum ($3 \times 10^8$ m/s or $9.8 \times 10^8$ft/s), and $t_1$ is the two-way travel time of the GPR signal within the surface layer. For bound pavement layers, such as hot-mix asphalt and Portland cement concrete, the following equation is widely used to estimate the dielectric constant of the surface layer, based on the GPR measurement:

$$\epsilon_{r,1} = \left( \frac{1 + \frac{A_0}{A_p}}{1 - \frac{A_0}{A_p}} \right)^2 \tag{7.5}$$

where $\epsilon_{r,1}$ is the dielectric constant of the first layer, $A_0$ is the amplitude of the surface reflection, and $A_p$ is the amplitude of the incident GPR wave, which is obtained by collecting data over a copper or aluminum reflector placed on the pavement surface.

However, it should be noted that the dielectric constant calculated using Equation 7.5 is based on the surface reflection of the GPR signal. Therefore, estimated surface layer thickness using this dielectric constant is based on the assumption that the material property of the surface layer

is uniform through the depth. This assumption is more reasonable in case of bound layers at early ages. However, for unbound granular layers, this assumption may lead to errors due to the relatively large variation of the material properties with depth; especially after being loaded. To obtain the average dielectric constant of the aggregate layer, another method, namely the extended common mid-point method, by using two air-coupled antenna systems, can be used [136]. The feasibility of employing this method to quantify the rutting in individual layers is suggested as future research scope in Chapter 9 of this PhD thesis.

## 7.6 Summary

The first part of this chapter presented results from non-destructive field modulus measurement techniques used in the current research to evaluate the effectiveness of these devices in identifying differences in aggregate quality, and for application in construction quality control. Field modulus measurements were taken using light weight deflectometer (LWD) and GeoGauge™ devices always at the same locations to eliminate effects of spatial variability in construction conditions. From testing on the engineered weak subgrades as well as constructed aggregate layers, it was observed that GeoGauge™ reported modulus values were consistently higher than those measured by the LWD due to the fact the moduli from the two devices were defined in different ways.

Both the GeoGauge™ and the LWD were successful in identifying anomalies in construction conditions, i.e., increasing or decreasing trends in moduli. The GeoGauge™ measured modulus values showed in general a decreasing trend with increasing moisture contents. However, the effects of dry density and material quality, associated with aggregate type and properties, were not reflected from the field modulus values. In that sense, the field modulus values could not be associated with the laboratory-measured modulus properties, which properly captured not only stress dependencies but also the effects of aggregate angularity and fines content.

The second part of this chapter presented the application of GPR technology for assessment of subsurface deformations in unsurfaced pavements. Basic principle of GPR operation was presented, followed by the installation of reflective strips at the aggregate-subgrade interface of full-scale test sections constructed during the scope of this research study. Typical GPR scan results for 2-layer unsurfaced pavement structures were presented, and the methodology for visual

identification of aggregate and subgrade rutting was explained. Results from the filed modulus measurements and transverse GPR scanning of unsurfaced pavement sections will be used in Chapter 8 to explain observed trends in test section performance under accelerated loading.

# CHAPTER 8

# ACCELERATED TESTING AND PERFORMANCE MONITORING

## 8.1 Introduction

This chapter reports results from accelerated pavement testing, and performance analyses of full-scale unsurfaced pavement sections constructed during the second phase of this PhD research. As discussed in Chapter 6, full scale pavement sections were constructed at the University of Illinois Advanced Transportation Research and Engineering Laboratory (ATREL) facility using aggregate types representing different combinations of the aggregate physical properties (test factors) of interest. The test sections were subsequently loaded using an Accelerated Transportation Loading Assembly (ATLAS) to apply channelized traffic and simulate the movement of heavy trucks and construction vehicles. Rut accumulation in the pavement sections under loading was monitored through surface profile measurements, as well as GPR scanning. After loading the test sections to failure, transverse trench sections were excavated across the wheel paths to get visual confirmation regarding the rut accumulation in aggregate and subgrade layers. Effect of different aggregate physical properties on field performance of unsurfaced pavement sections was then evaluated through analyses of mechanisms contributing to pavement failure.

---

This chapter includes results already reported in the following publications. Contribution of the coauthors is sincerely acknowledged:

1. *Mishra, D., Tutumluer, E., and Heckel, G.; "Performance Evaluation of Uncrushed Gravel Aggregates in Unsurfaced Road Applications through Accelerated Pavement Testing"; Accepted for Publication in Transportation Research Record: Journal of the Transportation Research Board (2012).*
2. *Mishra, D., and Tutumluer, E.; "Performance Evaluation of Unsurfaced Pavements using the UIUC Accelerated Transportation Loading Assembly"; Accepted for Presentation and Publication at the $4^{th}$ International Conference on Accelerated Pavement Testing, September 19-21, 2012, Davis, California, USA.*

## 8.2 Test Section Loading and Performance Monitoring

Design and construction of the full-scale unsurfaced pavement test cells representing different combinations of aggregate physical properties was presented in Chapter 6. Each test cell comprised three sections, numbered from West to East in an increasing order, (Sections 1, 2, & 3 respectively), characterized by different aggregate layer thicknesses constructed over a subgrade of controlled CBR. After construction, the pavement sections were loaded to failure by unidirectional, channelized application of a 44.5-kN (10-kip) wheel load using a super-single tire (455/55R22.5) at a tire pressure of 758 kPa (110 psi). The tire nomenclature denotes its dimensions and type in the form of AAA/BBXCC.C, where the first number (455) is the tire width from wall-to-wall in mm; the second number (55) is the side wall height given as a percentage of the tire width (250 mm for the tire in consideration); the letter 'R' indicates a radial tire; and the third number (22.5) is the rim diameter in inches.

The development of rutting with load application for each test section was monitored through surface profile measurements using a digital calliper. Average surface profile for each test section was calculated using two measurements separated by a distance of 152 cm (5 ft), located 152-cm (5-ft) away from the section boundaries on either side. Since the profile of an unsurfaced pavement is much more variable compared to that of a pavement with a bound surface layer, it was important to take several adjacent measurements to develop the average surface profile around a particular point. The surface profile was measured for up to a distance of 1.22 m (4 ft.) on either side of wheel path centerline. Wheel path wander effects were not considered in the current accelerated pavement testing effort to eliminate the "masking" of rut profiles resulting from collapse of the unbound aggregate surface materials into the rut path. In other words, loose aggregate particles from the surface would be "pushed" into the rut profile upon repeated loading along adjacent wheel paths, thus making it difficult to accurately monitor the rate of rut accumulation in the test sections. Moreover as unsurfaced pavements and low volume roads are often constructed under financial constraints, they are usually narrow and cannot accommodate significant wheel path wander. Therefore it is believed that channelized unidirectional loading of the test sections used in the current research study is "realistic".

Rut depths were calculated through subtraction of the original constructed pavement profile (corresponding to zero load applications) from the deformed profiles at different stages of loading.

Note that rut depth in this research study was defined as the deflection of any point on the pavement surface from its original profile. Therefore, points adjacent to the wheel path undergoing upward heaving were represented by negative rut depths representing the heave amounts. Trafficking of the test sections was continued up to a total rut depth of approximately 102 mm (4 in.) in most cases, as the ATLAS wheel could tolerate a maximum vertical movement of up to 102 mm (4 in.) into the rutted pavement surface before the internal vertical LVDT in the actuator of the wheel carriage assembly stroked out. However, this depth varied depending on the ATLAS track placements over individual test cells, and some sections could be tested to rut depths more than 102 mm. Transverse GPR scanning of the test sections at different number of load applications was also used for distinguishing between rutting in the subgrade, and aggregate layers. Figure 8.1 shows loading of the test sections and the surface profile measurement using a digital caliper.

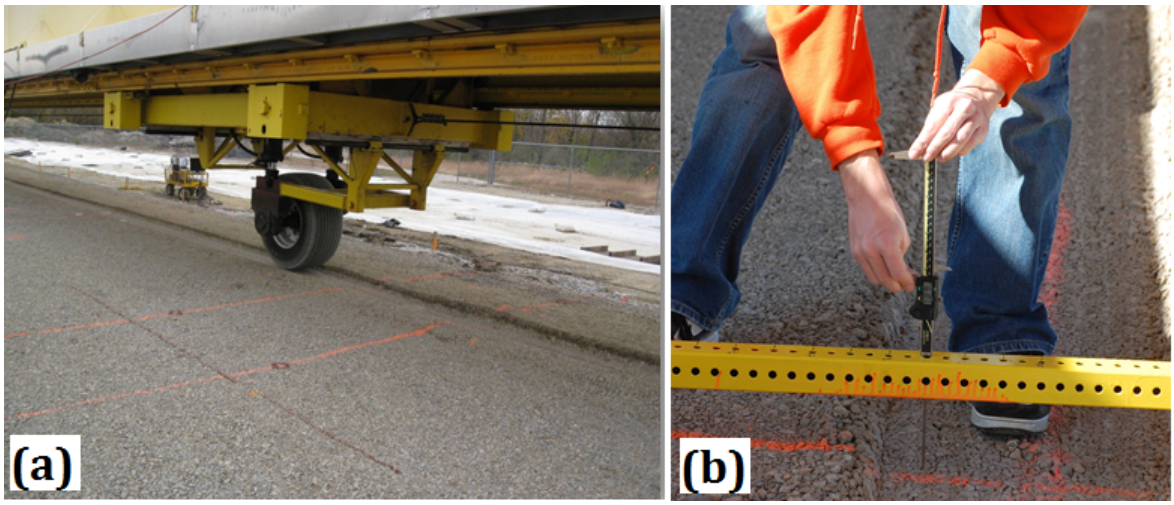


Figure 8.1: Photos Showing Unidirectional Accelerated Pavement Testing and Rut Measurement

### 8.2.1 Effect of Moisture Conditions on Unsurfaced Pavement Performance

As discussed in Chapter 3, one of the objectives of this research study was to evaluate the effect of moisture conditions on aggregate behavior. Accordingly, the pavement sections were constructed to be approximately 5.5 m (18 ft.) wide to accommodate loading along two different wheel paths (see Figure 8.2), separated by a distance of 2.44 m (8 ft.). The pavement sections were first tested at near-optimum conditions (North wheel path), before artificial flooding and

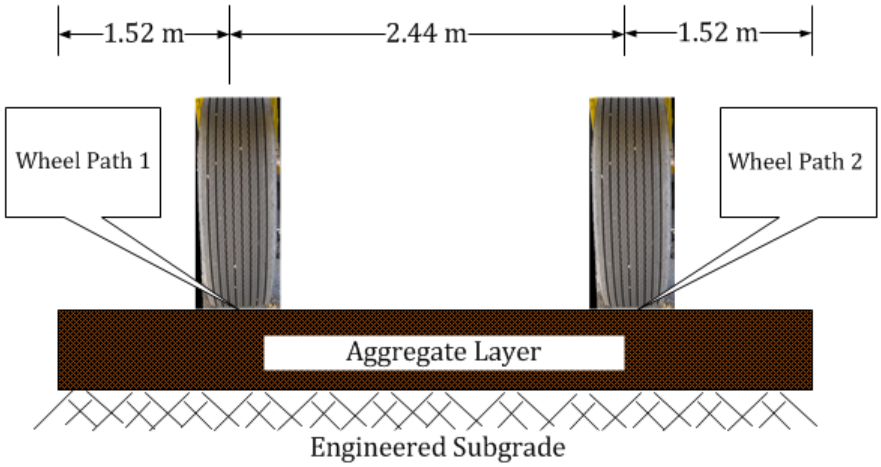


Figure 8.2: Wheel Path Locations

loading along the second (South) wheel path. Flooding of the test sections was achieved using perforated water sprinklers until excessive water was observed seeping through the boundaries of the aggregate sections. Both wheel paths were separated from the pavement edge by a distance of 1.52 m (5 ft.) to eliminate edge-effects induced by the unsupported aggregate boundaries.

A minimum time interval was maintained between artificial flooding and loading of the pavement sections to avoid material attrition through splashing, and development of excess pore water pressures. Note that due to the inaccuracies associated with layer boundary identification using GPR in the presence of excessive moisture, transverse GPR scanning of the test sections was not conducted under flooded conditions. After testing each pavement section to failure at near-optimum and flooded conditions, transverse trenches were excavated across the wheel paths for visual identification of subgrade and aggregate layer rutting.

The accelerated testing of full-scale test sections under the scope of this research study was conducted between October 2010, and May 2011. Cells 1, 2, 4, and 5 were tested between October and December 2010. However, testing of Cell 3 could not be carried out in 2010 due to inclement weather, and was completed in May 2011 after the spring thaw. Performance trends observed from loading of the test cells at near-optimum, and flooded conditions, are presented in the sections below, in the same order they were tested (cell 3 results presented last).

## 8.3 Cell 1: Uncrushed Gravel with High Amounts of Nonplastic Fines

This section presents analysis of probable rut-mechanisms contributing to failure of the uncrushed gravel pavement section constructed over an engineered subgrade of CBR, 3%. As explained in Chapter 6, this test cell (cell 1) was constructed using an uncrushed gravel material containing high amounts of nonplastic fines, and comprised three sections of aggregate layer thickness 356 mm, 305 mm, & 203 mm (14 in., 12 in., & 8 in. respectively) separated by 3.1-m (10-ft) long transition zones.

### 8.3.1 Performance under Near-Optimum Moisture Conditions

Figure 8.3 presents surface profile diagrams of the three test sections after different number of load applications along the North wheel path (near-optimum aggregate moisture conditions). As shown in Figure 8.3a, Section 1 (356-mm thick aggregate layer) performed the worst, and exhibited extensive heaving adjacent to the wheel path leading to failure after only 47 load applications. Section 2 (Figure 8.3b) performed better than Section 1, and could withstand up to 160 load applications before undergoing shear failure. Moreover, the surface heave for Section 2 was less severe compared to Section 1. It should be noted that rut accumulation accompanied by surface heaving adjacent to the wheel path is often considered to be an indicator of shear flow within the unbound granular layer [5]. Therefore, the deformed surface profiles of Sections 1 and 2 indicate failure of the aggregate layer within itself. However, as shown in Figure 8.3c, Section 3 (203-mm thick aggregate layer) could support a significantly higher number (400) of load applications before undergoing shear failure or developing excessive surface heave. This is in contradiction with the common assumption of thicker aggregate layers ensuring better resistance to permanent deformation. Note that the significantly better performance of Section 3 compared to the other two sections was clearly evident after 400 load applications. Therefore, loading of this section was stopped at this point, even though the total rut accumulation for the section was approximately 50 mm.

An investigation of aggregate layer moisture conditions was conducted to eliminate the possibility of excessive moisture in Section 1 leading to rapid rut accumulations. Aggregate samples were collected from different depths along the wheel path to determine the moisture content profiles in the three sections, and are presented in Table 8.1. As shown in the table, the

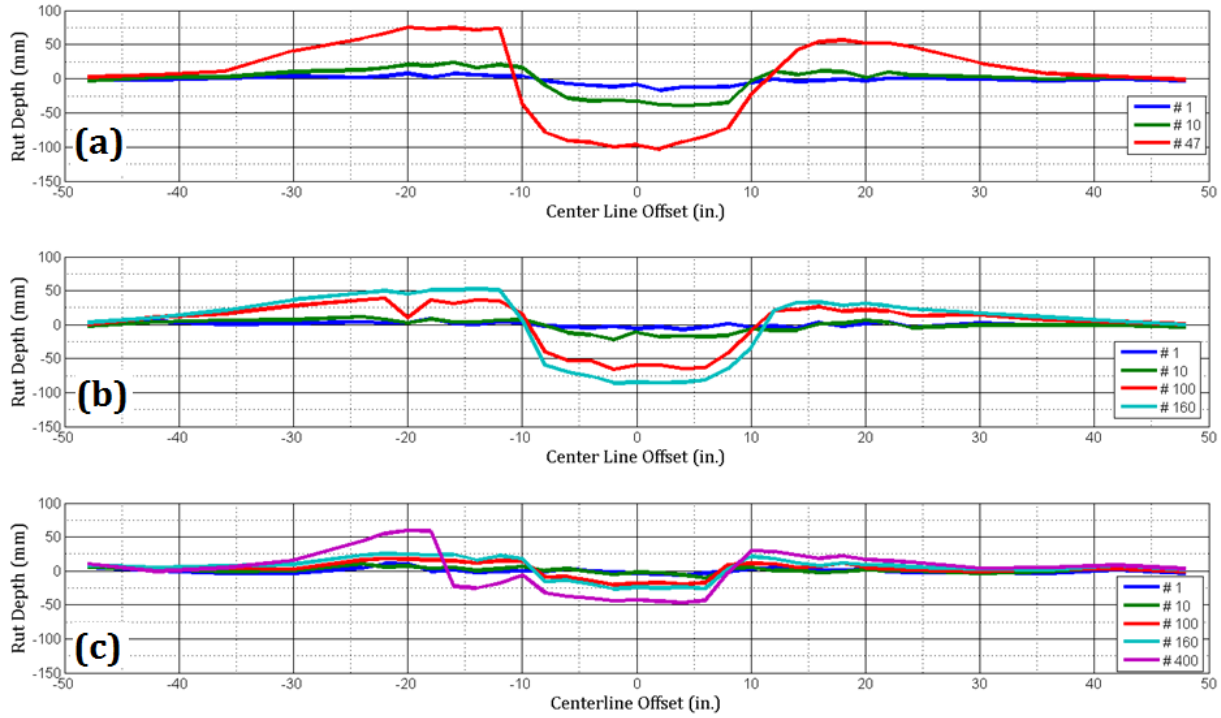


Figure 8.3: Rut Development in Uncrushed Gravel Sections (a) 1, (b) 2, and (c) 3 due to Unidirectional ATLAS Loading at Near-Optimum Conditions (1 in. = 25.4 mm)

moisture content profiles of the aggregate layers were uniform across the three test sections. This resulted in "moisture discrepancy" being ruled out as a plausible mechanism contributing to rapid failure of the thick uncrushed gravel sections. Close examination of GPR scans and layer boundaries obtained from excavated trench section was therefore pursued to identify the different rutting mechanisms involved.

Table 8.1: Cell 1: Moisture Content Investigation along Wheel Path

| **Point** | **Description** | **Aggregate Moisture Content (%)** |
|---|---|---|
| 1 | Section 1, West | 5.6 |
| 2 | Section 1, East | 5.9 |
| 3 | Section 2, West | 5.5 |
| 4 | Section 2, East | 5.2 |
| 5 | Section 3, West | 5.3 |
| 6 | Section 3, East | 5.7 |

Figure 8.4 shows the GPR B-scan, as defined in Chapter 7, from Section 1 (356-mm thick aggregate layer) of Cell 1 after different number of load applications. The yellow line in the figure shows the aggregate surface, whereas the red line shows the subgrade interface. Three different GPR scans, taken after 0, 10, and 47 load applications are shown in Figure 8.4. Figure 8.4a shows the undisturbed surfaces of the aggregate and the subgrade. As the number of load applications increased, the rut development in the surface is clearly visible from the broken nature of the solid yellow line (see Figures 8.4b and 8.4c). After 47 load applications, the aggregate surface underwent shear failure and the rut-depth became too deep for the ATLAS actuator controlling wheel load. It is important to note that even after 47 load applications, the GPR scan does not show significant depression in the subgrade layer. The small amount of subgrade depression noticed from the GPR scan is offset to the side of the wheel path. This is typically a result of material movement and shear flow due the development of a shear surface within the aggregate layer. The GPR scans present the possibility of rutting occurring primarily within the aggregate layer. It should be noted that as reported in Chapter 6, the uncrushed gravel with high fines used in this cell showed very poor performance in the laboratory testing as well.

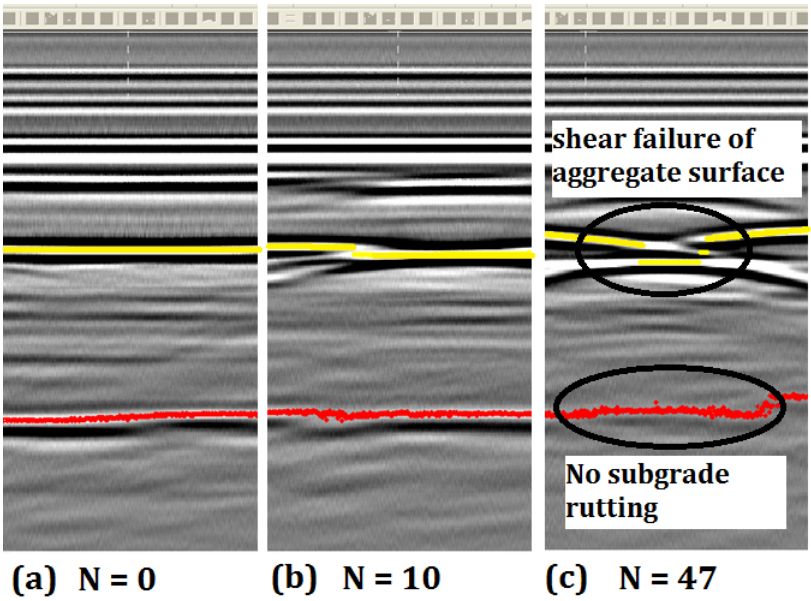


Figure 8.4: GPR Scans of 356-mm Thick Uncrushed Gravel Layer at Different Load Applications

Figure 8.5 shows the cross-section of the excavated trench alongside the GPR scan and the surface rut profile for the same test section (Section 1 of Cell 1). From the excavated trench

section, it was clear that the heave on the surface was much higher than the heave at the subgrade interface. Also, the depression in the subgrade (shown by the black trace on the photograph in Figure 8.5b) was offset from the surface rut observed under the wheel path. This was in agreement with the GPR scan results (see Figure 8.4) and supported the hypothesis regarding shear flow of material that resulted in a lateral offset of the subgrade depression from the wheel path. Analyzing Figures 8.4 and 8.5 together, shear movement within the aggregate layer was the primary mode of failure associated with performance of this uncrushed gravel section.

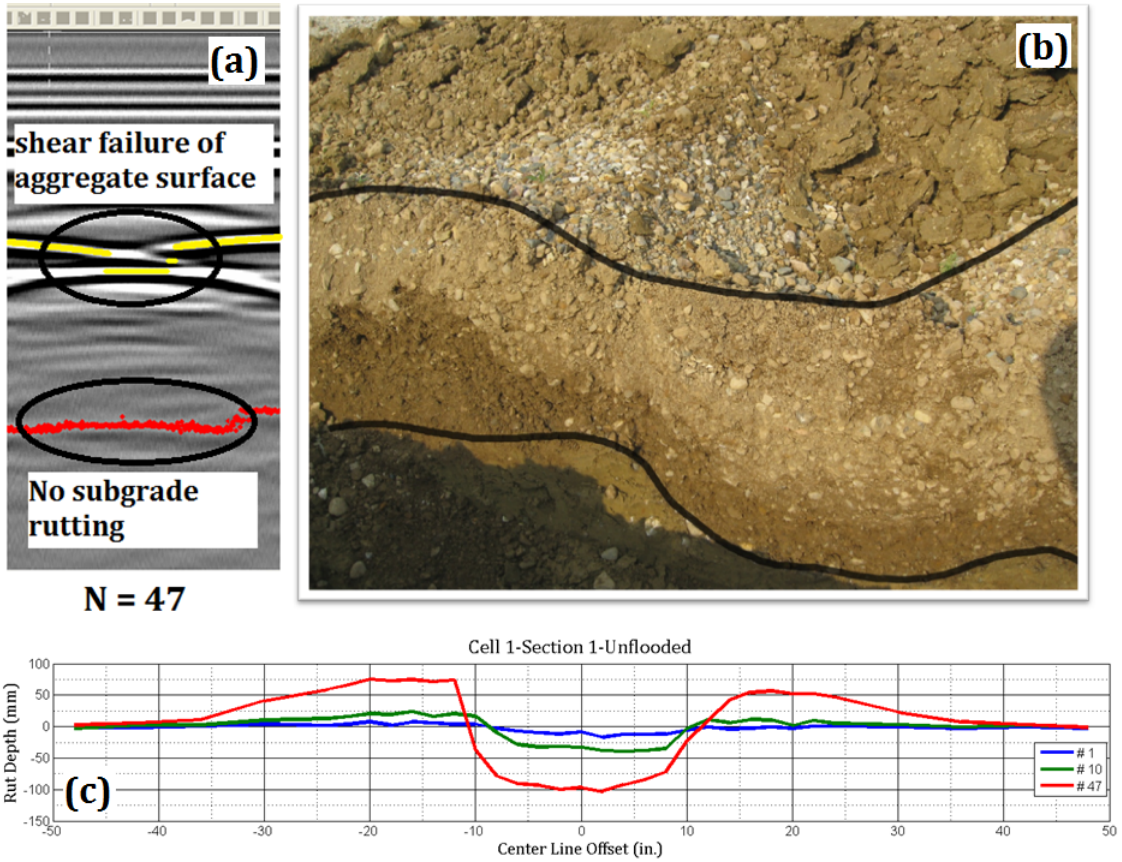


Figure 8.5: (a) GPR Scan, (b) Excavated Trench, and (c) Surface Rut Profile of the 356-mm Thick Uncrushed Gravel Aggregate Section (1 in. = 25.4 mm)

Figure 8.6 shows the deformed profile of the 305-mm thick uncrushed gravel in Section 2. Similar to the 356-mm thick aggregate section, the GPR scan of Section 2 clearly showed a much larger rutting in the aggregate (shown by the yellow line) compared to the subgrade (red line). However, it should be noted that the subgrade rutting in Section 2 was more significant than that

in Section 1. Also, looking at the cross-sectional profile from the excavated trench, the subgrade rutting in Section 2 was more pronounced than that in Section 1. This was primarily because of a thinner aggregate layer in Section 2, and the lack of aggregate depth for the development of a complete shear surface within the layer. As a result, the depression in the subgrade for Section 2 was less offset from the wheel path compared to that in Section 1. Therefore, performance under loading of Section 2 of Cell 1 indicated the combined action of aggregate shear flow and subgrade deformation contributing towards failure of the test section. As the aggregate layer thickness was reduced from Section 1 to Section 2, the subgrade soil was subjected to higher stress values leading to higher accumulation of permanent deformation. However, it should be noted that the aggregate layer was still the primary contributor to the failure of Section 2 under loading.

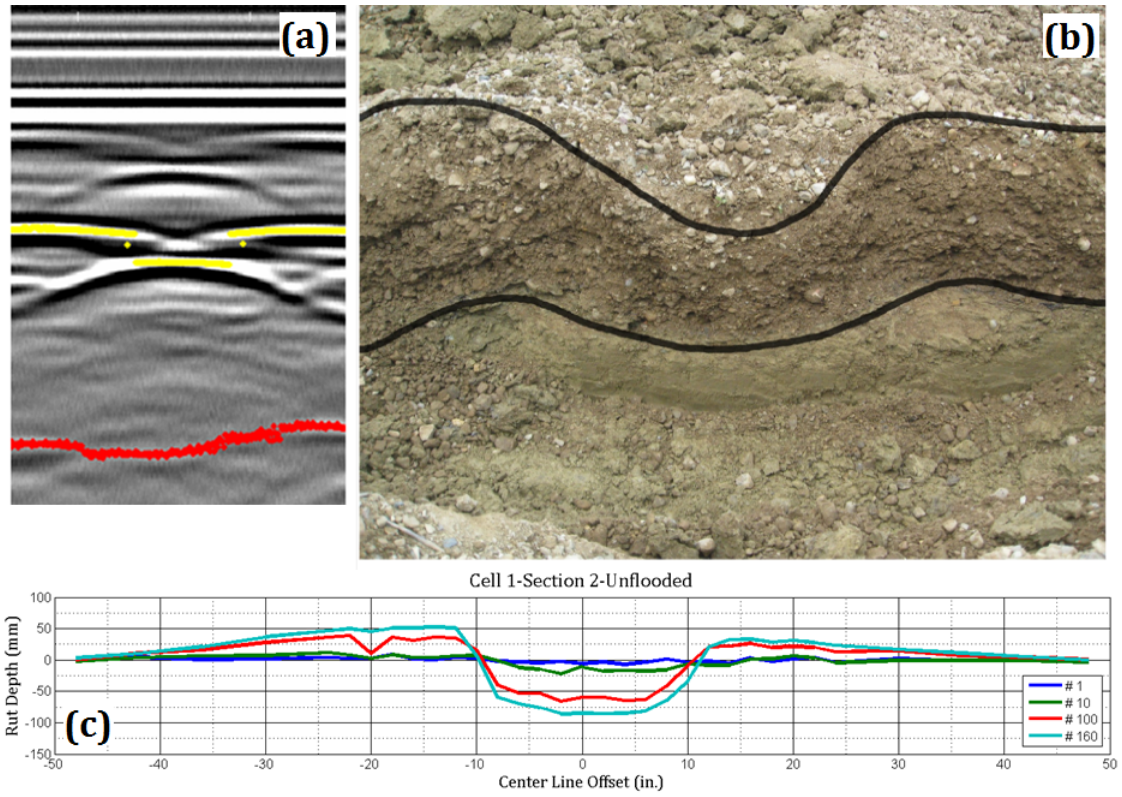


Figure 8.6: (a) GPR Scan, (b) Excavated Trench, and (c) Surface Rut Profile of the 305-mm Thick Uncrushed Gravel Aggregate Section (1 in. = 25.4 mm)

Figure 8.7 shows similar profiles for the 203-mm thick uncrushed gravel layer in Section 3. The absence of significant heave development at the aggregate-subgrade interface could clearly be noticed from Figure 8.7b. Moreover, the lack of significant heave development on the surface (see

Figures 8.7b, and 8.7c) implied no significant material movement within the aggregate layer. The subgrade deformation in Section 3 appeared to be less pronounced than Sections 1 and 2. This observation was in contradiction with common intuition regarding thick aggregate layers ensuring better pavement performance, and was attributed to the significantly higher subgrade moduli, and CBR values (refer to Figures 7.4 and 7.5) corresponding to Section 3, compared to Sections 1 and 2.

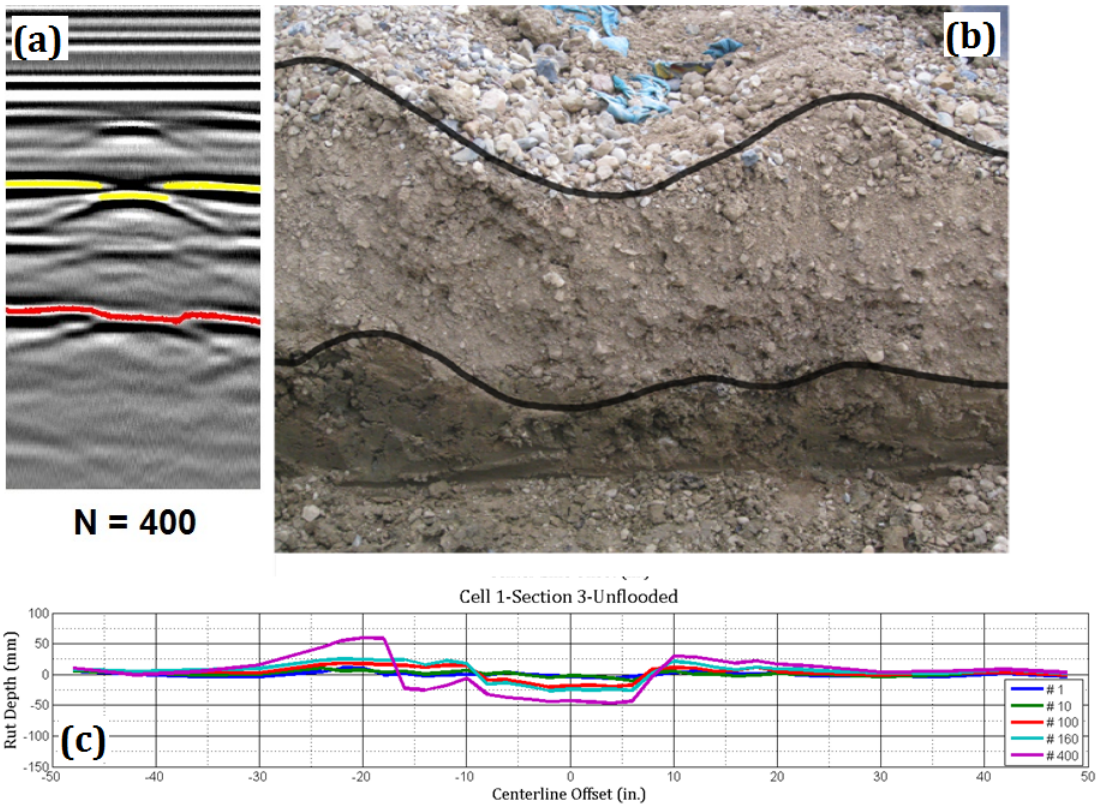


Figure 8.7: (a) GPR Scan, (b) Excavated Trench, and (c) Surface Rut Profile of the 203-mm Thick Uncrushed Gravel Aggregate Section (1 in. = 25.4 mm)

The stronger subgrade conditions in Section 3 of Cell 1 resulted in significantly lower subgrade deformations, compared to Sections 1 and 2. Note that besides presenting better resistance against Mode 2 rutting [5] (as defined in Chapter 2), a stronger subgrade layer facilitated better compaction of the overlying layers, which ultimately led to better performance through improved lateral distribution of traffic-induced stresses.

Significant material movement in the thick aggregate sections and the absence thereof in Section 3 could be confirmed from the subgrade compressive stress data collected along the North wheel path (near-optimum aggregate moisture conditions) of Sections 2 and 3. Figure 8.8 shows the subgrade vertical compressive stress values recorded for Sections 2 and 3 at different number of load applications (N). As shown in the figure, for low values of N, the subgrade stress levels in Section 2 (305-mm thick aggregate layer) were lower than those in Section 3 (203-mm thick aggregate layer) due to better load distribution achieved in the thicker aggregate layer. For example, for N = 2, the subgrade stress value recorded in Section 2 was 169.8 kPa (24.6 psi), whereas the recorded value for Section 3 was 195.5 kPa (28.4 psi). However, as the number of load applications increased, the subgrade stress values for Section 2 gradually increased, and subsequently became greater than those for Section 3. At N = 46, the subgrade stress values for Sections 2 and 3 were 206.0 kPa (29.9 psi) and 188.5 kPa (27.4 psi), respectively. This was attributed to the significant shear movement within the aggregate layer in Section 2 which resulted in a reduction in the effective aggregate cover thickness, thus subjecting the subgrade to higher stress levels. The 203-mm thick aggregate layer in Section 3 was constructed over a stiffer subgrade, and resisted internal shear movement supporting a significantly higher number of load applications without undergoing shear failure. Note that due to the stiffer subgrade conditions in Section 3 see (Figure 7.4), the aggregate layer could be compacted to higher densities when compared to the other two sections (96.2% relative compaction for Section 3, compared to 95.1% and 94.9% relative compaction values for Sections 1 and 2, respectively).

The field-measured subgrade vertical stress values were compared to those predicted from finite element analyses of the uncrushed gravel test sections in Cell 1. Accordingly, Figure 8.9 shows the predicted subgrade stress levels for Sections 2 and 3 (305-mm and 203-mm thick aggregate layers, respectively) in Cell 1 along with the measured stress levels corresponding to N = 2 load applications (representing relatively undisturbed state of the aggregate layers). The following three combinations of aggregate and subgrade layer modulus behavior were considered to predict the subgrade vertical stresses using GT-PAVE: 1) Isotropic stress-dependent aggregate layer over a subgrade of constant modulus, 2) Isotropic stress-dependent aggregate layer over a bilinear stress-dependent subgrade layer, and 3) cross-anisotropic stress-dependent aggregate layer over a bilinear stress dependent subgrade layer.

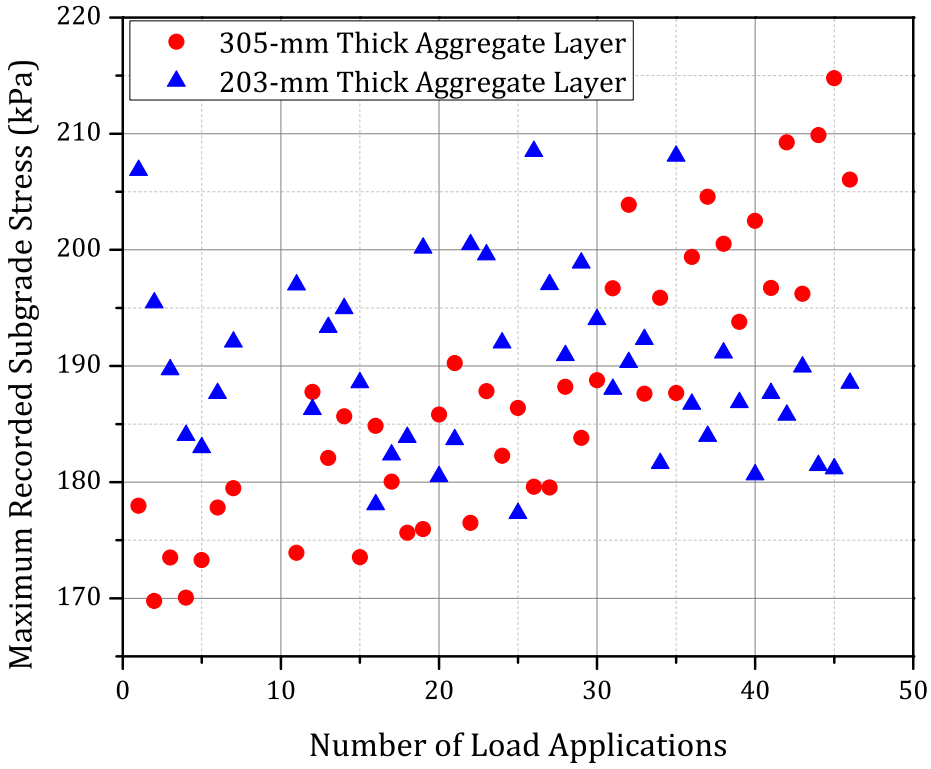


Figure 8.8: Subgrade Stress Levels Varying with Number of Load Applications for the Uncrushed Gravel Test Sections in Cell 1

As in Chapter 6, the following two assumptions were first made during analyses of the full-scale unsurfaced pavement test sections using GT-PAVE: 1) a constant modulus value was assumed for the subgrade layer, and 2) the aggregate layer was treated as isotropic, i.e. modulus and Poisson's ratio values were assumed to be the same in all directions. The first simplifying assumption was justified in Chapter 6 as stress-dependent subgrade behavior was not the primary focus of this research study, and the finite element analyses were primarily targeted to compare the effectiveness of different aggregate types in dissipating traffic-induced stresses. However to compare the predicted and measured subgrade vertical stress levels under accelerated loading, it was important to check the effect of incorporating stress-dependent subgrade behavior into the GT-PAVE analyses. Accordingly, Figure 8.9 also shows the predicted vertical subgrade stress values for Sections 2 and 3 upon modeling the subgrade using the bilinear stress-dependent resilient modulus model proposed by Thompson and Robnett [78]. As shown in the figure, no significant improvement in the difference between the predicted and measured subgrade vertical stress levels was observed upon considering the stress-dependent nature of subgrade modulus.

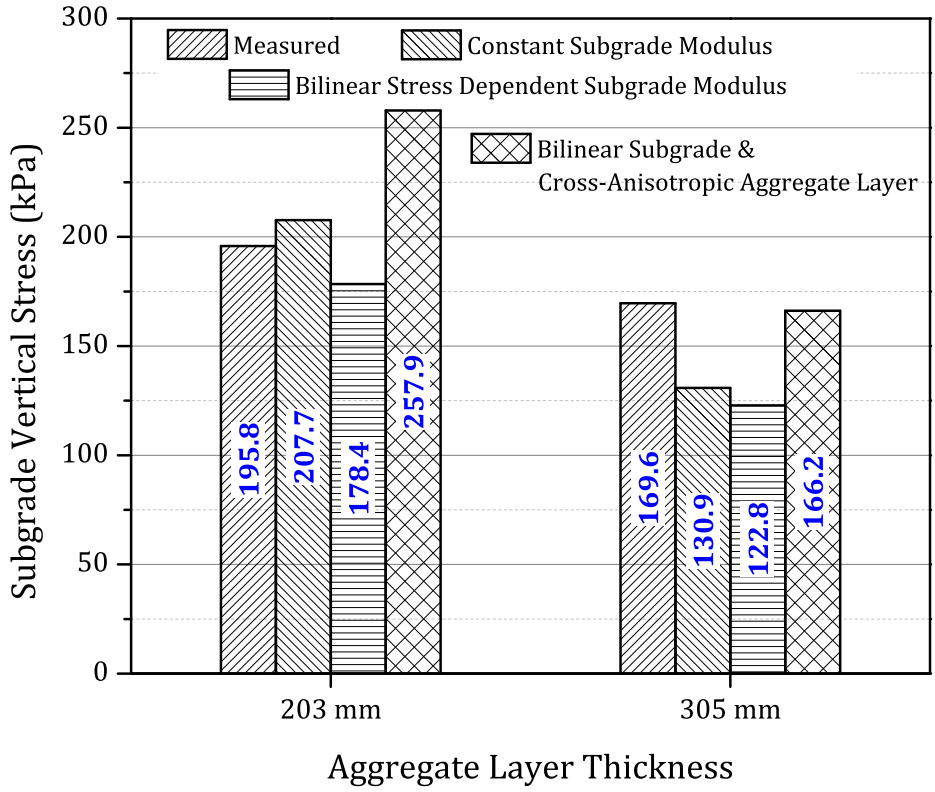


Figure 8.9: Comparing the Predicted and Measured Subgrade Stress Levels Underneath the Uncrushed Gravel Test Sections in Cell 1

Note that the unbound aggregate layer was still assumed to isotropic at this stage.

The next step involved consideration of the cross-anisotropic nature of the unbound aggregate layers resulting from particle reorientation during compaction, as well from traffic-induced stresses. This was accomplished by assigning different resilient modulus model parameters for the aggregate layer in the vertical and horizontal directions. The horizontal resilient modulus model parameters were determined from directional modulus testing of the aggregates in the laboratory, as discussed in Section 5.5. Note that anisotropic modulus characterization of unbound aggregate layers in general results in higher vertical stress predictions [21]. As shown in Figure 8.9, the predicted subgrade vertical stress (166.2 kPa) for Section 2 (305-mm thick aggregate layer) was significantly close to the measured value (169.6 kPa) upon consideration of the stress-dependent subgrade modulus, as well as cross-anisotropy of the unbound aggregate layer. Similar results have been reported in the literature; Tutumluer and Kwon [137] reported significant reduction in the discrepancies between field-measured and predicted pavement response parameters upon

consideration of the inherent cross-anisotropy in unbound aggregate layers. Note that the predicted subgrade vertical stress for Section 3 (257.9 kPa) was significantly higher than that measured in the field (195.8 kPa). This was primarily due to variabilities in construction conditions as well as nonuniform compaction of the subgrade and aggregate layers.

Failure patterns from trafficking the test sections under near-optimum aggregate moisture conditions indicated a definite internal shear failure mechanism of the uncrushed gravel layer. This field observation was reinforced by laboratory test results comparing the permanent deformation behavior of different aggregate types (refer to Figure 6.4) that clearly showed unstable behavior of the uncrushed gravel material compared to crushed aggregates.

### 8.3.2 Performance under Flooded Conditions

To evaluate the effects of excessive moisture on unsurfaced pavement performance, the uncrushed gravel test sections in Cell 1 were artificially flooded and tested along a second (South) wheel path separated from the first, by a distance of 2.44 m (8 ft.). The accumulated rut amounts were recorded through surface profile measurements after different number of load applications. Figure 8.10 shows the accumulations of permanent deformation in Sections (a) 1, (b) 2, and (c) 3 while testing under flooded conditions. Note that due to differences in ATLAS track elevations, different test sections could be tested to different rut depths before the vertical LVDT in the ATLAS wheel carriage assembly reached its maximum stroke.

The test section performances under flooded conditions were significantly different from those under near-optimum aggregate moisture conditions. All the three test sections showed rapid permanent deformation accumulation and failed after only 27 load applications. It is important to note from Figure 8.10 that the amount of surface heave in Section 1 (see Figure 8.10a) under flooded conditions was significantly lower than that under the near-optimum conditions indicating a somewhat lower degree of shear flow within the aggregate layer under flooded conditions. The amount of surface heave seen in Sections 2 and 3 (Figures 8.10b and 8.10c, respectively) were significantly higher than that in Section 1. Moreover, Section 3 with the thinnest (203-mm or 8-in. thick) aggregate layer, exhibited the highest rut accumulation after 27 load applications which was expected due to the wetting of the subgrade even though Section 3 had the highest as-constructed subgrade moduli for the near-optimum conditions (see Figure 7.4).

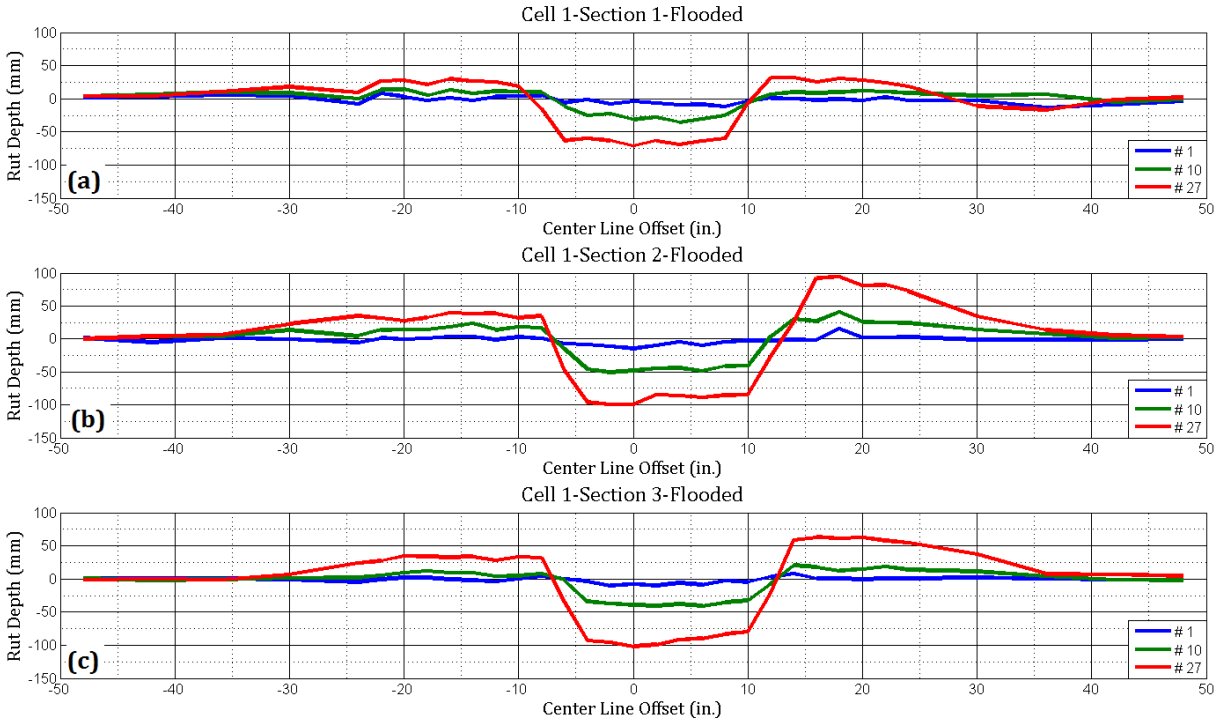


Figure 8.10: Rut Developments in Uncrushed Gravel Sections (a) 1, (b) 2, and (c) 3 due to Unidirectional ATLAS Loading under Flooded Conditions (1 in. = 25.4 mm)

Examination of transverse trench sections revealed a different mechanism contributing to failure of the uncrushed gravel test sections under flooded conditions. Figure 8.11 shows the deformed layer boundaries (from excavated trench sections) for the aggregate surface as well as the aggregate-subgrade interface after testing under flooded conditions. The subgrade deformation for Section 1 (Figure 8.11a) was more pronounced under flooded conditions, compared to that under near-optimum aggregate moisture conditions (Figure 8.5b). This resulted from penetration of the excessive moisture through the aggregate layer that weakened the subgrade significantly and led to failure due to excessive subgrade movement.

Figures 8.11b and 8.11c show the deformed layer boundaries under flooded conditions for Sections 2 and 3, respectively. In both cases, there was significant heaving of the subgrade leading to failure of the test sections. Moreover, any surface heave observed in these test sections appeared to be primarily reflections of the subgrade heave. Also, the extent of subgrade heave became significantly worse as the aggregate layer thickness was reduced (from Section 1 to Section 3). This could possibly be due to larger quantities of water getting into the subgrade

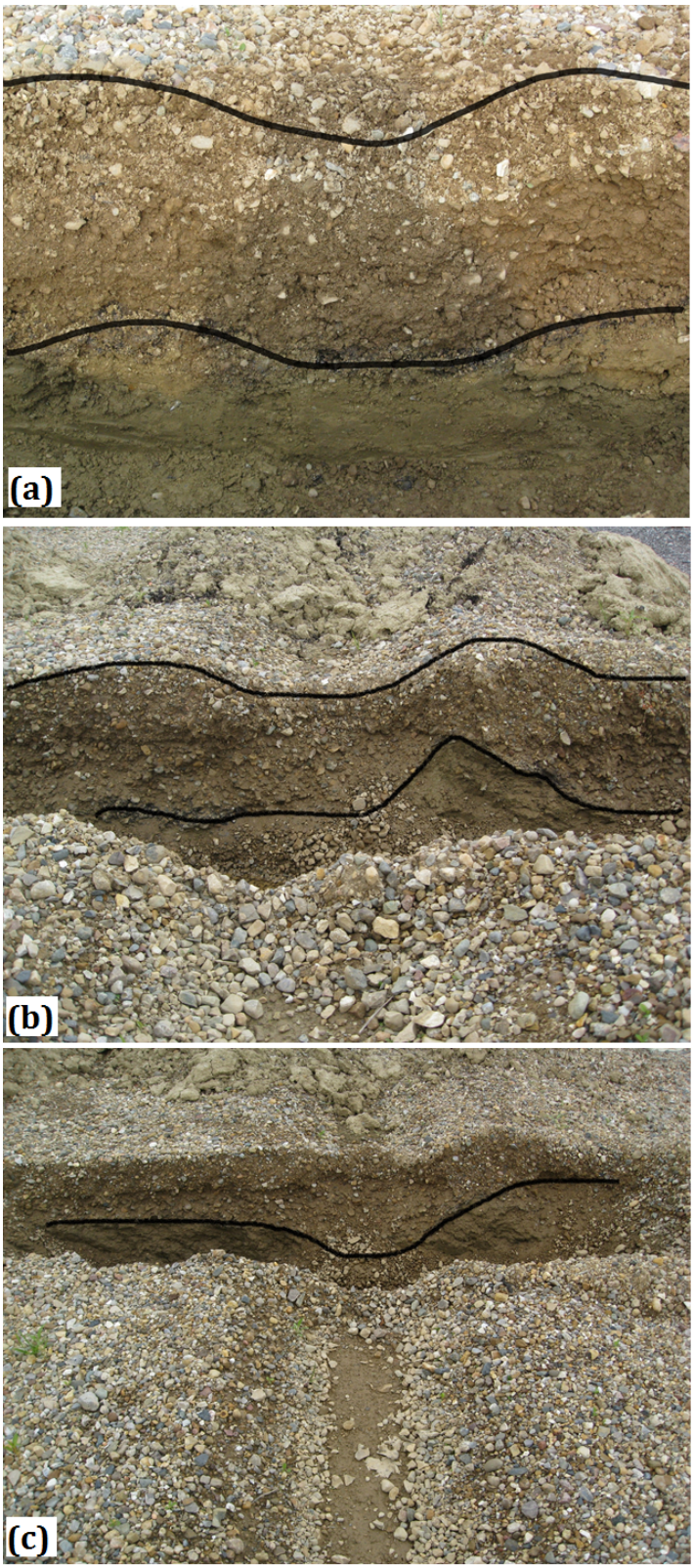


Figure 8.11: Excavated Trench Photos Showing Surface and Base-Subgrade Interface Deformations in Test Sections (a) 1, (b) 2, and (c) 3 for Cell 1 due to Loading under Flooded Conditions

under thinner aggregate layers that made the subgrade progressively weaker. On the other hand, assuming the ingress of water weakened the subgrade under all three sections equally, the thinner aggregate layers in Sections 2 and 3 would result in higher stresses on top of the subgrade, leading to excessive shear deformations.

Figure 8.12 shows changes in maximum rut depths with number of load applications for the three sections tested under near-optimum and flooded conditions. Note that Section 1 with the 356-mm (14-in.) thick uncrushed gravel layer showed a very high rate of rut accumulation even under near-optimum aggregate moisture conditions. It is therefore important to emphasize that subgrade rutting may not be the only mechanism leading to the failure of unsurfaced pavements, and even a thick layer of the poor quality, high fines uncrushed aggregate is likely to undergo internal shear flow resulting in rapid accumulation of permanent deformation. The North wheel path of Section 3 again showed the slowest rate of permanent deformation accumulation, which was attributed to the higher subgrade moduli as determined from the field modulus measurements.

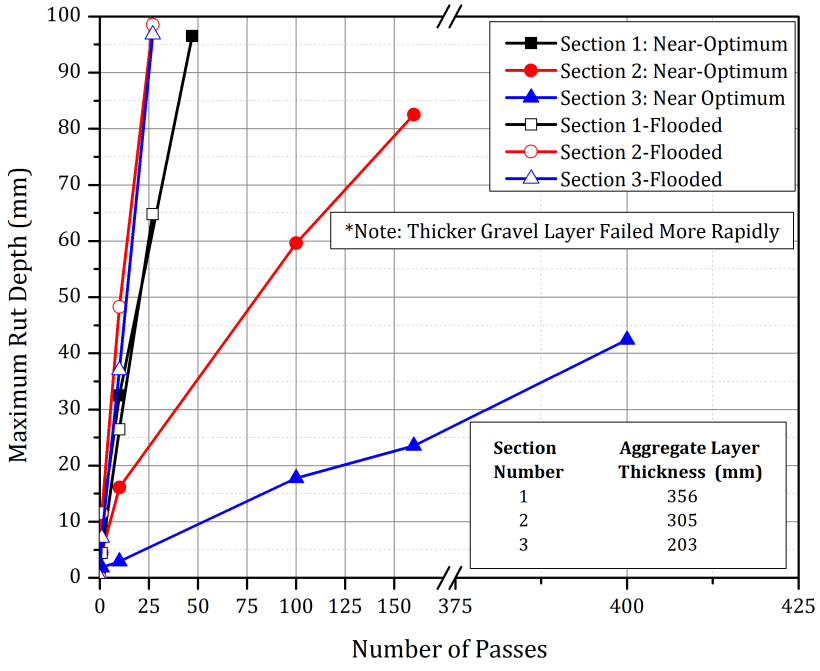


Figure 8.12: Cell 1 Permanent Deformation Accumulations under Near-Optimum and Flooded Conditions

## 8.4 Cell 2: Crushed Limestone with Low Amounts of Plastic Fines

The effect of low amounts of plastic fines on the performance of a crushed limestone was evaluated through accelerated testing of full-scale unsurfaced pavement sections constructed over an engineered subgrade of CBR, 3%. As mentioned in section 6.3.1, the aggregate material used in this test cell contained significantly lower amount ($\sim 5\%$) of fines (material passing No. 200 sieve, or finer than 0.075 mm) compared to the originally reported values ($\sim 12\%$) from the aggregate source, and was therefore categorized as a "low fines" content material with moderately plastic (PI = 5.7) fines. As reported in Chapters 4 and 5, the effect of fines plasticity on aggregate behavior was not apparent at low fines contents. Therefore, based on laboratory test results from phase I of this research, amount of fines in the aggregate matrix was expected to be the primary physical characteristic governing the performance of this particular test cell. As reported in Chapters 4 and 5, crushed aggregates (limestone and dolomite) exhibited unstable matrix behavior at very low fines contents, which was also observed from laboratory testing of the aggregate material used in cell 2 (refer to Chapter 6).

### 8.4.1 Performance under Near-Optimum Moisture Conditions

Performance of the test section at near-optimum moisture conditions was monitored through loading, and surface profile measurements along the North wheel path. Note that GPR scanning of this test cell could not be conducted due to unavailability of GPR equipment. Therefore, the mechanisms contributing to failure of this test cell were analyzed using surface profile measurements, and excavated trench sections only.

Figure 8.13 shows the (a) excavated trench section, and (b) surface rut profile, of Section 1 (356-mm thick aggregate layer) in Cell 2. As seen in Figure 8.13, the test section failed after only 52 load applications, by accumulating rut depths of 100 mm, accompanied by significant heaving adjacent to the wheel path. As already mentioned, development of significant heave adjacent to the wheel path is often an indicator of shear movement within the aggregate layer, and presented the possibility of internal shear failure of the crushed limestone layer. Close inspection of the excavated transverse trench sections showed no significant deformation of the subgrade (see Figure 8.13a), with the aggregate-subgrade interface remaining essentially horizontal even after failure of the test section to failure.

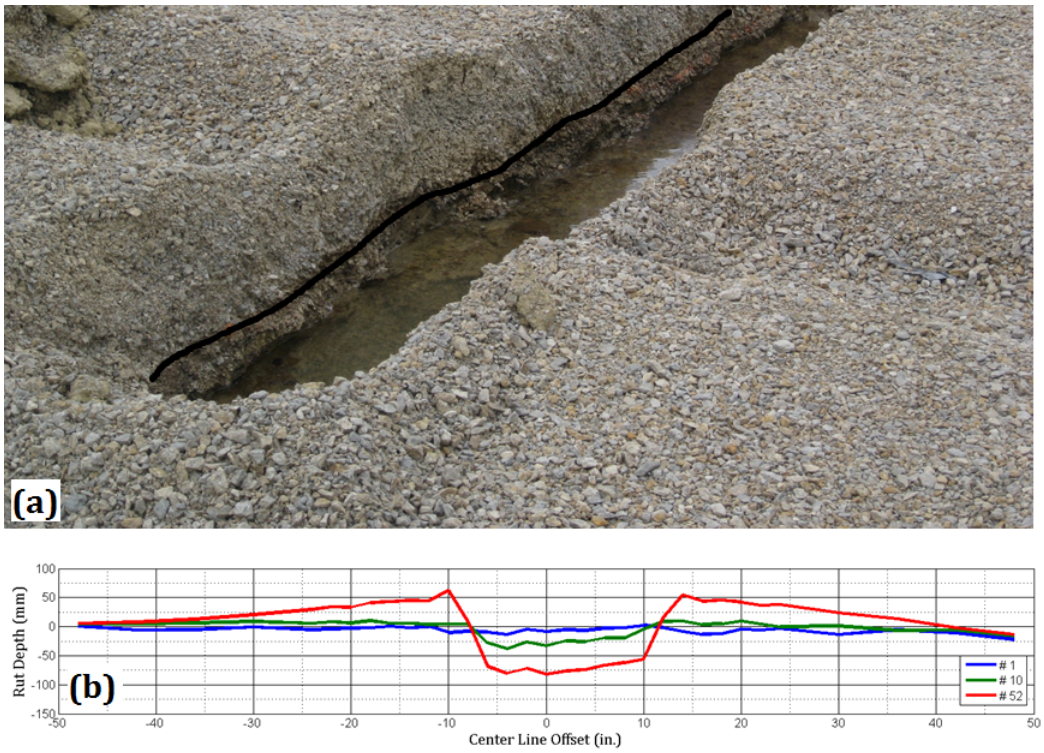


Figure 8.13: (a) Excavated Trench, and (b) Surface Rut Profile of the 356-mm Thick Crushed Limestone Section in Cell 2 (1 in. = 25.4 mm)

This behavior was in contradiction with the commonly observed trends regarding crushed aggregate layers resisting permanent deformation due to better particle interlock. However, it is important to note that the crushed limestone material used in Cell 2, showed unstable matrix behavior under standard compaction (ASTM D 698) conditions due to the significantly low fines contents, and could not be tested for permanent deformation characterization due to excessive bulging (refer to Chapter 6). Moreover, the material showed significantly low CBR values (18-19%) under standard compaction conditions. Laboratory test results therefore support the hypothesis of shear movement within the aggregate layer near standard compaction maximum densities due to the unstable matrix structure.

Figures 8.14, and 8.15 present deformed profiles of Sections 2 (305-mm thick aggregate layer) and 3 (203-mm thick aggregate layer), respectively, upon testing under near-optimum aggregate moisture conditions. From the figures, Sections 2, and 3 could sustain 100 and 350 load applications respectively, before accumulating significant rutting. Moreover, close inspection of the surface profiles and the excavated trench sections clearly indicates increased subgrade heaving

with decreasing aggregate layer thickness. The highest subgrade heaving was noticed for the 203-mm thick aggregate layer in Section 3.

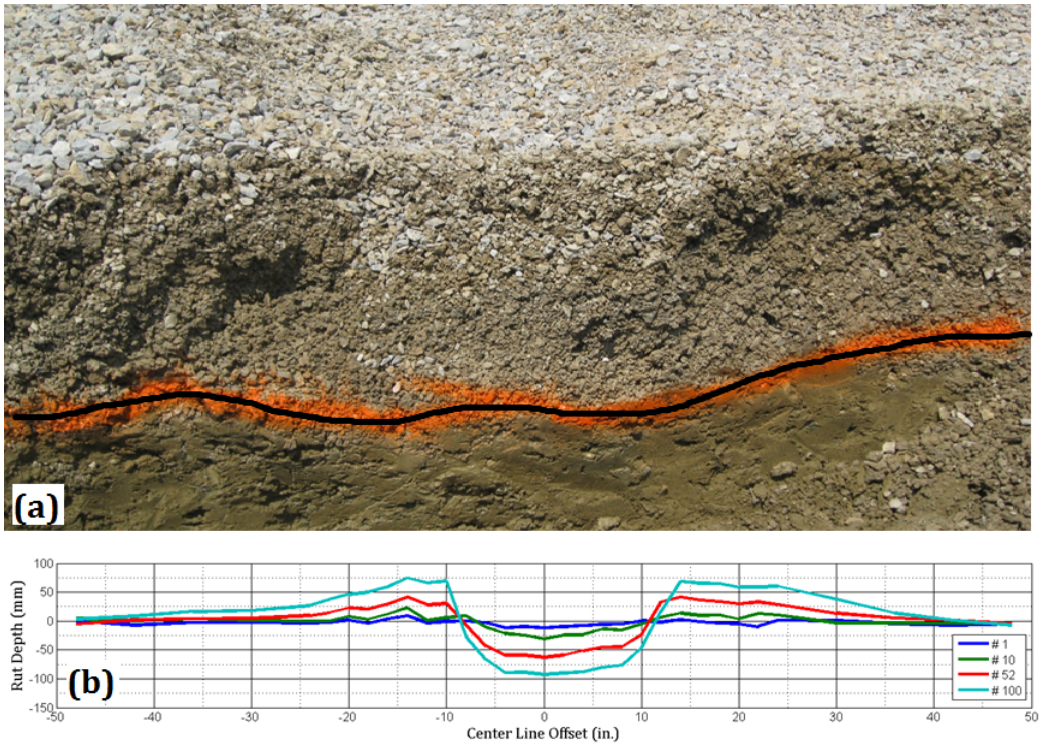


Figure 8.14: (a) Excavated Trench, and (b) Surface Rut Profile of the 305-mm Thick Crushed Limestone Section in Cell 2 (1 in. = 25.4 mm)

Similar to the near-optimum loading conditions for the uncrushed gravel material in Cell 1, failure of aggregate sections in Cell 2 under near-optimum aggregate moisture conditions could also be attributed to shear movement within the aggregate layer, which was also evident from the "wavy" nature of rut development along the wheel path. From preliminary investigation of the deformed surface profile and excavated trench sections, it was apparent that the crushed limestone material in Cell 2 experienced shear movement within the thick aggregate layers. However the crushed nature of the particles resulted in adequate stress reduction at the subgrade level, therefore protecting the subgrade from excessive deformation before significantly high number of load applications.

Further investigation of the test cell performance was conducted through analyses of the field moduli measured using LWD and GeoGauge™ on the compacted subgrade as well as aggregate

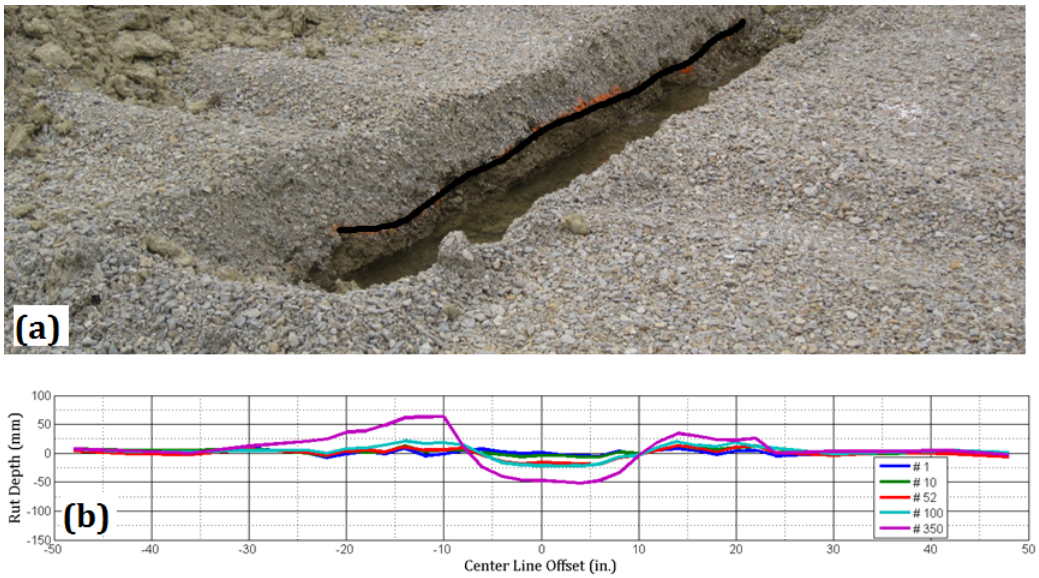


Figure 8.15: (a) Excavated Trench, and (b) Surface Rut Profile of the 203-mm Thick Crushed Limestone Section in Cell 2 (1 in. = 25.4 mm)

layers. Figure 8.16 shows the field moduli for the compacted (a) subgrade , and (b) aggregate layers for Cell 2. The subgrade moduli for Sections 2 and 3 were similar in magnitude, but were higher than those for Section 1 (as reflected from both LWD and GeoGauge$^{TM}$ results). Although the lower subgrade moduli for Section 1 could possibly be a contributing factor resulting in rapid failure of the thickest aggregate section (Section 1) under loading, the difference between performances of Sections 2 and 3 could not be explained on the basis of differences in subgrade moduli. Close inspection of the aggregate field moduli (see Figure 8.16b) reflected significantly higher moduli for Section 3 compared to Sections 1 and 2. This was linked to the achieved relative compaction (ASTM D 698) values for the three aggregate sections: 103.9%, 106.5%, and 108.7% for Sections 1, 2, and 3, respectively. Note that as discussed in Chapter 6, due to the free-draining nature of the crushed limestone aggregate used in Cell 2, the OMC and MDD values could not be easily established following the "impact hammer" methods. Therefore, the laboratory-determined MDD value of 18.1 kN/m$^3$(115.4 pcf) was not indicative of the maximum achievable densities in the field. This explained the high relative compaction values (> 100%) for all three test sections.

The 356-mm thick aggregate layer in Section 1 achieved the lowest relative compaction due to weaker subgrade conditions. The resulting inadequate particle interlock led to shear movement within the aggregate layer that ultimately failed after only 52 load applications. Sections 2 and 3

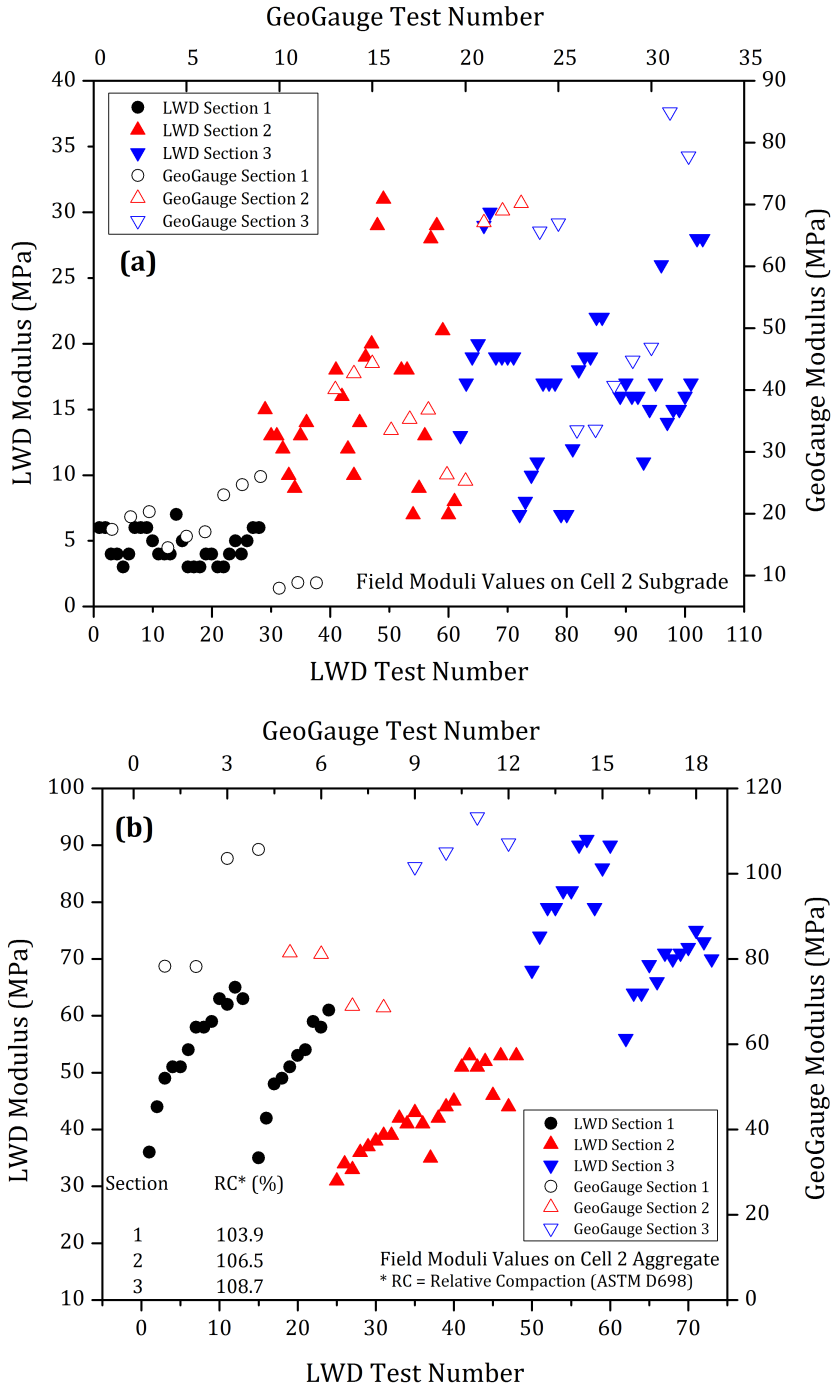


Figure 8.16: Field Modulus Values Measured by LWD and GeoGauge™ on the Compacted (a) Subgrade and (b) Aggregate Layers in Cell 2

were both constructed over similar subgrade conditions, with the aggregate layer in Section 3 compacted to higher densities (108.7% MDD) compared to Section 2 (106.5% MDD). Better compaction of the aggregate layer in Section 3 resulted in higher moduli values (adequately captured by the LWD and GeoGauge™), and better stress dissipation with depth. Reduced stress levels at the subgrade interface resulted in Section 3 sustaining significantly higher number of load applications (350) compared to Section 2 (100) without accumulating excessive rutting.

Higher compaction levels and in-place modulus values for Section 3 compared to Section 2 were also reflected from the measured vertical subgrade stress levels during accelerated pavement testing (see Figure 8.17). Figure 8.17 shows the subgrade vertical stress values for Sections 2 and 3 in Cell 2 corresponding to N = 4 (relatively undeformed aggregate layer configuration) plotted against time. The first peak in Figure 8.17 (shown in red, corresponding to t = 4 sec) represents the subgrade vertical stress level in Section 2, whereas the second peak (shown in black, corresponding to time = 6.4 sec) represents the stress on Section 3 subgrade. As shown the figure, higher subgrade stress values were recorded for Section 2 (305-mm thick aggregate layer) compared to Section 3 (203-mm thick aggregate layer). The same trend was observed at higher N values, and was attributed to the superior lateral dissipation of stresses within the stiffer aggregate layer in Section 3.

Analysis of Cell 2 performance under near-optimum aggregate moisture conditions therefore emphasized the importance of adequate compaction for crushed aggregates with low fines. Higher relative compaction percentages for the aggregate layers could be directly linked to better performance under loading. Note that laboratory testing of the aggregates showed similar trends (refer to Chapter 6). Although the crushed limestone matrix with low fines (used in Cell 2) was unstable under standard compaction conditions, it performed comparable to other crushed aggregate materials with high fines, under modified compaction OMC and MDD conditions (refer to Figure 6.4). Combined analyses of the laboratory and field test results lead to the conclusion that crushed aggregate materials should contain a minimum amount of fines to achieve a stable matrix structure. In the absence of sufficient fines in the void structure, the aggregate particles may become unstable under traffic loading and tend to increase movement and the permanent deformation. Higher compactive efforts can be used to somewhat improve the particle interlock in such aggregates with low fines. However, as achieving high relative compaction levels over weak

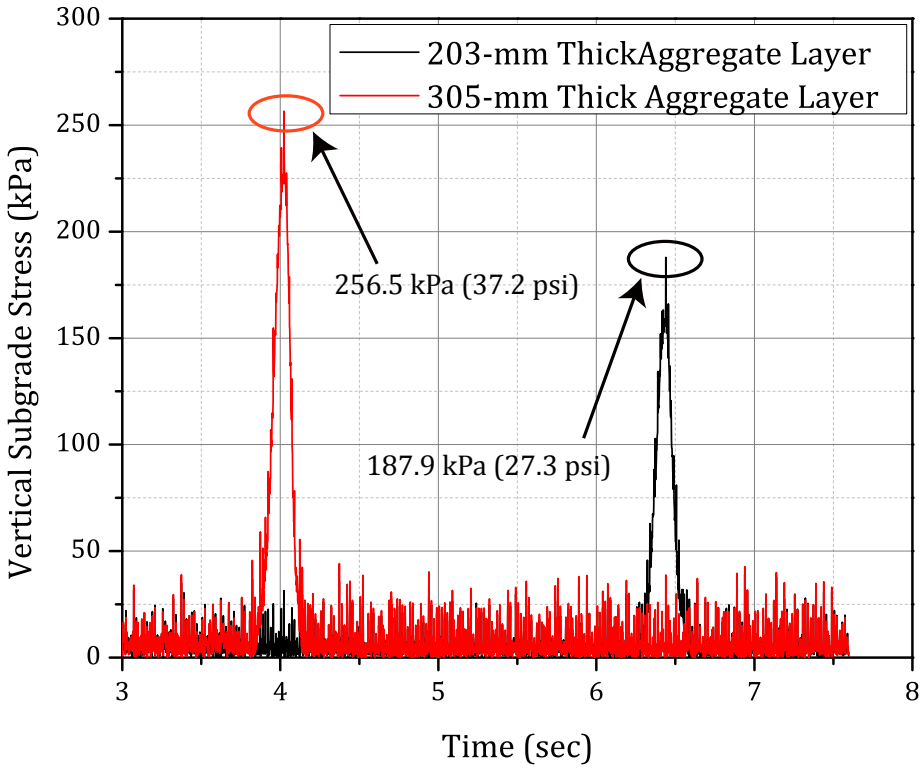


Figure 8.17: Subgrade Stress Levels underneath Sections (left) 2 and (right) 3 of Cell 2

subgrade conditions can often be challenging, it is recommended that crushed aggregate with very low fines contents should be avoided from unsurfaced pavement applications to eliminate the possibility of internal shear failure of the aggregate cover layer.

### 8.4.2 Performance under Flooded Conditions

Subsequent to testing at near-optimum aggregate moisture conditions, the test sections were artificially flooded and tested to failure under flooded conditions to evaluate the effect of excess moisture on pavement performance. Note that due to inclement weather conditions, testing of this cell under flooded conditions had to be stopped after only 34 load applications. Figure 8.18 shows the rut development in Cell 2 aggregate sections under flooded conditions. As shown in the figure, after 34 load applications, Section 2 (305-mm thick aggregate layer) showed the highest rut-accumulation as well as surface heave development. This was different from the trend observed in case of Cell 1, that showed rapid failure of the thinnest aggregate layer (Section 3) under flooded conditions, due to excessive subgrade deformations.

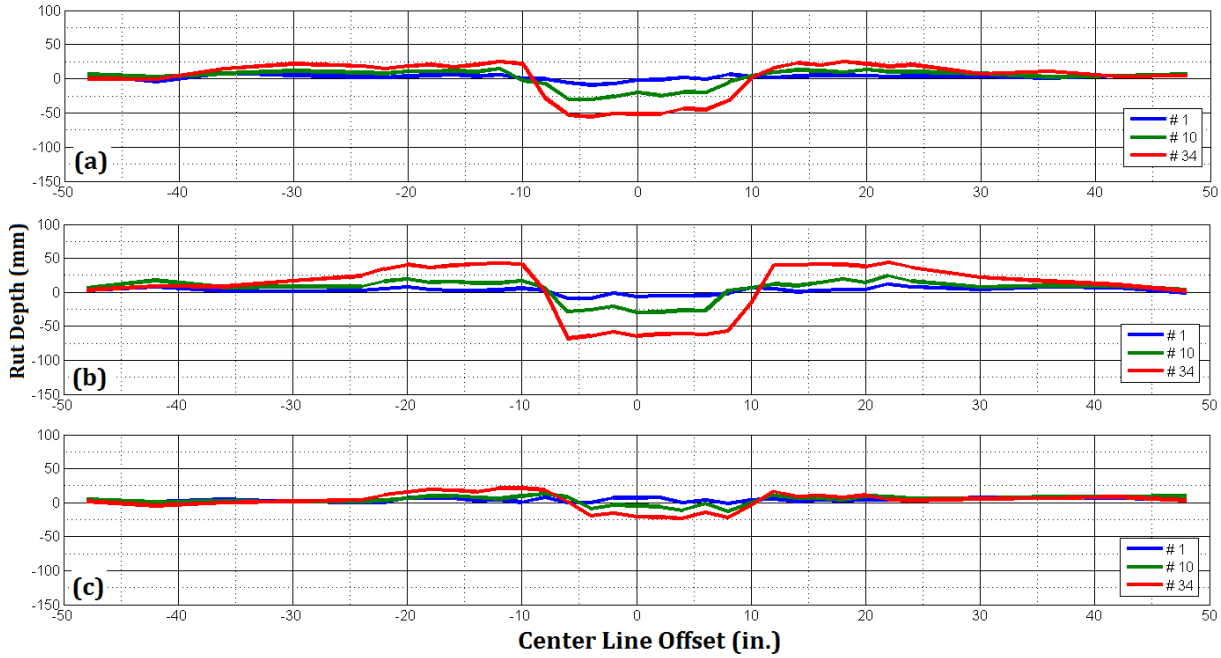


Figure 8.18: Rut Developments in Cell 2 Sections (a) 1, (b) 2, and (c) 3 due to Unidirectional ATLAS Loading under Flooded Conditions (1 in. = 25.4 mm)

Figure 8.19 shows the deformed layer boundaries for the aggregate surface as well as the aggregate-subgrade interface in Cell 2 after testing under flooded conditions. The subgrade deformation in Section 2 was clearly visible as shown in Figure 8.19b, whereas no significant subgrade deformation was observed for Sections 1 and 3. No logical explanation of this behavior could be deduced. However, one possible explanation could be related to inadequate flooding of Sections 1 and 3 resulting in not enough moisture wetting the subgrade to reduce the subgrade strength significantly.

An important observation should be made from the excavated trench sections shown in Figure 8.19. Significant amounts of subgrade intrusion into the aggregate layer was observed for all three sections under flooded conditions. It is apparent that due to the low fines content and free-draining nature of the crushed limestone used in Cell 2, subgrade pumping into the aggregate layer was more significant compared to the other aggregate types.

For the crushed limestone with low fines, degree of compaction played a significant role in governing aggregate layer behavior at near-optimum moisture conditions. The aggregate sections

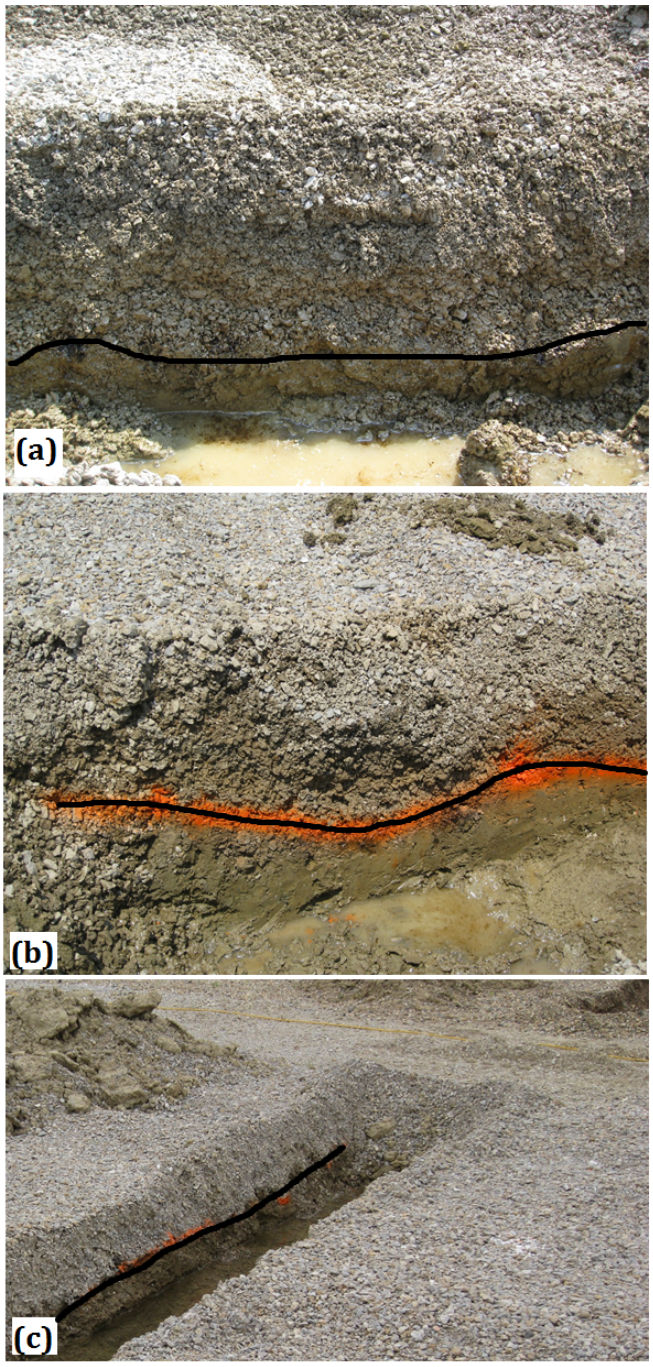


Figure 8.19: Excavated Trench Photos Showing Surface and Base-Subgrade Interface Deformations in Test Sections (a) 1, (b) 2, and (c) 3 due to Loading of Cell 2 under Flooded Conditions

with lower relative compaction levels, underwent internal shear failure that led to excessive rutting after relatively low number of load applications. Aggregate sections compacted to high densities on the other hand, sustained significantly higher number of load applications before failing due to subgrade deformation such as Section 3. The significant improvement in aggregate behavior under higher compactive efforts was also reflected from laboratory testing of the aggregates reported in Chapter 6. Significant subgrade intrusion into the aggregate layer was observed for all three test sections under flooded conditions. A fabric to be used at the subgrade interface would serve as a good separator for such low fines aggregate materials. The mechanism contributing to pavement failure under flooded conditions were not clear for this particular test cell.

## 8.5 Cell 4: Crushed Limestone with High Amounts of Nonplastic Fines

The effect of high amounts of nonplastic fines on the performance of a crushed limestone aggregate was evaluated through accelerated pavement testing of unsurfaced pavement sections at near-optimum and flooded conditions. As mentioned in section 6.3.1, the crushed limestone used in this cell (Cell 4) had higher fines contents ($\sim$ 10%) compared to those initially obtained during preliminary survey of potential aggregate sources, and was therefore classified as having "high" amount of fines. Like the uncrushed gravel used in Cell 1, the crushed limestone material in Cell 4 also comprised high amounts of nonplastic fines. Therefore, comparative analyses of Cell 1 and Cell 4 performances would emphasize the effect of aggregate shape and angularity.

### 8.5.1 Performance under Near-Optimum Moisture Conditions

Figure 8.20 shows the final deformed profile for the 356-mm (14-in.) thick aggregate section in Cell 4. The test section could sustain 168 load applications before accumulating rut depths of

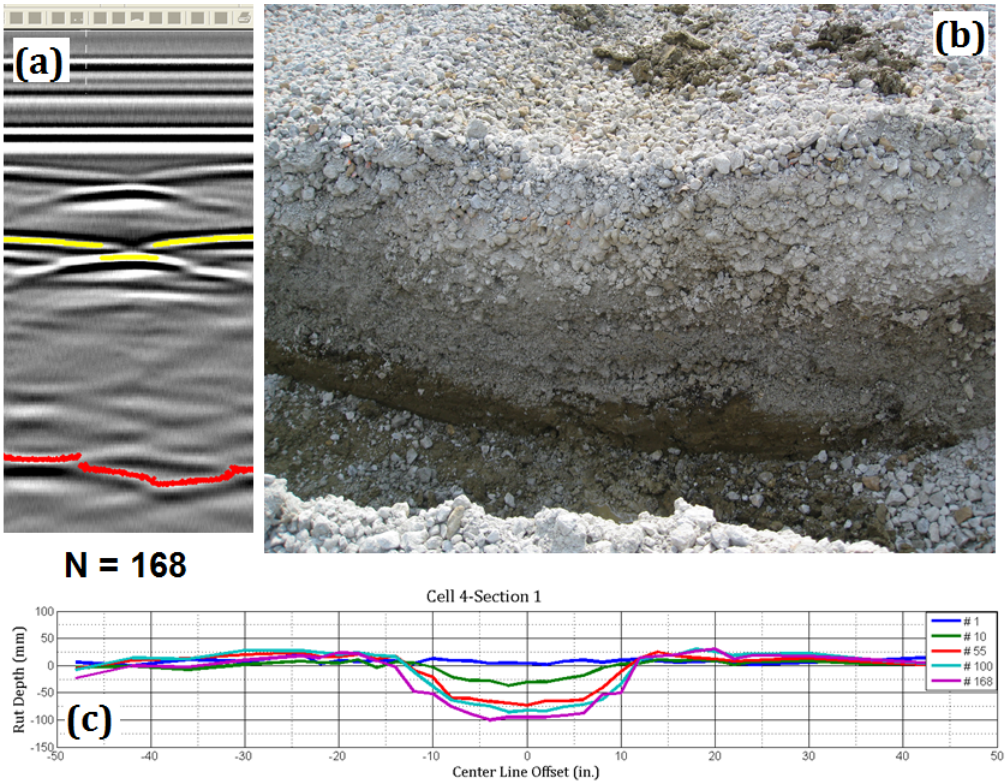


Figure 8.20: (a) GPR Scan, (b) Excavated Trench and (c) Surface Rut Profile of the 356-mm Thick Crushed Limestone Aggregate Section in Cell 4 (1 in. = 25.4 mm)

approximately 100 mm. Moreover, no surface heave was observed adjacent to the wheel path. The GPR scan and excavated trench sections (see Figures 8.20a and 8.20b) clearly indicate a more defined subgrade deformation pattern compared to those observed in Cell 1. Moreover, the subgrade depression is directly underneath the surface rut, indicating no significant shear movement within the aggregate layer due to improved particle-to-particle interlock. The basin-shaped subgrade deformed profile (see Figure 8.20b) can be attributed to the superior load spreading abilities of the crushed aggregate base course.

Figure 8.21 shows the final deformed profile of Section 2 (305-mm thick aggregate layer) of Cell 4. Unlike Section 1, this section showed significant heaving adjacent to the wheel path after 55

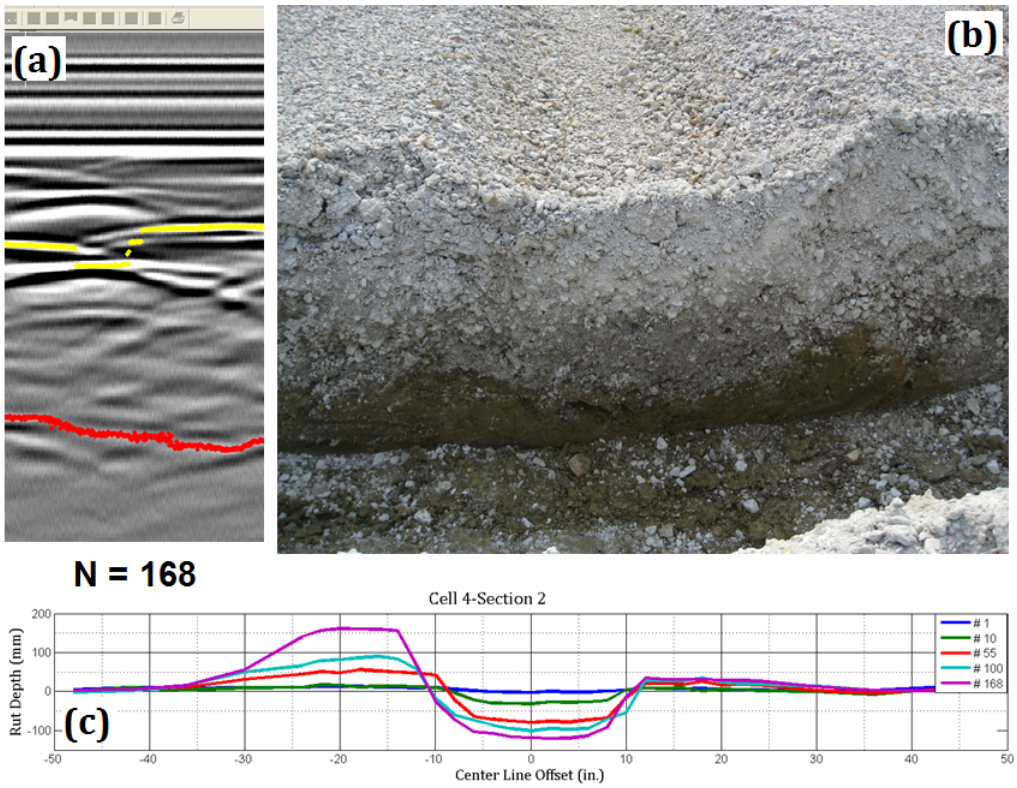


Figure 8.21: (a) GPR Scan, (b) Excavated Trench, and (c) Surface Rut Profile of the 305-mm Thick Crushed Limestone Aggregate Section in Cell 4 (1 in. = 25.4 mm)

load applications (see Figure 8.21c). Moreover, as can be seen from the GPR scan, the subgrade deformation is offset from the wheel path, and hence, shows the possibility of shear flow of the material. Close inspection of as-constructed moisture contents of the subgrade layer explained the excessive surface heave development in Section 2. Average moisture contents for the engineered

subgrade layer in Sections 1, 2, and 3 were 13.1%, 15.2%, and 13.3% respectively. As discussed in Chapter 6, a moisture content of approximately 13% was targeted for preparing an engineered subgrade of CBR = 3% (refer to Figure 6.18). However, as shown in Figure 6.18, the CBR value for the subgrade soil decreases rapidly with increasing moisture content; a moisture content of 15% corresponds to CBR values of less than 1%.

The significantly weaker subgrade conditions (owing to the higher moisture content) under the 305-mm thick aggregate layer in Section 2 resulted in failure of the section. The aggregate-subgrade layer interface observed from the excavated trench section (see Figure 8.21b) clearly showed significant subgrade movement, and the surface heave observed was a direct reflection of subgrade heave.

Figure 8.22 presents the deformed layer profiles for the 203-mm thick aggregate layer (Section 3) of Cell 4. As is apparent from the GPR scan and the trench sections (see Figures 8.22a and

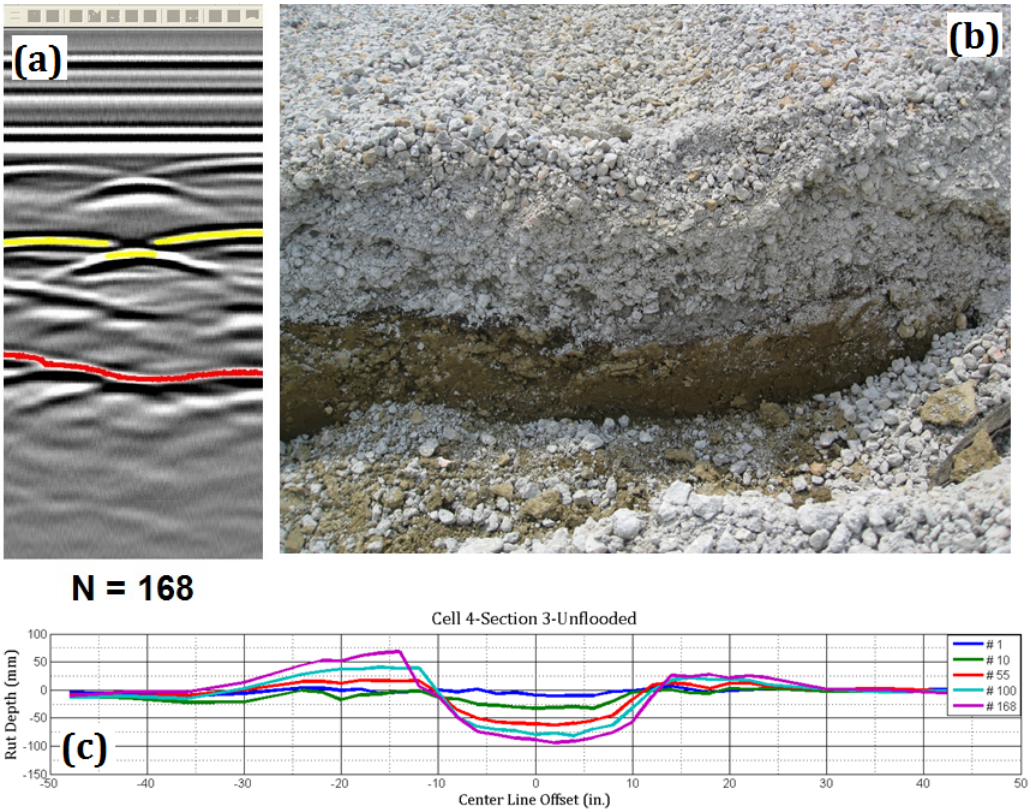


Figure 8.22: (a) GPR Scan, (b) Excavated Trench, and (c) Surface Rut Profile of the 203-mm Thick Crushed Limestone Aggregate Section in Cell 4 (1 in. = 25.4 mm)

8.22b), the subgrade deformation underneath the wheel path was clearly visible and the surface heave noticed, was primarily a reflection of the subgrade deformation.

### 8.5.2 Performance under Flooded Conditions

Figure 8.23 shows the development of rutting in Sections (a) 1, (b) 2 and (c) 3 under flooded conditions for the crushed limestone with high amounts of nonplastic fines. The layer interface boundaries as observed from excavated transverse trenches are shown in Figure 8.24. From

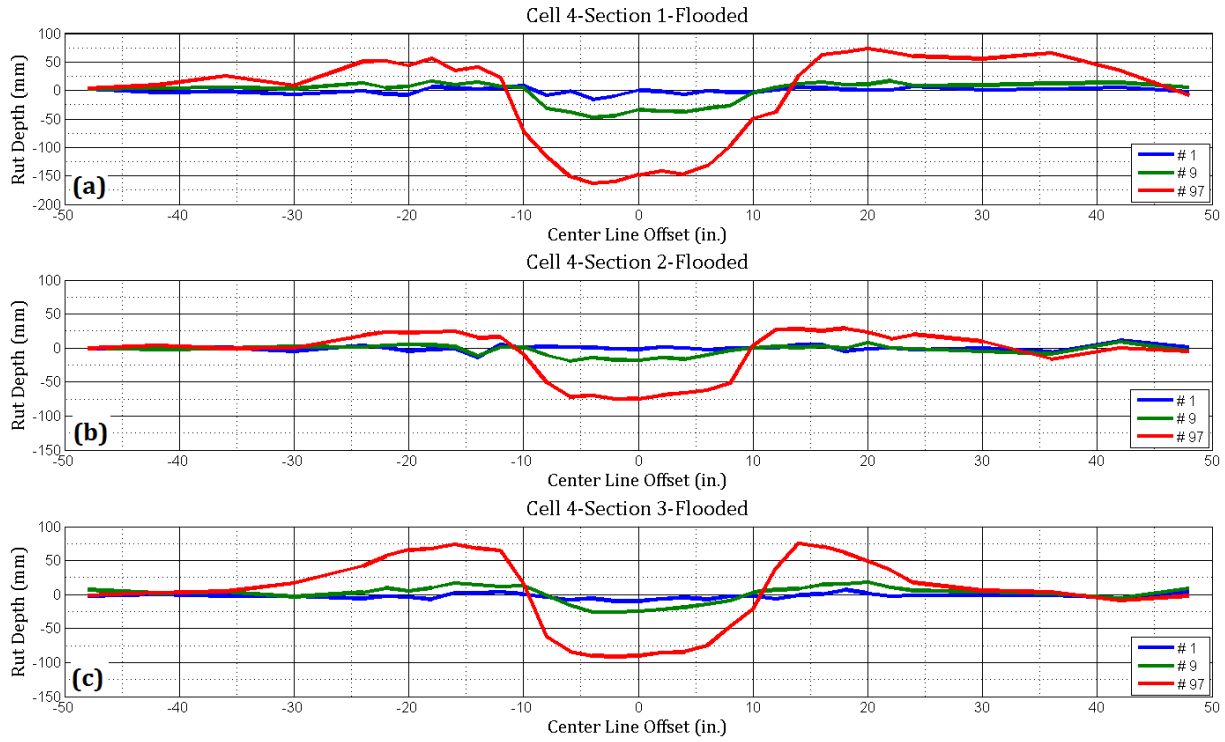


Figure 8.23: Rut Developments in Cell 4 Sections due to Unidirectional ATLAS Loading under Flooded Conditions (1 in. = 25.4 mm)

Figures 8.23 and 8.24, both Sections 1 and 3 underwent subgrade failure and showed significant heaving at the aggregate-subgrade interface, which was ultimately reflected on to the surface. After 97 load applications, Section 1 showed the highest rut accumulation (approximately 150 mm). This may have been caused by the combined effect of excess moisture and high amounts (10%) of fines in the aggregate matrix. Section 3 (203-mm thick aggregate layer) showed the highest amount of subgrade movement, which was attributed to the higher stress levels at the subgrade interface underneath the thinnest aggregate layer.

From testing at near-optimum as well as flooded conditions, the primary mechanism contributing to the pavement failure in Cell 4, was subgrade rutting. The crushed limestone with

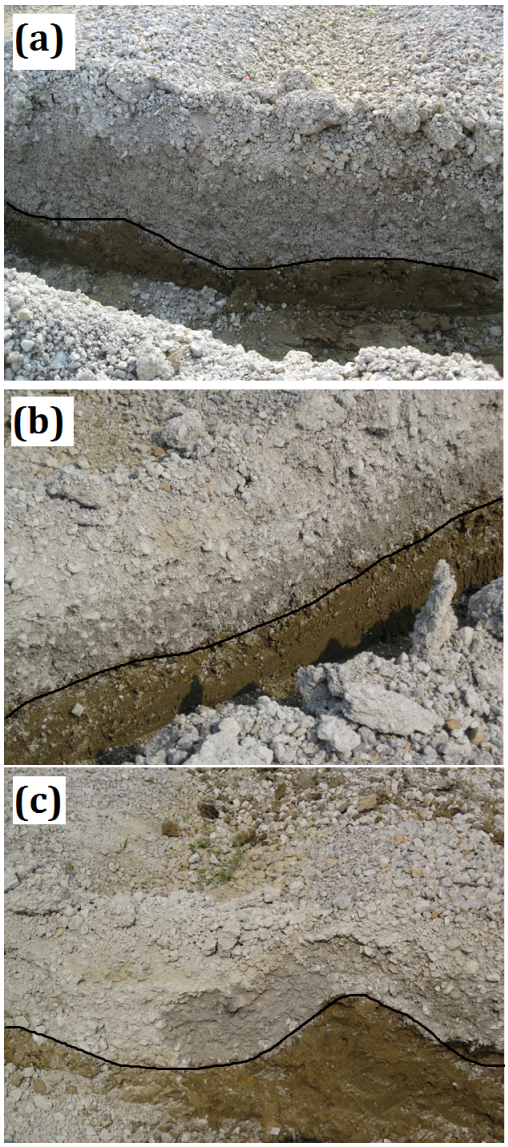


Figure 8.24: Excavated Trench Photos Showing Surface and Base-Subgrade Interface Deformations in Test Sections (a) 1, (b) 2, and (c) 3 due to Loading under Flooded Conditions

high fines did not undergo internal shear movement. Layer thickness was the primary factor governing pavement performance, with Section 3 (203-mm thick aggregate layer) failing first, due to inadequate stress dissipation at the subgrade interface. Section 1 (356-mm thick aggregate layer) performed consistently better than Section 3 (203-mm thick aggregate layer) under near-optimum aggregate moisture conditions. Section 1 showed the highest rut accumulation under flooded conditions, which may have been from the combined effect of excess moisture, and high amount of fines in the aggregate layer. Section 2 (305-mm thick aggregate layer) showed the highest surface heave at near-optimum conditions, which was attributed to significantly weaker subgrade conditions. The performance of Section 2 under flooded conditions, could not be explained.

## 8.6 Cell 5: Crushed Limestone with Low Amounts of Plastic Fines Over An Engineered Subgrade of Target CBR = 6%

Cell 5 was constructed using the same material as in Cell 2 (crushed limestone with low amounts of plastic fines) over a subgrade CBR value of 6%, and comprised aggregate layers of thicknesses 254 mm, 203 mm, and 152 mm (10 in., 8 in., and 6 in.) for Sections 1, 2, and 3 respectively. The primary objective behind construction of this test cell was to evaluate the effects of better subgrade conditions on unsurfaced pavement performance.

### 8.6.1 Performance under Near-Optimum Moisture Conditions

Figure 8.25 shows the (a) GPR Scan, (b) Excavated Trench, and (c) Surface Rut Profile of Section 1 (254-mm thick aggregate layer) in Cell 5, tested under near-optimum aggregate moisture conditions. From the figure, Section 1 of Cell 5 could sustain 478 load applications

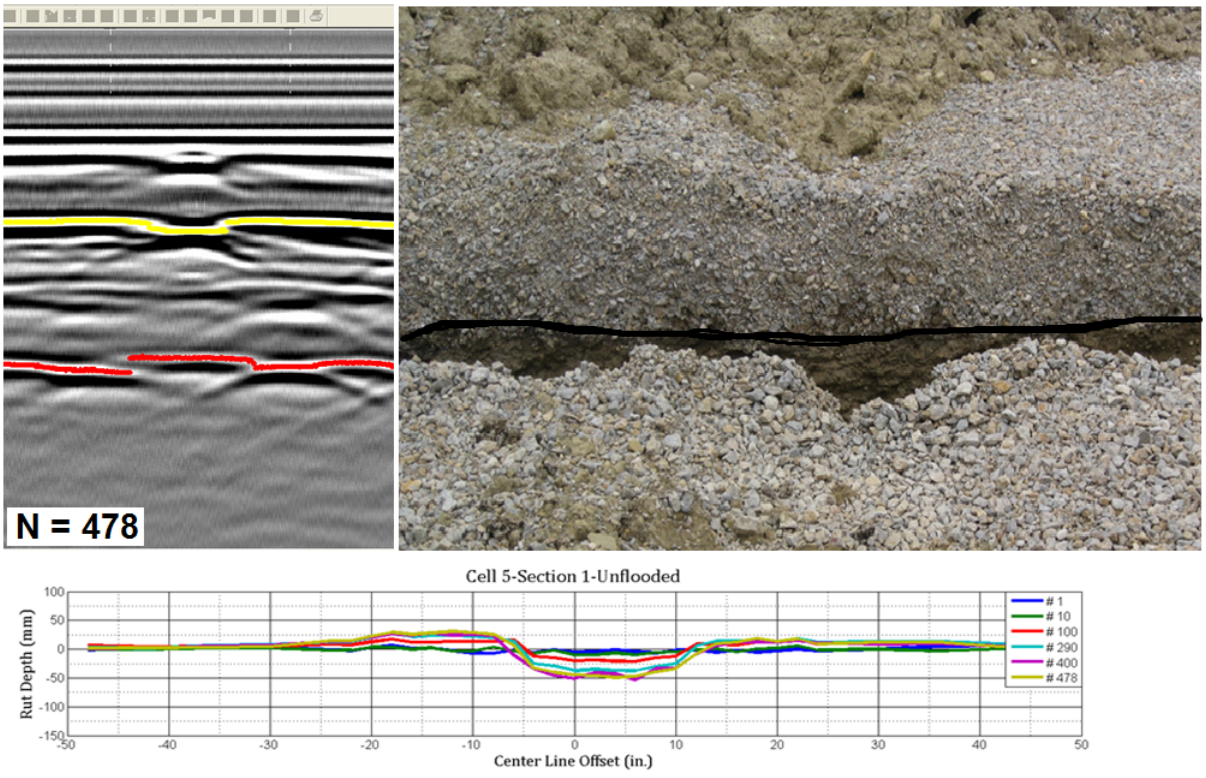


Figure 8.25: (a) GPR Scan, (b) Excavated Trench, and (c) Surface Rut Profile of the 254-mm Thick Aggregate Section in Cell 5 (1 in. = 25.4 mm)

without significant rut accumulation or development of surface heave. Moreover, close

examination of the GPR scan (Figure 8.25a) and excavated trench section (Figure 8.25b) clearly indicate the absence of subgrade shear failure. The rutting observed on the surface, was probably from subgrade movement that could not be visually identified from the trench sections.

Figure 8.26 shows the deformed layer profiles for Section 2 (203-mm thick aggregate layer) in Cell 5. As shown in the figure, no significant heaving of the surface was observed up to 100 load

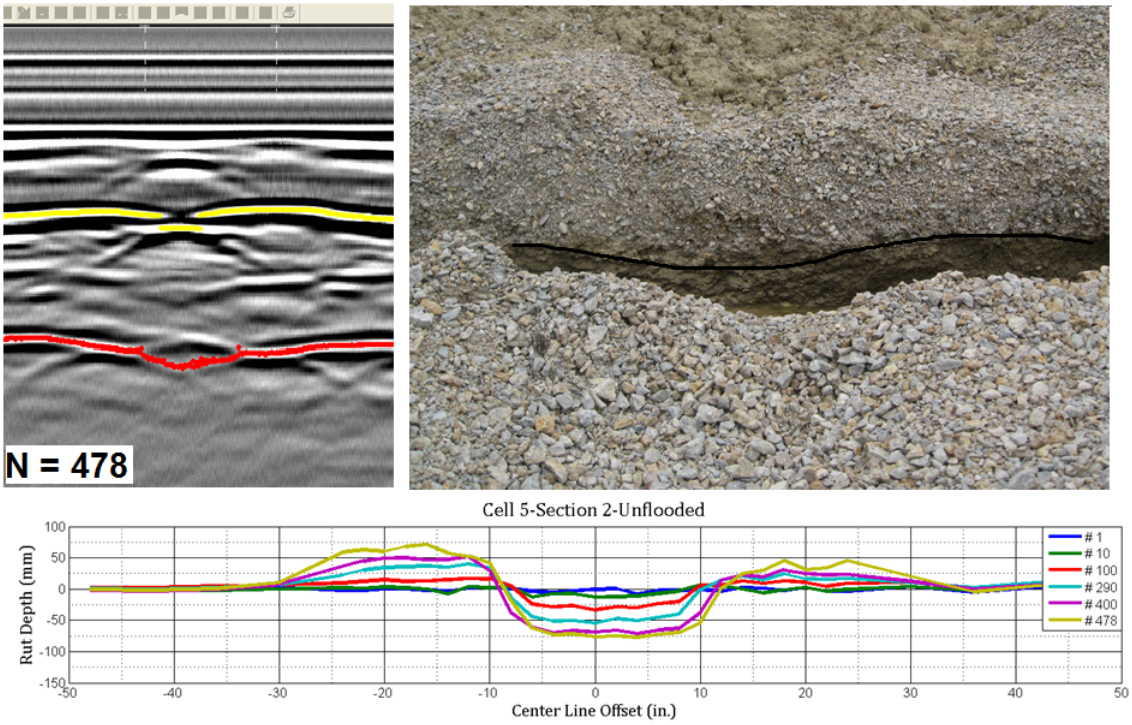


Figure 8.26: (a) GPR Scan, (b) Excavated Trench, and (c) Surface Rut Profile of the 203-mm Thick Aggregate Section in Cell 5 (1 in. = 25.4 mm)

applications. However, upon further loading, the surface heave became more and more apparent. The GPR scan and excavated trench sections showed clearly defined subgrade deformation under the wheel path. Moreover, the surface heave was a reflection of subgrade movement. This phenomenon was magnified in Section 3 (152-mm thick aggregate layer) as shown in Figure 8.27.

Close examination of GPR scans and excavated trenches for the three test sections identified the different modes contributing to failure. Section 1 performed the best without undergoing shear failure even after 478 load applications. The rutting in Section 1 was probably from subgrade deformations that could not be visually identified from the excavated trench sections.

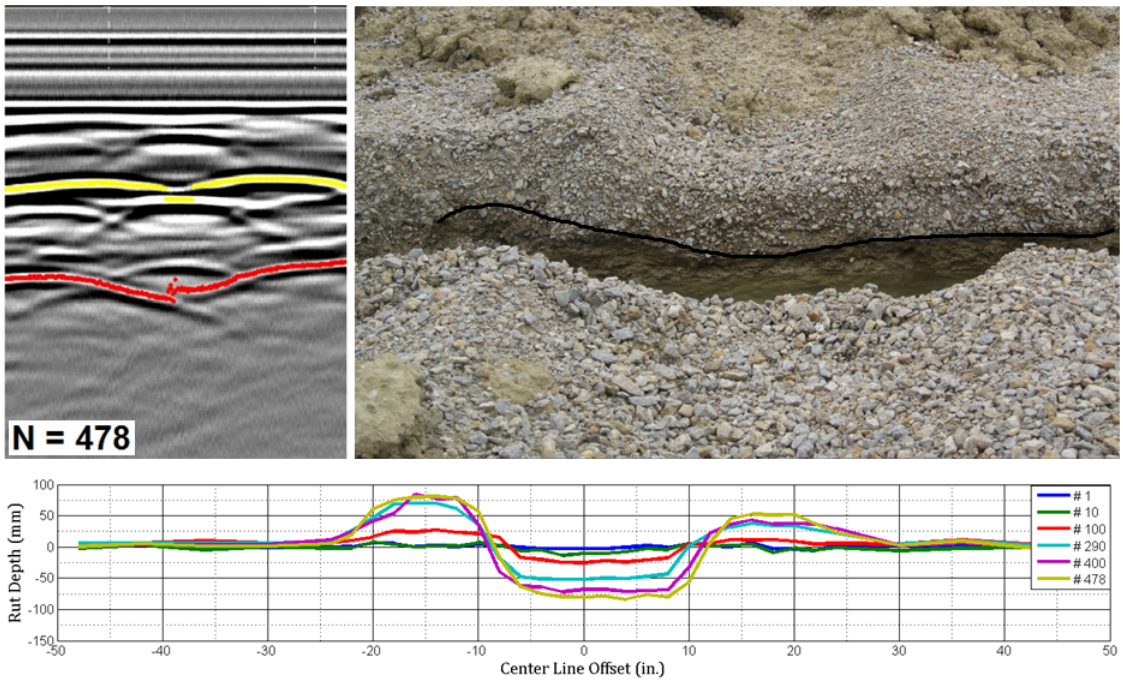


Figure 8.27: (a) GPR Scan, (b) Excavated Trench, and (c) Surface Rut Profile of the 152-mm Thick Aggregate Section in Cell 5 (1 in. = 25.4 mm)

The subgrade rutting pattern became clearly evident as the aggregate layer thickness decreased, and no significant shear movement within the aggregate layer was observed. For Sections 2 and 3, rapid heaving of the aggregate surface was observed after 100 load applications. The improvement in pavement performance achieved from better subgrade support is clearly evident from the performance of this test cell.

### 8.6.2 Performance under Flooded Conditions

Figure 8.28 shows the development of rutting in the three test sections of Cell 5 under flooded conditions. The test section performances under flooded conditions clearly showed the effect of excessive moisture on pavement performance, particularly for thin aggregate layers. Section 3 (152-mm thick aggregate layer) showed rapid permanent deformation accumulation and developed significant surface heave after 125 load applications. Test section performance was by far better for the thick aggregate sections, with Section 1 (254-mm thick aggregate layer) sustaining 216 load applications with much less rutting accumulated.

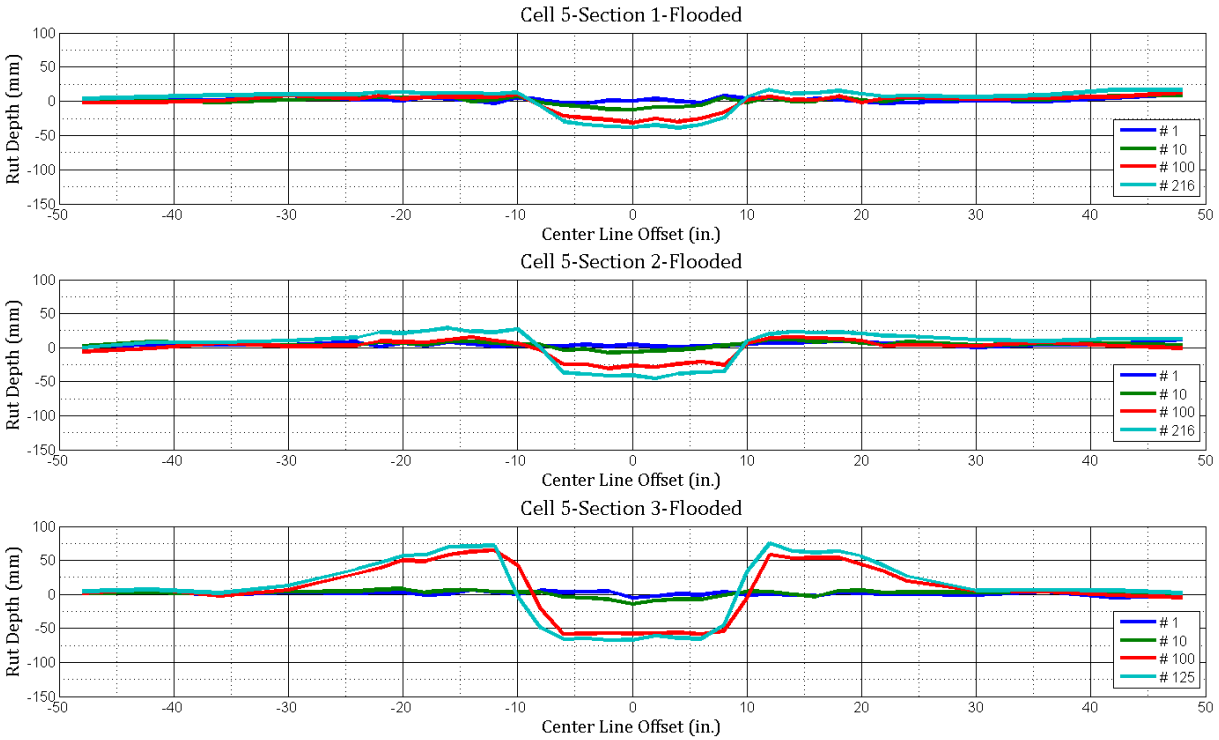


Figure 8.28: Rut Developments in Crushed Limestone Sections in Cell 5 due to Unidirectional ATLAS Loading under Flooded Conditions (1 in. = 25.4 mm)

Examination of transverse trench sections revealed subgrade deformation to be the primary mechanism contributing failure of the test sections under flooded conditions. Figure 8.29 shows the deformed layer boundaries for the aggregate surface as well as the aggregate-subgrade interface after testing under flooded conditions. As seen from the excavated trench sections, flooding of Cell 5 reduced the subgrade strength, and therefore the pavement sections failed at lower number of load applications as compared to the unflooded conditions. However, the modes of failure for the three aggregate sections were similar to those under near-optimum aggregate moisture conditions. Section 1 (254-mm thick aggregate layer) did not show any significant heave development adjacent to the wheel path, whereas progressively worse heaving was observed for Sections 2 and 3 (203-mm and 152-mm thick aggregate layers respectively). The worst surface heave was observed for Section 3, which can be attributed to the high subgrade stress levels underneath the 152-mm (6-in.) thick aggregate layer in Section 3. The high stresses applied on the weak subgrade (subgrade strength significantly reduced due to flooding) resulted in shear failure accompanied by surface heave development.

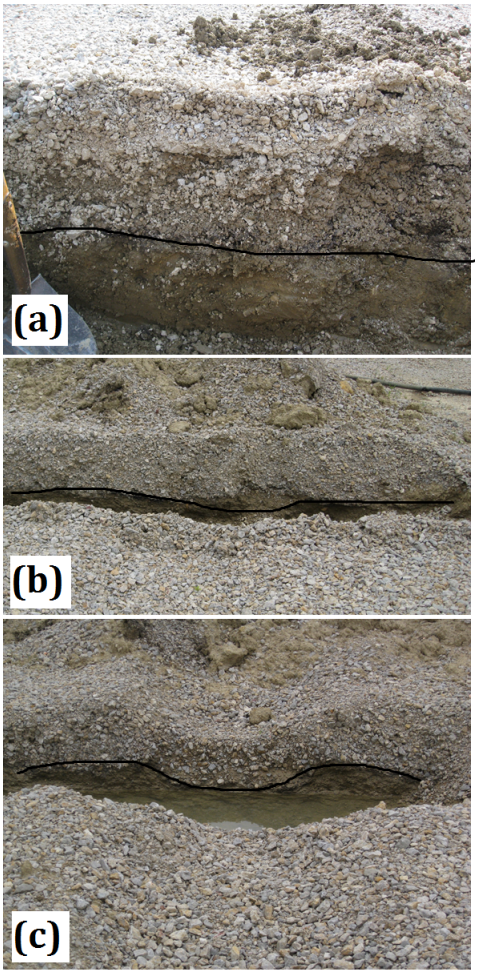


Figure 8.29: Excavated Trench Photos Showing Surface and Base-Subgrade Interface Deformations in Test Sections (a) 1, (b) 2, and (c) 3 of Cell 5 due to Loading under Flooded Conditions

## 8.7 Cell 3: Crushed Dolomite with High Amounts of Nonplastic Fines

The effect of high amounts of nonplastic fines on the performance of a crushed dolomite material was evaluated through accelerated testing of unsurfaced pavement sections under near-optimum and flooded aggregate moisture conditions. As already mentioned, testing of this cell was conducted in May 2011 after the test cell experienced winter freeze-thaw cycles. Testing took place approximately six weeks after the last freeze-thaw cycle to allow sufficient time for dissipation of any excessive moisture accumulation during the spring-thaw season.

The first task before loading of the test cell was to assess the existing conditions of the subgrade and aggregate layers. Accordingly, DCP testing was conducted at six different locations (two locations per test section) to determine the in-place CBR profiles in the top engineered subgrade and aggregate layers. Figure 8.30 shows the in-place CBR profile along the North wheel path of Section 1 (356-mm thick aggregate layer).

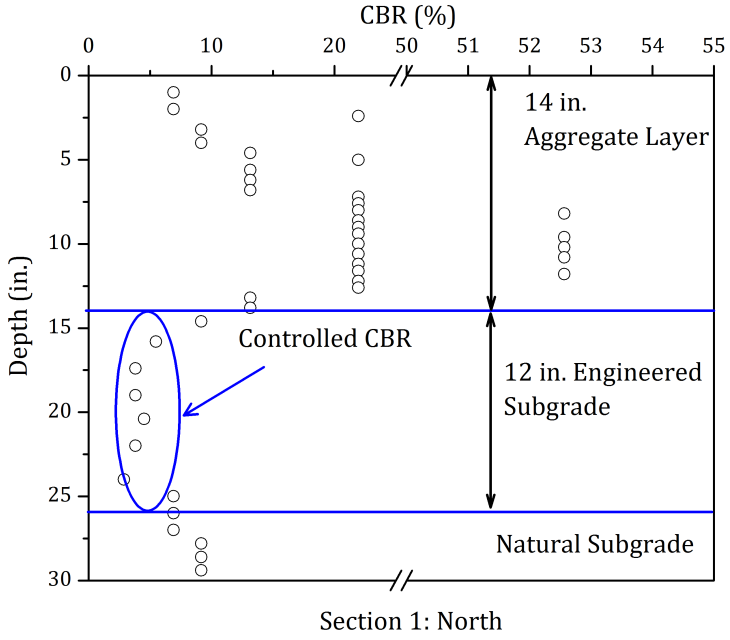


Figure 8.30: Cell 3 CBR Profiles with Depth along the North Wheel Path of the 356-mm Thick Aggregate Layer in Section 1 (1 in. = 25.4 mm)

As shown in Figure 8.30, the subgrade CBR values were consistently close to the as-constructed value (target CBR = 3%) throughout the depth (305 mm) of the engineered subgrade layer. DCP

results from the other five locations showed very similar results and are presented in Appendix D. No change in engineered subgrade CBR values due to the winter freeze-thaw cycles was therefore observed, which was primarily attributed to adequate removal of excessive moisture by the installed transverse and longitudinal drainage systems.

The effect of winter freeze-thaw cycles on the constructed aggregate layer was evaluated through comparison of field modulus values for the three sections measured before and after the freeze-thaw cycles using the GeoGauge™. As shown in Figure 8.31, the aggregate layer moduli for all three test sections after the freeze-thaw cycles were significantly higher (up to 225% ), when compared to the "as-constructed" values. This indicated significant strength gain by the crushed dolomite material after the winter.

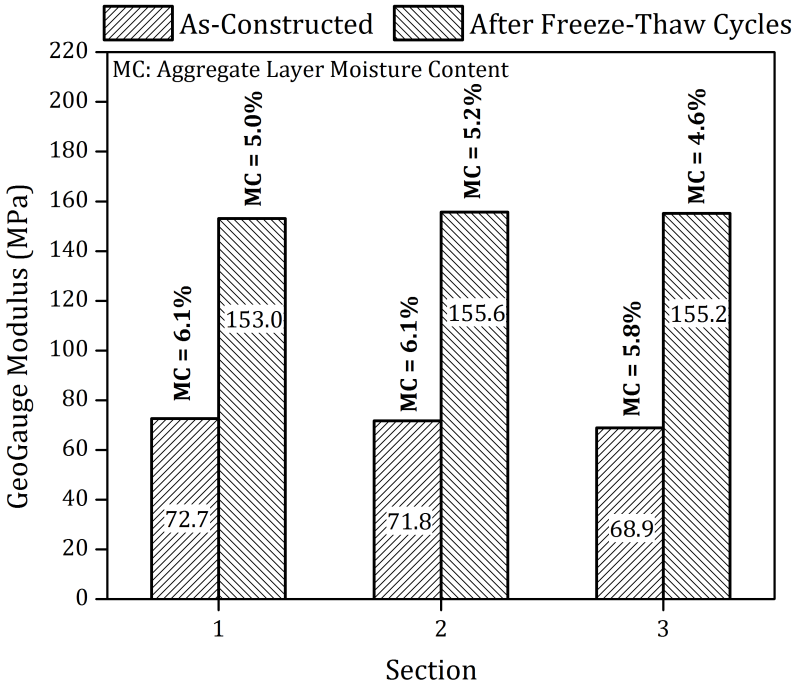


Figure 8.31: Comparison of Aggregate Layer Modulus Values before and after Freeze-Thaw Cycles

One plausible mechanism contributing to the strength gain within the crushed dolomite layer could be: "carbonate cementation" within the fines fraction [138]. Significant strength gain in high carbonate base course materials upon soaking has been reported in literature due to "cementation" of the fines fraction through dissolution and precipitation of Calcium Carbonate

($CaCO_3$) according to Equation 8.1 [138, 139].

$$CO_2 + H_2O + CaCO_3 = Ca^{2+} + H^+ + HCO_3^- + CO_3^{2-} \tag{8.1}$$

To further investigate the hypothesis regarding strength gain by the crushed dolomite material with high fines upon extended periods of soaking and exposure to freeze-thaw cycles, unconfined compressive strength (ASTM D 2166) tests were conducted on the aggregate fines (material finer than 0.075 mm, or passing No. 200 sieve). Two identical cylindrical specimens, 71 mm in diameter and 142 mm in height, were prepared at a target moisture content of 14%. Note that the target moisture content of 14% was selected through iterative trial-and-error approach to arrive at the minimum moisture content where the compacted specimen exhibited "cohesive" characteristics. One of the compacted specimens was immediately tested for the unconfined compressive strength, whereas the other was exposed to 24 hours of freezing (-16° C) followed by 24 hours of thawing (16° C) as specified in ASTM D 6035. Care was taken to ensure that no moisture was lost by the specimen during the freeze-thaw period. Figure 8.32 shows a picture of the "conditioned" specimen tested for unconfined compressive strength.

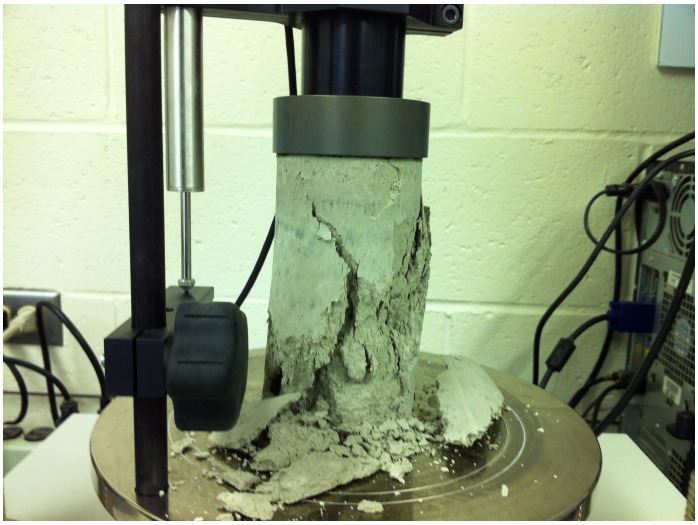

Figure 8.32: Unconfined Compressive Strength Testing of Fines Fraction

Figure 8.33 compares the unconfined compressive strength ($Q_u$) values for the two specimens described above. As shown in the figure, subjecting the specimen to one freeze-thaw cycle (24-hours of freezing followed by 24-hours of thawing) resulted in an increase in the unconfined

compressive strength value from 224 kPa (32.5) psi to 581 kPa (84.2 psi). This preliminary investigation supported the possibility of strength gain by the carbonate fines in the crushed dolomite material upon exposure to extended periods of soaking and freeze-thaw cycles, possibly due to the dissolution and precipitation of carbonates as illustrated in Equation 8.1. Further investigation of this phenomenon is required to verify the mechanism responsible for such strength gain. One possible approach may be to conduct X-Ray Diffraction (XRD) or Scanning Electron Microscope (SEM) testing of the fines fraction after different periods of "conditioning" to identify possible changes in the molecular structure. Such an investigation is beyond the scope of this PhD research, and has been listed in Chapter 9 as a recommended topic for future research.

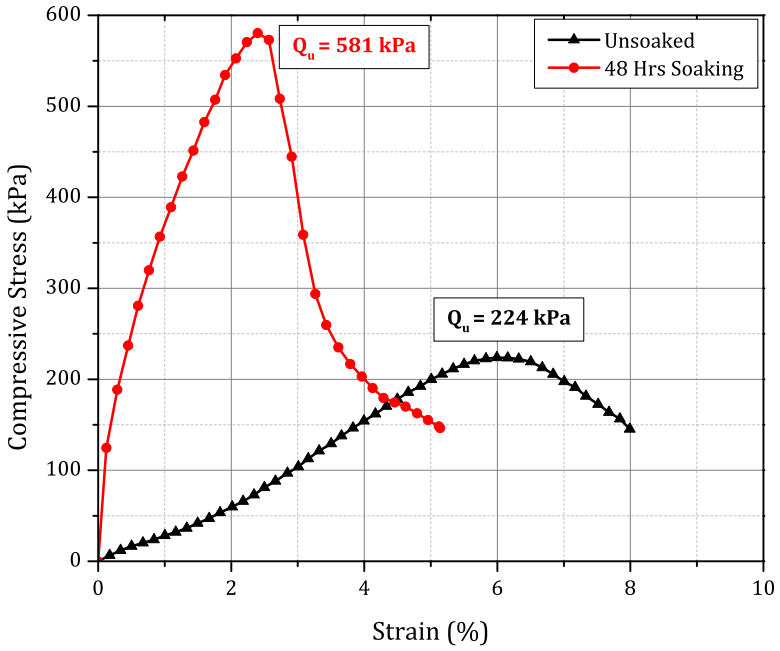


Figure 8.33: Effect of Freeze-Thaw Cycles on the Unconfined Compressive Strength of Carbonate Fines

It also important to note that the moisture contents of the aggregate sections in Cell 3 after the winter freeze-thaw cycles were consistently lower than the "as-constructed" values (see Figure 8.31). This loss of moisture in the crushed dolomite material with high fines might have led to changes in the layer suction characteristics, resulting in higher strength and field-modulus values. This hypothesis regarding lower moisture contents leading to higher shear strength was confirmed by comparing the unsoaked CBR values of crushed dolomite specimens prepared in the laboratory

with 12.4% nonplastic fines. Under optimum moisture conditions (ASTM D 698), the compacted specimen had an unsoaked CBR value of 65%, whereas under dry of optimum (90% $w_{opt}$) moisture conditions, the unsoaked CBR value was increased to 90%. Similarly, a reduction in permanent deformation accumulation was observed for the specimen tested at 90% of $w_{opt}$. As shown in Figure 8.34, a reduction in the moisture content by 0.7% led to a 33% reduction in the permanent deformation accumulation. Moreover, testing the two specimens for resilient modulus resulted in higher modulus values obtained under dry of optimum moisture conditions. These laboratory test results supported the hypothesis of improved performance for the crushed dolomite material with high amounts of nonplastic fines under reduced moisture contents. Further investigation of the effect of freeze-thaw cycles on aggregate suction characteristics is beyond the scope of this PhD research, and has been listed in Chapter 9 as a recommended topic for future research.

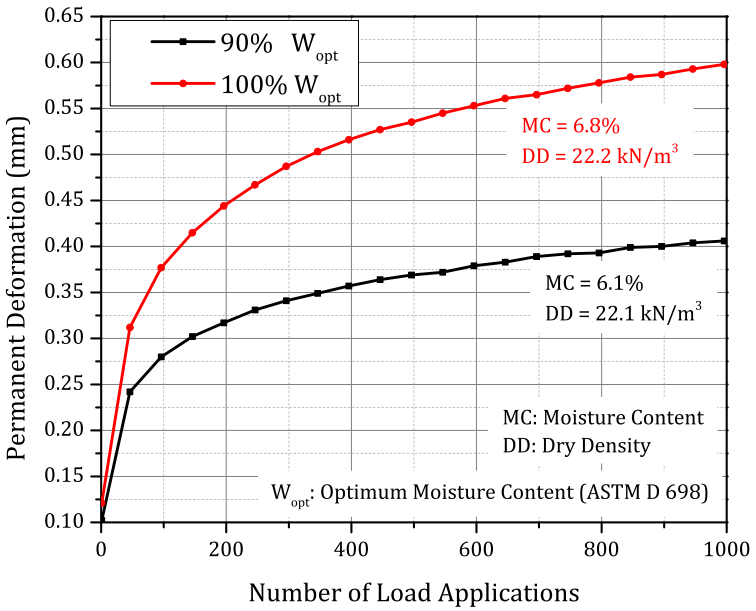


Figure 8.34: Comparing the Effect of Moisture Conditions on the Permanent Deformation Accumulation in Crushed Dolomite Specimens with 12.4% Nonplastic Fines

### 8.7.1 Performance under Near-Optimum Moisture Conditions

Apparent strength gain (reflected by high field modulus values) by the crushed dolomite material due to the freeze-thaw cycles was clearly reflected from performance of the test sections under

loading. Figure 8.35 shows the (a) GPR Scan, (b) Excavated Trench and (c) Surface Rut Profile of the 356-mm thick crushed dolomite section (Section 1) in Cell 3 upon testing at near-optimum moisture conditions. The most important thing to notice from Figure 8.35 is the significantly

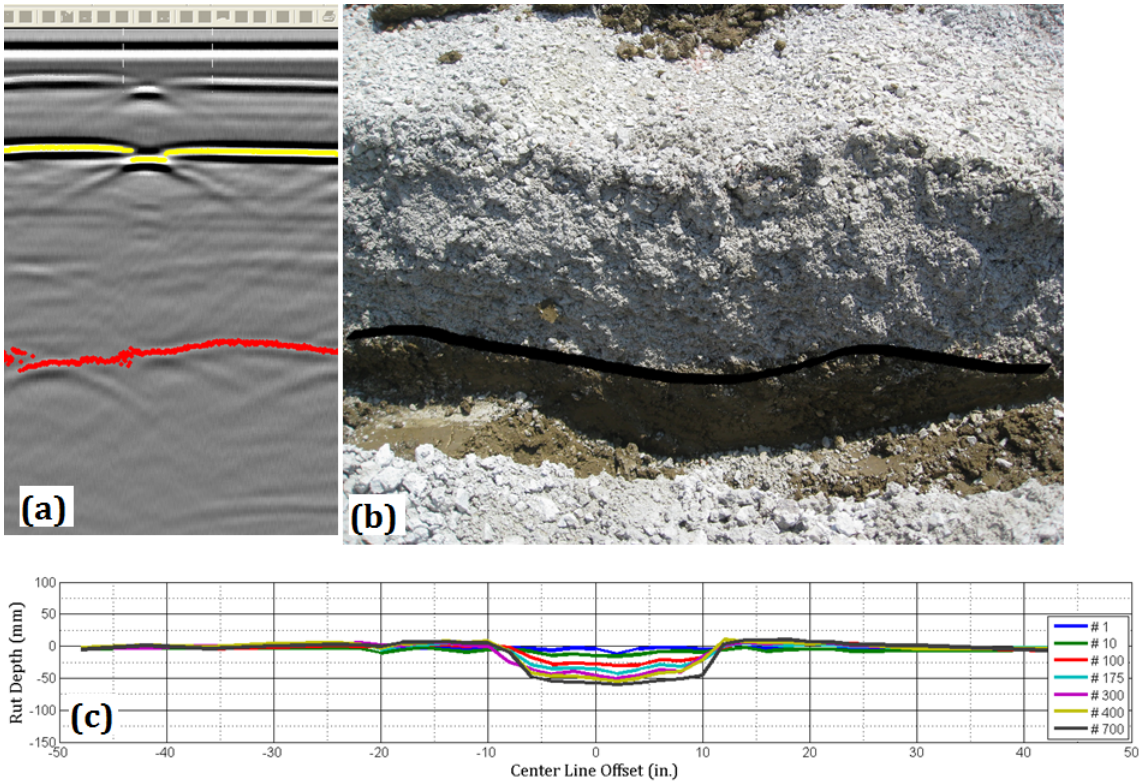


Figure 8.35: (a) GPR Scan, (b) Excavated Trench, and (c) Surface Rut Profile of the 356-mm Thick Crushed Dolomite Section in Cell 3 (1 in. = 25.4 mm)

higher number of load applications (700) this particular test section could sustain for accumulating only 50-mm rutting. Moreover, even after 700 load applications no surface heave was observed adjacent to the wheel path (see Figure 8.35c). This preliminary observation indicated the absence of significant shear movement within the aggregate layer. The GPR scan (see Figure 8.35a) and excavated trench section (see Figure 8.35b) both clearly indicate that rutting of the test section was due to subgrade deformation only.

Figures Figure 8.36, and Figure 8.37 show the deformed profiles for Sections 2 and 3 (305-mm and 203-mm thick aggregate layers), respectively. Sections 2 and 3 could sustain 400 and 175 load applications, respectively, before accumulating rut depths of approximately 100-mm. GPR scans, and excavated trench sections clearly showed subgrade deformation to be the primary

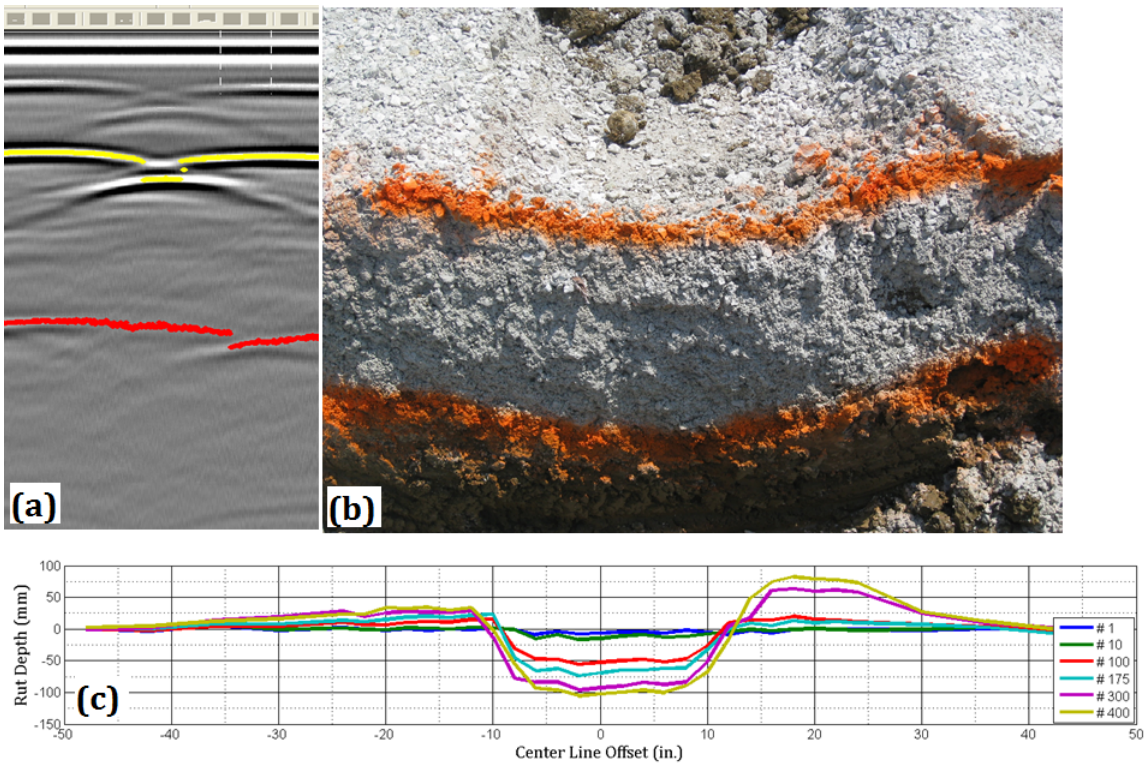


Figure 8.36: (a) GPR Scan, (b) Excavated Trench, and (c) Surface Rut Profile of the 305-mm Thick Crushed Dolomite Section in Cell 3 (1 in. = 25.4 mm)

mechanism responsible for failure of the test sections. As the aggregate layer thickness decreased, the subgrade was subjected to significantly higher stress levels, ultimately leading to shear failure. From the excavated trench sections (see Figures 8.36b and 8.37b) the aggregate layer clearly deformed as a "flexible mat" and observed surface heaves were merely reflections of subgrade movement.

Testing of Cell 3 at near-optimum conditions, showed that the performance of this test cell was significantly better than the other cells possibly due to carbonate-cementation within the fines fraction. Another mechanism that possibly contributed to "stiffening" of the aggregate layer was: increased suction potentials. The winter freeze-thaw cycles could have resulted in the formation of new interconnected voids within the aggregate layer, leading to increased suction potentials. Note that the aggregate layer moisture contents after the freeze-thaw cycles were less than the as-constructed conditions (see Figure 8.31), and support the plausible mechanism of improved suction potential. No significant shear movement within the aggregate layer was observed, and

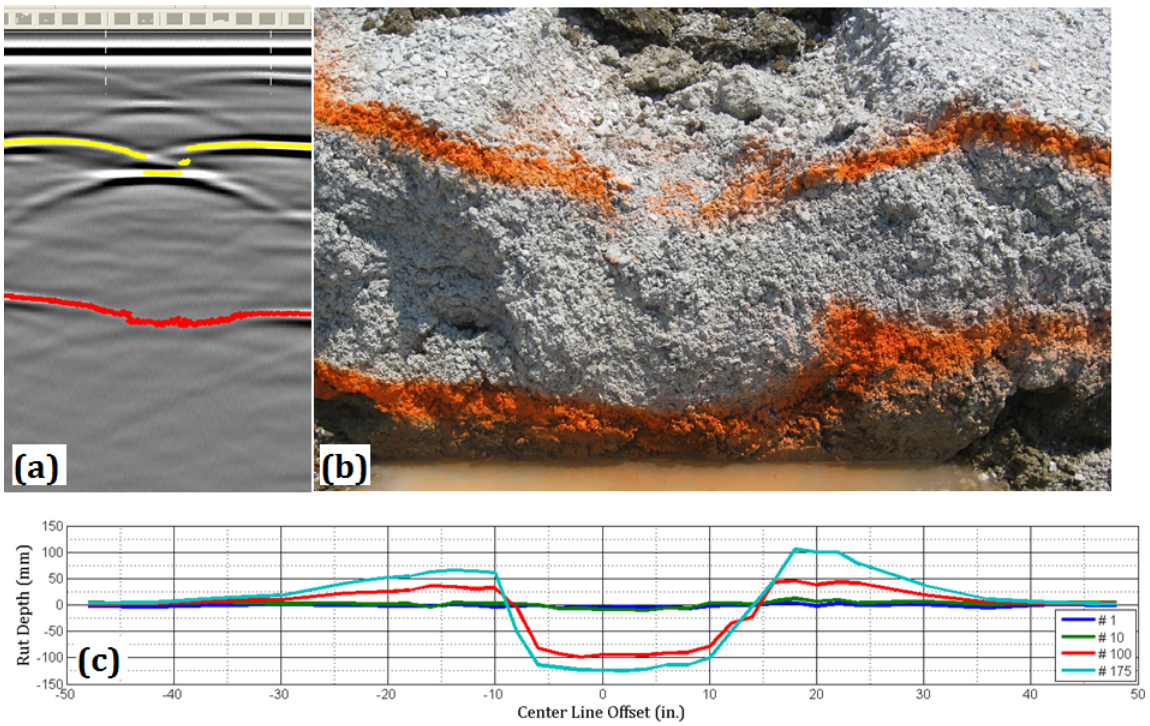


Figure 8.37: (a) GPR Scan, (b) Excavated Trench, and (c) Surface Rut Profile of the 203-mm Thick Crushed Dolomite Section in Cell 3 (1 in. = 25.4 mm)

subgrade rutting was the primary mechanism contributing to pavement failure.

### 8.7.2 Performance under Flooded Conditions

Subsequent to testing at near-optimum conditions, effect of excess moisture on performance of the crushed dolomite material with high fines was studied through accelerated pavement testing under flooded conditions. Figure 8.38 shows the development of rutting in the three test sections of Cell 3 under flooded conditions. As shown in the figure, no significant rutting was observed in the test sections up to 10 load applications. However upon further loading, the rutting in the sections became more apparent, with the 203-mm thick aggregate layer in Section 3 accumulating the most rutting. An important observation can be made regarding the "square" nature of the rut formations shown in Figure 8.38. Carbonate cementation of the fines fraction resulted in performance of the aggregate layer almost like a stiff bound layer showing punching failure due to penetration into the subgrade that was significantly weakened by flooding.

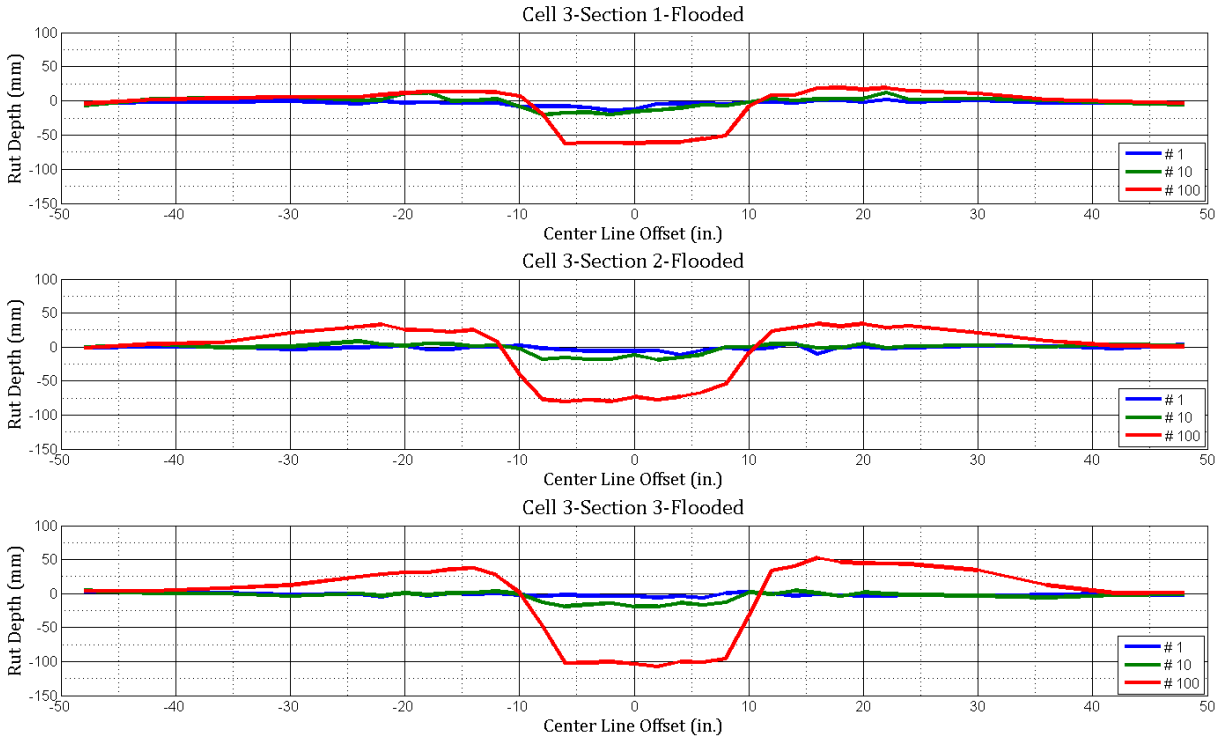


Figure 8.38: Rut Developments in Crushed Dolomite Sections in Cell 3 due to Unidirectional ATLAS Loading under Flooded Conditions (1 in. = 25.4 mm)

Figure 8.39 shows deformed layer boundaries as obtained from excavated transverse trenches in the three sections. Subgrade deformation and movement at the aggregate-subgrade interface became more apparent with decrease in the aggregate layer thickness. As observed in the case of other test cells, flooding of the test sections led to weakening of the subgrade, which failed by undergoing excessive deformation.

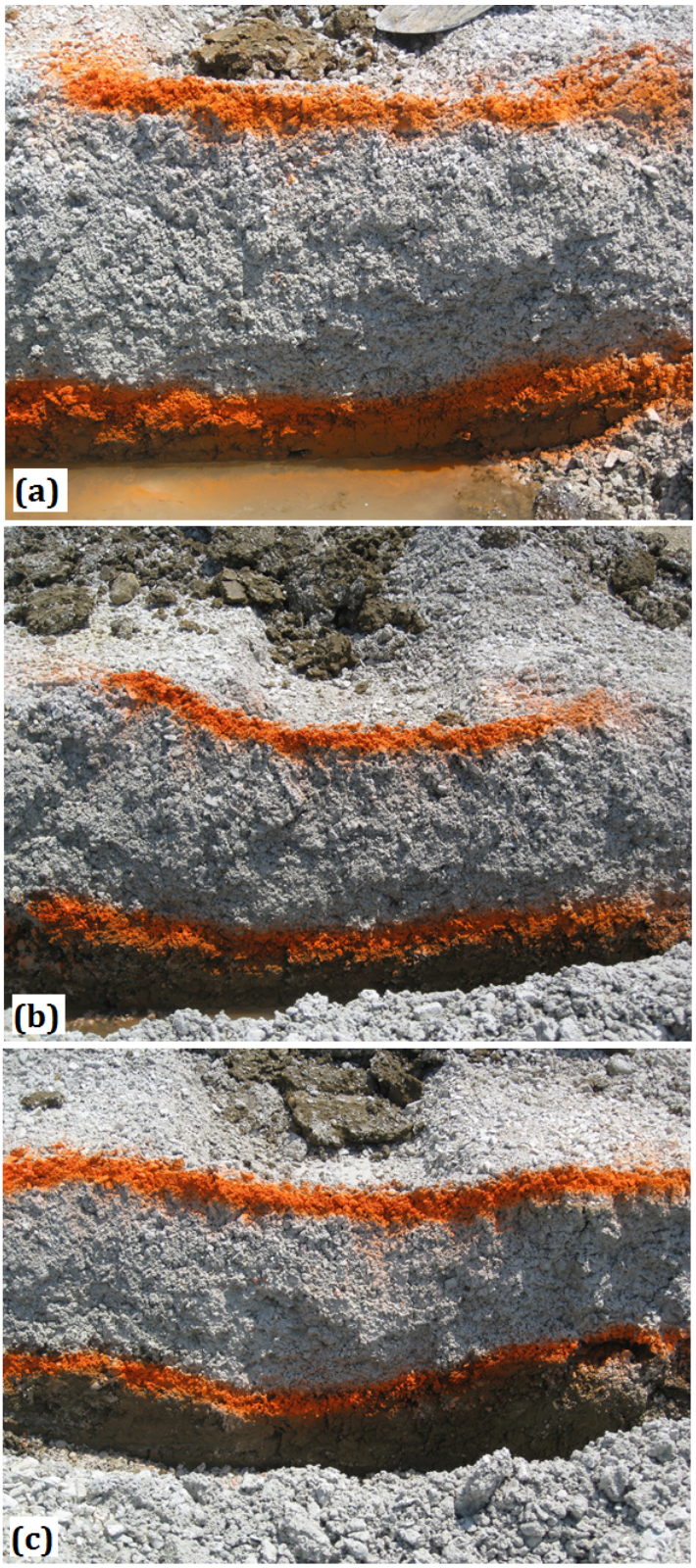


Figure 8.39: Excavated Trench Photos Showing Surface and Base-Subgrade Interface Deformations in Test Sections (a) 1, (b) 2, and (c) 3 due to Loading of Cell 3 under Flooded Conditions

## 8.8 Summary of Observations from Accelerated Testing of Full-Scale Unsurfaced Pavement Sections

This section summarizes the important observations from accelerated testing of the five unsurfaced pavement test cells constructed using different combinations of aggregate physical properties and subgrade conditions. Significant differences in aggregate qualities led to different mechanisms of rut-accumulation in the unsurfaced pavement sections under accelerated loading. For example, the uncrushed gravel in Cell 1 showed excessive shear movement within the aggregate layer, whereas the crushed aggregate sections in Cells 3, 4, and 5 failed primarily due to subgrade rutting. Table 8.2 lists the maximum rut depths (measured at the center of the wheel path) for all the test sections under near-optimum and flooded conditions after 1, 10, and 100 load applications to summarize the effects of aggregate material type and quality, as well as subgrade conditions on the performances of full-scale test sections.

Table 8.2: Maximum Rut Depths in the Full-Scale Unsurfaced Pavement Test Sections after 1, 10, and 100 Applications of Unidirectional ATLAS Loading

| Cell | Aggregate Layer Thickness (mm) | Rut Depth (mm) | | | | | |
|---|---|---|---|---|---|---|---|
| | | N = 1 | | N = 10 | | N = 100 | |
| | | Near-Optimum | Flooded | Near-Optimum | Flooded | Near Optimum | Flooded |
| 1 | 356 | 16.8 | 7.8 | 39.4 | 35.4 | N/A | N/A |
| | 305 | 7.4 | 14.4 | 22.1 | 50.6 | 66.2 | N/A |
| | 203 | 6.2 | 10.0 | 10.2 | 40.7 | 19.9 | N/A |
| 2 | 356 | 14.0 | 8.9 | 38.0 | 30.5 | N/A | N/A |
| | 305 | 11.7 | 9.3 | 30.8 | 29.7 | 92.6 | N/A |
| | 203 | 8.1 | 1.3 | 6.5 | 13.4 | 21.8 | N/A |
| 3 | 356 | 11.7 | 14.4 | 15.7 | 20.7 | 30.3 | 62.8 |
| | 305 | 8.3 | 11.8 | 16.0 | 18.8 | 55.6 | 80.6 |
| | 203 | 6.9 | 6.5 | 10.8 | 19.1 | 99.1 | 107.6 |
| 4 | 356 | -8.0* | 15.6 | 36.7 | 47.0 | 85.7 | 163.6** |
| | 305 | 2.5 | 13.9 | 31.5 | 19.1 | 101.1 | 75.1** |
| | 203 | 10.9 | 9.9 | 32.9 | 26.2 | 81.6 | 91.1** |
| 5 | 254 | 7.2 | 3.5 | 9.9 | 12.5 | 21.2 | 31.4 |
| | 203 | 7.8 | -0.3 | 13.2 | 7.2 | 32.9 | 30.4 |
| | 152 | 2.8 | 5.5 | 13.9 | 13.7 | 25.1 | 58.6 |

* No clear rutting was observed. The negative value indicates surface heave
** Surface profile measured after 97 load applications

As can be seen from Table 8.2, no consistent trend in the effects of material quality or moisture conditions on measured rut depths was observed after the first load application (N = 1). This was clearly evident from instances of higher rut depths under near-optimum aggregate moisture conditions compared to flooded conditions. This discrepancy was probably a result of particle rearrangement in the unbound aggregate surface layer under initial load applications. However, the effects of material quality and moisture conditions on performance became gradually apparent with an increase in the number of load applications. Note that due to internal shear movement of the aggregate layer under near-optimum moisture conditions, the 356-mm thick sections (Section 1) in Cells 1 and 2 could not be tested to 100 load applications. Similarly under flooded conditions, several test sections failed by accumulating rut amounts greater than 100 mm (4 in.) Rut depths corresponding to such sections have been listed as "N/A" in Table 8.2.

The crushed limestone material with low fines used in Cell 2 showed unstable matrix behavior under standard compaction conditions, leading to internal shear failure of Section 1 (356-mm thick aggregate layer) in Cell 2. However at higher relative compaction levels, the material showed adequate performance, and no significant shear movement within the aggregate layer was observed. Excessive subgrade deformation was the primary mechanism contributing to failure of pavement sections under such conditions.

The 203-mm thick aggregate sections of Cells 1 and 2 yielded 10.2 mm and 6.5 mm permanent deformations, respectively (see Table 8.2), after 10 load applications due to the much stronger subgrade CBR values achieved during construction (for Cell 1), and better compaction of aggregate layer (for Cell 2), respectively. Upon testing all sections to 100 load applications, the measured ruts often exceeded 50 mm (2 in.) with certain sections accumulating nearly 4-in. rutting. Therefore depending on the threshold rut-depth used to define pavement "failure", the test section "failed" after different number of load applications. However upon careful analyses of aggregate and subgrade layer construction conditions, as well as taking into account the laboratory aggregate test results, effects of different aggregate physical properties on construction platform performance could still be identified.

The effect of stronger subgrade conditions on unsurfaced pavement performance was clearly evident from the significantly higher number of load applications sustained by Cell 5 before

failure. For example, all three test sections in Cell 5 (target subgrade CBR = 6%) consistently accumulated lower rut amounts when compared to the other test cells after 100 load applications. This was a clear indication of improved performance due to better subgrade conditions. A comparison of the aggregate layer compaction information presented in Table 6.5 indicated that the test sections in Cells 2 and 5 (both constructed using material No. 2) were compacted to similar densities. However, the better subgrade conditions in Cell 5 (CBR = 6% compared to CBR = 3% for Cell 2) provided stronger "platforms" for compaction of the aggregate layers, which ultimately resulted in lower rut depths. Note that unlike the 356-mm thick aggregate layer in Cell 2, none of the layers in Cell 5 showed internal shear movement. For the same aggregate material type, stronger subgrade conditions consistently resulted in significantly improved test section performances. This could clearly be established by comparing the maximum rut depths for the test sections in Cells 2 (subgrade CBR = 3%) and 5 (subgrade IBV = 6%). For the stronger subgrade conditions in Cell 5, lower rut depths were observed even for sections with reduced aggregate layer thicknesses when compared to Cell 2.

Test Cell 3, constructed using a crushed dolomite material with high amounts of nonplastic fines was subjected to several over the winter effects i.e. freeze-thaw cycles which resulted in significant strength gain. Such strength gain was attributed to carbonate cementation of the fines fraction and improved suction characteristics due to the freeze-thaw cycles. The improved strength and modulus characteristics were apparent from the change in aggregate layer moduli measured using a GeoGauge™ before and after the freeze-thaw cycles (aggregate moduli increased by up to 225%), as well as by comparing the shear strength and permanent deformation behavior of similar aggregate specimens prepared in the laboratory at different moisture contents. The resulting stiffer aggregate layers sustained much higher number of load applications without undergoing significant rutting.

Test section failures under flooded conditions were primarily due to excessive shear movements observed in the subgrade layer. Ingress of moisture upon flooding significantly reduced the subgrade strength for all the test cells and ultimately caused more rapid subgrade deformations due to the applied unidirectional ATLAS loading.

## 8.9 Finite Element Analyses of Constructed Full-Scale Test Sections

Finite element analyses of the constructed full-scale test sections were conducted to identify the subgrade rutting potentials corresponding to the different aggregate material types and subgrade conditions. The finite element mesh shown in Figure 6.7 was used for this purpose. Subgrade properties for the individual test cells were assigned based on previous laboratory test results for the subgrade soil at the University of Illinois ATREL facility. Accordingly, the subgrade layer for Cells 1 through 4 (target CBR = 3%) was modeled using a constant modulus value of 31 MPa (4.5 ksi) and an unconfined compressive strength ($Q_u$) value of 158 kPa (23 psi). On the other hand, the subgrade for Cell 5 (target CBR = 6%) was assigned a constant modulus value of 62 MPa (9 ksi) and an unconfined compressive strength ($Q_u$) of 269 kPa (39 psi). To primarily focus on the effectiveness of different aggregate types in dissipating traffic-induced stresses and thus protecting the subgrade from excessive rutting, the test sections were modeled as an isotropic stress-dependent unbound aggregate layer placed over a subgrade of constant modulus. Resilient modulus model parameters for the aggregate layers were determined from laboratory testing of the four aggregate materials used for constructing the test sections. As in Section 6.4, the vertical compressive stresses at the subgrade interface were computed, and the corresponding Subgrade Stress Ratio (SSR) values were calculated as indicators of the subgrade rutting potential. Table 8.3 lists the subgrade vertical stress and the corresponding SSR values for the different constructed full-scale test sections.

Table 8.3: Subgrade Vertical Stress and Subgrade Stress Ratio (SSR) Values for Individual Full-Scale Test Sections from GT-PAVE Analyses

| Cell Number | Subgrade CBR (%) | Subgrade $Q_u$ (kPa) | Subgrade Modulus (MPa) | Subgrade Vertical Stress (kPa) / SSR | | |
|---|---|---|---|---|---|---|
| | | | | Section 1 | Section 2 | Section 3 |
| 1 | 3 | 158 | 31 | 113.1 / 0.71 | 131.0 / 0.83 | 207.5 / 1.31 |
| 2 | | | | 98.6 / 0.62 | 111.0 / 0.70 | 154.4 / 0.97 |
| 3 | | | | 89.6 / 0.57 | 105.5 / 0.67 | 183.4 / 1.16 |
| 4 | | | | 82.7 / 0.52 | 96.5 / 0.61 | 164.8 / 1.04 |
| 5 | 6 | 269 | 62 | 174.4 / 0.65 | 206.8 / 0.77 | 266.8 / 0.99 |

From Table 8.3, the SSR values for Sections 1 and 2 were in the acceptable range (∼0.6-0.7) for all five test cells, whereas the SSR values for Section 3 often exceeded unity (>1.0) representing subgrade shear failure. Therefore based on the principle of subgrade protection, only Section 3

(thinnest aggregate cover) of each test cell should have undergone significant rutting, with all the other test sections performing adequately for at least 500 load applications [43]. However as discussed in the preceding sections, most of the test sections failed by accumulating approximately 100-mm rutting after significantly lower number of load applications. This was primarily a result of different mechanisms contributing to failure of the test sections depending on the aggregate material quality and subgrade conditions. Note that due to differences in achieved compaction levels of the constructed aggregate layers and other field variabilities, performances of the test sections were often different from those predicted from the GT-PAVE analyses. For example, due to better laboratory-measured resilient modulus values for the crushed limestone material used in Cell 4 compared to the crushed dolomite material used in Cell 3, the predicted subgrade stress levels corresponding to Cell 3 were consistently higher than those for Cell 4. However as reported in this chapter, the test sections in Cell 3 performed significantly better than those in Cell 4 due to apparent strength gain by the crushed dolomite material with high fines upon exposure to the freeze-thaw cycles. This emphasized the difficulty associated with getting consistent results from modeling and accelerated testing of full-scale pavement sections. This difficulty becomes even more magnified for unsurfaced pavements due to inherent variabilities associated with the compaction levels, and construction conditions of the unbound aggregate layers. Although finite element analyses of the full-scale test sections presented reasonable indications regarding the subgrade rutting potentials associated with individual test sections, it did not present any indications regarding different mechanisms possibly contributing towards failure of the pavement sections. It is important to note that commonly used pavement analysis programs often consider only the recoverable (elastic) components of pavement layer deformations. As unsurfaced pavement performance under loading often involves large deformations representing plastic material flow, modeling such pavement systems using "plasticity theory" may give better indications regarding shear flow within the aggregate layers. Such advanced modeling of unsurfaced pavement systems is beyond the scope of this PhD research.

## 8.10 Discussions and Recommendations

Based on results from laboratory testing of aggregates as well as accelerated testing of full-scale unsurfaced pavement sections, several recommendations are presented in this section regarding the material selection and construction practices for unsurfaced pavements. Due to different

mechanisms as well as factors contributing to the high permanent deformation accumulations in the test sections, merely increasing/decreasing or adjusting the aggregate cover layer thicknesses to account for aggregate material quality may not be the most efficient approach to ensure adequate performance of unsurfaced pavements. For example, an uncrushed gravel material with high amounts of fines will not perform satisfactorily in the field even though its layer thickness is increased. This is because such poor quality aggregate cover material will tend to internally fail due to low shear resistance and a much thicker layer of this failing material will not prevent excessive rut accumulation observed on the surface. Similarly, wet of optimum construction conditions are expected to produce excessive permanent deformations. Accordingly, thicker gravel layer constructed in wet (or flooded) conditions will not necessarily outperform a 356-mm (14-in.) thick gravel layer with high amounts of fines. In fact, they will both fail due to excessive internal shear movement. In summary, merely adjusting the constructed aggregate layer thicknesses to account for aggregate material quality may not represent the best approach for ensuring adequate performance of unsurfaced pavements. Although the detrimental effects of some of the factors studied in this research project on aggregate performance were clearly apparent from the laboratory test results, not all hypotheses drawn from the laboratory testing could be verified through accelerated pavement testing. Accordingly, based on the laboratory and field test results, the current research study recommends the following guidelines for material selection and construction practices to ensure adequate performance of unsurfaced pavements.

### 8.10.1 Aggregate Type

Both laboratory as well as field test results indicated aggregate angularity to be the most important factor governing aggregate layer behavior. Therefore, the current research findings warrant caution on the use of uncrushed gravel (irrespective of the fines content) for unsurfaced pavement applications. Although the current research study evaluated the performance of an uncrushed gravel material with high amounts of nonplastic fines, Heckel [140] studied the performance of an uncrushed gravel material with moderate amounts ($\sim$ 7%) of plastic fines. From monitoring the performance of several test sections under controlled loading, he reported significantly poor performance for the uncrushed gravel material compared to crushed aggregates [140].

The uncrushed gravel material tested in this research study (Cell 1) exhibited significant shear movement within the aggregate layer. Therefore, subgrade deformation was not the primary factor contributing to pavement failure under such conditions. Moreover, lack of adequate compaction was not believed to be the reason behind inadequate performance of the uncrushed gravel test sections. This was based on the observation that the uncrushed gravel material accumulated significantly higher amounts of permanent deformation in the laboratory compared to the crushed aggregates, even under modified (ASTM D 1557) compaction conditions. Heckel [140] suggested the use of uncrushed gravel as a capping layer over large size aggregates (e.g. primary crusher run). However, as the performance of uncrushed gravel in capping layer applications was not evaluated during this PhD research, the current study does not have sufficient information to validate/contradict the adequacy of uncrushed gravel layer performance in such applications.

Both the laboratory and field test results from the two phases of this research project highlighted the importance of fines content (material finer than 0.075 mm or passing No. 200 sieve) for ensuring stability of a crushed aggregate matrix. At very low fines contents (often around 4%), the crushed aggregate particles tend to move with respect to each other, resulting in a less stable matrix for higher permanent deformations that can ultimately lead to shear failure. This was particularly evident for the crushed limestone with $\sim 5\%$ fines used in Cells 2 and 5, which showed unstable matrix behavior under standard compaction conditions. Although improved test section performances were observed under higher relative compaction levels, it is important to note that such high compaction levels may not be easy to achieve over weak subgrade conditions. Therefore, careful attention should be paid to the minimum amount of fines required in a crushed aggregate material for use in pavement applications. For example, current Illinois Department of Transportation (IDOT) specifications prescribe fines contents between 4% and 12% for aggregate materials satisfying a typical dense-graded aggregate (CA-6) specification. However based on the laboratory and field test results, it is recommended that the minimum amount of fines required for crushed aggregates be increased to 6% from the currently specified value of 4%. As uncrushed aggregate matrices often comprise lower amount of voids compared to crushed aggregates, stability of the aggregate matrix can potentially be achieved at lower fines contents. Therefore, the current lower limit of 4% may be retained for uncrushed aggregate materials. However note that due to inadequate performance of uncrushed gravel aggregates in

the laboratory as well as in the field, the current research findings warrant caution on its use for unsurfaced pavement applications.

### 8.10.2 Compactive Effort

The level of relative compaction or compactive effort was found to have a significant effect on the performance of full-scale aggregate sections tested under accelerated loading. For example, a 3% difference in the achieved relative compaction levels with respect to laboratory determined maximum dry densities was found to have a significant effect on the failure mechanism of the test sections in Cell 2. It is therefore recommended that all unsurfaced pavement sections be compacted to at least 95% of the laboratory determined maximum dry densities under standard compactive effort. Achieving adequate compaction levels is particularly important for crushed aggregate materials with low amounts of fines. Due to insufficient packing of the voids by fines, such aggregate types may exhibit unstable matrix behavior unless compacted to very high densities. In cases where weak subgrade conditions limit aggregate compaction levels, discing, or tilling of the subgrade layer should be performed to achieve uniform distribution of the subgrade moisture.

### 8.10.3 Effect of Moisture Conditions

Although slight moisture increases beyond optimum moisture content were found to have a significant effect on the performance of aggregate specimens in the laboratory (as discussed in Chapters 4 and 5), field sections when tested under flooded (saturated) conditions primarily failed from excessive subgrade deformations. This was attributed to the ingress of excessive moisture into the subgrade leading to its significant weakening. In such cases, the aggregate layer thickness played a secondary role as far as governing pavement performance was concerned. Therefore, increasing the aggregate layer thickness may not be effective in ensuring adequate performance under flooded conditions. As unsurfaced pavement performance under flooded conditions is primarily governed by subgrade strength, changing the aggregate layer thickness by 2-3 inches will not necessarily ensure adequate performance. It is therefore recommended that sufficient time be allowed for the aggregate layers to dry in the event of rain before subjecting the unsurfaced pavement sections to traffic loading. However, as closing in-service low volume roads to traffic may not be feasible, installation of subsurface drainage systems is strongly

recommended to quickly remove excessive moisture from the aggregate and subgrade layers. Moreover, controlling the moisture content of the aggregate layer during placement is also likely to help especially for aggregate materials with high fines contents. Both laboratory and field testing indicated that excessive moisture conditions had a more severe effect on aggregate materials with high fines compared to those with low or moderate amount of fines.

# CHAPTER 9

# CONCLUSIONS & RECOMMENDATIONS FOR FUTURE RESEARCH

## 9.1 Research Framework

This thesis research evaluated the effects of different aggregate physical properties on the response and performance of unsurfaced pavement systems through laboratory experimentation and accelerated loading of full-scale test section. Extensive review of technical literature identified the following physical properties (test factors) as critical in governing aggregate behavior in pavement layers: particle shape, texture and angularity, fines content (material passing No. 200 sieve, or finer than 0.075 mm), type of fines (nonplastic or plastic based on the Plasticity Index measured on material finer than 0.425 mm), and compaction (moisture-density) conditions. Particle size distribution or gradation was used as the primary control parameter for comparing individual effects of the test factors on aggregate behavior.

Three different aggregate types, namely crushed limestone, crushed dolomite and uncrushed gravel, commonly used in the state of Illinois for pavement applications were selected for laboratory experimentation and construction of the full-scale unsurfaced pavement test sections. A factorial laboratory test matrix was developed by assigning different values to individual test factors within pre-determined ranges. Aggregate behavior at different test factor combinations was then studied through the following laboratory tests: standard compaction moisture-density, unsoaked California Bearing Ratio (CBR), monotonic triaxial testing for rapid shear strength, and repeated load triaxial testing for permanent deformation and directional modulus characteristics.

Important findings from laboratory characterization of the aggregates at different test factor combinations served as the basis for material selection and thickness design of full-scale unsurfaced pavement sections for accelerated testing. Five different test "cells" were constructed at different combinations of aggregate quality and engineered subgrade strength, and were tested

to failure using an Accelerated Transportation Loading Assembly (ATLAS) at near-optimum and flooded aggregate moisture conditions. Test section performances under simulated traffic loading were monitored through surface profile measurements after different number of load applications. Earth pressure cells were installed on top of the subgrade at the aggregate-subgrade interface to measure the vertical subgrade stress levels under loading and evaluate the effect of aggregate material type and quality on subgrade rutting potential. Transverse scanning of the test sections with Ground-Penetrating Radar (GPR) was also pursued to identify the development of subsurface deformations and to differentiate between subgrade and aggregate rutting. Subsequently, visual confirmation of layer interface deformations were obtained through excavation of transverse trenches across the test sections. Non-destructive field modulus measurements using light weight deflectometer (LWD) and Soil Stiffness Gauge (GeoGauge™) type devices were performed on the compacted subgrade as well as aggregate layers to identify construction anomalies, and to evaluate the applicability these techniques for pavement performance prediction based on material quality.

## 9.2 Summary of Findings

Significant findings from this research study are summarized below:

- Particle shape and angularity played the most important role in governing aggregate behavior irrespective of other physical properties. Crushed aggregates showed consistently higher shear strength, modulus, and lower susceptibility to permanent deformations when compared to the uncrushed "river-run" gravel.
- An aggregate matrix comprising crushed particles exhibited higher tolerance to the amount of fines and showed lower moisture sensitivity even at high fines contents. For nonplastic fines, the variation in shear strength (CBR used as shear strength index) with moisture content was erratic and did not indicate any significant trends at low fines contents. However at higher fines contents, the effect of moisture was significant and caused a rapid reduction in shear strength values. High moisture contents combined with high amounts of plastic fines presented the worst combination and rapidly deteriorated aggregate matrix conditions.
- The effect of fines type (nonplastic or plastic) was not significant for aggregate matrices

comprising low amount of fines. However, as the amount of fines in a matrix was increased, specimens with plastic fines clearly showed poor performance compared to those with nonplastic fines.

- Individual effects of test factors were found to be significantly dependent on other test factor levels. For example, the effect of moisture on aggregate behavior changed significantly depending on the amount of fines in the aggregate matrix. Similarly, the type of fines (plastic or nonplastic) affected aggregate behavior significantly only for materials comprising high amounts of fines. Therefore, aggregate specifications currently used by transportation agencies need to be modified to consider the effect of the fines plasticity and set different threshold limits for nonplastic and plastic fines as far as maximum allowable fines content in an aggregate matrix is concerned.

- Permanent deformation test results clearly identified the importance of fines in an aggregate matrix. Crushed aggregate specimens with low fines contents (around 4%) showed unstable behavior compared to the ones with moderate amount (around 8%) of fines. This behavior was attributed to the higher amounts of voids in the aggregate matrix comprising crushed particles. At low fines contents, the aggregate particles moved and reoriented with respect to each other thus resulting in higher permanent deformations and lower resilient modulus values. As the fines content increased to around 8%, a larger proportion of voids in the aggregate matrix were filled by the fines and a "stable" matrix behavior was observed. The uncrushed gravel matrix did not show any such stabilizing behavior due to the low amount of voids in an aggregate matrix comprising uncrushed particles. Based on these findings, different threshold values for the allowable fines content in an aggregate material were proposed for crushed and uncrushed aggregates. The allowable fines content for crushed aggregates should be set around 8%, whereas the value for uncrushed gravel should be around 6%. It is also important to note that crushed aggregate matrices showed higher tolerance to variations in fines content compared to uncrushed ones.

- Slight variations in test factor values did not reflect clearly on the resilient modulus behavior of aggregates. For example, increasing the amount of fines by 4% did not result in significant changes in aggregate modulus values. However, large variations induced in the fines content (increase from 4% to 16%) was often reflected as a significant reduction in

resilient modulus values. Crushed aggregates showed consistently higher modulus values compared to uncrushed ones due to better particle to particle interlock.

- Anisotropic modulus ratios (defined as the ratio of horizontal to vertical resilient modulus values) adequately identified significant differences in aggregate material quality. Anisotropic modulus ratios for "good quality" materials typically showed increasing trends with increasing deviator stress levels, and the horizontal moduli were consistently lower than vertical moduli.

- Finite Element analyses of unsurfaced pavement sections highlighted the importance of considering both the resilient modulus and permanent deformation characteristics of aggregates together during material selection for satisfactory mechanistic response and rutting performance in unsurfaced pavement applications. Although the aggregate resilient modulus values (and hence subgrade rutting potential) did not change significantly with different aggregate physical property combinations, the permanent deformation trends clearly captured the effects of aggregate material quality. This is particularly important for unsurfaced pavement applications, as a thick layer of "poor" quality material may undergo internal shear failure.

- Effects of individual aggregate physical properties on resilient modulus and permanent deformation model parameters were evaluated through statistical Analyses of Variance (ANOVA). Although the results showed varying levels of influence of individual aggregate physical properties on modulus and permanent deformation model parameters, aggregates with a stable matrix, i.e. not all the voids filled with fines, demonstrated improved behavior in terms of both resilient modulus and permanent deformation trends.

- Field modulus measurements using LWD and GeoGauge™ successfully identified anomalies in construction conditions, i.e. increasing or decreasing trends in subgrade strength, aggregate compaction levels, etc. However, direct comparison of the modulus values reported by the two devices did not yield any definitive conclusions. GeoGauge™ measured modulus values showed in general a decreasing trend with increasing moisture contents. However, the effects of dry density and material quality, associated with aggregate type and properties, were not reflected from the field modulus values. In that sense, the field modulus values could not be associated with the laboratory-measured modulus properties, which

properly captured not only stress dependencies but also the effects of aggregate angularity and fines content.

- Significant differences in aggregate qualities led to different mechanisms of rut-accumulation in the unsurfaced pavement sections under accelerated pavement testing. Uncrushed gravel layers in Cell 1 showed excessive internal shear movement, whereas the crushed aggregate sections in Cells 3, 4, and 5 failed primarily due to subgrade rutting. The crushed limestone material with low fines used in Cells 2 and 5 showed unstable matrix behavior under standard compaction conditions. The resulting particle reorientation led to internal shear failure of the 356-mm aggregate layer in Cell 2. However, at higher relative compaction levels, the material showed adequate performance, and no significant shear movement within the aggregate layer was observed.

- Earth pressure cells installed on top of the subgrade at the aggregate-subgrade interface helped identify different mechanisms contributing towards failure of the test sections under loading. Out of a total of 10 earth pressure cells installed in the full-scale test sections, only four survived the construction process, and successfully recorded the traffic-induced vertical stress levels on top of the subgrade. Field-measured subgrade stress levels in Section 2 of Cell 1 indicated significant movement of the uncrushed gravel aggregate layer. This was clearly evident from the consistent increase in measured subgrade stress levels with number of load applications. Higher compaction levels and stronger subgrade conditions (primarily due to nonuniform moisture distribution during subgrade preparation) in Section 3 of Cell 1 resulted in no significant material movement reflected by no apparent increase in the measured subgrade vertical stress levels with number of load applications. Similarly for the crushed limestone material with low amounts of fines Cell 2, field-measured subgrade stress values highlighted the importance of adequate compaction to achieve better stress dissipation with depth.

- Finite element analyses of the uncrushed gravel test sections in Cell 1 indicated the importance of considering compaction and stress-induced cross-anisotropy in unbound aggregate layers; close agreement between the predicted and field-measured subgrade vertical stress levels was achieved upon consideration of the stress-dependent nature of subgrade modulus as well as cross-anisotropy of the aggregate layer.

- The effect of stronger subgrade conditions on unsurfaced pavement performance was clearly evident from the significantly higher number of load applications sustained by Cell 5, which was constructed over an engineered subgrade with CBR of 6%. Although constructed using the same aggregate material as Cell 2, the aggregate sections in Cell 5 did not exhibit significant shear movement due to better confinement provided by the stronger subgrade conditions.

- Cell 3, constructed using a crushed dolomite material with high amounts of nonplastic fines, was subjected to several freeze-thaw cycles during the winter, and demonstrated significant strength gain possibly due to the combined action of carbonate cementation of fines as well as suction effects at lower moisture contents. This strength gain resulted in significantly higher number of load applications that this particular test cell could sustain without undergoing shear failure. Transverse trench sections excavated across the wheel paths showed a basin-shaped subgrade deformed profile, which is characteristic of subgrade deflections under bound pavement layers. Significant increase in the aggregate layer stiffness probably due to the combined action of carbonate cementation and suction effects were clearly reflected from the field moduli measured using GeoGauge™ after the freeze-thaw cycles (aggregate moduli increased by up to 225%).

- An innovative application of the nondestructive Ground-Penetrating Radar (GPR) technology was established for assessing subsurface deformations and distinguishing between the different rut mechanisms contributing to unsurfaced pavement failure. A thin aluminum strip foil was placed at the aggregate-subgrade interface to serve as a pure reflector of GPR waves and identify the layer boundaries. Comparison of GPR scans and excavated trench sections for the rutting mechanisms and failure patterns of the full-scale unsurfaced pavement test sections proved the effectiveness of transverse GPR scanning for monitoring rut accumulations in unsurfaced pavement structures.

- Failure of the test sections under flooded conditions was primarily due to excessive shear movement of the subgrade layer. Ingress of additional moisture upon flooding significantly reduced the subgrade strength for all the test cells, which ultimately failed the weaker subgrade under the ATLAS traffic loading.

- As different mechanisms contributed to failure of the unsurfaced pavement test sections

depending on aggregate material type and quality as well as subgrade conditions, changing the constructed aggregate layer thickness to account for variations in aggregate material quality was not the best approach to ensure adequate pavement performance. Accordingly based on the laboratory and field-test results, several guidelines were presented for material selection and construction practices to facilitate the design and construction of better performing unsurfaced pavements and construction platforms.

## 9.3 Recommendations for Future Research

Based on findings from the current research study, the following recommendations are made for future research activities:

- Evaluate the effects of aggregate physical properties on permanent deformation behavior using the shakedown theory through laboratory testing at different stress ratios (defined as the ratio of applied stress to material shear strength). Such test results can be used to identify threshold values for aggregate properties corresponding to response in shakedown ranges A, B, and C [15].
- Use laboratory permanent deformation tests conducted at different stress states to develop transfer functions for relating laboratory and field rut development.
- Use of GPR scanning for quantitative estimation of aggregate and subgrade layer deformations in unsurfaced pavements using the "extended common mid-point method" [136].
- Backcalculation of aggregate and subgrade layer moduli from light weight deflectometer (LWD) data collected with a three-sensor configuration; and develop correction factors to predict field moduli from laboratory resilient modulus test results for different aggregate types.
- Use the field rutting data along with aggregate and subgrade strength parameters to evaluate the adequacy of bearing-capacity based design methods for unsurfaced pavement structures constructed with different aggregate types.
- Investigate carbonate cementation as a means of dissolution and precipitation effects in

crushed limestone and dolomite materials with high fines, and quantify the resulting increase in strength and modulus characteristics.

- Investigate the changes in suction potentials of crushed limestone and dolomite materials at different fines contents and the effects of repeated freeze-thaw cycles on strength and modulus characteristics.

# REFERENCES


[1] Y. H. Huang. *Pavement Analysis and Design*. Prentice Hall, Upper Saddle River, NJ, 2nd edition, 2004.

[2] A. T. Papagiannakis and E. A. Masad. *Pavement Design and Materials*. John Wiley & Sons, Inc., 1st edition, 2008.

[3] P. R. Donovan. *Analysis of Unbound Aggregate Layer Deformation Behavior From Full Scale Aircraft Gear Loading with Wander*. PhD Thesis, University of Illinois at Urbana-Champaign, Urbana, Illinois, 2009.

[4] K. Skorseth and A. A. Selim. *Gravel Roads: Maintenance and Design Manual*. South Dakota Local Transportation Assistance Program (SD LTAP), Federal Highway Administration, 2000.

[5] A. R. Dawson and P. Kolisoja. *Permanent Deformation: ROADEX II Final Report*. Roadscanners, Rovaniemi, Finland, 2005.

[6] *Subgrade Stability Manual*. Bureau of Bridges and Structures, Illinois Department of Transportation, 2005.

[7] E. Tutumluer, D. Mishra, and A. A. Butt. Characterization of Illinois Aggregates for Subgrade Replacement and Subbase. Technical Report ICT-R-27-1, Illinois Center for Transportation, University of Illinois at Urbana-Champaign, 2009.

[8] R. D. Barksdale, editor. *The Aggregate Handbook*. National Stone Association, Washington, D.C., 1991.

[9] F. Lekarp, U. Isacsson, and A. R. Dawson. State of the Art. I: Resilient Response of Unbound Aggregates. *Journal of Transportation Engineering, ASCE*, 126(1):66–75, 2000.

[10] B. N. Jorenby and R. G. Hicks. Base Course Contamination Limits. *Transportation Research Record: Journal of the Transportation Research Board*, 1095:86–101, 1986.

[11] J. Allen. *The Effect of Non-Constant Lateral Pressures on the Resilient Response of Granular Materials*. PhD Thesis, University of Illinois at Urbana-Champaign, Urbana, Illinois, 1973.

[12] M. R. Thompson and K. Smith. Repeated Triaxial Characterization of Granular Materials. *Transportation Research Record: Journal of the Transportation Research Board*, 1278:7–17, 1990.

[13] ASTM D698-07: Standard Test Methods for Laboratory Compaction Characteristics of Soil Using Standard Effort (12400 ft-lbf/ft$^3$ (600 kN-m/m$^3$)). In *ASTM Annual Book of Standards*. ASTM International, 2011.

[14] ASTM D1557-09: Laboratory Compaction Characteristics of Soil Using Modified Effort (56,000 ft-lbf/ft$^3$ (2700 kN-m/m$^3$)). In *ASTM Annual Book of Standards*. ASTM International, 2011.

[15] S. Werkmeister. *Permanent Deformation Behaviour of Unbound Granular Materials in Pavement Constructions*. PhD Thesis, Dresden University of Technology, Dresden, Germany, 2003.

[16] E. Tutumluer. *CEE 509: Transportation Soils Lecture Notes*. Department of Civil and Environmental Engineering, University of Illinois at Urbana-Chamapign, 2010.

[17] R. G. Hicks and C. L. Monismith. Factors Influencing the Resilient Properties of Granular Materials. *Transportation Research Record: Journal of the Transportation Research Board*, 345:15–31, 1971.

[18] G. Rada and M. W. Witczak. Comprehensive Evaluation of Laboratory Resilient Moduli Results for Granular Material. *Transportation Research Record: Journal of the Transportation Research Board*, 810:23–33, 1981.

[19] J. Uzan. Characterization of Granular Materials. *Transportation Research Record: Journal of the Transportation Research Board*, 1022:52–59, 1985.

[20] R. W. May and M. W. Witczak. Effective Granular Modulus to Model Pavement Responses. *Transportation Research Record: Journal of the Transportation Research Board*, 810:1–9, 1981.

[21] E. Tutumluer. *Predicting Behaviour of Flexible Pavements with Granular Bases*. PhD Thesis, Georgia Institute of Technology, Atlanta, Georgia, 1995.

[22] M. W. Witczak and J. Uzan. *The Universal Aiport Pavement Design System Report I of V: Granular Material Characterization*. University of Maryland, Department of Civil Engineering, 1988.

[23] M. Kim and E. Tutumluer. Validation of a Three-Dimensional Finite Element Model using Airfield Pavement Multiple Wheel Load Responses. *Road materials and pavement design*, 11(2):387–408, 2010.

[24] *NCHRP1-37 A. Development of the Mechanistic-Empirical Design Guide of New and Rehabilitated Pavement Structures*. 2004.

[25] A. Yau and H.L. Von Quintus. Study of LTPP Laboratory Resilient Modulus Test Data and Response Characteristics. Technical Report FHWA-RD-02-051, Office of Infrastructure Research and Development, Federal Highway Administration, 2002.

[26] H. L. Theyse. *The Development of Mechanistic-Empirical Permanent Subgrade Deformation Models from Heavy Vehicle Simulator Data*. MS Thesis, University of Johannesburg, Johannesburg, Republic of South Africa, 2001.

[27] I. T. Kim. *Permanent Deformation Behavior of Airport Flexible Pavement Base and Subbase Courses*. PhD Thesis, University of Illinois at Urbana-Champaign, Urbana, Illinois, 2005.

[28] R. Sharp. *Shakedown Analyses and the Design of Pavement Under Moving Surface Load*. PhD Thesis, University of Sydney, New South Wales, Australia, 1983.

[29] R. W. Sharp and J. R. Booker. Shakedown of Pavements under Moving Surface Loads. *Journal of Transportation Engineering*, 110(1):1–14, 1984.

[30] J. H. Maree. *Design Parameters for Crushed Stone in Pavements*. MS Thesis, University of Pretoria, South Africa, 1978.

[31] S. Werkmeister, A. R. Dawson, and F. Wellner. Permanent Deformation Behavior of Granular Materials and the Shakedown Concept. *Transportation Research Record: Journal of the Transportation Research Board*, 1757:75–81, 2001.

[32] H. L. Theyse. *A Mechanistic-Empirical Design Model for Unbound Granular Pavement Layers*. PhD Thesis, University of Johannesburg, Johannesburg, Republic of South Africa, 2007.

[33] M. Boulbibane, D. Weichert, and L. Raad. Numerical Application of Shakedown Theory to Pavements with Anisotropic Layer Properties. *Transportation Research Record: Journal of the Transportation Research Board*, 1687:75–81, 1999.

[34] R. D. Barksdale. Laboratory Evaluation of Rutting in Base Course Materials. In *Proceedings of the 3rd International Conference on Structural Design of Asphalt Pavements*, pages 161–174, 1972.

[35] C. L. Monismith, N. Ogawa, and C. R. Freeme. Permanent Deformation Characteristics of Subgrade Soils Due to Repeated Loading. *Transportation Research Record: Journal of the Transportation Research Board*, 537:1–17, 1975.

[36] M. R. Thompson and D. Nauman. Rutting Rate Analyses of the AASHO Road Test Flexible Pavements. *Transportation Research Record: Journal of the Transportation Research Board*, 1384:36–48, 1993.

[37] H. Wolff. *Elasto-Plastic Behavior of Granular Pavement Layers in South Africa*. PhD Thesis, University of Pretoria, Pretoria, Republic of South Africa, 1992.

[38] A. A. Van Niekerk and M. Huurman. Establishing Complex Behavior of Unbound Road Building Materials from Simple Material Testing. Technical Report No. 7-95-200-16, Delft University of Technology, Delft, 1995.

[39] M. Huurman. *Permanent Deformation in Concrete Block Pavements*. PhD Thesis, Delft University of Technology, Delft, Netherlands, 1997.

[40] O. J. Porter. Foundations for Flexible Pavements. In *Highway Research Board Proceedings*, volume 22, pages 100–143, 1942.

[41] E. H. Davis. The California Bearing Ratio Method for the Design of Flexible Roads and Runways. *Geotechnique*, 1(3):249–263, 1949.

[42] G. W. Jameson. Origins of AUSTROADS Design Procedures for Granular Pavements. Technical Report ARR 292, ARRB Transport Research Ltd., Victoria, Australia, 1996.

[43] M. R. Thompson, T. C. Kinney, M. L. Traylor, J. R. Bullard, and J. L. Figueroa. *Subgrade Stability: Final Report, Project IHR-605.* Illinois Cooperative Highway and Transportation Research Program, Department of Civil Engineering, University of Illinois at Urbana-Champaign, Urbana, Illinois, 1977.

[44] M. W. Frost, P. R. Fleming, and C. D. F. Rogers. Assessment of Performance Specific Approach for Pavement Foundations. *Transportation Research Record: Journal of the Transportation Research Board*, 1757:100–108, 2001.

[45] *Design Manual for Roads and Bridges.* HD 25/94 Pavement Design and Maintenance-Foundations (DMRB 7.2.2), 1994.

[46] G. Garcia and M. R. Thompson. Working Platform Requirements for Pavement Construction. Technical Report A White Paper Prepared for the Technical Review Panel, Project IHR-R30, "Upgrade Subgrade Stability Manual", 2003.

[47] P. R. Flemming, C. D. F. Rogers, and M. W. Frost. Performance Parameter and Target Values for Construction of UNITED KINGDOM Road Foundations. In *Proceedings of Fifth International Conference on the Bearing Capacity of Roads and Airfields*, 1998.

[48] *Interim Advice Note 73/06 Revision 1 (2009): Design Guidance for Road Pavement Foundations (Draft HD25).* Department of Transport, London, UK, 2009.

[49] Austroads. Pavement Design - A Guide to the Structural Design of Road Pavements. Technical report, Austroads, Sydney, Australia, 2004.

[50] S. Y. Oloo, D. G. Fredlund, and J. K-M Gan. Bearing Capacity of Unpaved Roads. *Canadian Geotechnical Journal*, 34(3):398–407, 1997.

[51] S. Y. Oloo. *A Bearing Capacity Approach to the Design of Low-Volume Traffic Roads.* PhD Thesis, University of Saskatchewan, Saskatoon, Canada, 1994.

[52] N. W. McLeod. Some Basic Problems in Flexible Pavement Design. In *Highway Research Record Proceedings*, volume 32, pages 90–118, 1953.

[53] N. W. McLeod. The Ultimate Strength Approach to Flexible Pavement Design. In *Proceedings of The Association of Asphalt Paving Technologists*, volume 23, 1954.

[54] B. B. Broms. The Bearing Capacity of Pavements Subjected to Frost Action. *Highway Research Record*, 39:66–180, 1963.

[55] B. B. Broms. The Effect of Degree of Saturation on the Bearing Capacity of Flexible Pavements. *Highway Research Record*, 71:1–14, 1964.

[56] G. W. E. Milligan, R. A. Jewell, G. T. Houlsby, and H. J. Burd. A New Approach to the Design of Unpaved Roads, Part I. *Ground Engineering*, 22(3):25–29, 1989.

[57] D. A. Bender and E. J. Barenberg. Design and Behavior of Soil-Fabric-Aggregate Systems. *Transportation Research Record: Journal of the Transportation Research Board*, 671:64–75, 1978.

[58] J. P. Giroud and L. Noiray. Geotextile-Reinforced Unpaved Road Design. *Journal of the Geotechnical Engineering Division, ASCE*, 107(GT9):1233–1254, 1981.

[59] A. R. Dawson, P. Kolisoja, N. Vuorimies, and T. Saarenketo. Design of Low-Volume Pavements Against Rutting: Simplified Approach. *Transportation Research Record: Journal of the Transportation Research Board*, 1989:165–172, 2007.

[60] J. E. Gray. Characteristics of Graded Base Course Aggregates Determined by Triaxial Tests. *Engineering Research Bulletin No. 12*, 1962.

[61] M. A. Kamal, A. R. Dawson, O. T. Farouki, D. A. B. Hughes, and A. A. Sha'at. Field and Laboratory Evauation of the Mechanical Behavior of Unbound Granular Materials in Pavements. *Transportation Research Record: Journal of the Transportation Research Board*, 1406:88–97, 1993.

[62] R. D. Barksdale and S. Y. Itani. Influence of Aggregate Shape on Base Behavior. *Transportation Research Record: Journal of the Transportation Research Board*, 1227:173–182, 1989.

[63] A. R. Dawson, N. H. Thom, and J. L. Paute. Mechanical Characteristics of Unbound Granular Materials as a Function of Condition. In *Proceedings of European Symposium Euroflex 1993*, pages 35–44. Balkema, 1996.

[64] N. H. Thom and S. F. Brown. The Effect of Grading and Density on the Mechanical Properties of a Crushed Dolomitic Limestone. In *Proceedings of the 14th ARRB Conference, Part 7*, pages 94–100, 1988.

[65] J. J. Allen and M. R. Thompson. Resilient Response of Granular Materials Subjected to Time Dependent Lateral Stresses. *Transportation Research Record: Journal of the Transportation Research Board*, 510:1–13, 1974.

[66] N.H. Thom. *Design of Road Foundations*. PhD Thesis, University of Nottingham, 1988.

[67] N. Thom and S. Brown. The Mechanical Properties of Unbound Aggregates from Various Sources. In *Proceedings of the Third International Symposium on Unbound Aggregates in Roads, UNBAR3*, pages 130–142, 1989.

[68] C. Rao, E. Tutumluer, and I. T. Kim. Quantification of Coarse Aggregate Angularity Based on Image Analysis. *Transportation Research Record: Journal of the Transportation Research Board*, 1787:117–124, 2002.

[69] T. Pan, E. Tutumluer, and S. H. Carpenter. Effect of Coarse Aggregate Morphology on Resilient Modulus of Hot Mix Asphalt. *Transportation Research Record: Journal of the Transportation Research Board*, 1929:1–9, 2005.

[70] E. Tutumluer and T. Pan. Aggregate Morphology Affecting Strength and Permanent Deformation Behavior of Unbound Aggregate Materials. *Journal of Materials in Civil Engineering*, 20(9):617–627, 2008.

[71] U. Seyhan. *Characterization of Anisotropic Granular Layer Behavior in Flexible Pavements*. PhD Thesis, University of Illinois at Urbana-Champaign, Urbana, Illinois, 2001.

[72] R. M. Knutson and M. R. Thompson. Resilient Response of Railway Ballast. *Transportation Research Record: Journal of the Transportation Research Board*, 651:31–39, 1977.

[73] R. P. Elliot and S. I. Thornton. Resilient Modulus and AASHTO Pavement Design. *Transportation Research Record: Journal of the Transportation Research Board*, 1196:116–124, 1988.

[74] M. A. Rowshanzamir. *Resilient Cross Anisotropic Behavior of Granular Base Materials Under Repeatitive Loading*. PhD Thesis, University of New South Wales, Australia, 1995.

[75] E. Tutumluer and U. Seyhan. Neural Network Modeling of Anisotropic Aggregate Behavior from Repeated Load Triaxial Tests. *Transportation Research Record: Journal of the Transportation Research Board*, 1615:86–93, 1998.

[76] A. A. Van Niekerk. *Mechanical Behavior and Performance of Granular Bases and Sub-Bases in Pavements*. PhD Thesis, Delft Technological University, Delft, The Netherlands, 2002.

[77] I. Holubec. Cyclic Creep of Granular Materials. Technical Report No. RR147, Department of Highways, Ontario, Canada, 1969.

[78] M. R. Thompson and Q. L. Robnett. Resilient Properties of Subgrade Soils. *Transportation Engineering Journal, ASCE*, 105(1):71–89, 1979.

[79] B. J. Dempsey. Laboratory and Field Studies of Channeling and Pumping. *Transportation Research Record: Journal of the Transportation Research Board*, 849:1–12, 1982.

[80] N. H. Thom and S. F. Brown. Effect of Moisture on the Structural Performance of a Crushed-Limestone Road Base. *Transportation Research Record: Journal of the Transportation Research Board*, 1121:50–56, 1987.

[81] J. H. Maree, C. R. Freeme, N. J. Van Zyl, and P. F. Savage. The Permanent Deformation of Pavements with Untreated Crushed Stone Bases as Measured in Heavy Vehicle Simulator Tests. In *Proceedings of the 11th ARRB Conference, Part 2*, pages 16–28, 1982.

[82] E. Tutumluer, C. Rao, and J. A. Stefanski. Video Image Analysis of Aggregates. Technical Report FHWA-IL-UI-278, Civil Engineering Studies UILU-ENG-2000-2015, University of Illinois at Urbana-Champaign, Urbana, Illinois, 2000.

[83] C. Rao. *Development of 3-D Image Analysis Techniques to Determine Shape and Size Properties of Coarse Aggregates*. PhD Thesis, University of Illinois at Urbana-Champaign, Urbana, Illinois, 2001.

[84] C. Rao, E. Tutumluer, and J. A. Stefanski. Flat and Elongated Ratios and Gradation of Coarse Aggregates Using a New Image Analyzer. *ASTM Journal of Testing and Standard*, 29(5):79–89, 2001.

[85] C. Rao, T. Pan, and E. Tutumluer. Determination of Coarse Aggregate Surface Texture Using Image Analysis. In *Proceedings of the Pavement Mechanics Symposium at the 16th ASCE Engineering Mechanics Division Conference (EM2003)*, Seattle, Washington, 2003.

[86] T. Pan, E. Tutumluer, and S. H. Carpenter. Imaging Based Evaluation of Coarse Aggregate Used in the NCAT Pavement Test Track Asphalt Mixes. In *Proceedings of the 1st International Conference on Design and Construction of Long Lasting Asphalt Pavements*, Auburn, Alabama, 2004.

[87] E. Tutumluer, T. Pan, and S. H. Carpenter. Investigation of Aggregate Shape Effects on Hot Mix Asphalt Performance Using an Image Analysis Approach. Technical Report Pooled Fund Study TPF-5(023), UILU-ENG-2005-2003, Federal Highway Administration IL Division, University of Illinois, Urbana, 2005.

[88] N. Garg and M. R. Thompson. Triaxial Characterization of Minnesota Road Research Project Granular Materials. *Transportation Research Record: Journal of the Transportation Research Board*, 1577:27–36, 1997.

[89] A. Saeed, J. W. Hall, and W. Barker. *NCHRP Report 453: Performance-Related Tests of Aggregates for Use in Unbound Pavement Layers*. Transportation Research Board, National Research Council, Washington, DC, 2001.

[90] AASHTO T 307-99 (R 2007): Standard Method of Test for Determining the Resilient Modulus of Soils and Aggregate Materials. In *Standard Specifications for Transportation Materials and Methods of Sampling and Testing, 30th Edition*. AASHTO - American Association of State Highway and Transportation Officials, 2010.

[91] U. Seyhan and E. Tutumluer. Anisotropic Modular Ratios as Unbound Aggregate Performance Indicators. *Journal of Materials in Civil Engineering, ASCE*, 14(5):409–416, 2002.

[92] E. Tutumluer and U. Seyhan. Effects of Fines Content on the Anisotropic Response and Characterization of Unbound Aggregate Bases. In A.R. Dawson, editor, *Unbound Aggregates in Road Construction, Proceedings of the Unbound Aggregates in Roads (UNBAR5) Symposium*, pages 153–161, University of Nottingham, UK, 2000. A. A. Balkema.

[93] ASTM D 1883-07: Standard Test Method for CBR (California Bearing Ratio) of Laboratory-Compacted Soils. In *ASTM Annual Book of Standards*. ASTM International, 2011.

[94] *AASHTO Guide for Design of Pavement Structures* . American Association of State Highway and Transportation Officials, Washington, D.C., 1986.

[95] E. Tutumluer and U. Seyhan. Laboratory Determination of Anisotropic Aggregate Resilient Moduli using an Innovative Test Device. *Transportation Research Record: Journal of the Transportation Research Board*, 1687:13–21, 1999.

[96] O. Pekcan, E. Tutumluer, and M. R. Thompson. Nondestructive Pavement Evaluation using Illi-Pave Based Artificial Neural Network Models. Technical Report FHWA-ICT-08-022, A Report of the Findings of ICT-R39-2, Illinois Center for Transportation, University of Illinois at Urbana-Champaign, Urbana, Illinois, 2008.

[97] N. Garg. *Mechanistic-Empirical Evaluation of the Mn/Road Low-Volume Road Test Sections*. PhD Thesis, University of Illinois at Urbana-Champaign, Urbana, Illinois, 1997.

[98] E. Tutumluer and R. D. Barksdale. Behavior of pavements with granular basesprediction and performance. In *Proceedings of the UNBAR4 Symposium, Nottingham, UK*, pages 173–183. Nottingham, UK, 1995.

[99] ASTM D 2487-10: Standard Practice for Classification of Soils for Engineering Purposes (Unified Soil Classification System). In *ASTM Annual Book of Standards*. ASTM International, 2011.

[100] AASHTO M 145-1991 (R 2008): Standard Specification for Classification of Soils and Soil-Aggregate Mixtures for Highway Construction Purposes. In *Standard Specifications for Transportation Materials and Methods of Sampling and Testing, 30th Edition*. AASHTO - American Association of State Highway and Transportation Officials, 2010.

[101] E. Kleyne, J. Maree, and P. Savage. The Application of a Portable Pavement Dynamic Cone Penetrometer to Determine in Situ Bearing Properties of Road Pavement Layers and Subgrades in South Africa. In *Proceedings of the 2nd European Symposium on Penetration Testing, Amsterdam*, volume 1, pages 272–282. National Institute for Transport and Road Research, 1982.

[102] C. T. Senseney and M. A. Mooney. Characterization of two-layer soil system using a lightweight deflectometer with radial sensors. *Transportation Research Record: Journal of the Transportation Research Board*, 2186:21–28, 2010.

[103] C. Gros. *Use of a Portable Falling Weight Deflectometer;" Loadman"*. Oulun yliopisto, 1993.

[104] W. Kudla, R. Floss, and C. Trautmann. Dynamic Plate Compression Test-Rapid Testing Method for Quality Assurance of Unbound Course. *Autobahn*, 42(2), 1991.

[105] C. D. F. Rogers, A. J. Brown, and P. R. Fleming. Elastic stiffness measurement of pavement foundation layers. In *Proceedings of the 4th International Symposium on Unbound Aggregates in Roads (UNBAR4)*, pages 271–280, 1995.

[106] Carl Bro Pavement Consultants Website. http://www.carlbro.dk/prima100, December 2010.

[107] P. R. Flemming, M. W. Frost, and C. D. F. Rogers. A Comparision of Devices for Measuring Stiffness In-Situ. In *Unbound Aggregates in Road Construction, Proceedings of the Unbound Aggregates in Roads (UNBAR5) Symposium*, pages 193–200. A. A. Balkema, Rotterdam, Netherlands, 2000.

[108] M. A. Mooney and P. K. Miller. Analysis of Lightweight Deflectometer Test Based on In Situ Stress and Strain Response. *Journal of Geotechnical and Geoenvironmental Engineering*, 135(2):199–208, 2009.

[109] K. P. George. *Portable FWD (Prima 100) for In-situ Subgrade Evaluation*. Mississippi Dept. of Transportation Research Division, and University of Mississippi Dept. of Civil Engineering, and Portland Cement Association, 2006.

[110] M. W. Frost, P. R. Fleming, M. Gordon, and J. P. Edwards. Pavement Foundation Stiffness Testing: a New Regime. In *Transport (Proceedings of the ICE)*, volume 163. © Thomas Telford.

[111] D. J. White, P. K. R. Vennapusa, and M. J. Thompson. Field Validation of Intelligent Compaction Monitoring Technology for Unbound Materials. Technical Report MN/RC-2007-10, Center for Transportation Research and Education, Iowa State University, 2007.

[112] P. R. Fleming, M. W. Frost, and J. P. Lambert. Lightweight Deflectometers for Quality Assurance in Road Construction. In *Bearing Capacity of Roads, Railways and Airfields. Proceedings of the 8th International BCR2A'09 Conference*, pages 809–818, 2009.

[113] P. R. Fleming, M. W. Frost, and J. P. Lambert. Review of Lightweight Deflectometer for Routine In Situ Assessment of Pavement Material Stiffness. *Transportation Research Record: Journal of the Transportation Research Board*, 2004:80–87, 2007.

[114] Dynatest International. *Dynatest 3031 LWD: Light Weight Deflectometer, Owner's Manual, Version 1.0.1.* 2009.

[115] Humboldt Mfg. Co. *GeoGauge User Guide: Model H-4140 Soil Stiffness/Modulus Gauge, Version 4.1.* 2007.

[116] A. Sawangsuriya. *Evaluation of the Soil Stiffness Gauge.* M.S. Thesis, University of Wisconsin at Madison, Madison, Wisconsin, 2001.

[117] E. Ekrem. *Laboratory Evaluation of In-Situ Tests as Potential Quality Control/Quality Assurance Tools.* MS Thesis, Louisiana State University, Baton Rouge, Louisiana, 2003.

[118] N. Ryden and M.A. Mooney. Analysis of Surface Waves from the Light Weight Deflectometer. *Soil Dynamics and Earthquake Engineering*, 29(7):1134–1142, 2009.

[119] H. L. Von Quintus, C. Rao, R. E. Minchin, S. Nazarian, K. R. Maser, and B. Prowell. *NCHRP Report 626: NDT Technology for Quality Assurance of HMA Pavement Construction.* Transportation Research Board, National Research Council, Washington, D.C., 2009.

[120] M. Nazzal. *Field Evaluation of In-Situ Test Technology for QC/QA Procedures During Construction of Pavement Layers and Embankments.* MS Thesis, Louisiana State University, Baton Rouge, Louisiana, 2003.

[121] M. D. Nazzal, M. Y. Abu-Farsakh, K. Alshibli, and L. Mohammad. Evaluating the Light Falling Weight Deflectometer Device for In Situ Measurement of Elastic Modulus of Pavement Layers. *Transportation Research Record: Journal of the Transportation Research Board*, 2016:13–22, 2007.

[122] K. Black and P. Kopac. The Application of Ground-Penetrating Radar in Highway Engineering. *Public Roads*, 56(3):96–103, 1992.

[123] I. L. Al-Qadi, S. Lahouar, and A. Loulizi. Successful Application of Ground-Penetrating Radar for Quality Assurance-Quality Control of New Pavements. *Transportation Research Record: Journal of the Transportation Research Board*, 1861:86–97, 2003.

[124] I. L. Al-Qadi, S. Lahouar, K. Jiang, K. K. McGhee, and D. Mokarem. Accuracy of Ground-Penetrating Radar for Estimating Rigid and Flexible Pavement Layer Thicknesses. *Transportation Research Record: Journal of the Transportation Research Board*, 1940:69–78, 2005.

[125] I. L. Al-Qadi and S. Lahouar. Measuring Layer Thicknesses with GPR-Theory to Practice. *Construction and Building Materials*, 19(10):763–772, 2005.

[126] K. R. Maser, T. J. Holland, R. Roverts, and J. Popovics. NDE Methods for Quality Assurance of New Pavement Thickness. *International Journal of Pavement Engineering*, 7(1):1–10, 2006.

[127] A. Loizos and C. Plati. Accuracy of Pavement Thicknesses Estimation using Different Ground-Penetrating Radar Analysis Approaches. *NDT&E International*, 40(2):147–157, 2007.

[128] T. Saarenketo and T. Scullion. Ground Penetrating Radar Applications on Roads and Highways. Technical Report 1923-2F, Texas Transportation Institute, College Station, Texas, United States, 1994.

[129] D. H. Chen and T. Sucllion. Detecting Subsurface Voids using Ground-Coupled Penetrating Radar. *Geotechnical Testing Journal*, 31(3):217–224, 2008.

[130] I. L. Al-Qadi and S. Lahouar. Measuring Rebar Cover Depth in Rigid Pavements with Ground-Penetrating Radar. *Transportation Research Record: Journal of the Transportation Research Board*, 1907:81–85, 2005.

[131] *Design Manual for Roads and Bridges, Vol. 7, Section 3, Part 2: HD29/94 Structural Assessment Methods, Chapter 6 Ground Radar.* Department of Transport, London, UK, 2001.

[132] Z. Leng, I. L. Al-Qadi, and S. Lahouar. Development and Validation for in-Situ Asphalt Mixture Density Prediction Model. *NDT&E International*, 44(4):369–375, 2011.

[133] I. L. Al-Qadi, Z. Leng, S. Lahouar, and J. Baek. In-Place Hot-Mix Asphalt Density Estimation using Ground-Penetrating Radar. *Transportation Research Record: Journal of the Transportation Research Board*, 2152:19–27, 2010.

[134] M. Silvast. *Air Void Content Measurement using GPR Technology at Helsinki-Vantaa Airport: Runway No. 3. Survey Report.* Roadscanners, Rovaniemi, Finland, 2001.

[135] Z. Leng, I. L. Al-Qadi, and S. Lahouar. Selection of Antenna Type and Frequency for Pavement Survesy using Ground-Penetrating Radar (GPR). *TRB 88th Annual Meeting Compendium of Papers DVD*, 2009.

[136] Z. Leng. *Prediction of In-Situ Asphalt Mixture Density Using Ground-Penetraing Radar:Theoretical Development and Field Validation.* Ph.d. dissertation, University of Illinois at Urbana-Champaign, Urbana, Illinois, 2011.

[137] E. Tutumluer and J. Kwon. Validations of Anisotropic Aggregate Base Behavior from Full-Scale Tests. In *ASCE Geotechnical Special Publication No. 187: Contemporary Topics in Gound Modification, Problem Soils, and Geo-Support*, pages 441–448, 2009.

[138] R. E. Graves. *Strength Developed from Carbonate Cementation in Silica/Carbonate Systems As Influenced by Cement-Particle Mineralogy.* MS Thesis, University of Florida, Gainsville, Florida, 1987.

[139] R. E. Graves, J. L. Eades, and L. L. Smith. Strength Developed from Carbonate Cementation in Silica/Carbonate Base Course Materials. *Transportation Research Record: Journal of the Transportation Research Board*, 1190:24–30, 1988.

[140] G. Heckel. Aggregate Subgrade Thickness Determination. Technical Report Final Report: Experimental Features Project IL 03-01, Illinois Department of Transportation, Bureau of Materials and Physical Research, Springfield, Illinois, 2009.

# APPENDIX A

# PARTICLE SIZE DISTRIBUTION OF AGGREGATES TESTED IN THE LABORATORY

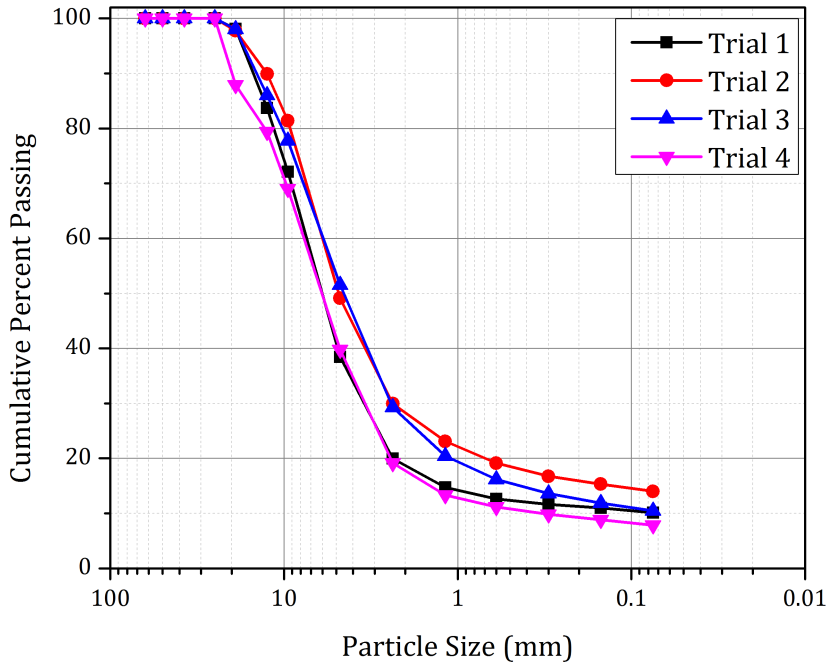


Figure A.1: As-Received Gradation of Crushed Dolomite tested in the Laboratory

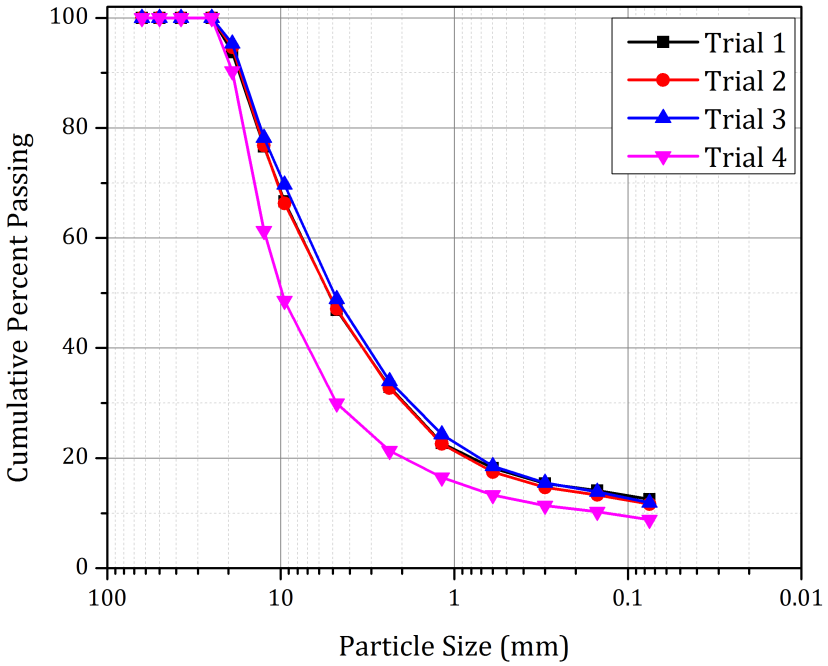


Figure A.2: As-Received Gradation of Crushed Limestone tested in the Laboratory

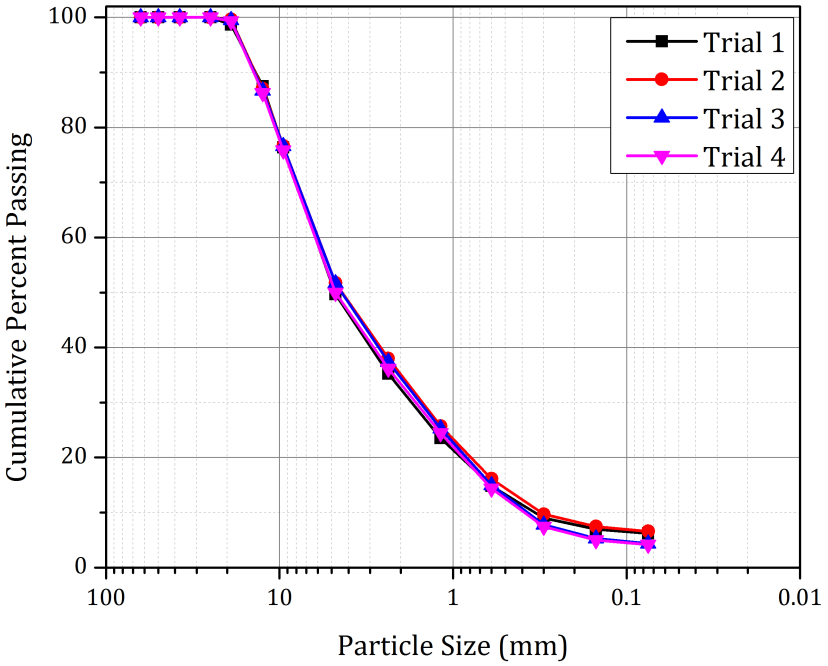


Figure A.3: As-Received Gradation of Uncrushed Gravel tested in the Laboratory

# APPENDIX B

# CHARACTERIZATION OF AGGREGATES USED IN FIELD SECTIONS

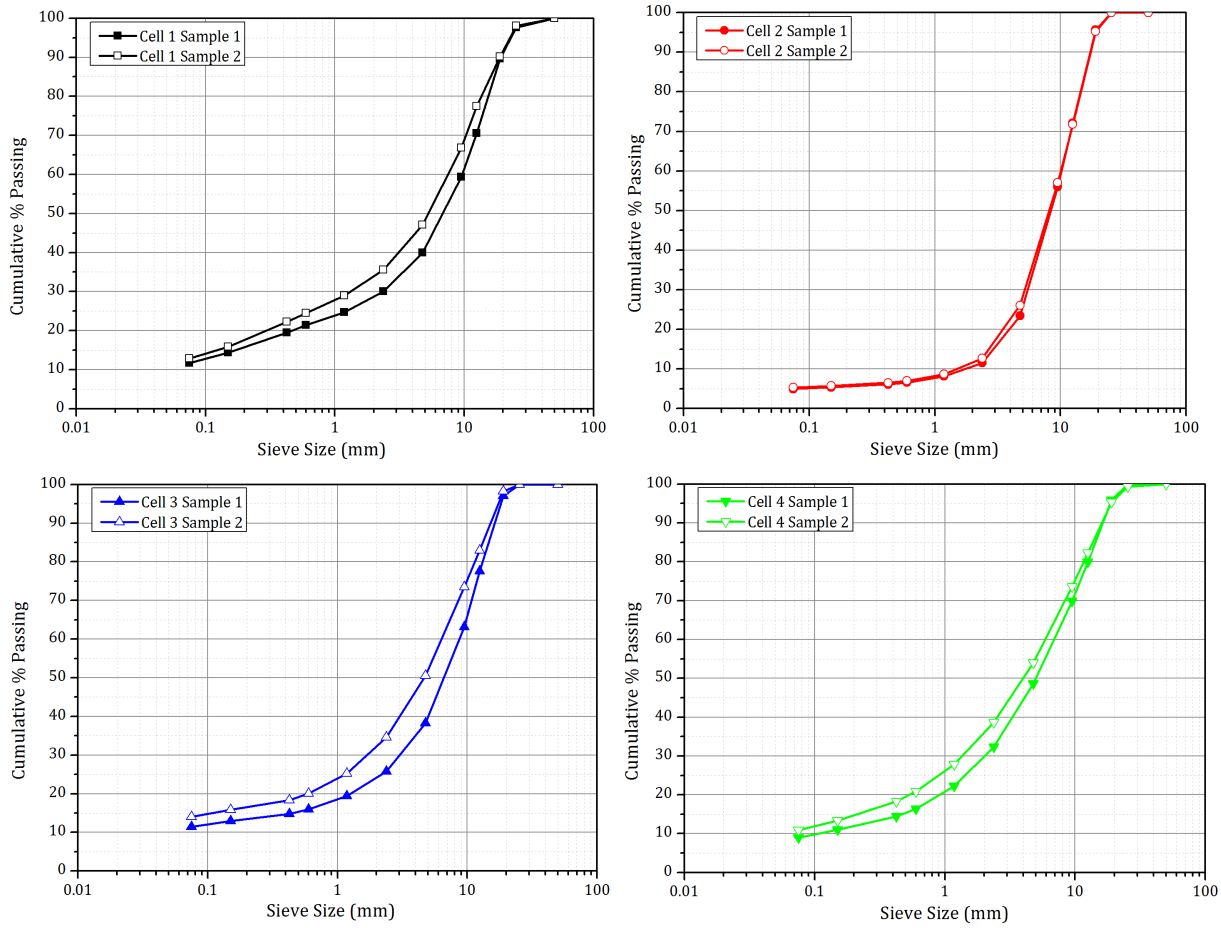


Figure B.1: Particle Size Distribution of the Four Aggregate Materials used in Construction of the Full-Scale Test Sections

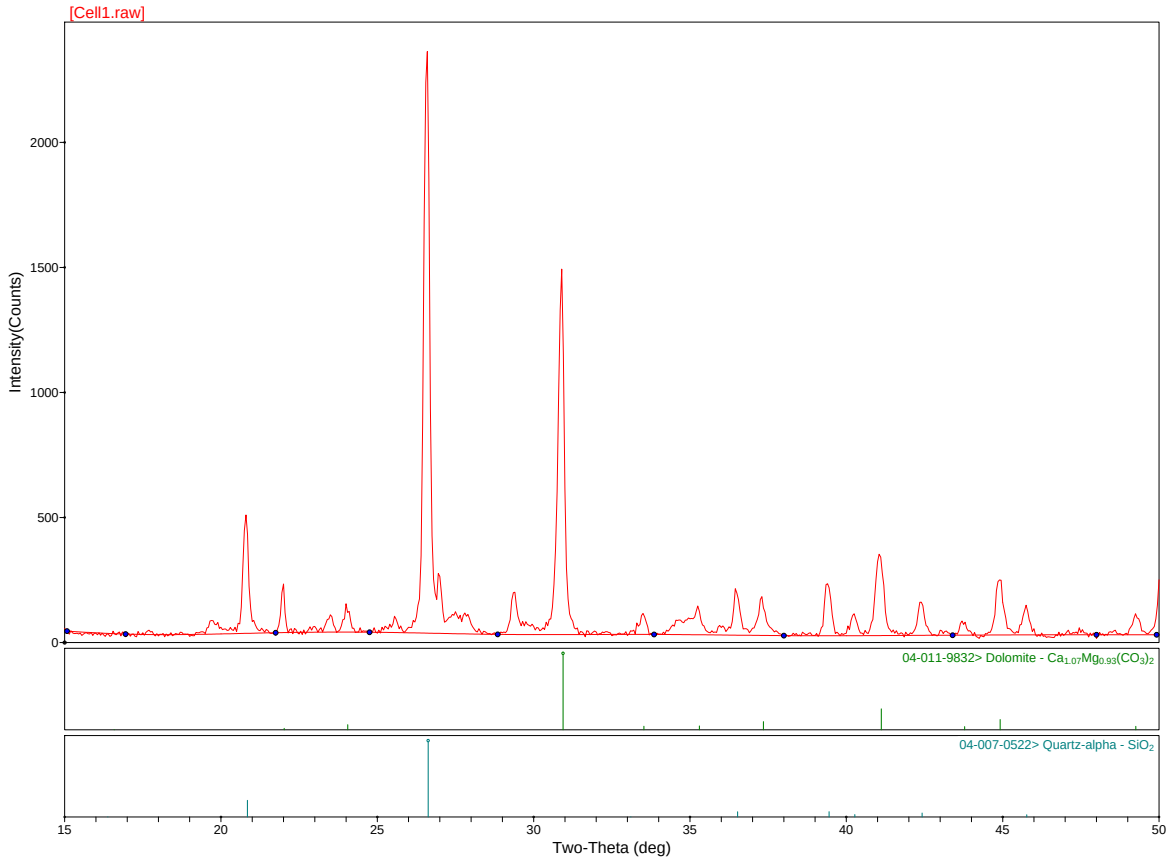


Figure B.2: X-Ray Diffraction (XRD) Results for the Uncrushed Gravel Aggregate Material (Material No. 1)

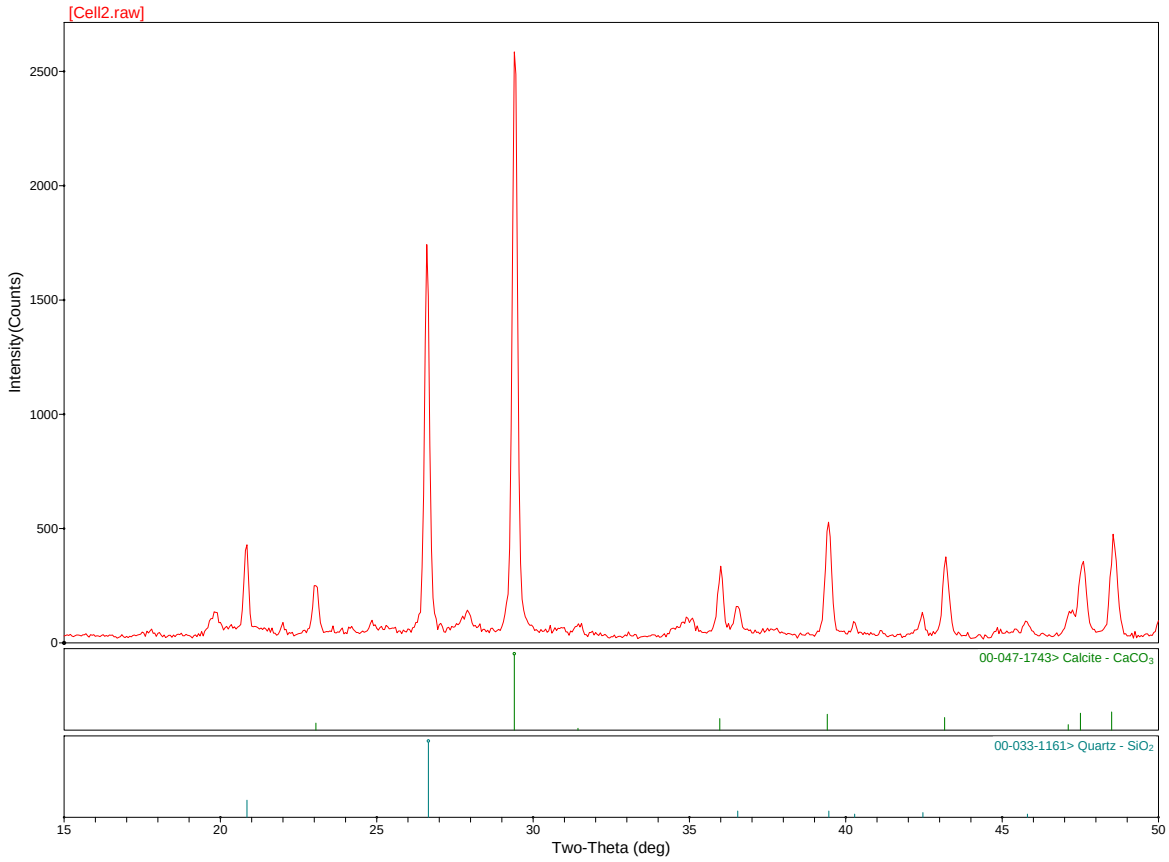


Figure B.3: X-Ray Diffraction (XRD) Results for the Crushed Limestone Aggregate Material (Material No. 2)

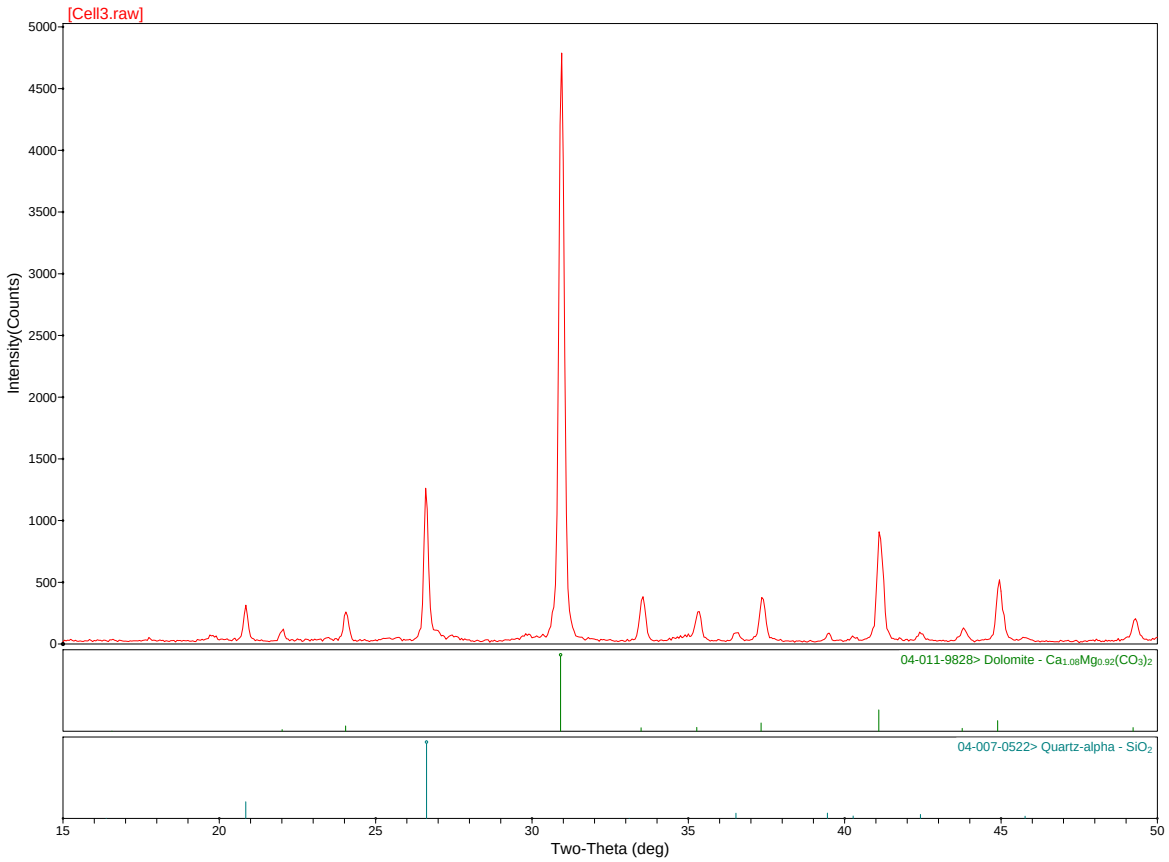


Figure B.4: X-Ray Diffraction (XRD) Results for the Crushed Dolomite Aggregate Material (Material No. 3)

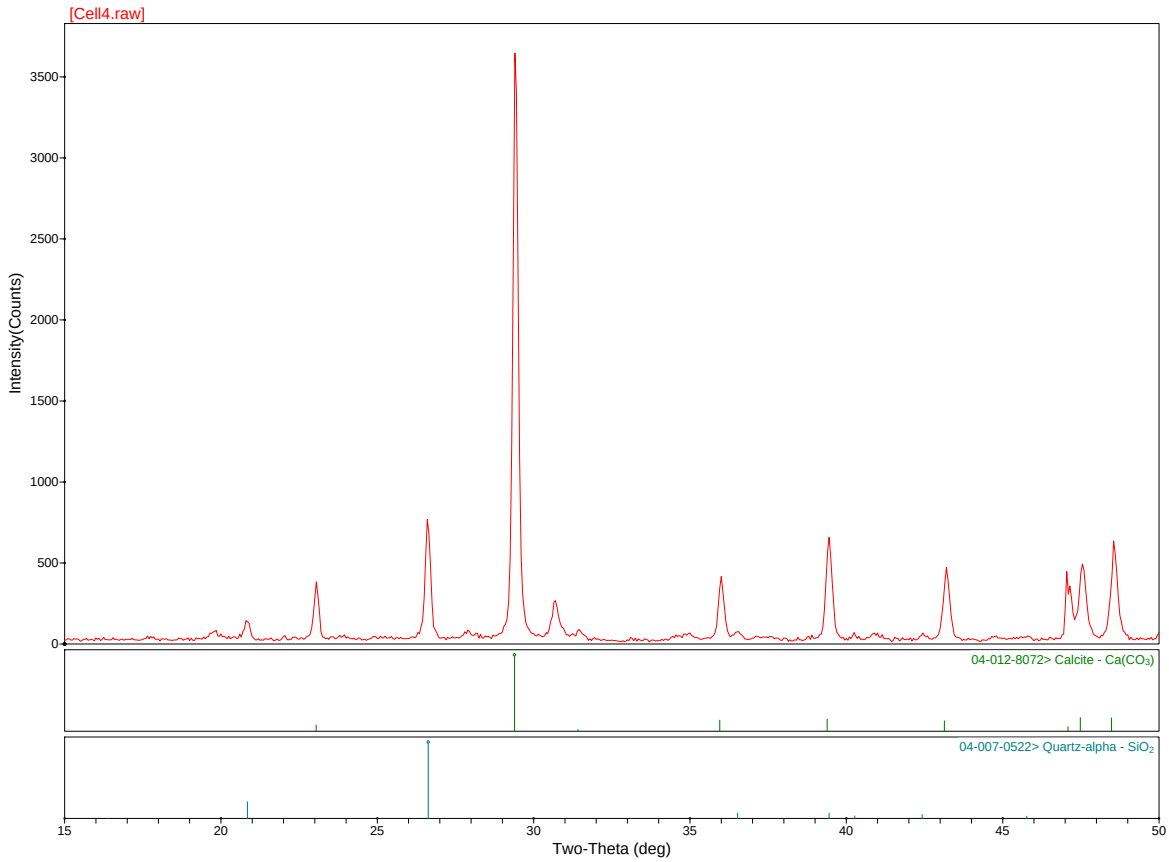


Figure B.5: X-Ray Diffraction (XRD) Results for the Crushed Limestone Aggregate Material (Material No. 4)

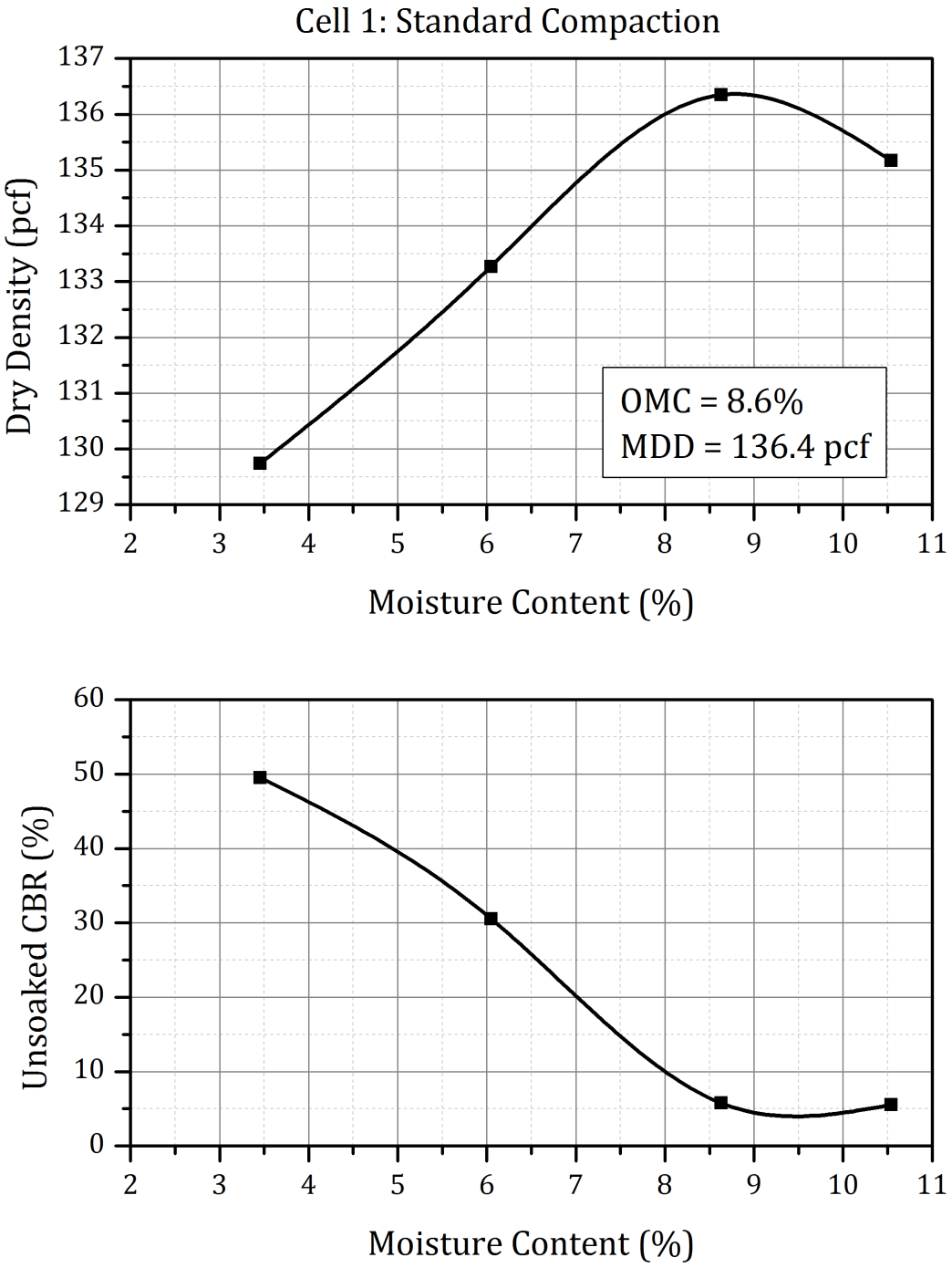


Figure B.6: Moisture-Density and Unsoaked CBR for Uncrushed Gravel with High Amounts of Nonplastic Fines-Standard Compactive Effort (1 pcf = 0.157 kN/m$^3$)

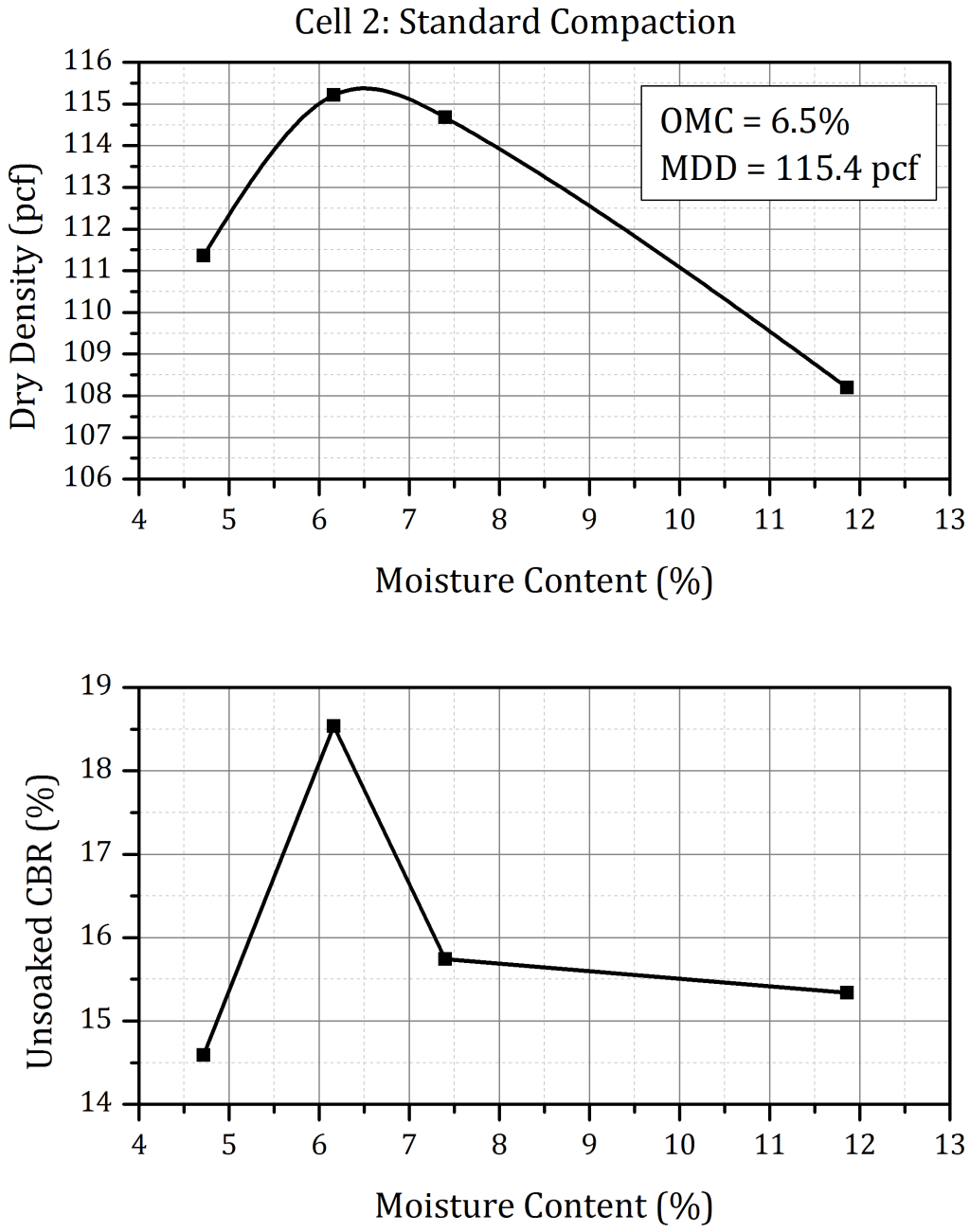


Figure B.7: Moisture-Density and Unsoaked CBR for Crushed Limestone with Low Amounts of Plastic Fines-Standard Compactive Effort (1 pcf = 0.157 kN/m$^3$)

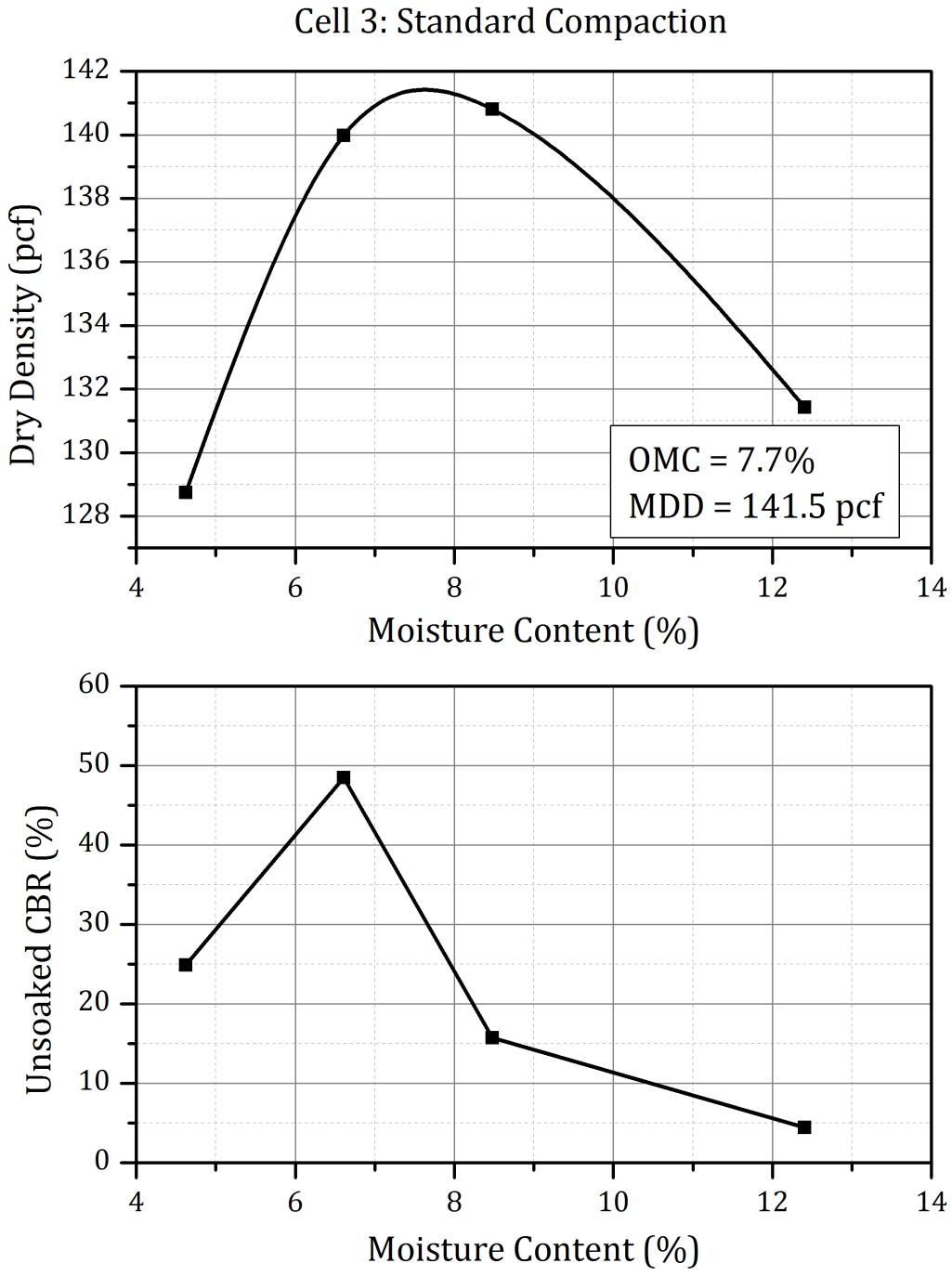


Figure B.8: Moisture-Density and Unsoaked CBR for Crushed Dolomite with High Amounts of Nonplastic Fines-Standard Compactive Effort (1 pcf = 0.157 kN/m$^3$)

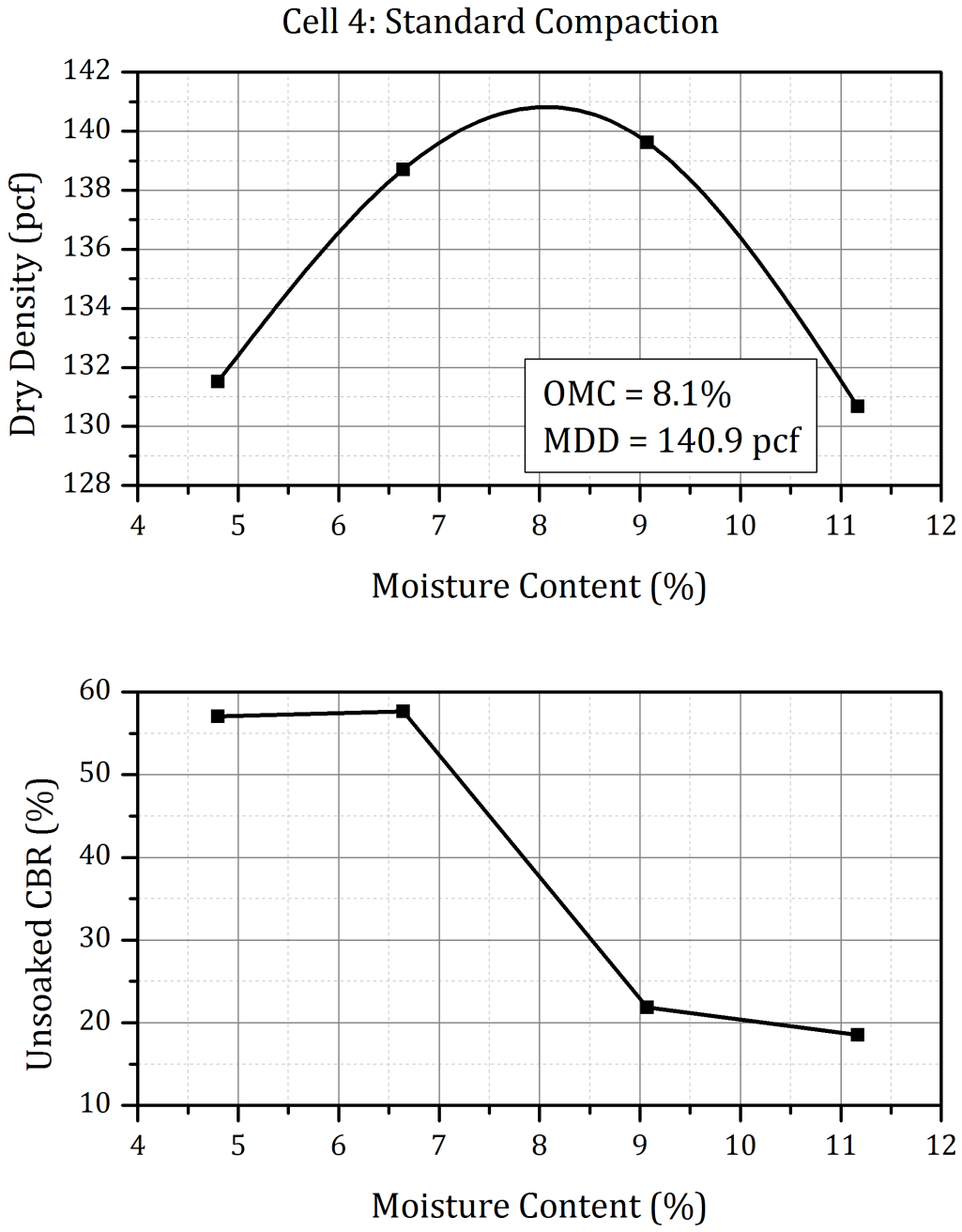


Figure B.9: Moisture-Density and Unsoaked CBR for Crushed Limestone with High Amounts of Nonplastic Fines-Standard Compactive Effort (1 pcf = 0.157 kN/m$^3$)

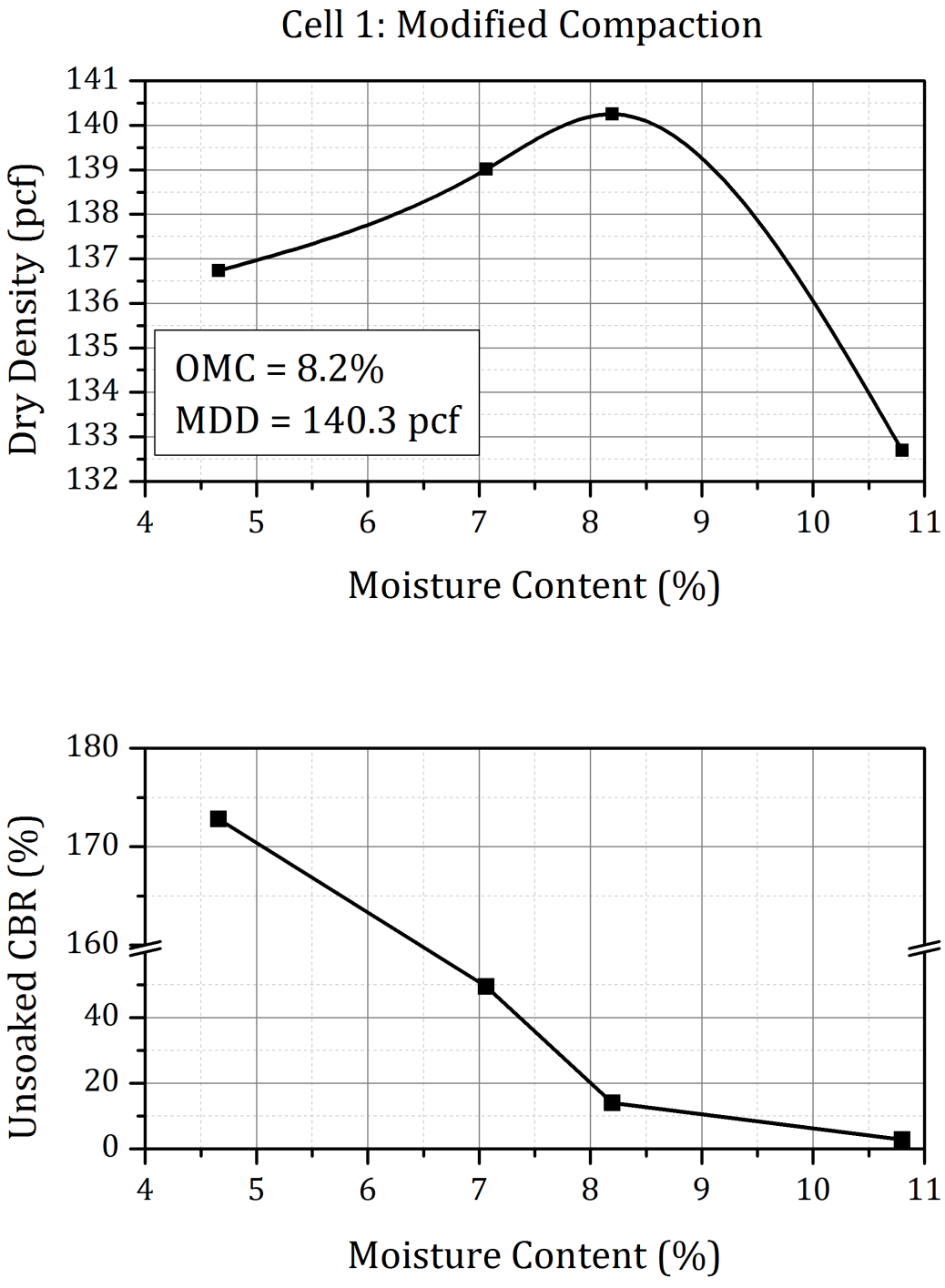


Figure B.10: Moisture-Density and Unsoaked CBR for Uncrushed Gravel with High Amounts of Nonplastic Fines-Modified Compactive Effort (1 pcf = 0.157 kN/m$^3$)

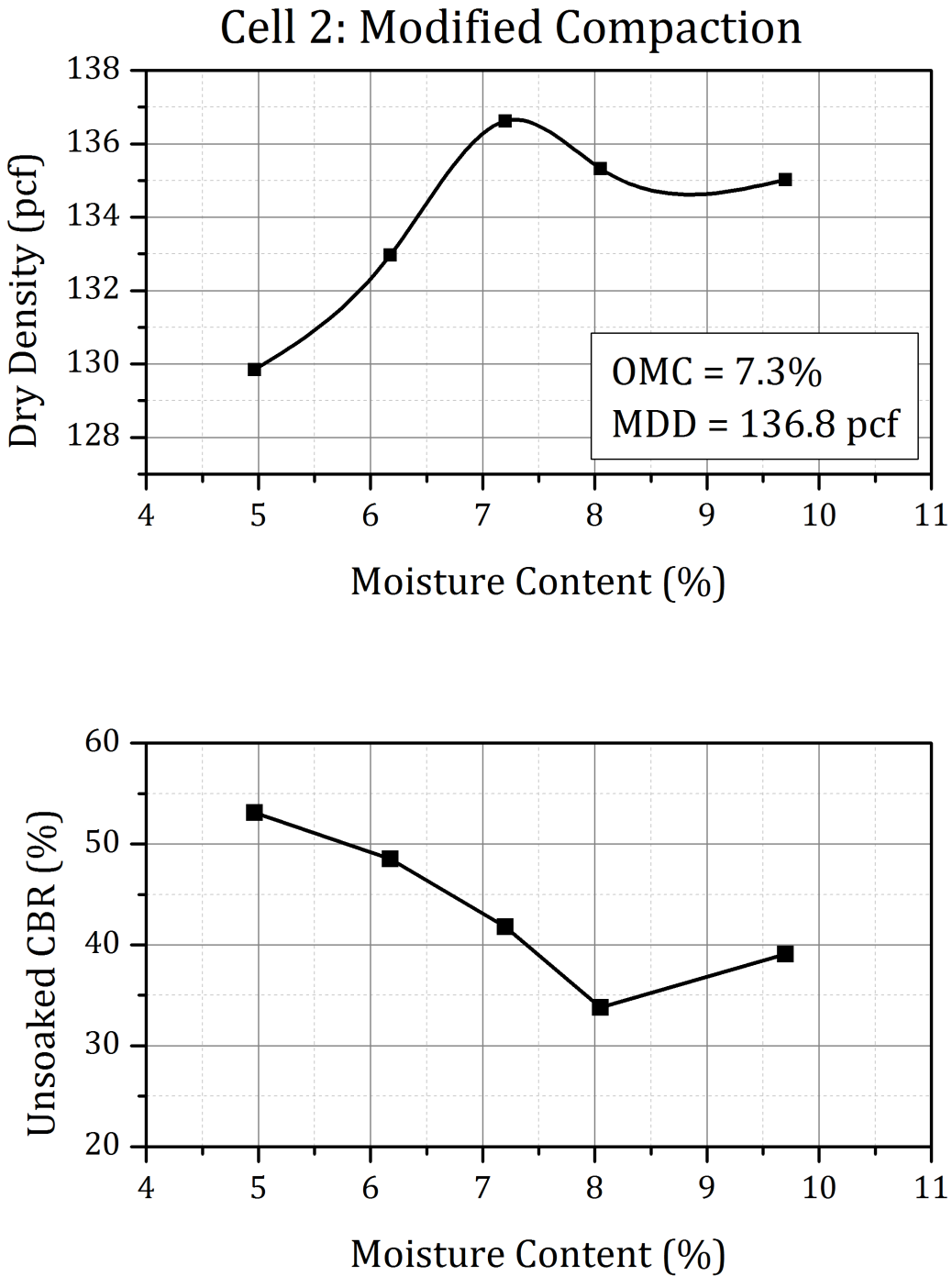


Figure B.11: Moisture-Density and Unsoaked CBR for Crushed Limestone with Low Amounts of Plastic Fines-Modified Compactive Effort (1 pcf = 0.157 kN/m$^3$)

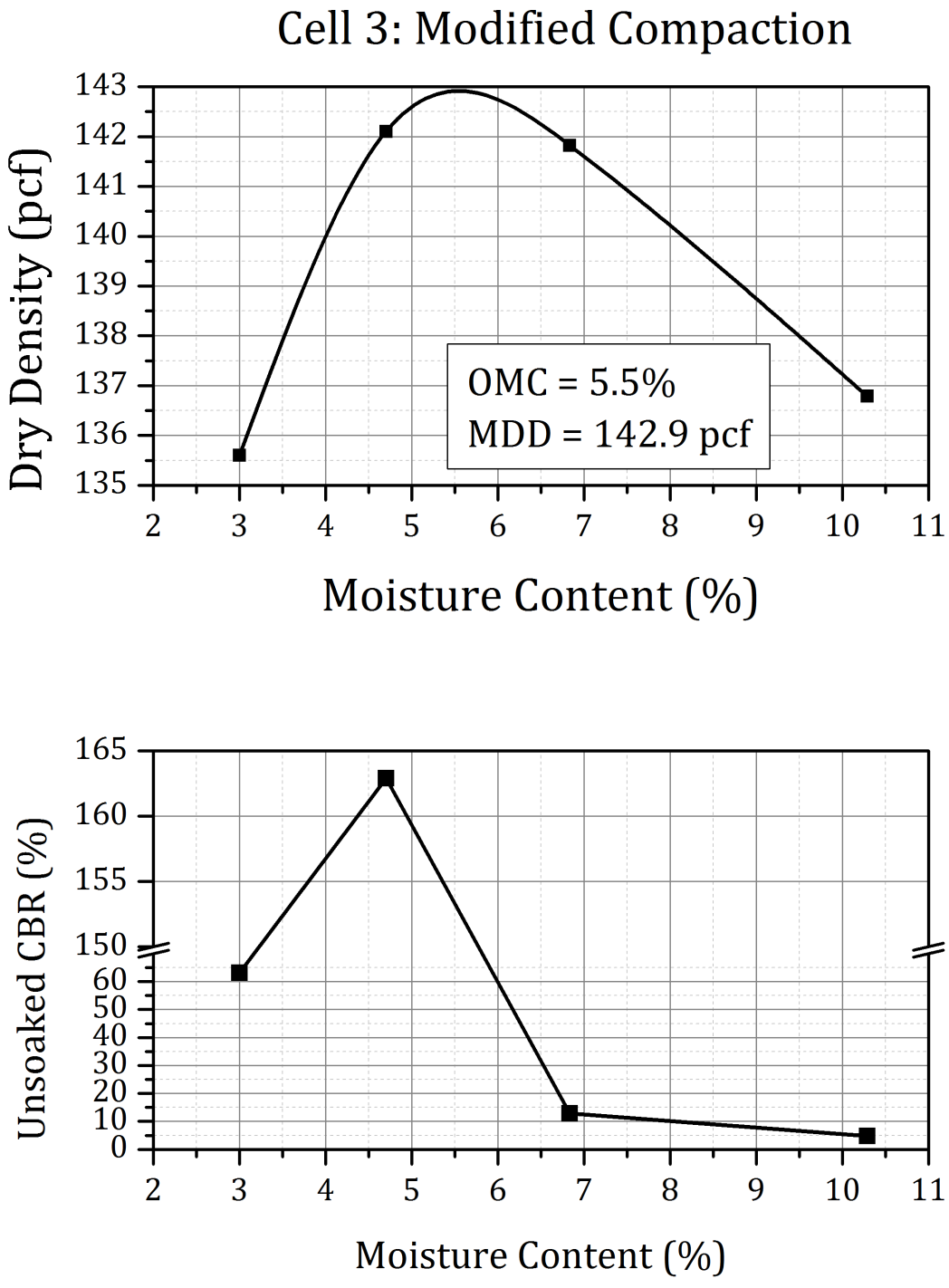


Figure B.12: Moisture-Density and Unsoaked CBR for Crushed Dolomite with High Amounts of Nonplastic Fines-Modified Compactive Effort (1 pcf = 0.157 kN/m$^3$)

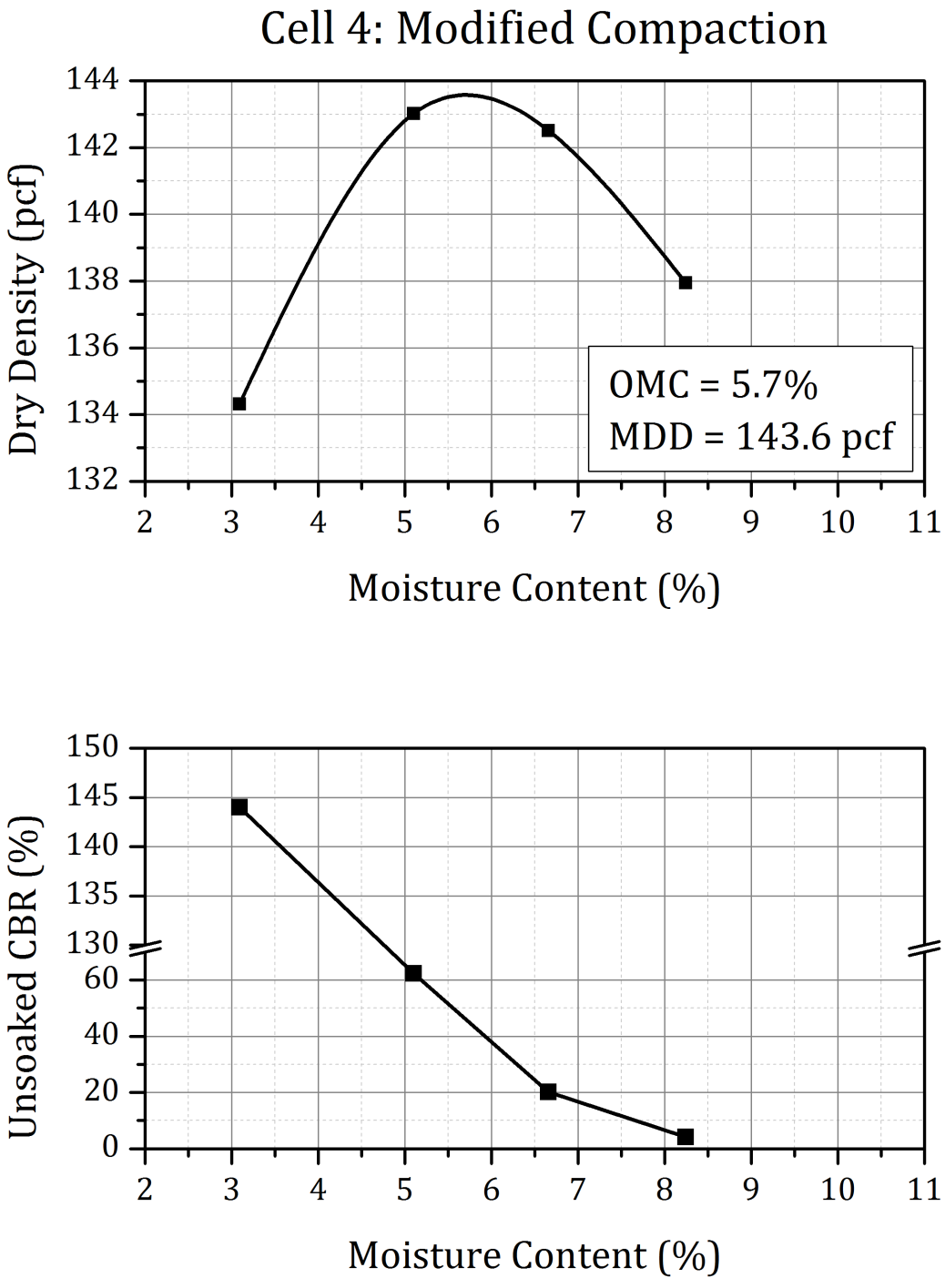


Figure B.13: Moisture-Density and Unsoaked CBR for Crushed Limestone with High Amounts of Nonplastic Fines-Modified Compactive Effort (1 pcf = 0.157 kN/m$^3$)

# APPENDIX C

# LIGHT WEIGHT DEFLECTOMETER SPECIFICATIONS

1. Loading
    - Loading Plate Diameter: 150 mm (5.9 in) and 300 mm (11.8 in)
    - Drop Weight Mass: 10 kg (22 lb)
    - Loading Type: Essentially Half Sine
    - Pulse Duration: 15-30 ms
2. Load Cell
    - Range: 0-25.0 kN (0-5,500 lbf)
    - Accuracy: 2% $\pm$ 2 kPa (2.25 lbf)
    - Precision: 0.0003 kN (0.067 lbf)
3. Deflection Sensors
    - Type of sensor: Velocity Transducer (Geophone)
    - Number: 1 central sensor with 2 offset sensors
    - Range: 0-2200 $\mu$m (0-87 mil) (preferrably 500 $\mu$m - 1500 $\mu$m)
    - Sampling Frequency: 4000 Hz on each sensor
    - Sampling Period: 60-120 ms (set by user)
    - Accuracy: 2% $\pm 2\mu$m (0.08 mil)
    - Precision: 0.1 $\mu$m

# APPENDIX D

# INVESTIGATION OF FREEZE-THAW EFFECT WITH DCP

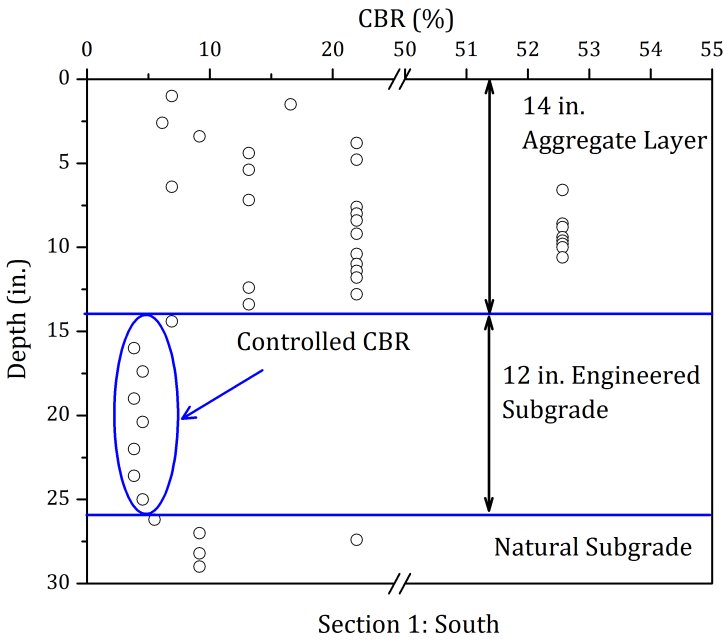


Figure D.1: CBR Profile with Depth for Section 1-South

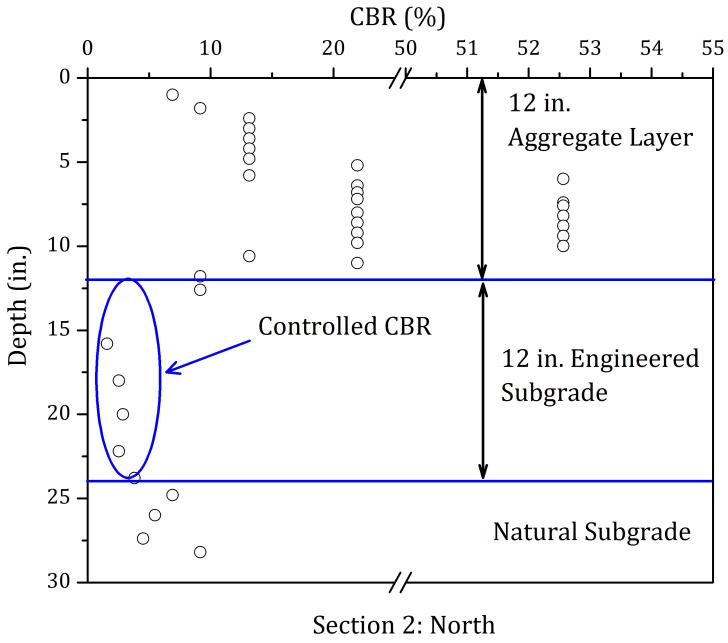


Figure D.2: CBR Profile with Depth for Section 2-North

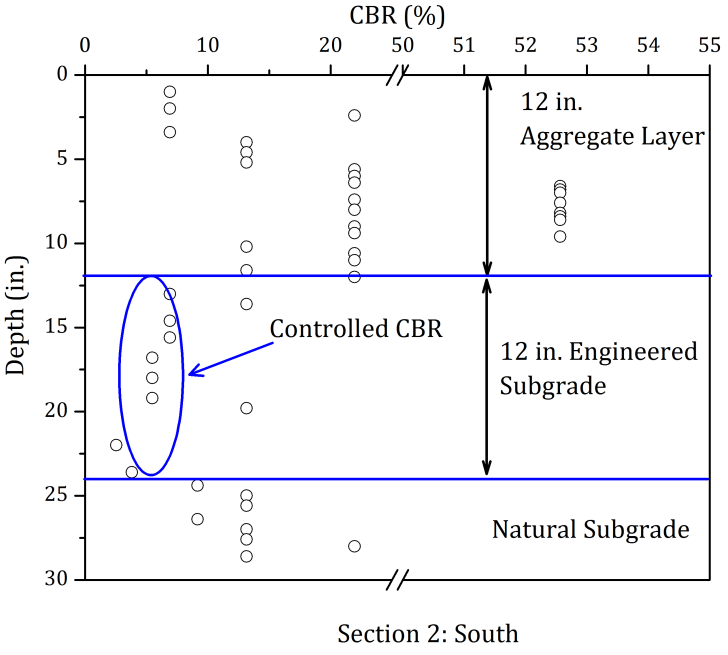


Figure D.3: CBR Profile with Depth for Section 2-South

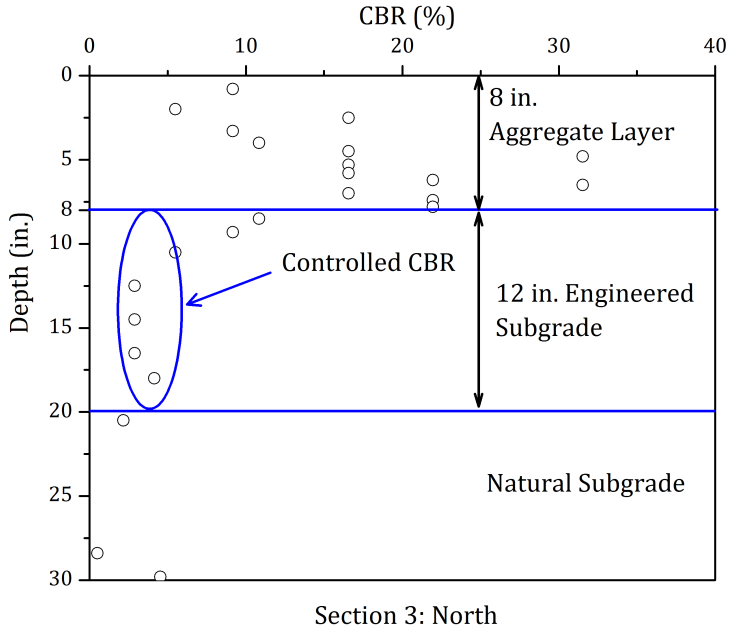


Figure D.4: CBR Profile with Depth for Section 3-North

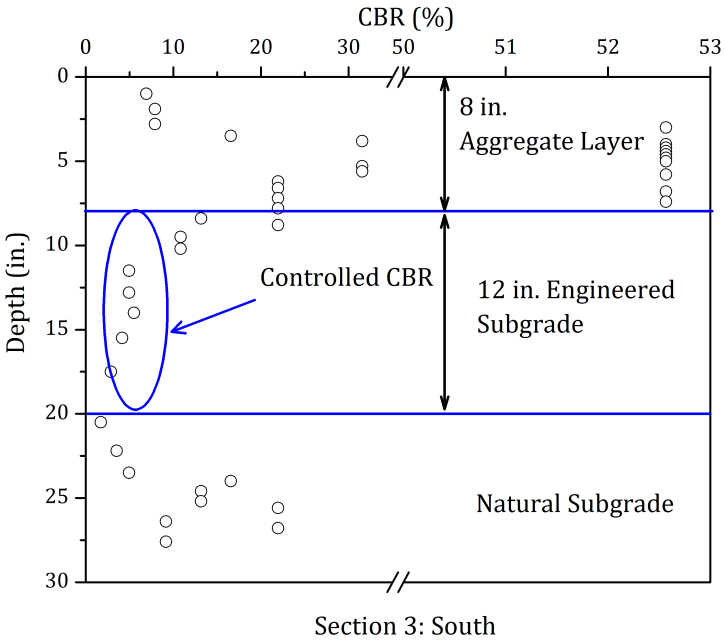


Figure D.5: CBR Profile with Depth for Section 3-South